P WAVE VELOCITY STRUCTURE OF THE UPPER MANTLE IN THE AUSTRALIAN REGION

A thesis submitted for

the degree of

DOCTOR OF PHILOSOPHY

in the

AUSTRALIAN NATIONAL UNIVERSITY

by

DAVID WILLIAM SIMPSON

February 1973

STATEMENT

The studies described in this thesis were carried out while I was a full-time research scholar in the Department of Geophysics and Geochemistry at the Australian National University during the period October 1969 to February 1973.

Except where mentioned in the text or in the acknowledgements, the research described in this thesis is my own.

This thesis has never been submitted to another university or similar institution.

David W. Simpson

DAVID W. SIMPSON

Canberra,
February 28, 1973

Acknowledgements

I sincerely wish to thank Dr J.R. Cleary for his guidance and encouragement throughout this study.

Dr R.F. Mereu and Mr D.W. King were responsible for developing the array processing system used in the WRA study. They analysed many of the events and made useful comments and criticisms on that part of the work. Dr Mereu also kindly provided an unpublished velocity model of the Canadian shield and made a number of useful comments on the presentation of the travel time diagrams in Chapter 2.

Dr K.J. Muirhead designed the instruments described in Chapter 3 and he and Mr M.H. Worthington have been involved in useful discussion on many aspects of this study.

Dr C. Wright and Mr H.A. Doyle were involved in the initial stages of this work and Dr Wright was responsible for an early version of the travel time program used in Chapter 2.

Dr D. Denham organized the Ord River experiments and provided original records from the Bureau of Mineral Resources stations. Dr D. Sutton made records available from the University of Adelaide stations.

Professor A.E. Ringwood, Dr D.H. Green and Dr R.C. Liebermann discussed many aspects of the geochemistry and physical properties of the upper mantle and they are responsible for initiating many of the ideas presented in Chapter 8.

Many members of the Department of Geophysics and Geochemistry, especially Dr T.J. Fitch, Dr A.R. Crawford and Dr R. Underwood, have made useful comments and criticisms.

Summary

A P wave velocity model for the upper 800 km of the mantle has been determined using travel times to 20° from large explosions in northern Australia and observations at the WRA array of travel times and slownesses from earthquakes in the New Guinea region in the distance range 17° to 30°.

In the uppermost mantle, the explosion data indicate velocity discontinuities at 85 and 175 km and a gradual increase in velocity between these depths. Observations of the Cannikin nuclear explosion at portable stations along a line crossing the Precambrian boundary in eastern Australia suggest that a low velocity layer for P, absent beneath the Precambrian shield, exists in the younger area to the east.

The combined interpretation of WRA travel time and slowness data reveals a number of later arrival branches in the travel time curve between 15° and 30°. A velocity model based on these data shows a low velocity gradient above 300 km, a gradual increase in velocity from 300 to 400 km, a minor zone of high velocity gradient near 520 km, a low velocity gradient from 550 km to 680 km and an abrupt increase in velocity near 680 km. The main features of this model are in substantial agreement with the changes in physical properties expected from mineralogical variations in a pyrolite upper mantle.

P WAVE VELOCITY STRUCTURE OF THE UPPER MANTLE IN THE AUSTRALIAN REGION

TABLE OF CONTENTS

TABLES

FIGURES

CHAPTER 1

INTRODUCTION

1.1 The Velocity Structure of the Upper Mantle

Refinements to the determination of body wave velocities in the upper mantle have been an important part of recent developments in our understanding of the properties of this region of the Earth's interior. Advances in instrumentation, data handling, and interpretation techniques have made it possible to distinguish both lateral and vertical variations in velocity structure which have important implications concerning the composition of the mantle and the part which it plays in tectonic processes.

The most direct evidence about the P wave velocity distribution in the upper 800 km of the mantle comes from observations of refracted P wave arrivals at epicentral distances of less than 30°. Since early in this century (see Gutenburg and Richter, 1935, for a review of early work) it has been known that one of the most striking features of this part of the travel time curve is a significant change in slope near 20°, which, under the name "20° discontinuity", was assumed to result from a rapid increase in velocity in a transition zone between 300 and 700 km. The other main feature of arrivals in this distance range is a low amplitude region between 5° and 18°, which has been associated with low or negative velocity gradients at depths less

than 250 km. These two general properties of the velocity structure of the upper mantle - a zone of low or negative velocity gradient above 250 km (the "low velocity zone") and regions of high velocity gradient between 300 and 700 km (the "transition zone") - are now generally accepted*. However, recent attempts at establishing the exact nature of velocity changes in these anomalous regions have led to models which differ significantly in detail. This may reflect real regional variations in structure, but is more likely a result of difficulties in the interpretation of the observed data - data which may often be "inaccurate, insufficient and inconsistent" (Johnson, 1972).

It is now well established that high velocity gradients in at least two zones near 400 and 600 km cause multiplicity in the P-wave travel time curve

---

*A note on terminology: The early subdivision of the outer 1000 km of the Earth into crust and upper mantle is no longer adequate to describe the detail of structure now known to exist in this region. The revival of the terms lithosphere, asthenosphere and mesosphere within the framework of plate tectonics (Isacks, Oliver and Sykes, 1968) is useful in the discussion of tectonic processes, but the thicknesses and properties of these layers are vaguely defined. In this thesis the following general terms will be used when describing velocity structure. Upper mantle will refer to depths from the base of the crust to a depth of 1000 km. Transition zone will refer to the region containing a number of zones of high velocity gradient from approximately 250 km to below 800 km (the maximum depth of interest in this thesis). This comprises the depths reached by rays emerging at distances from 17° to 30°. Uppermost mantle will refer to depths above approximately 250 km which may or may not contain a low velocity zone centered near 100 km.

between 10^{o} and 30^{o} (see review by Hales, 1972). The later arrivals from this complex region are difficult to identify and correlate over an extended distance range, and it is mainly the interpretation of these arrivals which leads to differences in velocity models. The travel times and amplitudes of body waves are very sensitive to minor variations in velocity structure, and although this makes them useful for delineating fine structure, it also means that any lateral variation in velocity will cause significant differences in travel times for different regions. Within the resolving power of early travel time observations, world wide data were sufficient to define the general features of the upper mantle. In order to achieve the resolution required in recent studies, it has been necessary to confine observations to more limited regions. Similarities in models derived for different regions should make it possible to define more precisely the general character of upper mantle fine structure, while differences will indicate the extent of regional variations.

1.2 Limitations in Velocity Determination

There are three major limitations in the extent to which a "correct" velocity model can be found for any region of the upper mantle; 1) lateral variations in velocity, 2) incomplete and inaccurate data, and 3) the non-uniqueness of the geophysical inverse problem.

Lateral variations in velocity - An attempt to define uniquely velocity as a function of a single variable, depth, implies that the velocity does not vary laterally within the region sampled. The determination of upper mantle velocities by refraction methods requires observations of travel times over a distance range of up to 30° and it is unlikely that any region of the Earth has a homogeneous velocity distribution over such a range. Observations of earthquake sources are especially susceptible to this problem, as the very existence of the earthquakes implies the existence of an anomalous region. In studies of the uppermost mantle, the problem has been minimized by using observations of artificial explosions at temporary stations set up along profiles within regions where the velocity structure may be nearly homogeneous (e.g., the Early Rise Project, Iyer et al., 1969). Even these studies have sometimes indicated regional variations in structure that are greater than originally expected (e.g., the thick crust found beneath Lake Superior, Smith et al., 1966). Observations of nuclear explosions at distances which sample the transition zone are limited by the location of test sites. The American test sites in Nevada and the Aleutians are both situated in regions of recent tectonic activity where it is likely that the upper mantle structure is atypical.

Recent attempts to utilize three dimensional ray theory (Jacob , 1970, Sorrells et al., 1971) have provided insight into the effects of lateral variations

in velocity, but the usefulness of this approach as an inversion tool is limited at this stage by the increased non-uniqueness of the inversion process in three dimensions.

Incomplete and inaccurate data - The global distributions of earthquakes, nuclear explosions and recording stations impose severe restrictions on the determination of a complete travel time curve by routine observations alone. Special studies using explosions have helped to alleviate this problem also, but the limitations in size of non-nuclear explosions has restricted their usefulness mainly to the investigation of the uppermost mantle.

The present state of seismic instrumentation has virtually eliminated problems associated with timing errors. Once identified, the arrival time of a clear phase can be read to adequate precision. The major unresolved problem in interpretation of the multi-branched travel time curve near 20° is the proper identification of later arrivals; i.e., the data are incomplete and inaccurate because of errors in interpretation rather than observation. As will be shown in Chapter 6, seismic arrays are perhaps most useful in this context. The ability to determine dT/Δ directly makes it possible to relate each arrival to a particular branch of the travel time curve and thus eliminate much of the uncertainty in phase identification.

The non-uniqueness of the geophysical inverse problem - It has been shown that the nature of the

inverse problem in seismology is such that it is impossible, with only a finite amount of data, to determine a unique solution to fit these data (Backus and Gilbert, 1967). Using Monte Carlo methods (Press, 1968, 1972; Wiggins, 1969; Worthington et al., 1972) and extremal techniques (McMechan and Wiggins, 1972) it is possible to place bounds on the range of solutions that are consistent with observed data. The limits of these bounds can be refined as the amount and quality of data increase. At any stage, a geophysically useful estimate of the "correct" model is the simplest valid solution within the current bounds which satisfies the observed data and meets any constraints imposed from independent sources (e.g., geochemical models).

1.3 Other Methods of Velocity Determination

The observation of travel times of refracted arrivals at less than 30° provides the most direct means of determining body wave velocities in the upper mantle, but recently two less direct methods have been successful in describing average structure and detecting regional variations in velocity.

Body wave residuals - In a revision of the P wave travel time curve from 32° to 100° Cleary and Hales (1966) were able to separate regional differences in travel times into residuals associated with source and receiver areas. These residuals showed definite correlation with tectonic regions. Negative residuals (early arrivals) were associated with stable shield areas

and positive residuals (late arrivals) were found for younger tectonic regions. Hales et al. (1968) showed that these variations could be explained by changes in the thickness of the low velocity zone in the upper mantle. This technique is especially suited to the study of regional variations in structure since the rays involved pass through the upper mantle at a steep angle and hence sample a region that is limited in lateral extent.

Underside reflections - Gutenburg (1960) suggested that precursors to the main arrivals of phases such as PP, P'P' or pP may be reflections from the crust and from discontinuities in the upper mantle. Bolt et al. (1968) identified arrivals before the onset of PP which they ascribed to underside reflections (PdP) from discontinuities near depths of 400 and 600 km. Some doubt now exists as to the proper interpretation of these arrivals, and Wright (1972) and Angoran and Davies (1972) showed that they are likely to be confused with asymmetrical reflections from the Earth's surface. This criticism does not apply, however, to observations of precursors, P'dP', to the core phase P'P'. Adams (1968, 1971) and Whitcomb and Anderson (1970) have identified P'dP' arrivals which originate from reflectors at depths between 280 and 650 km. The amplitudes of the arrivals suggest that the transition at 650 km is much more abrupt than those at shallow depths (Richards, 1972). The virtual absence of the reflection from 400 km on short period records,

contrasted with its prominence on long period records, also indicates that the shallower transition is gradual.

1.4 Relevance of Velocity Studies to Related Fields

With the development of the theory of plate tectonics, studies of the structure of the upper mantle have taken on great importance because of the role this part of the Earth must play in the motion of plates. The properties of the low velocity zone vary widely. For P waves, it is best developed in areas of recent tectonic activity and appears to be almost absent from shield regions (Cleary and Hales, 1966, Kanamori, 1970). If the low velocity layer is assumed to provide the region over which plates move, then variations in its properties have important implications on the mobility of plates. Further insight into the mechanism of the formation and growth of continents may lie in an understanding of the reasons for differences to considerable depths in the structure beneath shields and tectonic regions and the persistence of these differences over long periods of time.

The significance of high velocity gradients in the transition zone has become apparent with the identification of phase transitions in upper mantle mineral assemblages using high pressure and temperature techniques (see reviews by Anderson, 1967b, and Ringwood, 1970). A mantle of predominantly olivine composition would undergo abrupt changes in properties at the pressures and temperatures expected near 400 and 650 km.

When assumptions are made concerning the composition of the mantle and the variations of pressure and temperature and depth, it is now possible to predict fine structure in considerable detail, but the validity of such geochemical models depends on confirmation by the observation of fine structure in the velocity distribution.

1.5 The Scope of This Thesis

The Australian sub-continent has a number of features which make it a particularly fruitful region for upper mantle studies. In general terms, the area consists largely of Precambrian shield, which is bounded to the west and south by ocean, to the east by a region of recent uplift and to the north by an intensely active zone of plate subduction (Figure 1-1). The seismic area to the north is confined to a narrow belt and the transition from the active region to the stable continent is relatively abrupt. Unlike most other areas in the circum-Pacific belt, the Benioff zones in this region generally dip away from the continent, so that seismic waves travelling to a receiver on the continent spend little time in the anomalous source region. The location of the Warramunga seismic array (WRA) in the central part of the continent thus provides one of the few locations on the Earth where rays with relatively pure transmission paths through the transition zone of the upper mantle can be observed using earthquake sources. An automated array analysis technique developed by King, Mereu and Muirhead (1973), which is described in Chapter

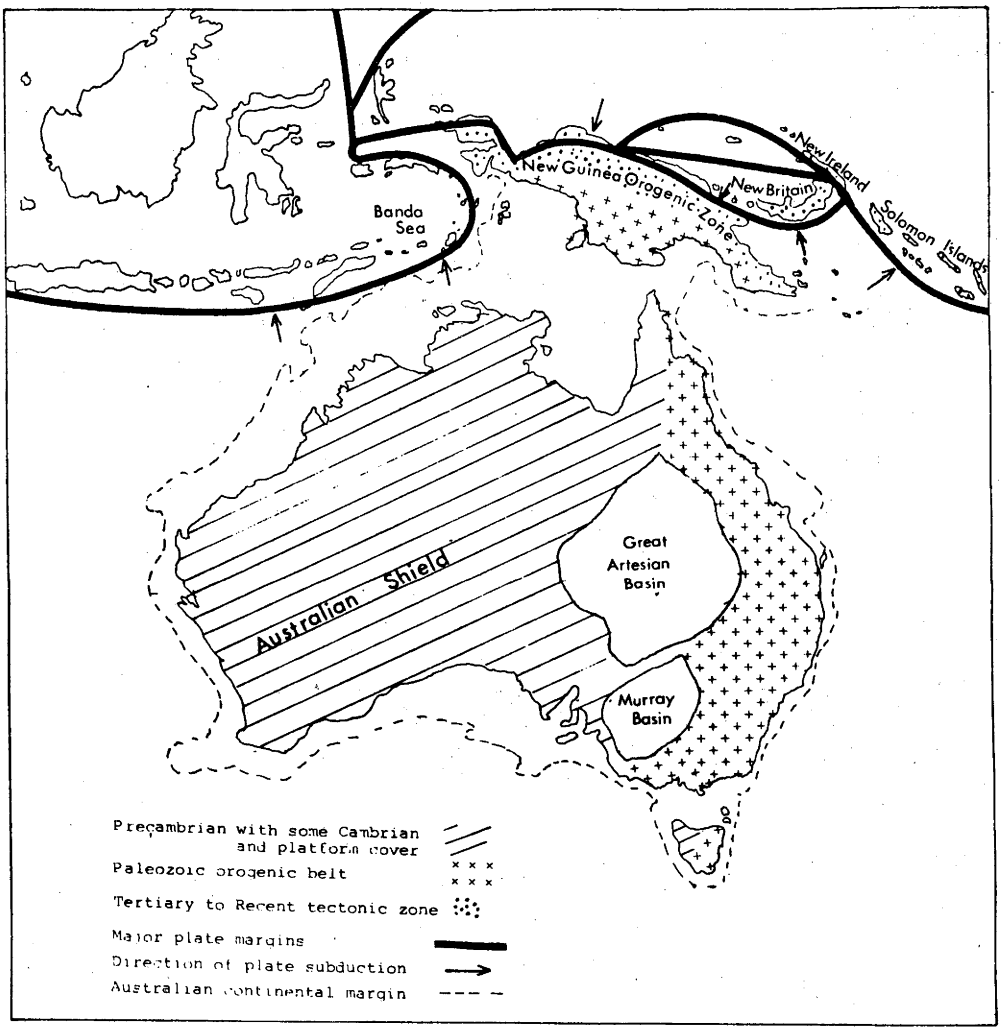

Figure 1-1. Tectonic sketch map of Australia and surrounding regions.

5, has made it possible to analyze WRA data in great detail. The ability to measure $dT/d\Delta$ for later, as well as first, arrivals makes this method especially well suited for unravelling the complexity in the travel time curve near 20°. A combined travel time and $dT/d\Delta$ approach (Chapter 6) has been used to identify the nature of travel time branches in the range 15° to 30°, using array-analysed data from approximately 200 earthquakes in the New Guinea region. Velocity models derived from these data (Chapter 7) show details in structure that have not previously been identified.

The timely occurrence of three large explosions during the course of study related to this thesis provided the opportunity for two other investigations of the upper mantle in the Australian region (Chapter 4). Two large explosions at the Ord River damsite in northern Australia were observed at distances up to 24° and provided the basis for a study of velocities in the uppermost mantle beneath the Australian shield. A set of portable instruments (Chapter 3) developed for this project was also used to record the large American nuclear explosion Cannikin. The location of this explosion in the Aleutian Islands was particularly fortunate, as a line perpendicular to the great circle path from the shot point cuts directly across the boundary between the Precambrian shield and the younger highlands of eastern Australia. Travel time residuals at a series of temporary stations along the line were used to define variations in upper mantle structure across the Precambrian boundary (Chapter 4).

CHAPTER 2

TRAVEL TIMES FOR UPPER MANTLE MODELS - A REVIEW

2.1 Introduction

Among the important parameters of seismic body waves which can be observed as a function of distance (Δ) at the Earth's surface are the travel time (T), slowness ($dT/d\Delta$, corresponding to the inverse of the apparent velocity, v_a) and amplitude (A). The slowness and amplitude are related to the travel time curve through its first and second derivatives, and the slowness can be related to the velocity (v) of the medium at the maximum depth (d_p) to which a ray penetrates.

In this chapter a graphical presentation will be used to show the interrelationship between the four distance-dependent parameters (T, $dT/d\Delta$, A and d_p) and the depth-dependent velocity (v) for a number of upper mantle velocity models. The historical development of velocity models is interesting in its own right, but a study of these models and the travel times derived from them has also proved useful in providing a basis for comparison with the data presented in this thesis and by indicating the extent of regional variations in velocity structure. The wide variety of velocity distributions represented by these models has also shown the effects of various types of velocity structure on the parameters derived from them.

Slowness - The first distance derivative of the travel time curve ($dT/d\Delta$) can be shown to equal the seismic ray parameter p and it is this parameter, as a function of distance, which is required in the classical Herglotz-Wiechert inversion technique in order to derive a velocity-depth distribution (Appendix A). Until recent years $dT/d\Delta$ could only be obtained by smoothing observed travel time data and finding the slope of the smoothed curve. With the advent of modern seismic arrays, it is now possible to measure $dT/d\Delta$ directly and independently of absolute time, thus removing many of the errors associated with the earlier technique. Because $dT/d\Delta$ is now a readily observable quantity its importance as an analytical parameter has increased in recent years.

Amplitude - The second distance derivative ($d^2T/d\Delta^2$) gives the curvature of the travel time curve. If the curvature at a particular distance is large, rays are focussed at that distance and the amplitude of arrivals is high. If the curvature is low (i.e. the travel time curve is almost linear), the rays are spread out and the resulting amplitude is low. A complete discussion of this geometrical spreading effect on the amplitude of body waves is given by Bullen (1963, Chapter 8) (see also Julian and Anderson, 1970). It is sufficient here to simply state that, in the absence of attenuation, amplitude is proportional to $d^2T/d\Delta^2$.

Depth of penetration - The true velocity (v_t) at the maximum depth of penetration (d_p) for a given ray is

related to the apparent velocity (v_a) at the Earth's surface (radius R_E) by

$$v_t = \frac{v_a (R_E - d_p)}{R_E} \qquad (2\text{-}1)$$

(see Appendix A)

It is obvious from equation 2-1 that the slope ($dT/d\Delta \propto v_a^{-1}$), and hence the shape, of any part of the travel time curve is determined by the velocity at the maximum depth of penetration for the rays arriving over that part of the curve. Conversely, if the apparent velocity at the surface is known as a function of distance, the true velocity at depth can be found by determining the corresponding depths of penetration as a function of distance, using the Herglotz-Wiechert inversion technique.

2.2 Graphical Presentation

An example of the graphical presentation which will be used in all subsequent travel time plots is shown in Figure 2-1, for a hypothetical upper mantle velocity model. Slowness ($dT/d\Delta$, in s/deg), reduced travel time ($T-\Delta/10$ km/s, in s) and depth of penetration (in km) are shown as a function of distance (Δ, in both km and deg). Velocity (in km/s) is given as a function of depth (in km). Crosses are placed on the travel time curve at points corresponding to the arrivals of rays separated by equal intervals of slowness (0.05 s/deg). The density of crosses (i.e. the change of slowness with distance) is a measure of $d^2T/d\Delta^2$, and thus provides a qualative

indication of the amplitude of arrivals. When reflections occur due to a first order discontinuity in the velocity model, the travel time curve beyond the critical distance is included and is indicated by circles, instead of crosses.

This unified presentation emphasises the inter-relationship between the velocity model and the various parameters derived from it. It is possible to relate a point on any curve (viz. velocity-depth, depth-distance, time-distance or slowness-distance) with the corresponding points on the other curves in the manner shown in Figure 2-1. The vertical line through 18.1^{o} shows that at this distance two phases (a, c) arrive simultaneously with a reduced travel time of 51.5 s. The slownesses of the two arrivals are 13 s/deg (a) and 11 s/deg (c) and they correspond to rays which have penetrated to depths of 200 km and 410 km where the velocities are 8.3 km/s and 9.5 km/s, respectively. A larger amplitude later arrival, b, on the retrograde branch, has a slowness of 12 s/deg and penetrates to a depth of 360 km where the velocity is 8.9 km/s. The times, slownesses, depths of penetration, velocities and relative amplitudes of the later (d, e) arrivals at this distance can be found in a similar manner.

This presentation also stresses the importance of later arrivals in determining velocity structure. The vertical lines in Figure 2-1 at the cross-over distances near 18^{o} and 24^{o} show that the first arrival portions of the travel time curve correspond to rays which reach

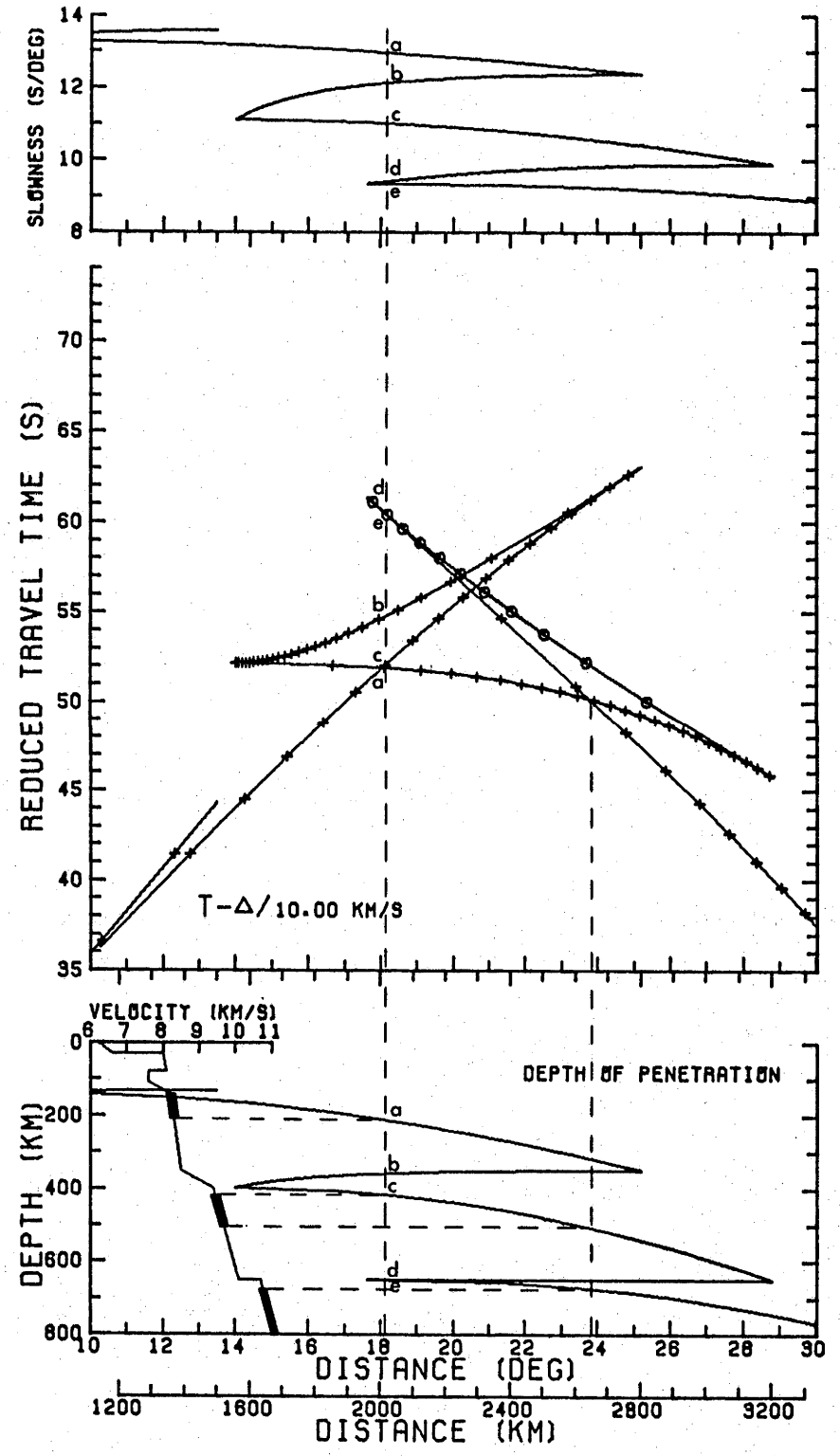

Figure 2-1. Hypothetical upper mantle model. For description see text.

their maximum depths of penetration over a very limited range. Between depths of 200 and 700 km, first arrivals in this model correspond to a total depth interval of only 100 km. Depths near the two discontinuities at 400 and 650 km are always related to later arrivals. Thus if the details of later arrivals are unknown, much of the velocity distribution is beyond the scope of the data.

2.3 Computational Methods

The calculation of travel time, slowness and depth of penetration is based on the discussion of ray theory given by Bullen (1961). An outline of the method is given in Appendix A. The velocity is assumed to follow a law of the form $v = a \cdot r^b$ between the tabulated values of velocity and depth. Wesson (1970), Shimshoni and Ben-Menahem (1970) and Chapman (1971) have discussed problems associated with the use of this velocity function when deriving amplitude curves. Discontinuities in the gradient of the velocity-depth curve are introduced at the tabulated depths and this leads to singularities in the amplitude curve. The effects on the travel time and slowness are minimal however, and in the presentation used here the problem has been avoided by treating the amplitudes in a qualative manner and not explicitly presenting amplitude-distance curves.

2.4 Velocity Models

Velocity models for the upper mantle can conveniently be divided in two groups: 1) the classical and gross Earth models which include those of Jeffreys, Gutenberg and Lehmann, as well as the more recent gross Earth model of Herrin et al. (1968); and 2) the recent models, which include numerous models with the general characteristic of high velocity gradients near 400 and 650 km, as first suggested by Niazi and Anderson (1965).

The velocity models to be considered in this chapter are shown in Figures 2-2, 2-3 and 2-4. The source of the data used in determining the models and the main features of the models are briefly discussed below. More details can be found in the original papers and in reviews by Lehmann (1967), Julian and Anderson (1968) and Hales (1972).

2.4.1 The classical and gross Earth models

The identification of a change in slowness and amplitude at the "20° discontinuity" (Byerly, 1926, Neumann, 1933, Lehmann, 1934, Gutenberg and Richter, 1935, Jeffreys, 1939) prompted a long series of papers in which Jeffreys, Gutenberg and Lehmann debated the proper interpretation of this feature (see reviews by Jeffreys, 1970, pp. 113-124; Gutenberg, 1959b, chapter 4; and Lehmann, 1967).

Jeffreys - The study of travel times by Jeffreys and Bullen which led to the J-B tables of 1940 was used in the derivation by Jeffreys (1939) of the velocity model shown in Figure 2-5 (Figures 2-5 to 2-24 are

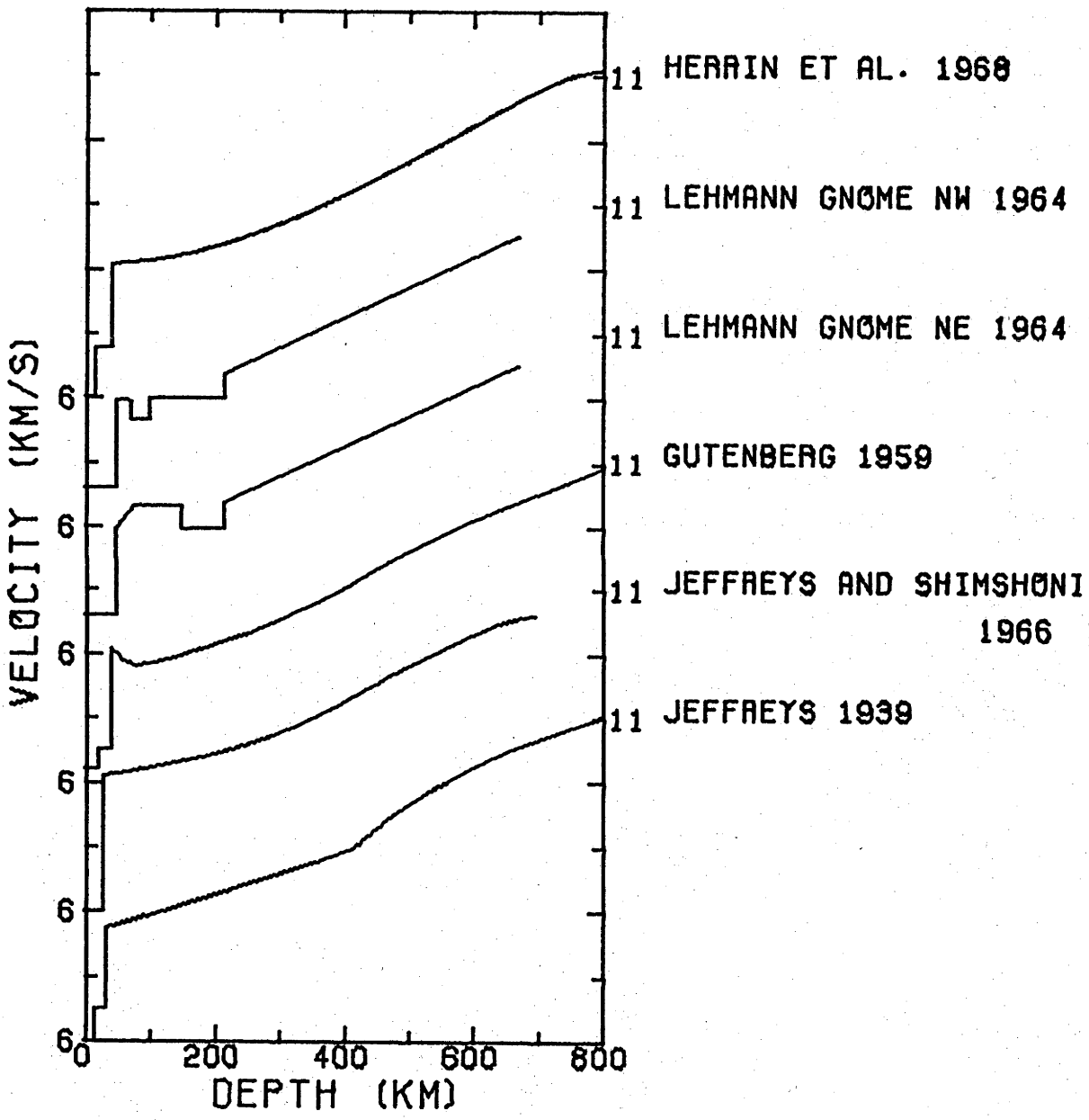

Figure 2-2. Classical and gross earth velocity models.

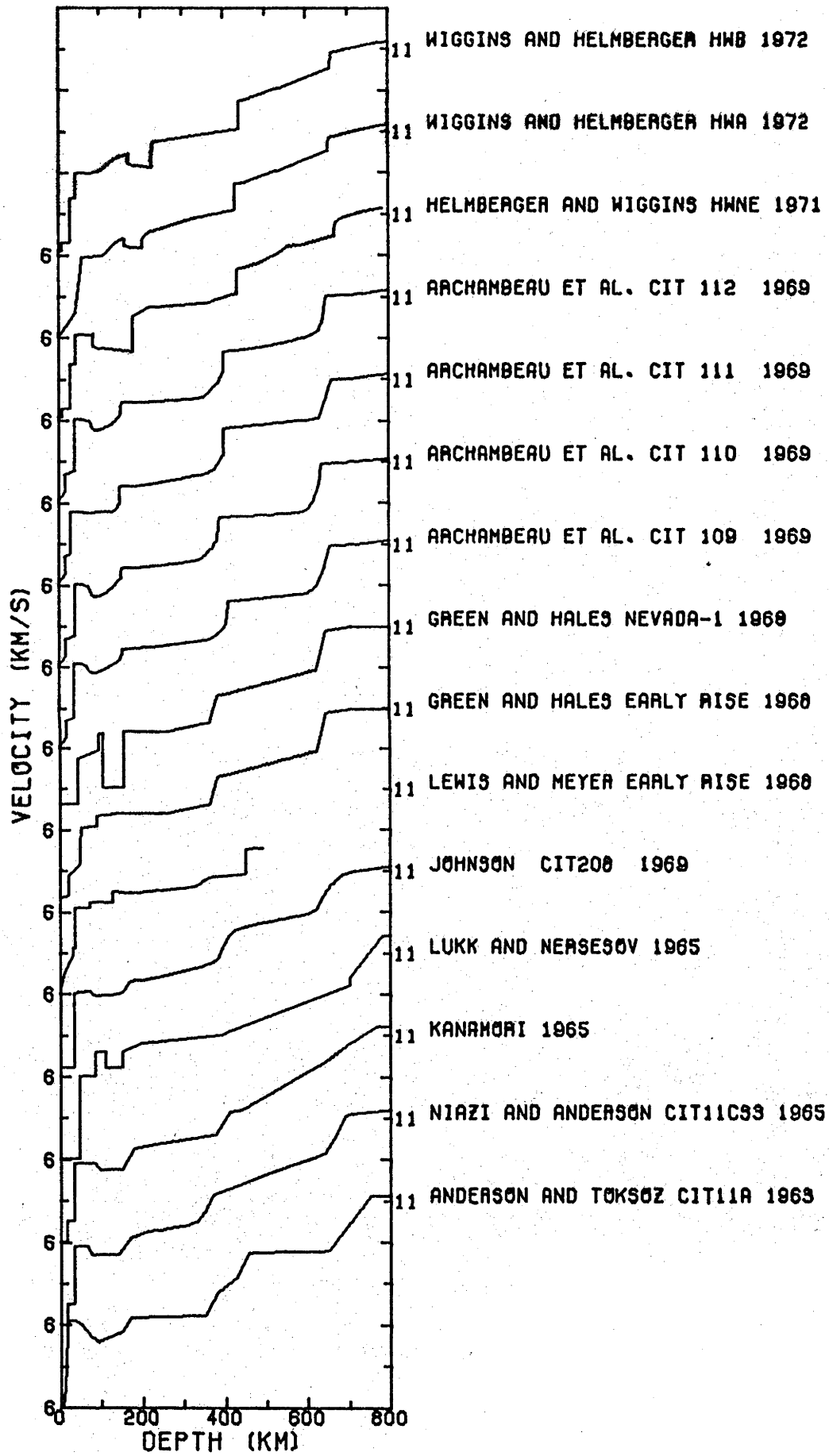

Figure 2-3. Recent velocity models.

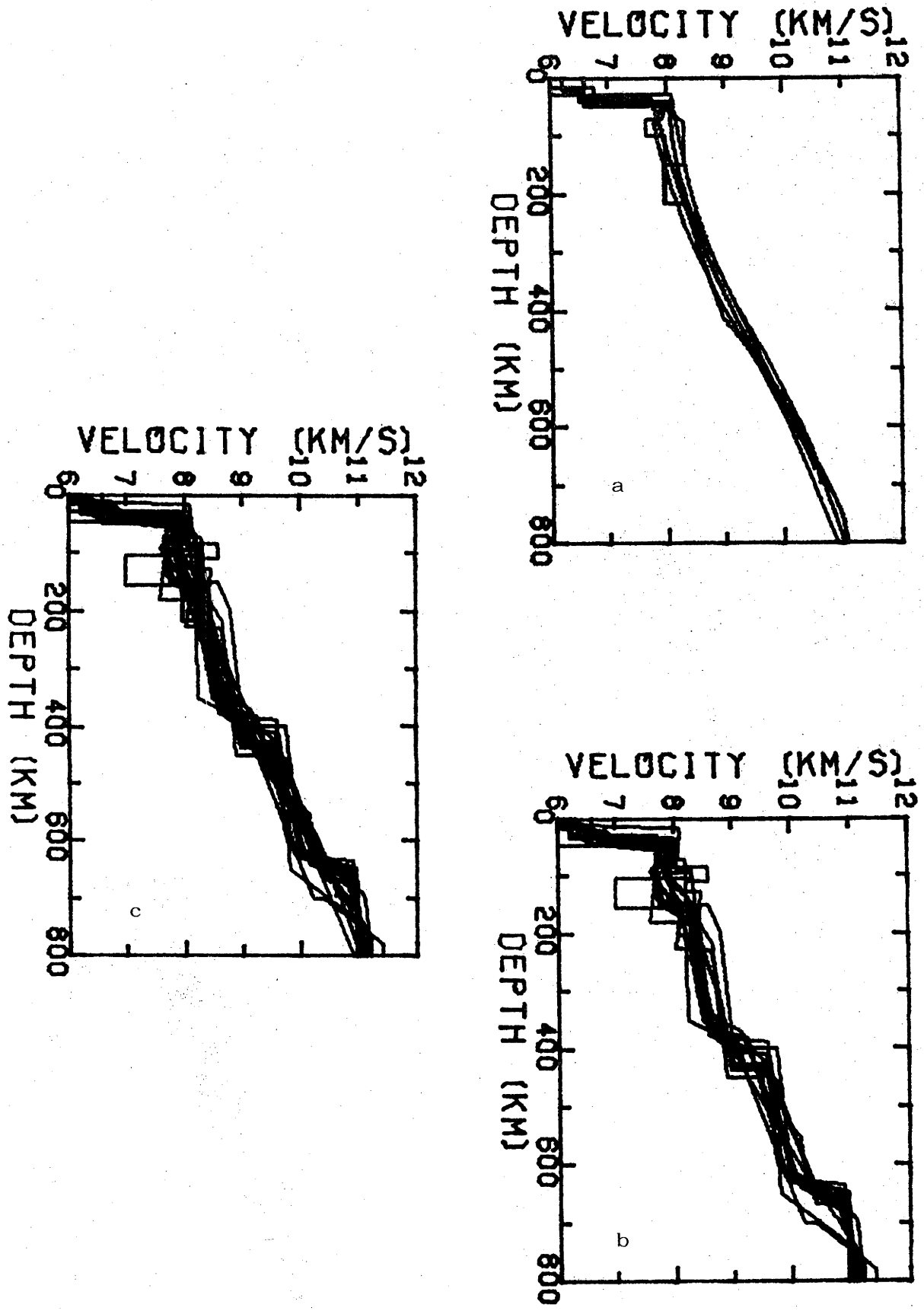

Figure 2-4. a) Classical and gross earth, b) recent and c) classical, gross earth and recent velocity models.

grouped together at the end of this chapter). The velocity is continuous throughout the mantle but has a discontinuity in slope near 410 km which causes the minor triplication at 20°. As Jeffreys (1966) has pointed out, this model resulted from the use of travel times from different regions - the times up to 10° coming mainly from Japan, European times extending the data to 25°. It was this "patchwork" that caused the break in slope at 20° (Jeffreys, 1966). "The 20° discontinuity in the travel time curve and the corresponding discontinuity at 413 km depth were derived from the Jeffreys-Bullen time curve, but when this was found to be in error at small epicentral distances there was no longer any support for the existence of the discontinuity. Nevertheless, it has continued to figure in the literature" (Lehmann, 1967, p. 50). Figure 2-6 shows a more recent model of Jeffreys and Shimshoni (1966), based on European travel time and amplitude data, which, while retaining the high amplitudes near 20°, does not show the abrupt change in slowness or the minor triplication given by the earlier model.

Gutenberg - The velocity model of Gutenberg (Figure 2-7) is characterized by a low velocity zone extending from just below the crust to a depth of 200 km, and an absence of any discontinuity in velocity or velocity gradient below this zone. The method used by Gutenberg (1959) was based on the observation of inflections in the travel time curves from earthquakes at various focal depths. Jeffreys (1966) expressed

severe reservations concerning the accuracy of this method. Gutenberg supported the presence of the low velocity layer with amplitude data from shallow focus earthquakes, which show a rapid decrease in amplitude up to 7^{o}, low amplitudes in a shadow zone from 7^{o} to 13^{o}, which he attributed to diffracted energy, and a sudden increase in amplitude at 14^{o} caused by the focussing of arrivals from below the low velocity zone.

Lehmann - Lehmann (1934) introduced the notations P_d and P_r to describe two travel time branches which she first observed to cross near 20^{o} in times from the Azores earthquake of 1931 (Lehmann, 1934). She related the P_r branch to a discontinuity in velocity at a depth near 250 km. Figure 2-8 shows a model determined from travel times to the northeast of the Gnome nuclear test site in the south-central United States (Lehmann, 1964). The P_r branch becomes a first arrival near 20^{o}, thus corresponding to the "20^{o} discontinuity". In a second model from the same paper (Figure 2-9), using times from the more tectonic region between the Gnome and Nevada test sites, the low velocity layer is at a shallower depth, causing the distance at which the P_r branch becomes a first arrival to move back to 14^{o}. These models explain the same general features as those in the Gutenberg model - low amplitudes on the P_d branch up to some distance beyond 14^{o}, where the phase P_r appears with higher amplitude and higher apparent velocity. This higher velocity branch can usually be observed as a second arrival at distances less than the

cross-over with the P_d branch. Lehmann finds no evidence for the high amplitudes required by the caustic at 14^o in the Gutenberg model and hence she attributes the higher velocity arrival as coming from an abrupt velocity increase at 220 km, which may (Figure 2-8) or may not (Figure 2-9) correspond to the bottom of the low velocity layer.

Herrin et al. - The revision of travel times in the "1968 Seismological Tables for P Phases" (Herrin et al., 1968) involved the determination of an average upper mantle structure (Figure 2-10). They state that the model for times up to 20^o "is not intended to represent the actual velocity structure beneath ... any ... part of the Earth. This arbitrary model has a much simpler structure than is expected to exist anywhere in the upper mantle. ... An over-simplified model of the upper mantle is postulated as a basis for travel time estimation in the hope that regional differences with respect to this model can be determined through future studies." (Herrin et al., 1968, p. 1274)

2.4.2 Recent Models

By the mid 1960's, a number of travel time studies (e.g. Carder, 1964; Doyle and Webb, 1963. For summary see Johnson, 1967, Table 4) and a $dT/d\Delta$ study by Niazi and Anderson (1965) had indicated abrupt changes in the slope of the P wave travel time curve near 18^o and 24^o. At the same time, surface wave dispersion studies (Anderson and Toksoz, 1963) showed rapid increases in shear wave velocity at 350 and 650 km. The interpretation

of the body wave data was strongly influenced by the surface wave results, and most of the upper mantle P wave models published since 1965 have tended to follow the general character of the CIT11A model (Figure 2-3) (Anderson, 1967) which was based on the Anderson and Toksoz (1963) shear wave model CIT11.

Lukk and Nersesov - Using data from intermediate depth earthquakes in the Hindu Kush region, recorded along a line to the northeast across central Asia, Lukk and Nersesov (1965) derived the velocity model shown in Figure 2-11. The main features of their model are a low velocity layer from 110 km to 150 km, a change in velocity gradient at 400 km, and a layer of high velocity gradient from 700 km to 780 km.

Tonto Forest array models - Niazi and Anderson (1965) made measurements of $dT/d\Delta$ for first arrivals in the distance range 12° to 30° using the Tonto Forest array in Arizona. Model CIT11CS3 (Figure 2-12) is a smoothed version of the CIT11 model and was considered by Niazi and Anderson to agree with their data, although they stressed that the absence of later arrival data did not allow them to distinguish between various models with differing structure near the discontinuities at 350 and 650 km.

In a later study using an extended version of the Tonto Forest array, Johnson (1967) included dT/d measurements for later arrivals. The CIT208 model in Figure 2-13 shows high velocity gradients near 400 and 650 km, producing triplications at 18° and 24°.

Kanamori - Using the Japanese Wakayama microearthquake observatory and its substations as an array of approximately 1^{o} aperture, Kanamori (1967) determined the apparent velocity ($d\Delta/dT$) for first arrivals from earthquakes along the western margin of the Pacific Ocean. In his preliminary model (Figure 2-14) the velocity increase at 375 km causes a triplication near 18^{o} similar to that in Johnson's model. Because of the paucity of Kanamori's data near 25^{o} he was not able to identify an abrupt change of slope in this range and therefore his model shows a rapid, but continuous, velocity increase near 650 km which does not produce the major triplication seen near 24^{o} in Johnson's model.

Early Rise models - Explosions fired in Lake Superior during Project Early Rise in 1966 provided travel time data along a series of profiles covering a large part of the North American continent (Iyer et al., 1969). Two of the longest profiles have been studied in detail by Lewis and Meyer (1968) and Green and Hales (1968). Figure 2-15 shows the model of Lewis and Meyer as determined from times to the west of Lake Superior. The 450 km discontinuity in this model is based on a change in slope at 2400 km and a later arrival branch which extends back to 1600 km.

Green and Hales supplemented data from a profile to the south of Lake Superior with observations of the Gnome explosion in New Mexico to produce the model in Figure 2-16. In the same paper they use data from

Nevada Test Site explosions to derive the model in Figure 2-17. The rapid increases in velocity near 370 and 640 km in these models were introduced on the basis of breaks in the slope of the travel time data at 2150 and 2500 km. "The authors regret that they have not been able to confirm the structure deduced from first arrivals on the basis of later arrivals, as indeed they have not." (Lehmann, 1970, p. 371). Later arrivals are observable in their record sections but they do not appear to follow a definite trend.

CIT100 series - Archambeau et al. (1969) made a detailed study of travel times and amplitudes of first and later arrivals along four profiles to the northeast and southeast of two explosion sites in Nevada. The four profiles sample distinct upper mantle provinces at short distances, and differences in the structure of the uppermost mantle are reflected in the four velocity models. Beyond 1500 km the profiles all extend into the Central Plains area, and the structure below 300 km depth is essentially the same for all models. The models are shown in Figure 2-18 (CIT109, eastern Basin and Range - northern Rocky Mountains), Figure 2-19 (CIT110, Colorado Plateau - Rocky Mountains), Figure 2-20 (CIT111, Basin and Range) and Figure 2-21 (CIT112, Snake River Plains - northern Rocky Mountains). CIT111 is classified as tectonic, the others as intermediate-tectonic.

HW series - Helmberger and Wiggins (1971) and Wiggins and Helmberger (1972) have also used data from western United States explosions and earthquakes. In

the technique which they use, velocity models are first derived using observed travel time and amplitudes. Synthetic seismograms are produced for these models using the Cagniard-de Hoop technique, and the models are modified until the synthetic seismograms explain the feature observed in the real data. Their first model HWNE (Figure 2-22) has discontinuities at 430 and 650 km and a decrease in velocity gradient at 520 km. In two later models HWA (Figure 2-23) and HWB (Figure 2-24) the extent of the discontinuity at 650 km has been decreased. The HWNE and HWB models are from data to the area northeast of Nevada, the model HWA is from data to the southeast.

2.5 Discussion

The models in Figures 2-5 to 2-24 show the increasing resolution of the complex nature of the P wave travel time curve which has resulted from detailed regional studies of travel times, slownesses and amplitudes. As the main features of travel time curve become better known, emphasis has shifted from the well established arrivals to various unidentified phases. Such an approach has been profitable, for example, in the identification of precursors to the core phase P'P' as reflections from upper mantle discontinuities (Adams, 1968; Whitcomb and Anderson, 1970); in the suggestion that precursors to the phase PKP result from scattering near the core mantle boundary (Cleary and Haddon, 1972); and in the identification of the multiply reflected core phases PmKP (Buchbinder, 1972; Bolt and Qamar, 1972). However, care must

be taken to ensure that a complex interpretation is not given to signals which might more readily be explained in terms of known structure.

As the basis of an argument which relates the complexity of P signals from underground explosions to zones of anomalous Q in the upper mantle, Douglas et al. (1971) compare the signals from an explosion recorded at the GBA array in India ($\Delta = 27.4^{\circ}$) with that recorded at the EKA array in Scotland (Δ approximately 45°). While the EKA record is a simple arrival characteristic of explosions, the GBA record shows a first arrival (P) with slowness of 9.2 s/deg, followed approximately 4 s later by a larger amplitude arrival (P_{H1}) with slowness of 10.3 s/deg. Presumably on the basis of the Herrin model (Figure 2-10), Douglas et al. assume that the 10.3 s/deg arrival originates from an apparent source at 22° and they suggest that "one possible ray path for P_{H1} which agrees with the travel time and phase velocity measurements would be a reflection path of the P_dP type from a discontinuity at a depth of about 500 km". However, Figure 2-13 (for example) shows that the triplication of the travel time curve resulting from a discontinuity near 650 km produces at 27.4°, in the Johnson model, a first arrival with slowness of 9 s/deg followed 5 s later by two closely spaced, larger amplitude arrivals with slowness of approximately 10 s/deg. Thus, it would appear that the P_{H1} arrival is more simply explained as a phase refracted from a depth near 650 km.

It is hoped that this unified presentation of the parameters derived from standard velocity models will prove useful as a comparison with observed data and as a basis for interpretation of this complex portion of the travel time curve.

Addenda

After this chapter was completed, two models became available which are included in this discussion as Figures 2-25 and 2-26.

Jordan model B1 - Jordan (1973) has presented a gross Earth model of velocities and density within a spherically symmetrical Earth based on an inversion of free oscillations and differential travel times. The upper mantle P wave structure from his model B1 is shown in Figure 2-25.

Massé et al. model SDL-UT-BR1 - Using travel times to western United States stations from Nevada Test Site explosions, Massé et al. (1972) derived the velocity model shown in Figure 2-26. A double discontinuity near 400 km (315 km and 422 km), similar to that suggested by Simpson et al. (1971), produces an extra triplication in the travel time curve near 18°.

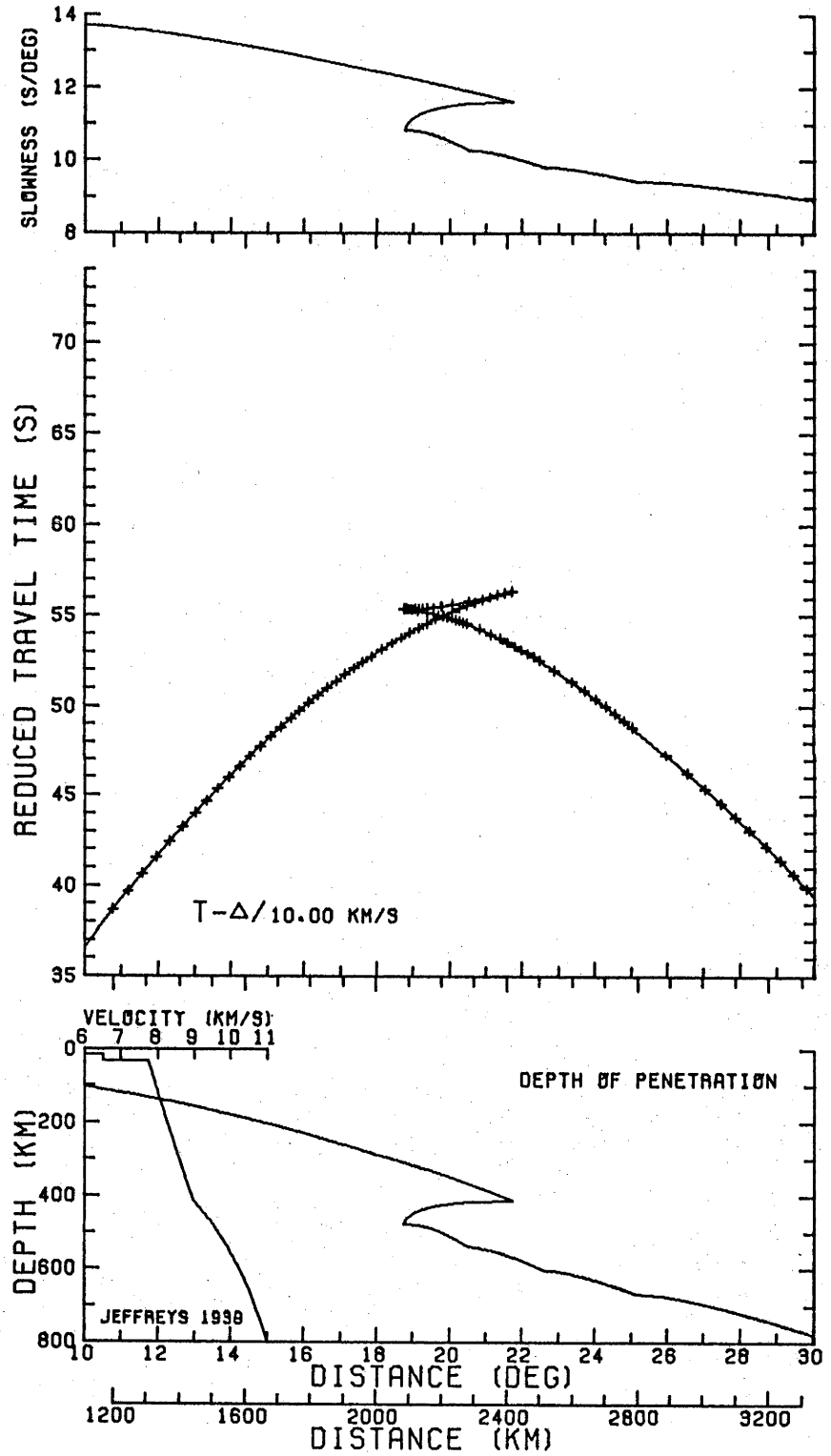

Figure 2-5. The Jeffreys (1939) model.

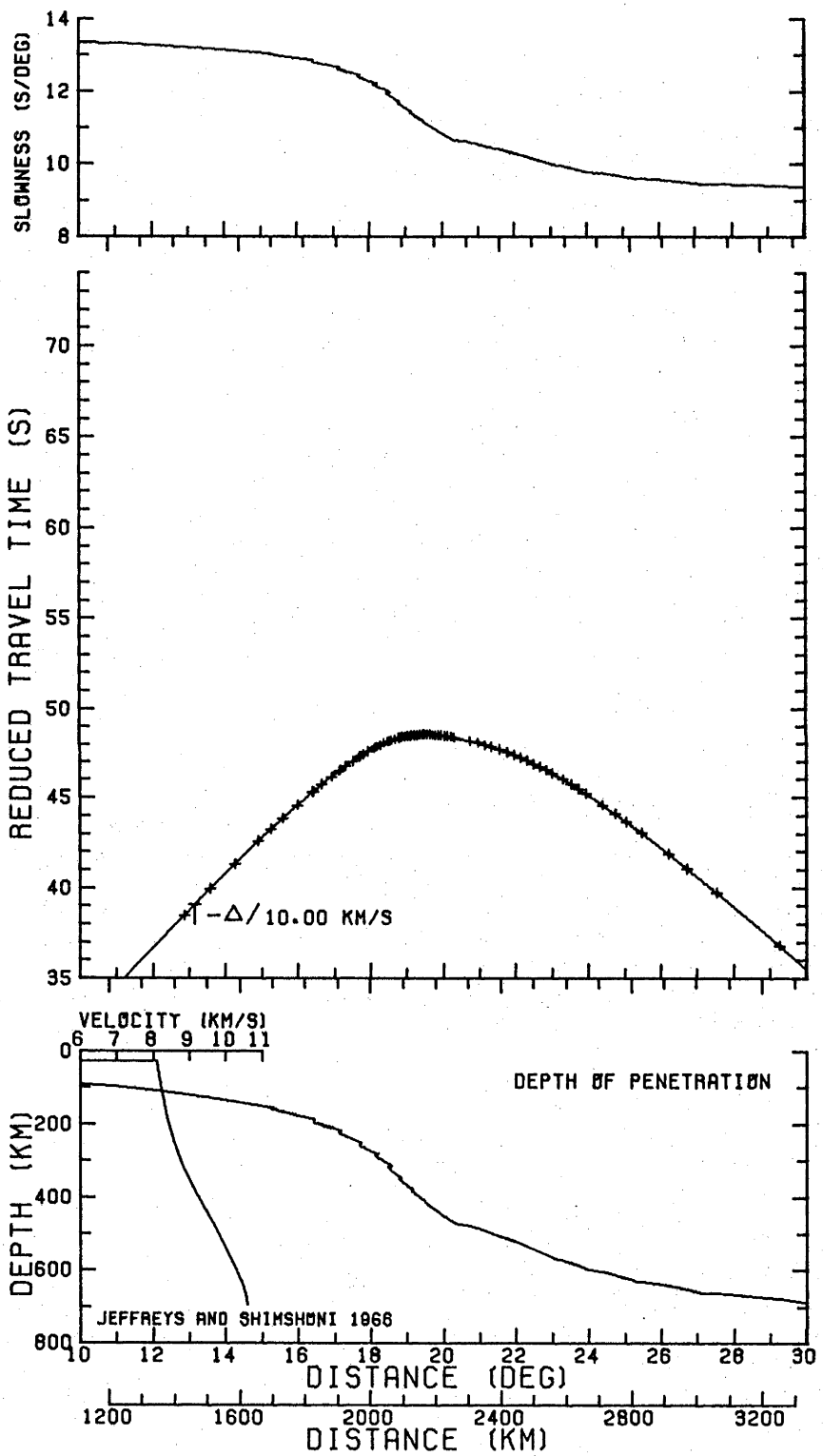

Figure 2-6. The Jeffreys and Shimshoni (1966) model.

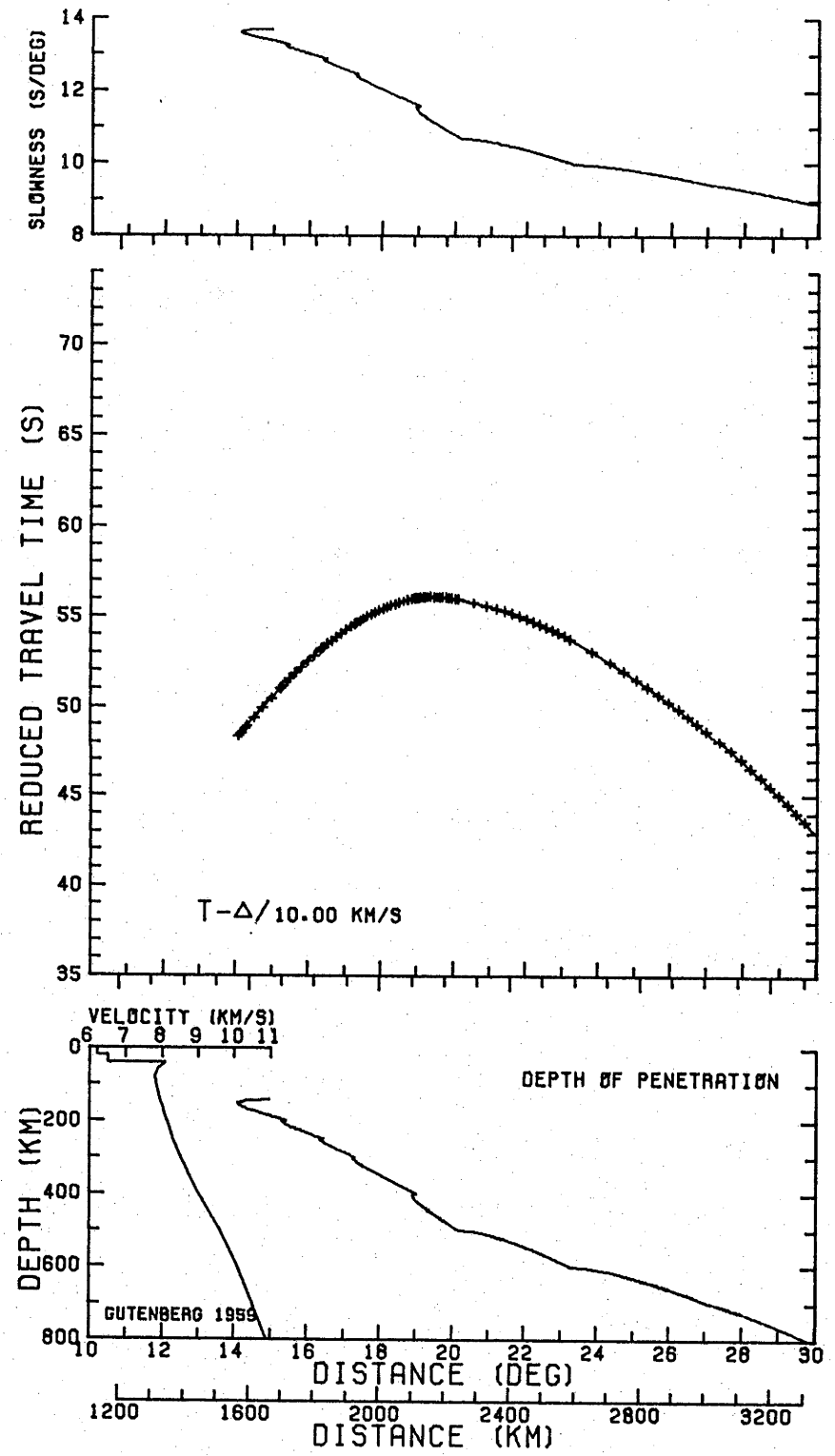

Figure 2-7. The Gutenberg model. Velocities above 400 km from Gutenberg (1959), below 400 km from Bullard (1957).

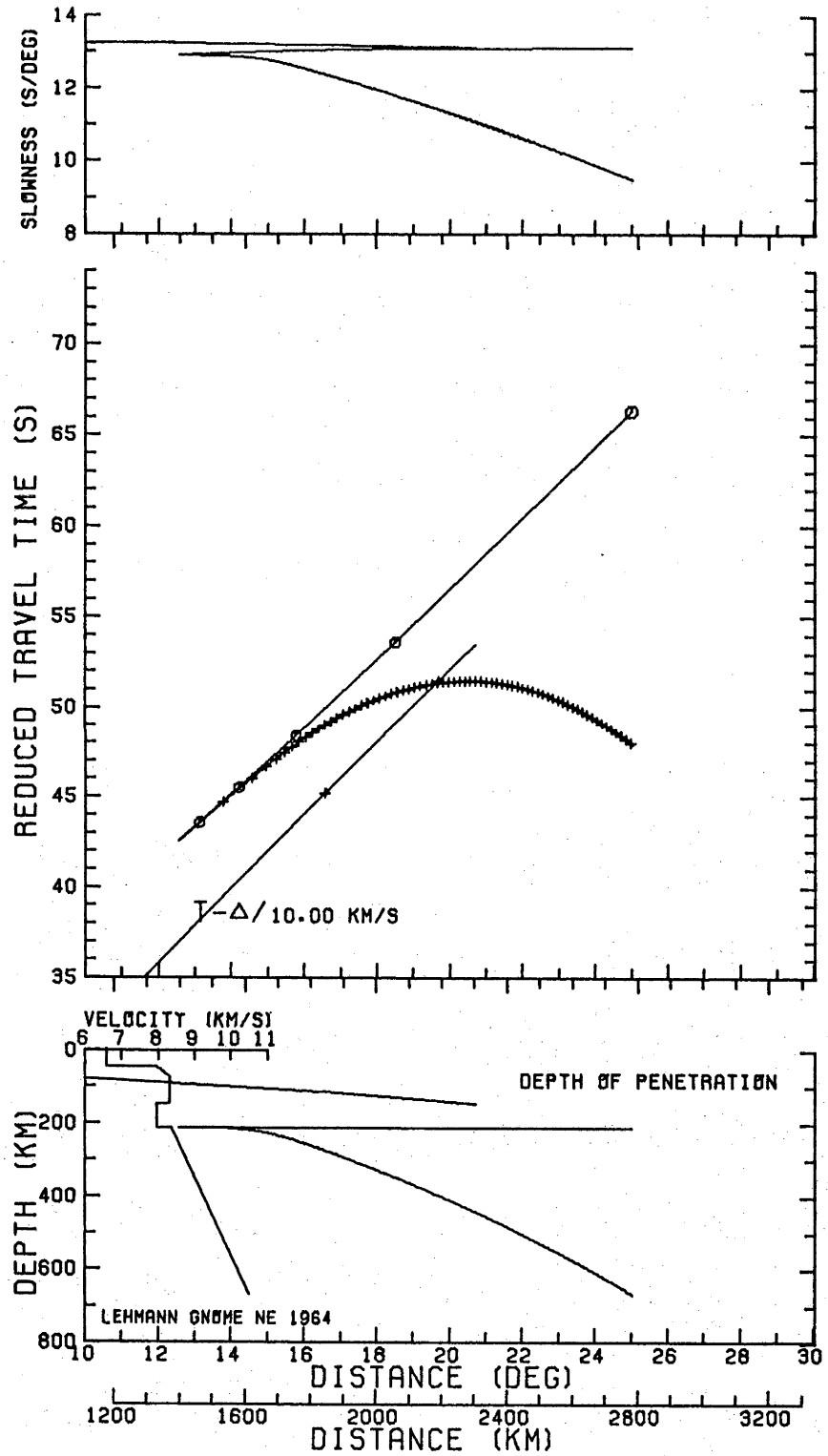

Figure 2-8. The Gnome northeast model of Lehmann (1964).

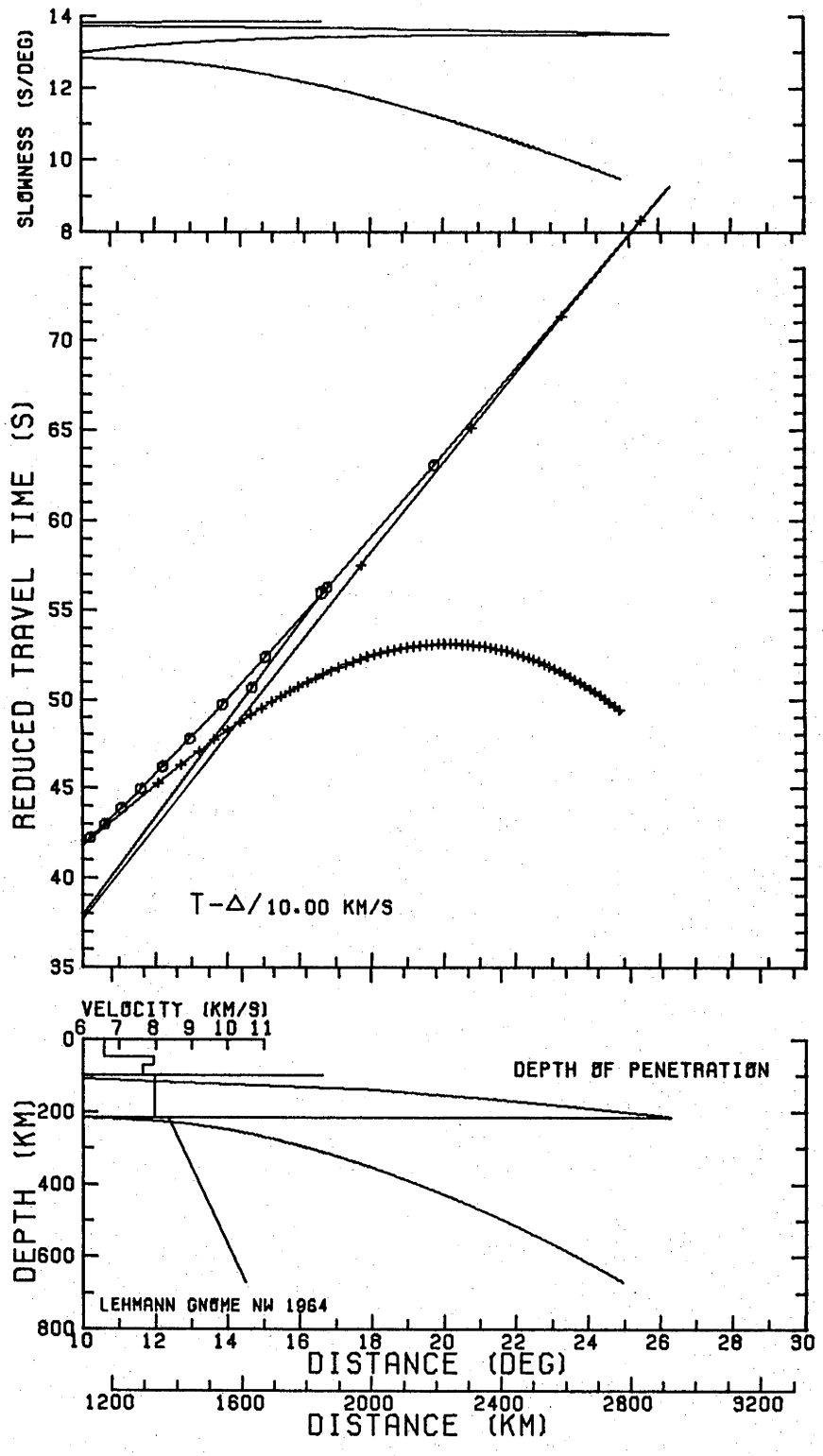

Figure 2-9. The Gnome northwest model of Lehmann (1964).

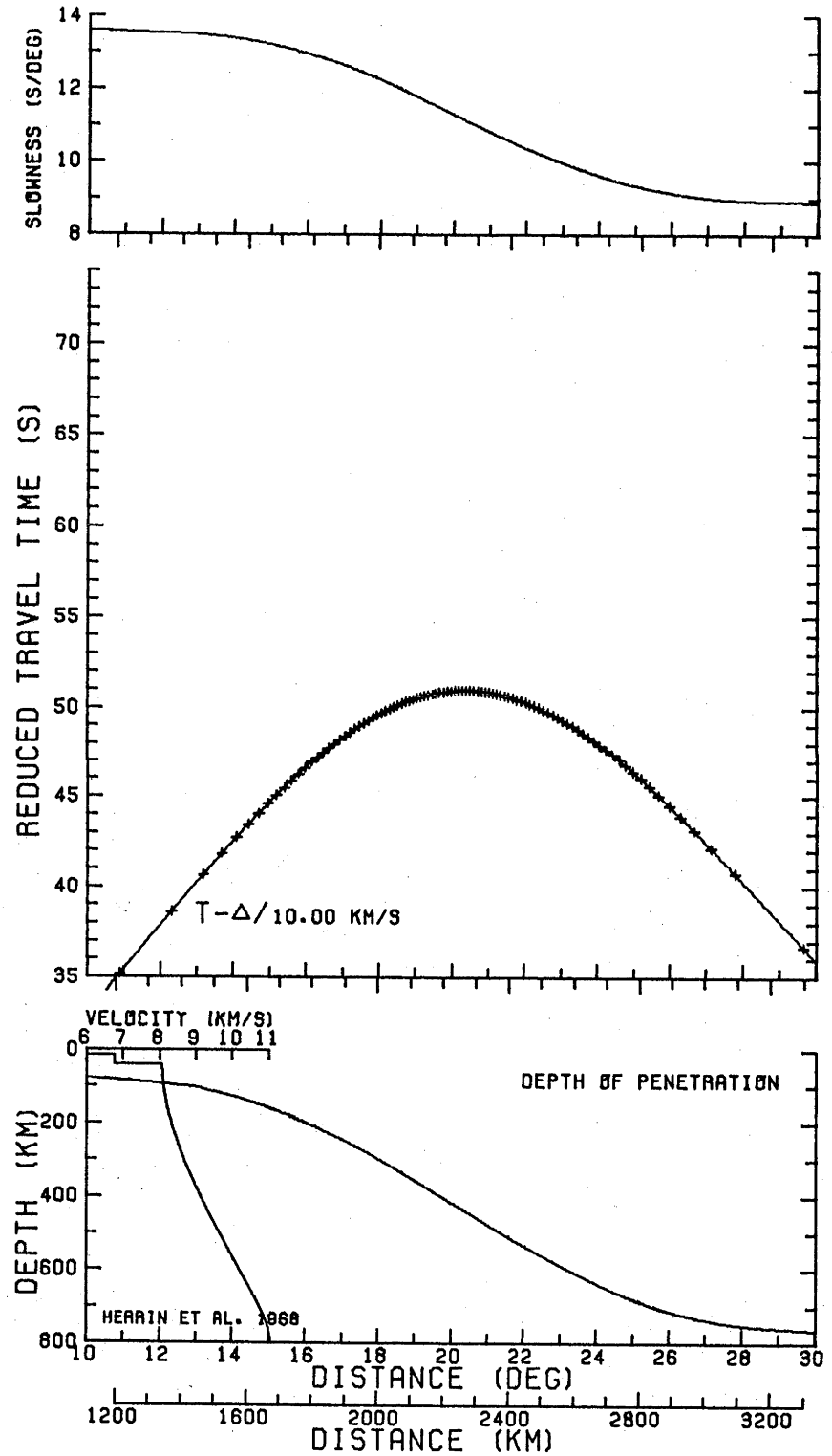

Figure 2-10. The Herrin et al. (1968) model from the "1968 Seismological Tables for P Phases".

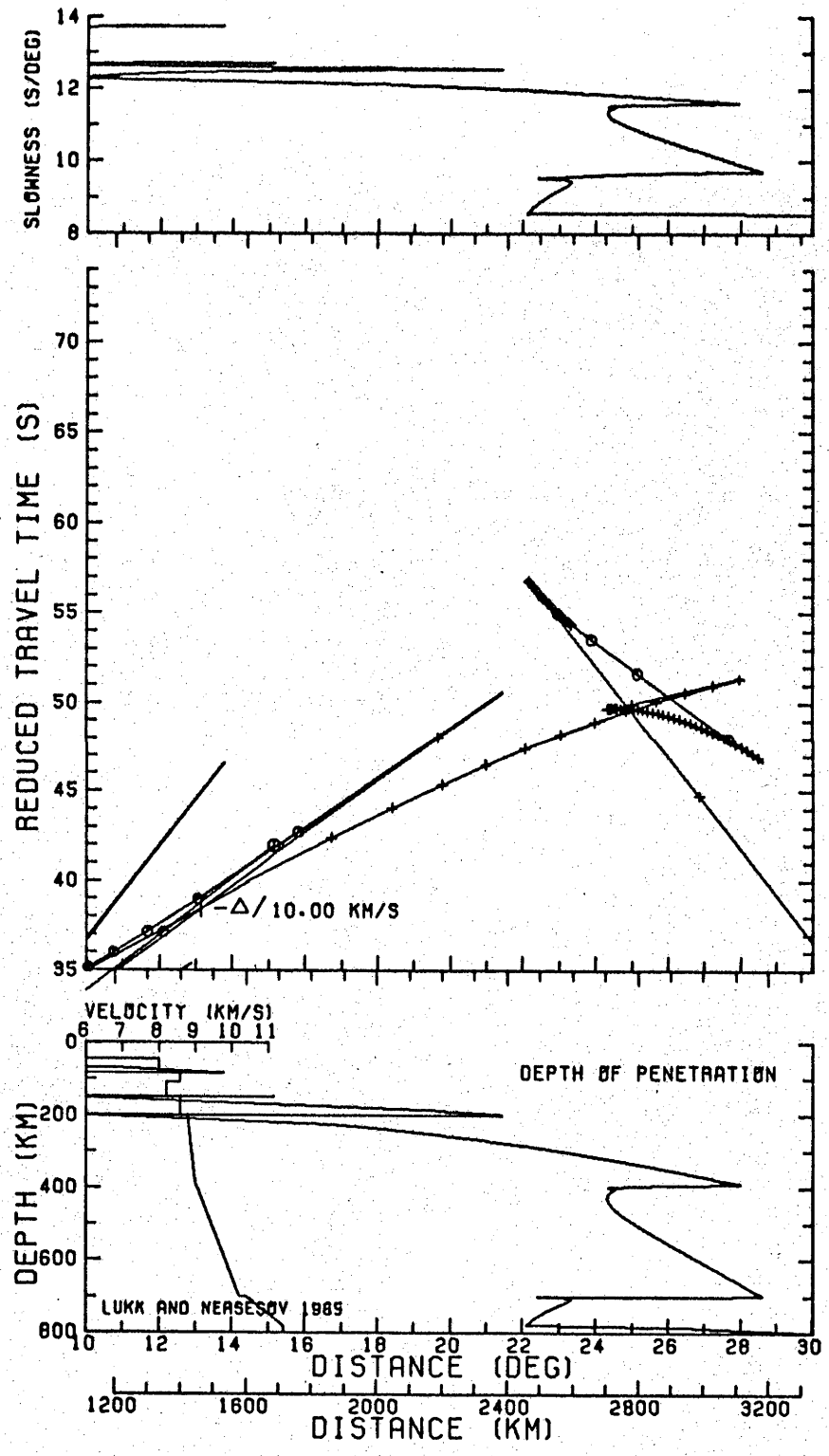

Figure 2-11. The Lukk and Nersesov (1965) model.

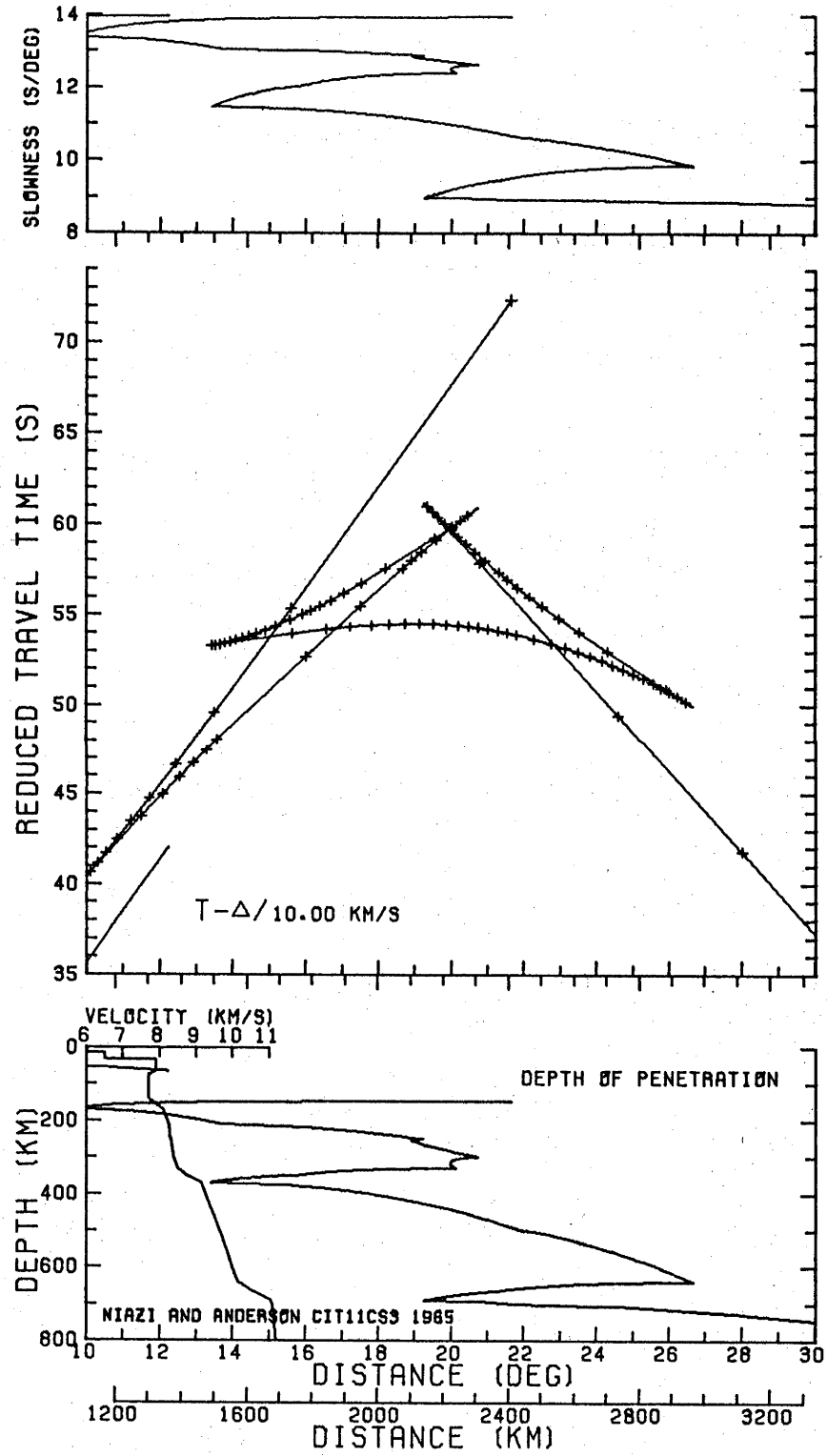

Figure 2-12. The CIT11CS3 model of Niazi and Anderson, 1965, tabulated in Kanamori (1967).

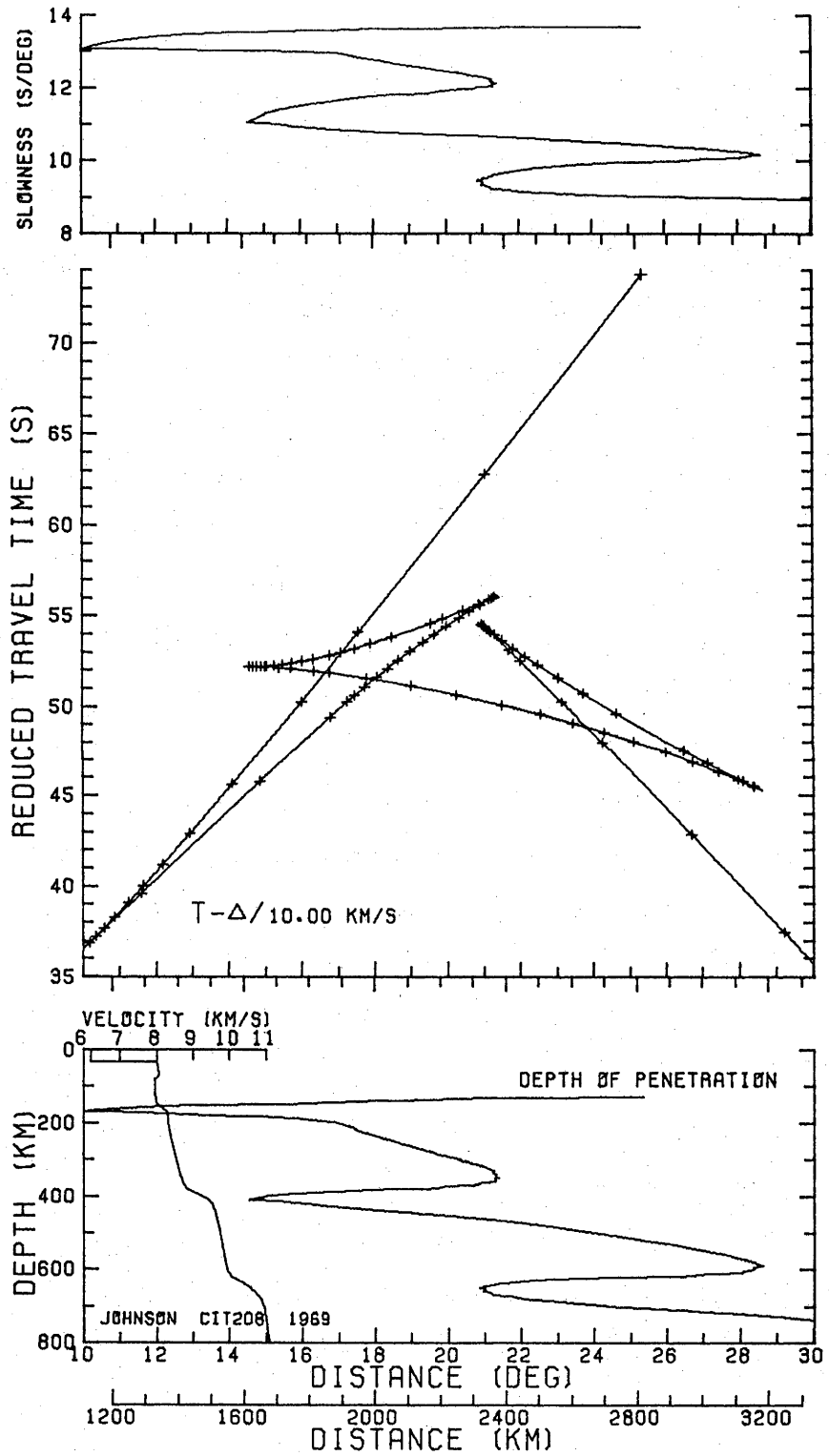

Figure 2-13. The CIT208 model of Johnson (1967), tabulated by Johnson (1969).

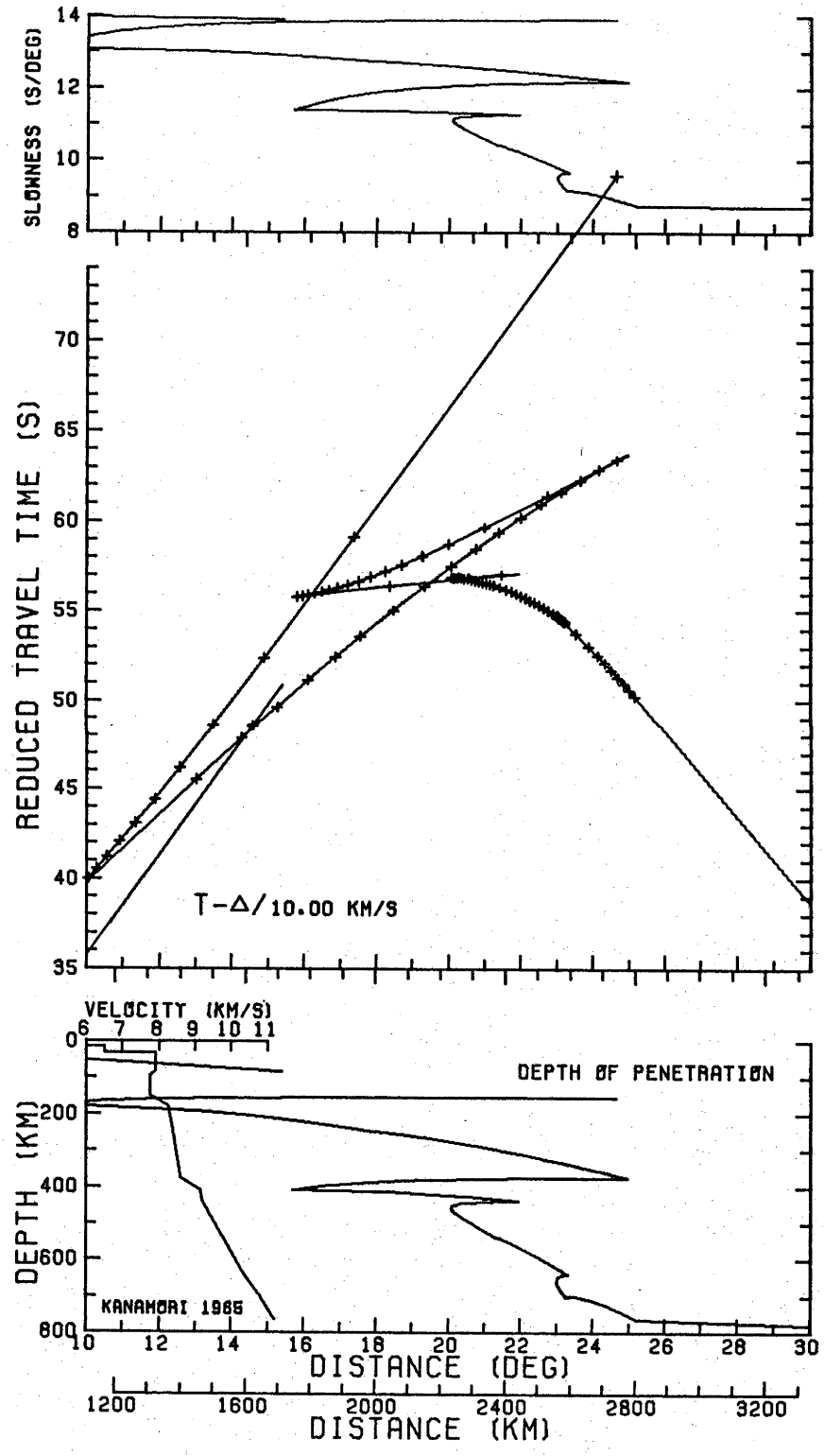

Figure 2-14. The Kanamori (1967) model.

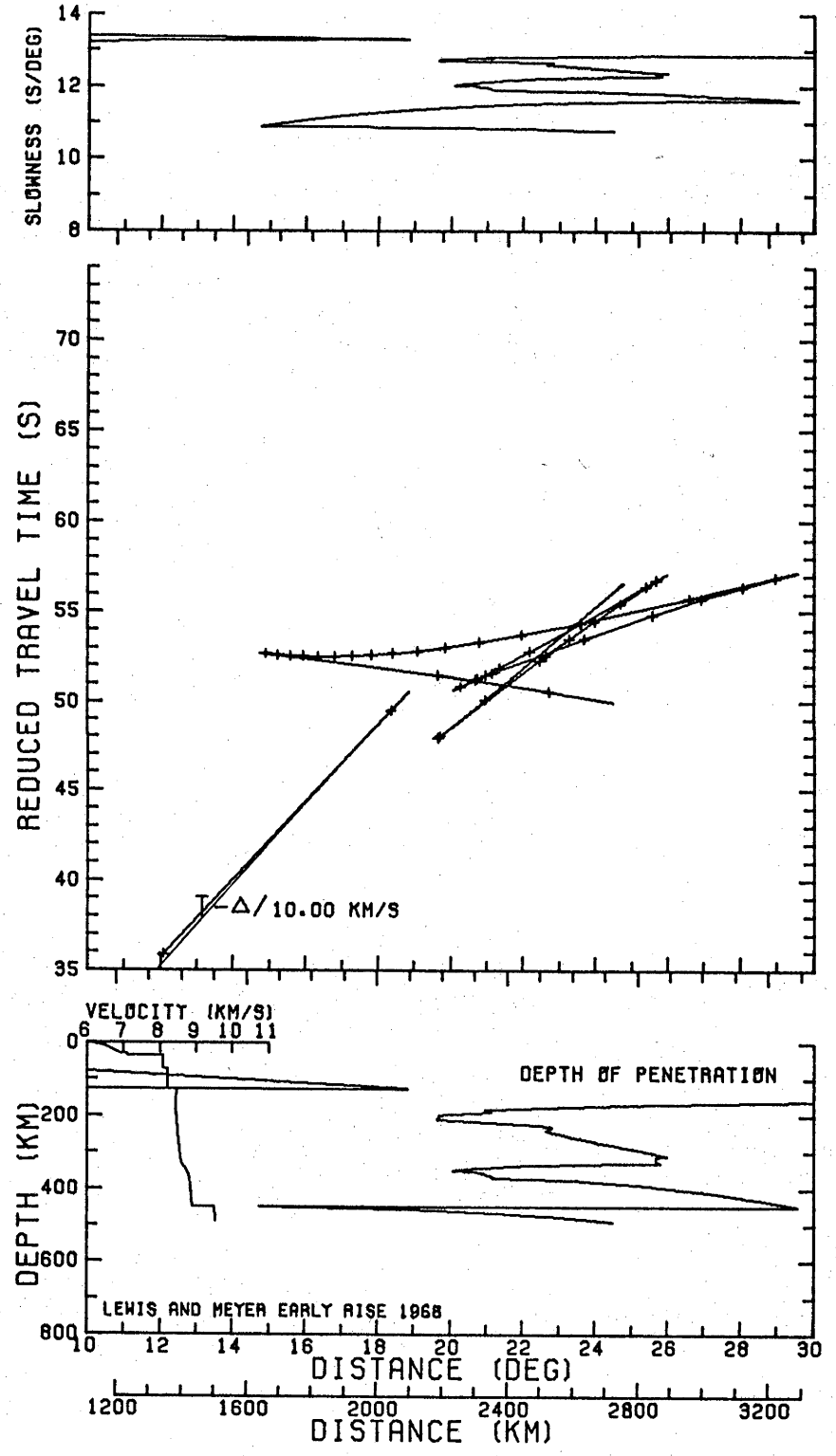

Figure 2-15. The Lewis and Meyer (1968) model.

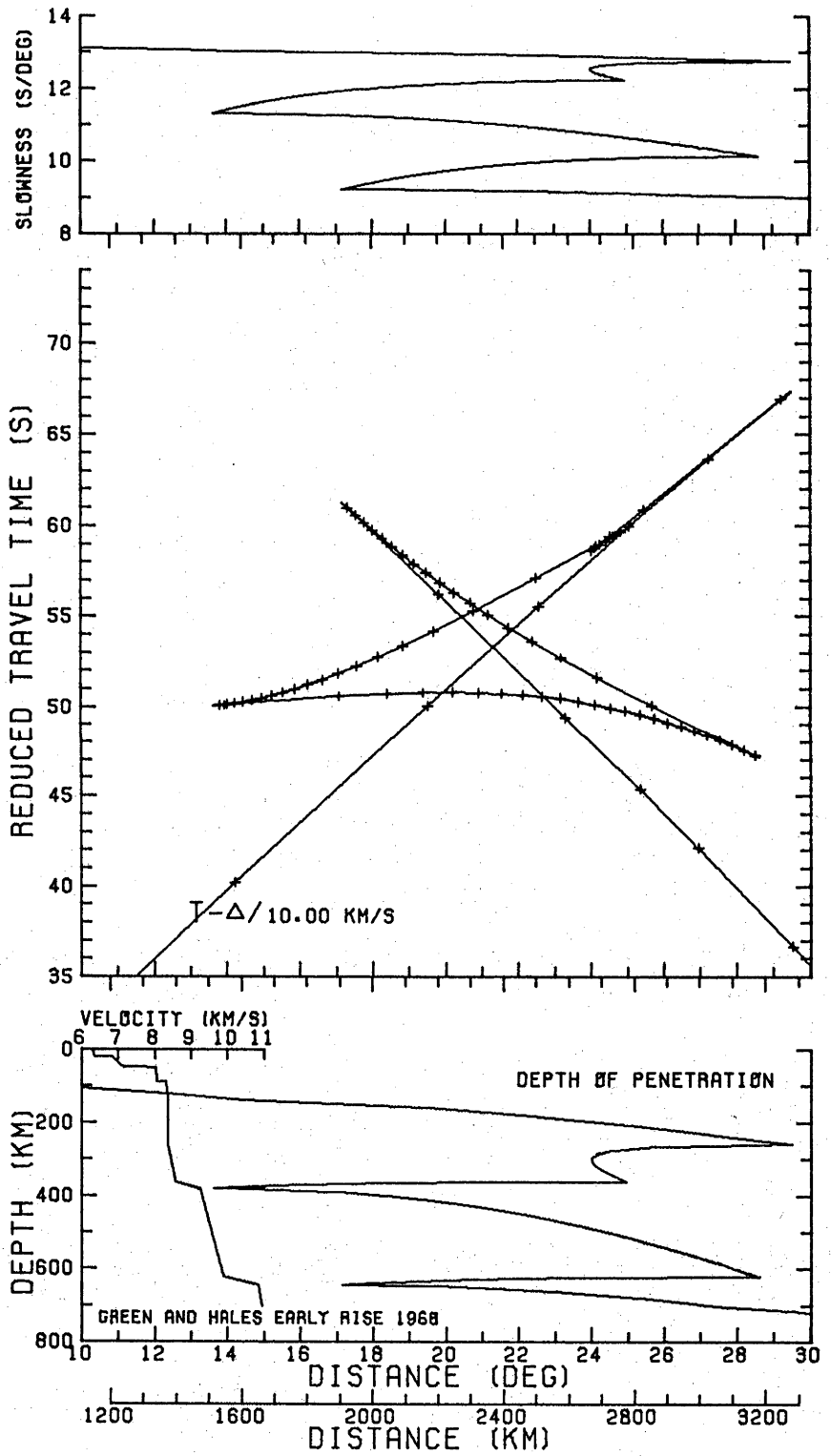

Figure 2-16. The Green and Hales (1968) Early Rise model.

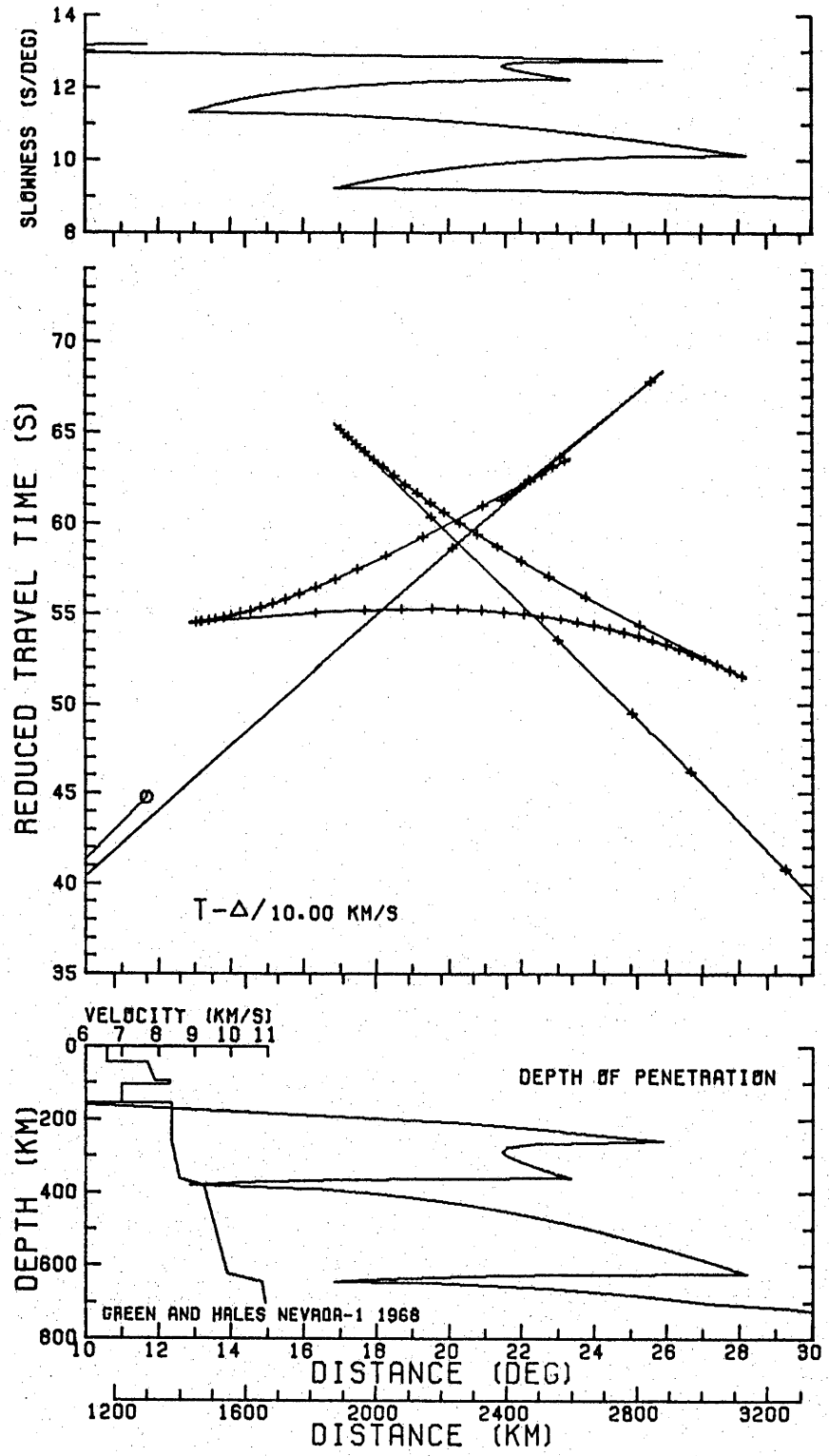

Figure 2-17. The Green and Hales (1968) Nevada model.

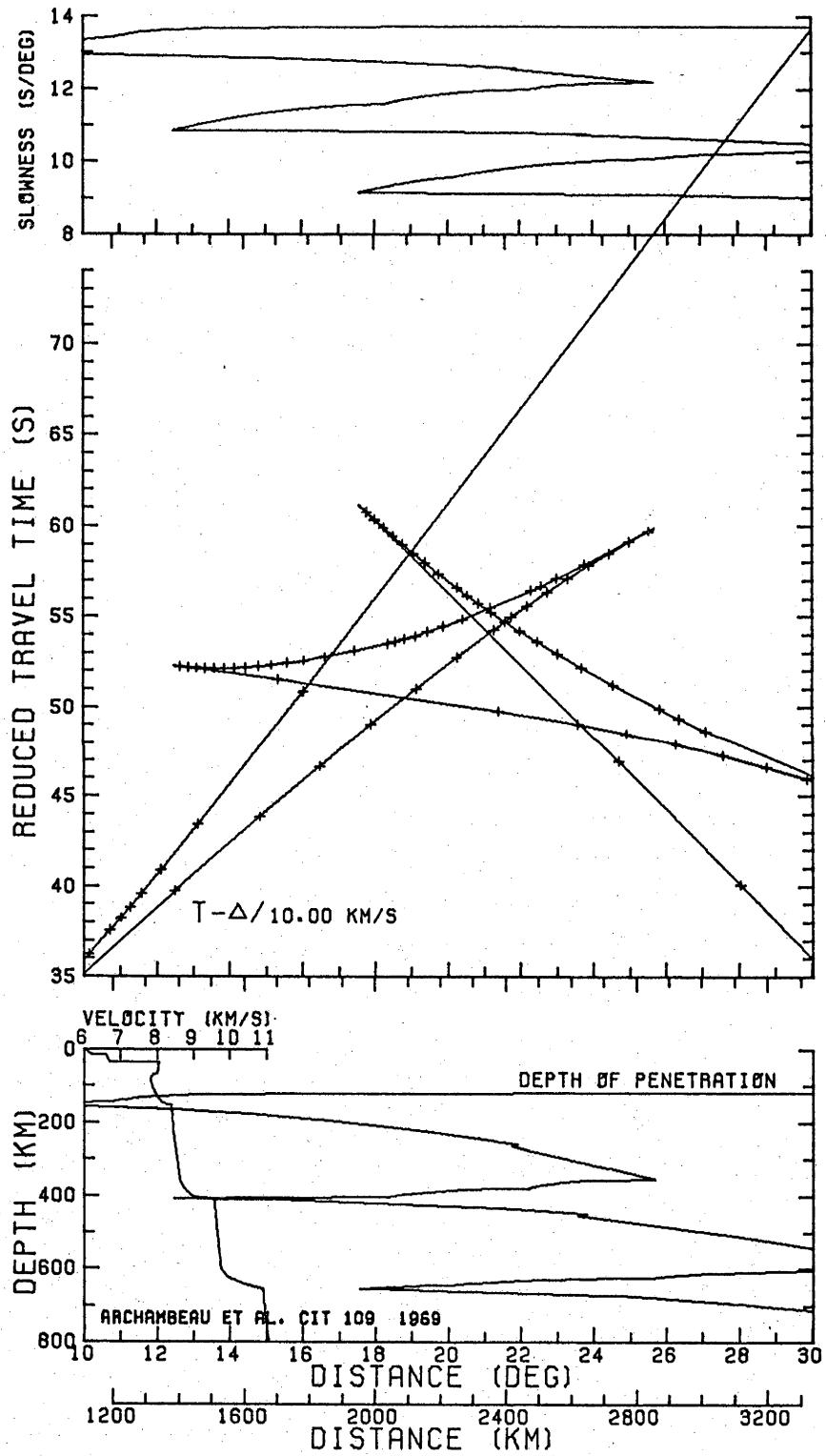

Figure 2-18. The Archambeau et al. (1969) CIT109 model (eastern Basin and Range - northern Rocky Mountains).

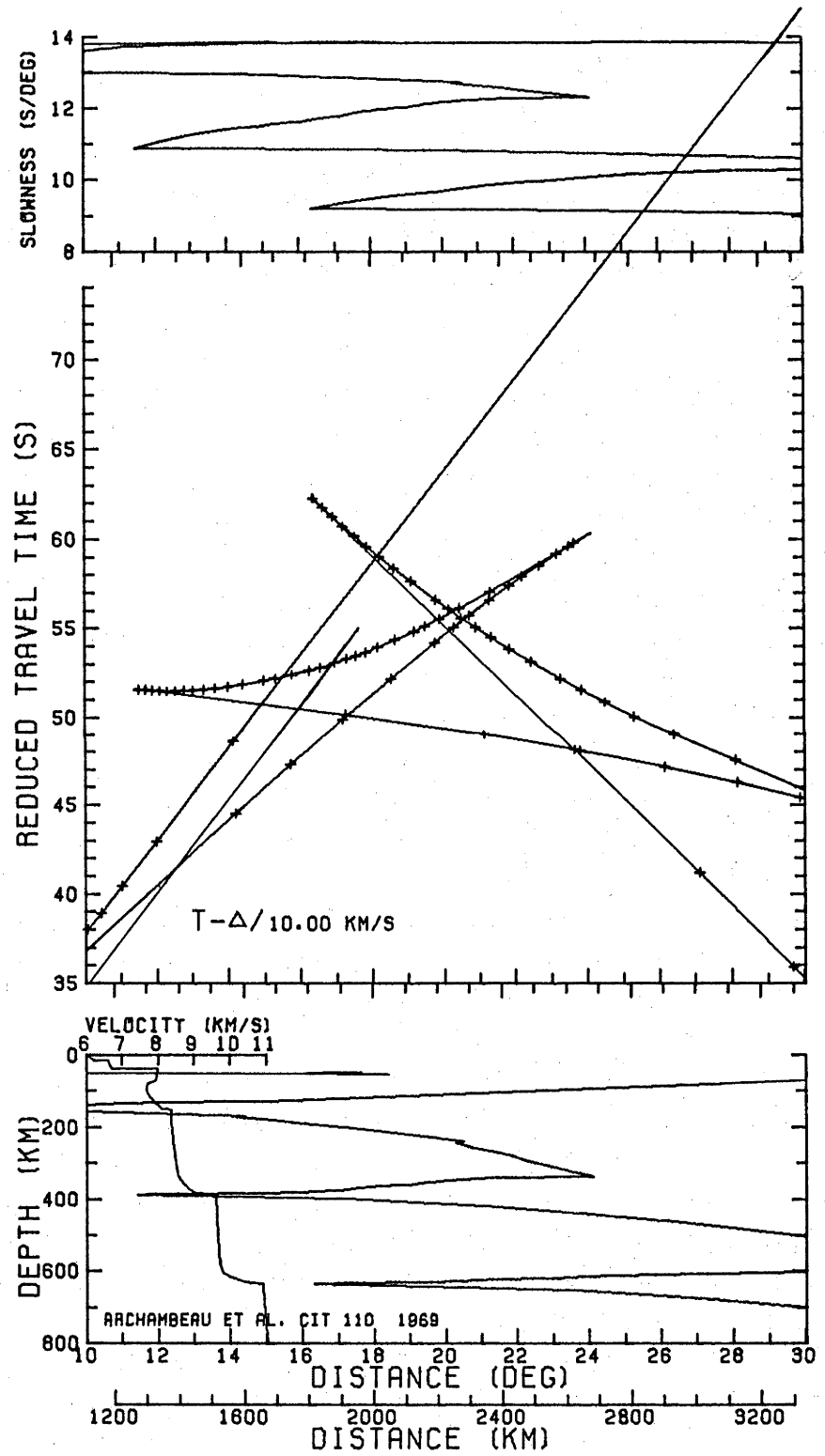

Figure 2-19. The Archambeau et al. (1969) CIT110 model (Colorado Plateau - Rocky Mountains).

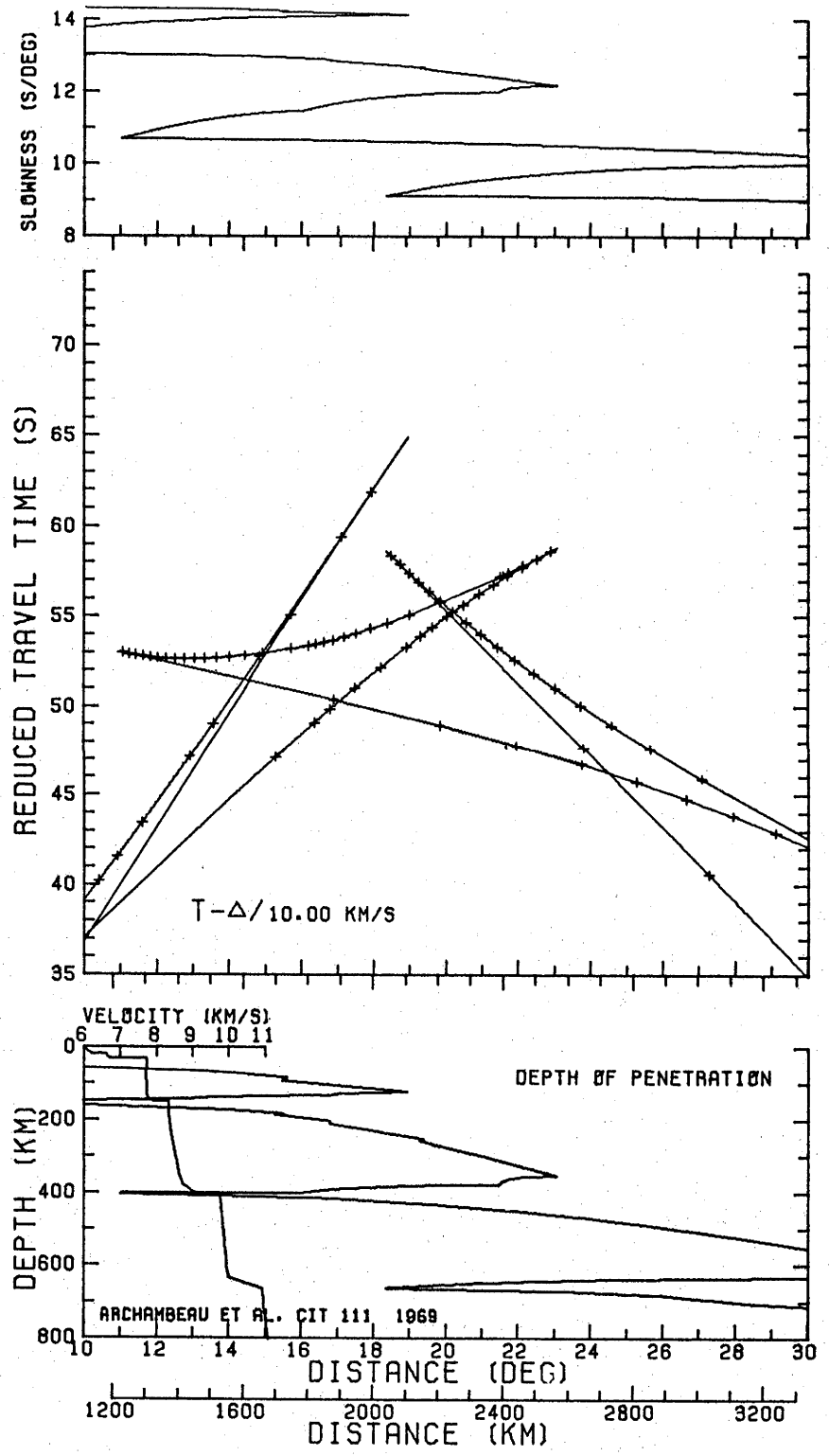

Figure 2-20. The Archambeau et al. (1969) CIT111 model (Basin and Range).

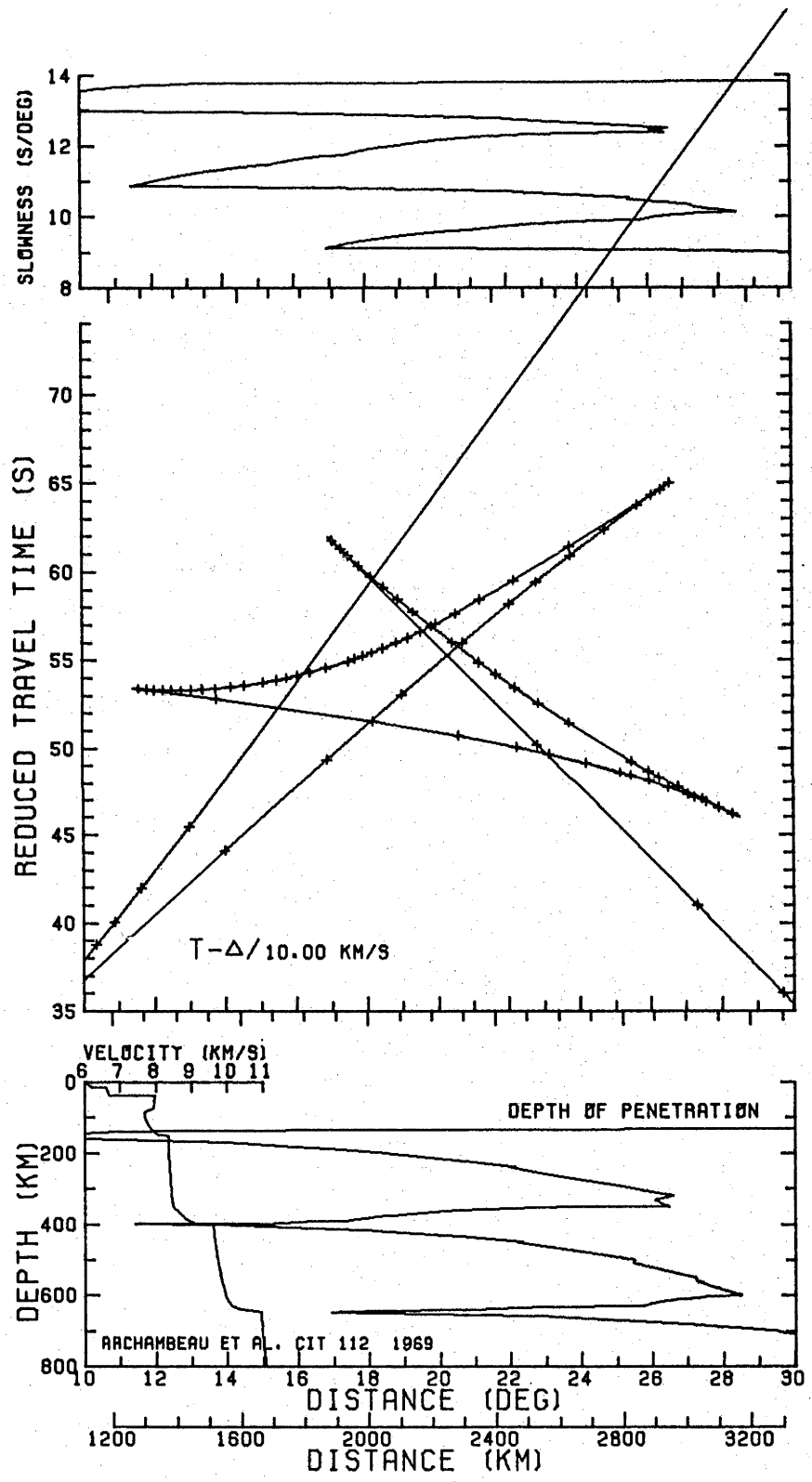

Figure 2-21. The Archambeau et al. (1969) CIT112 model (Snake River Plains - northern Rocky Mountains).

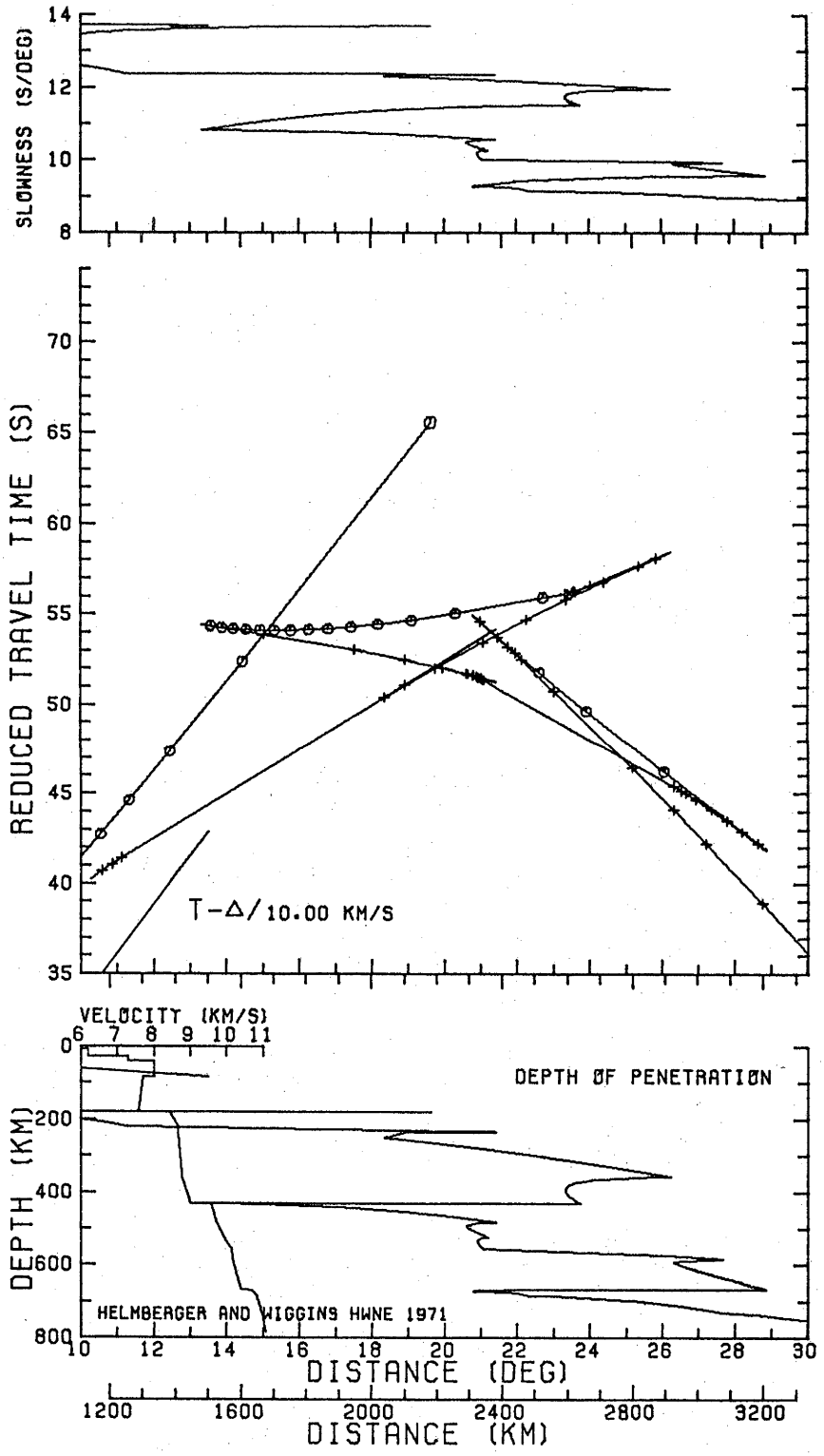

Figure 2-22. The Hemberger and Wiggins (1971) model HWNE.

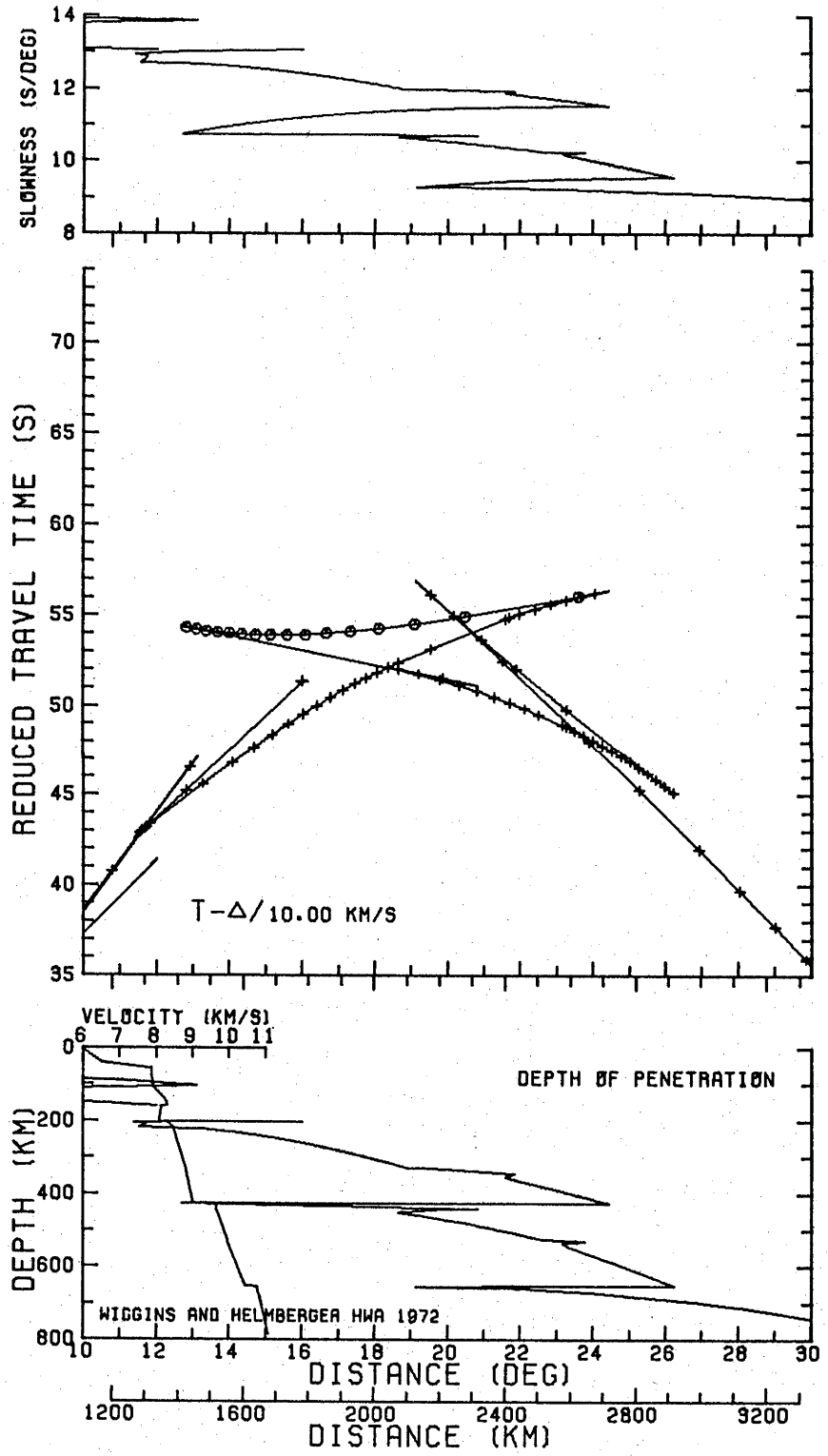

Figure 2-23. The Wiggins and Helmberger (1972) model HWA.

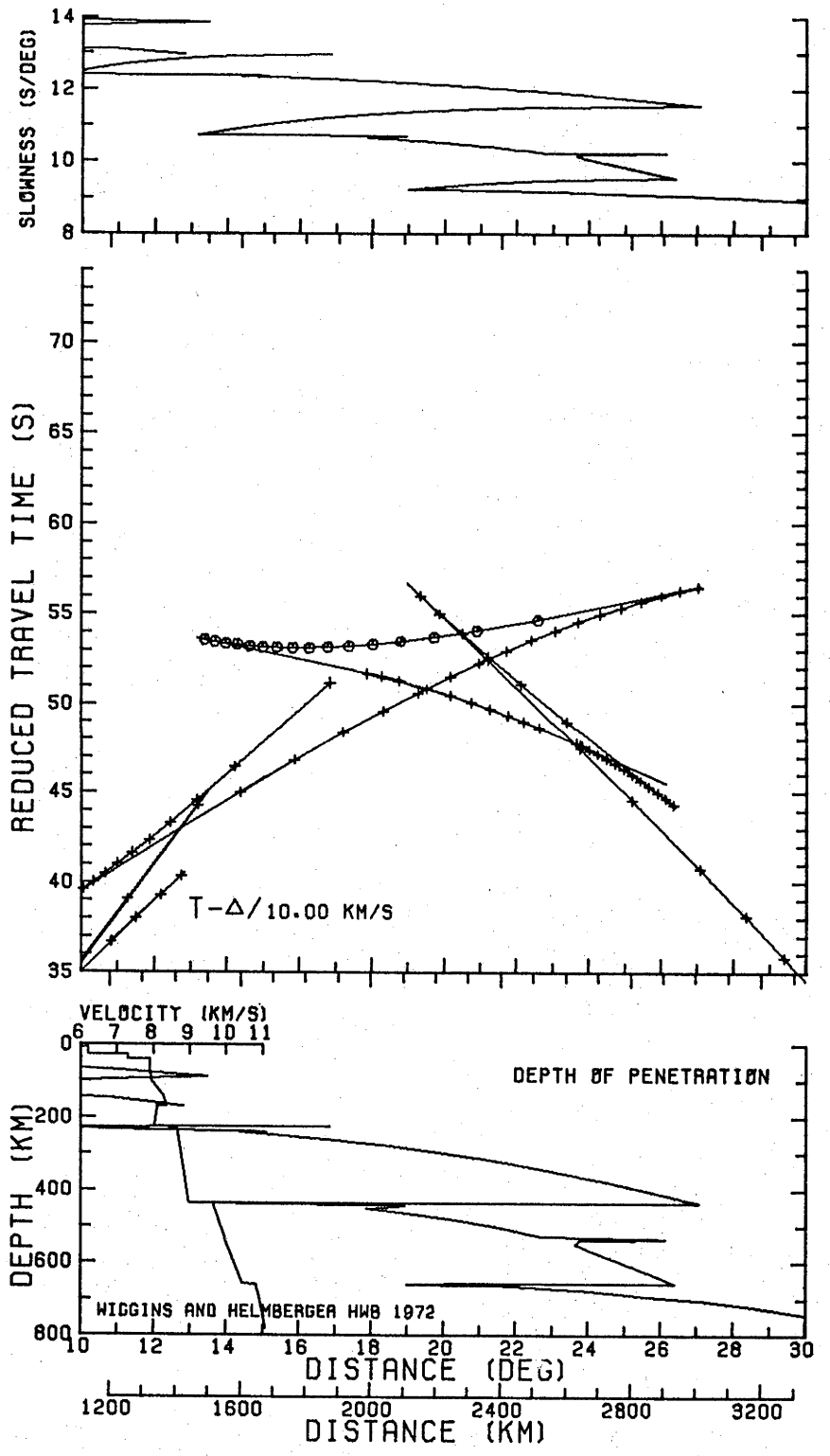

Figure 2-24. The Wiggins and Helmberger (1972) model HWB.

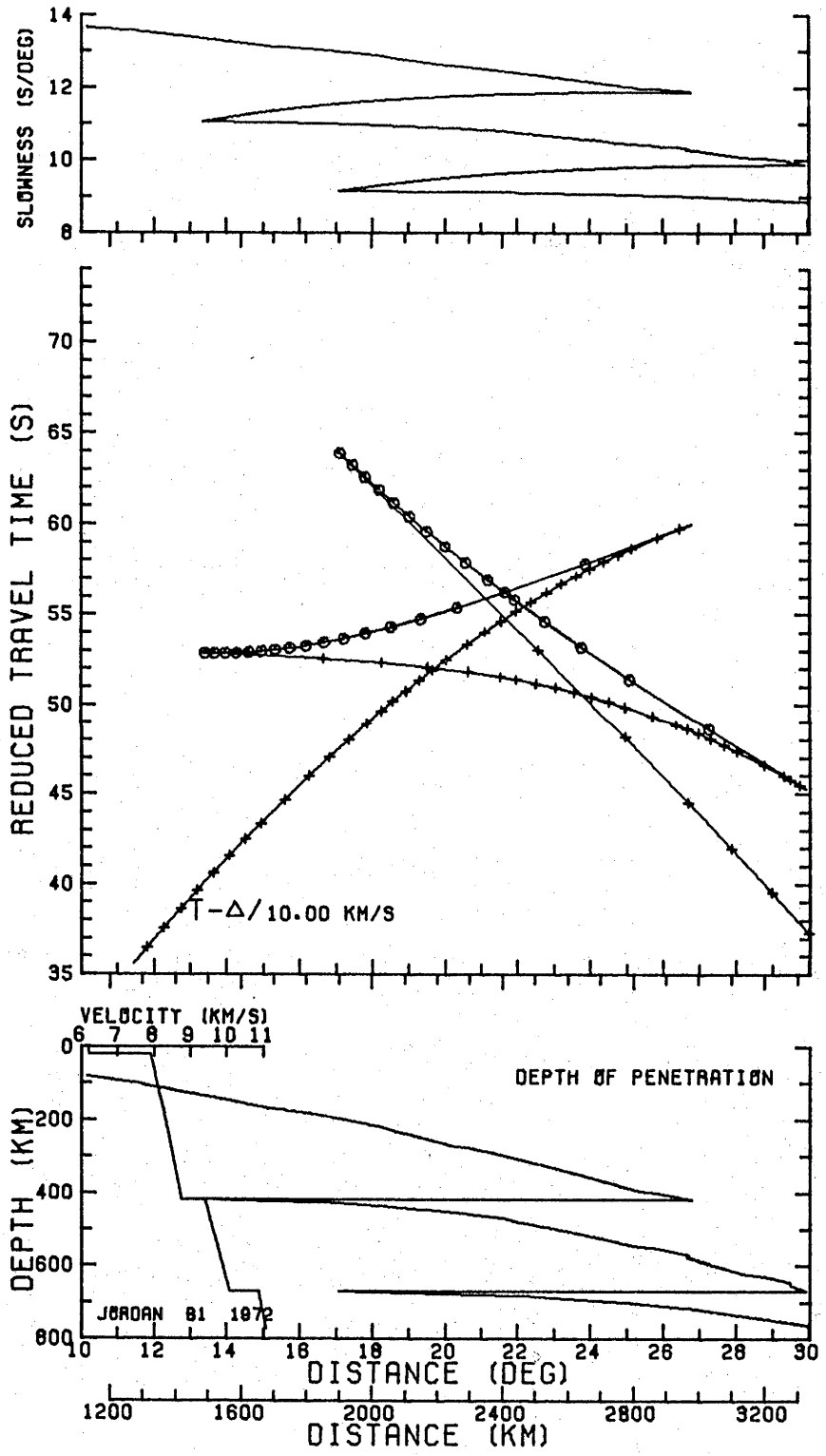

Figure 2-25. The Jordan (1972) model B1.

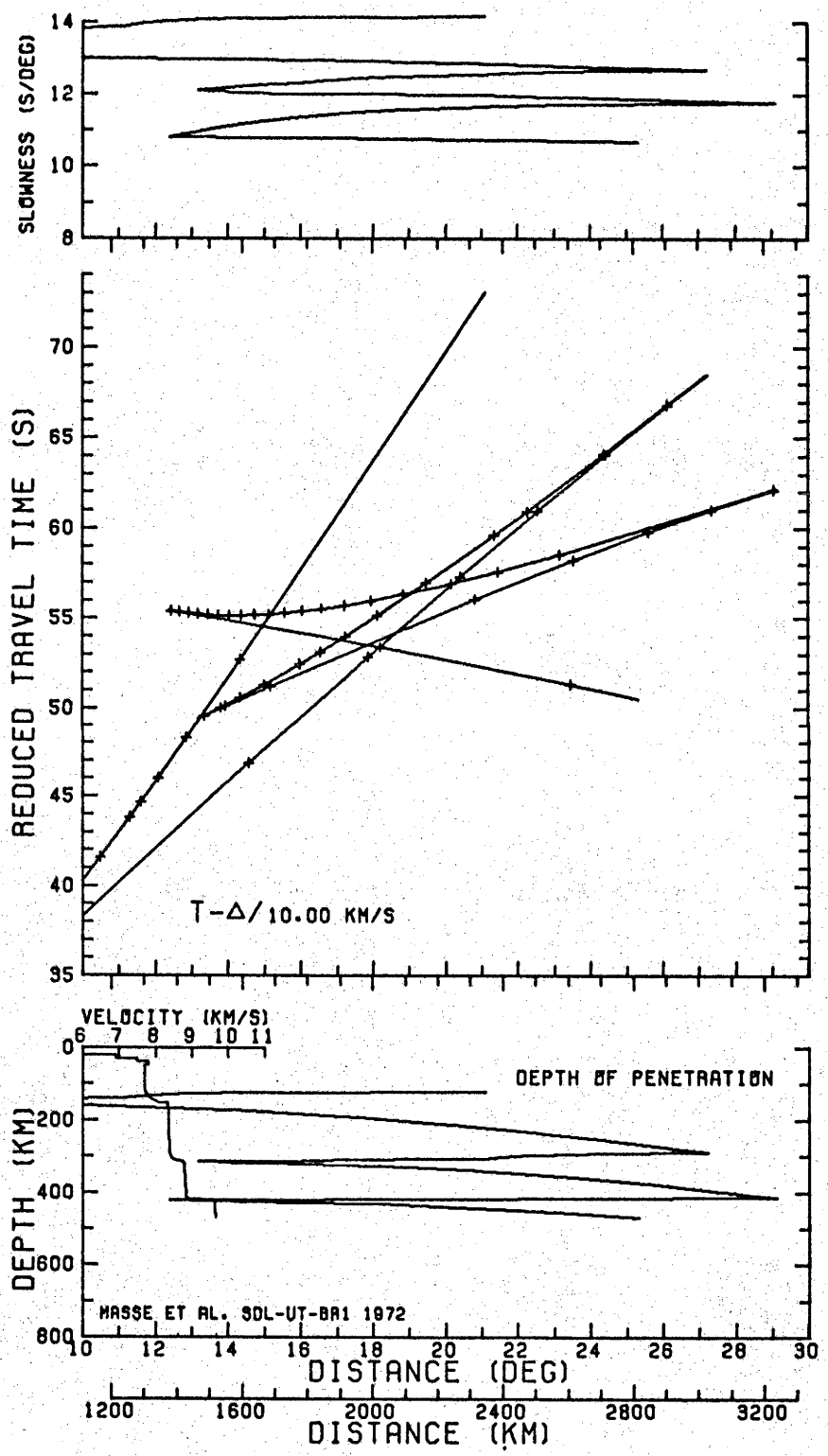

Figure 2-26. The Massé et al. (1972) model SDL-UT-BR1.

CHAPTER 3

PORTABLE SEISMIC INSTRUMENTATION

3.1 Introduction

In May 1970 a 500 t explosion at the Ord River damsite in northern Australia was recorded by most of the permanent seismic stations on the Australian continent. The large distance range over which this explosion was detected indicated that a similar explosion, planned for the following year, would be very suitable for a study of the uppermost mantle beneath Australia. It was the need for portable instruments to record this second explosion which initially prompted the development of the recording system to be described in this chapter.

Although the immediate need was for instruments to record the Ord River explosion, many other applications for such instruments were foreseen, including the monitoring of localized earthquake or aftershock activity, as well as the recording of controlled explosions and quarry blasts. As many of these applications would involve naturally occurring events or explosions for which there may be no foreknowledge of the origin time, it was decided that the recorders should be capable of long periods of continuous unattended recording. Using direct recording on magnetic tape, it is possible to achieve continuous recording in excess of four weeks using standard tape lengths and slightly modified inexpensive recorders. This method

has been used successfully by K.J. Muirhead in Tasmania (Muirhead and Read, 1966) using a system similar to that developed by Dibble (1964). The main drawbacks of these earlier systems were that accurate clocks were not included and the power consumption was so high that battery supplies for long term recording were unwieldly. Recent advances in low-power semiconductor technology have made it possible to develope low-power, high-stability clocks, and to greatly reduce the power required by other components in the recording system. Thus, it was decided to design and construct a set of direct recording instruments, based on the earlier Muirhead design and meeting the following design criteria:

a) Instrumental Performance:

1. continuous recording with a life in excess of one month,
2. a frequency range of at least 0.1 -20 Hz,
3. a dynamic range sufficient to allow for expected variations in signal strength,
4. a timing accuracy of 0.1 s throughout the recording period,
5. power consumption low enough to allow a convenient battery supply to power the system for the total recording period,

b) Logistics:

6. low weight and bulk to allow easy handling and transport,
7. simple installation, operation and repair,
8. rugged construction,

c) Cost:

9. low cost so that a number of instruments could be constructed for a reasonable financial commitment.

3.2 The Direct Recording Method

A reasonable "figure of merit" for the highest frequency response of the direct recording method is 4000 cycles/in of tape (Weber, 1963). Thus, if the maximum frequency of interest is in the order of 40 Hz, a tape speed as low as 0.01 in/s can be used. Using a standard 7 in reel of 2400 ft of tape, this speed allows 33 days of continuous recording. The lower end of the frequency range in the direct recording process is determined by the response of the playback system. Below 20 Hz the output of conventional playback heads approaches the noise level of playback amplifiers, and thus frequencies below this are difficult to recover in real-time playback. If the playback speed is increased to a standard speed of 1 7/8 in/s, the frequency of a 40 Hz signal recorded at 0.01 in/s is reproduced as 7.5 kHz, and a recorded frequency of 0.4 Hz is reproduced as 75 Hz. This range is then well within the response of a standard audio playback system. An additional advantage is gained by time compression on playback, since the recorded seismic frequencies are brought into the audio range, so that the tapes can be edited aurally.

3.3 Instrumentation

3.3.1 Recording

A block diagram of the recording system is shown in Figure 3-1.

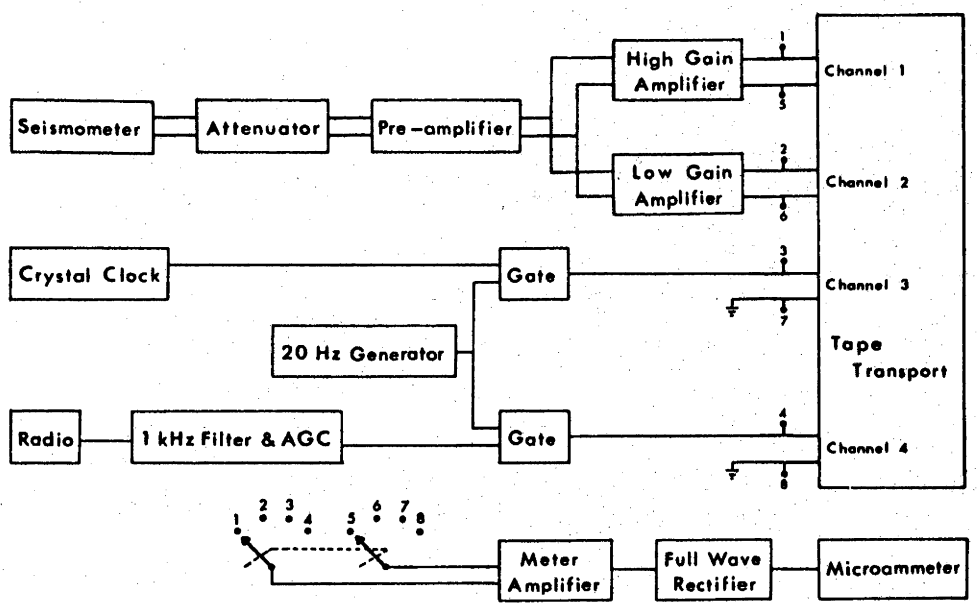

Figure 3-1. Block diagram of portable recording system.
(from Muirhead and Simpson, 1972)

The instrument system was designed by K.J. Muirhead and is described in the appended publication by Muirhead and Simpson (1972). The tape transport is adapted from a domestic tape recorder, modified with a slow speed motor and gearbox to give tape speeds of 0.005, 0.01 and 0.02 in/s. A second two-track head is added to provide for four channel recording. The output of a Willmore Mk II seismometer is passed through a 0-30 db attenuator and low-noise preamplifier before being recorded on two channels with a gain separation of 26 db, giving a total dynamic range of greater than 70 db.

Absolute timing is obtained from a domestic radio receiver tuned to the Australian Post Office time service (VNG) on 7.5 MHz. The VNG transmission consists of a 0.05 s long 1 kHz burst each second, with the minute identified by the omission of the 59th second and a double length tone on the minute. To prevent drift of the radio receiver, a crystal is added to the superheterodyne oscillator, and the signal-to-noise ratio is improved by adding a narrow band, 1 kHz filter and automatic gain control to the radio output. After full wave rectification the 1 kHz second tone is used to gate the output of a 20 Hz oscillator which is recorded on the third tape channel.

Because radio signal fading occurs at night, continuity of time signals is provided by a crystal clock, the output of which is recorded on the fourth tape channel. A complete time code provides a method of determining the time on any part of the tape. The clock consists of a 4.194304 MHz crystal-controlled oscillator and a series of dividing and decoding circuits. The oscillator frequency is reduced to 1 pulse per second using straight binary division, after which binary dividers incorporating feedback loops are used to provide minute, hour, and day counts. Each minute, the outputs of these counters are gated into a parallel-to-serial shift register, and, from this they are gated onto the tape, giving a binary registration of the hour, minute and day during the first 30 sec of each minute. A sample time code recovered from the tape is shown in

Figure 3.2.

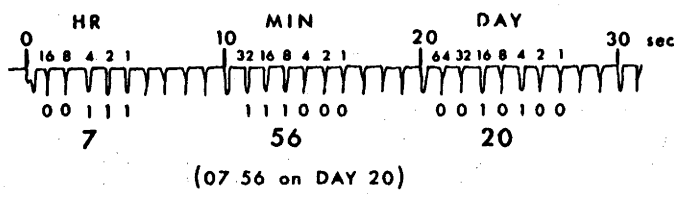

Figure 3-2. Sample time code.
(from Muirhead and Simpson, 1972)

A 0.5 s pulse identifies the start of the minute, a 0.25 s pulse identifies 10 s intervals as well as logical "ones" in the time code, while a 0.125 s pulse is used for all other seconds. To keep power consumption to a minimum, COS-MOS integrated circuits have been used throughout the clock logic, and the use of a crystal oven has been avoided by selecting a crystal with a stability of better than $\pm$ 0.5 ppm over the temperature range 0 to 60^{o}C, which corresponds to a variation of less than $\pm$ 0.05 s per day. A separate circuit incorporating a digital display is used to set the clock at commencement of recording.

The operation of the seismic amplifiers, radio, clock (together with its encoding circuitry) and bias oscillator, can be checked by switching an inbuilt test amplifier to the input of the four tape channels. This feature together with a spare set of printed circuit boards allows damage incurred in transporting the system to be detected and repaired in the field.

The complete recording system, shown in Figure 3-3 consists of the seismometer, a long-wire radio aerial, a fiberglassed wooden box containing the tape recorder, radio and all timing and amplifier circuits, and a battery supply, which may consist either of dry cells, as shown in the figure, or an external wet cell. The only other equipment required is a clock set-up box, also shown in the figure, which is used to set the clock to a standard time and to monitor the clock at the start and end of the recording period.

To prevent vandalism and to maintain a constant temperature for the clock, the instruments are normally completely buried except for the radio aerial. Waterproofing is achieved by using a tight-fitting brass lid, which is sealed to the fiberglassed box with a 2 in wide moisture resistent tape.

The weight of the complete field system is 88 lb, including 17 lb of dry cells and the 32 lb Willmore seismometer. The instrument box measures 22 in x 18 in x 9 in. Total power consumption is 0.65 W including 0.40 W for the motor and 0.10 W for the radio. This is low enough to allow one month's recording using eight Eveready no. 6 dry cells.

3.3.2 Playback

The same type of tape recorder used in the field system has been modified for playback to give seven tape speeds between 15/64 and 15 in/s (corresponding to time compressions of 23.4 to 1500, assuming a recording speed of 0.01 in/s). Four amplifiers, with frequency response

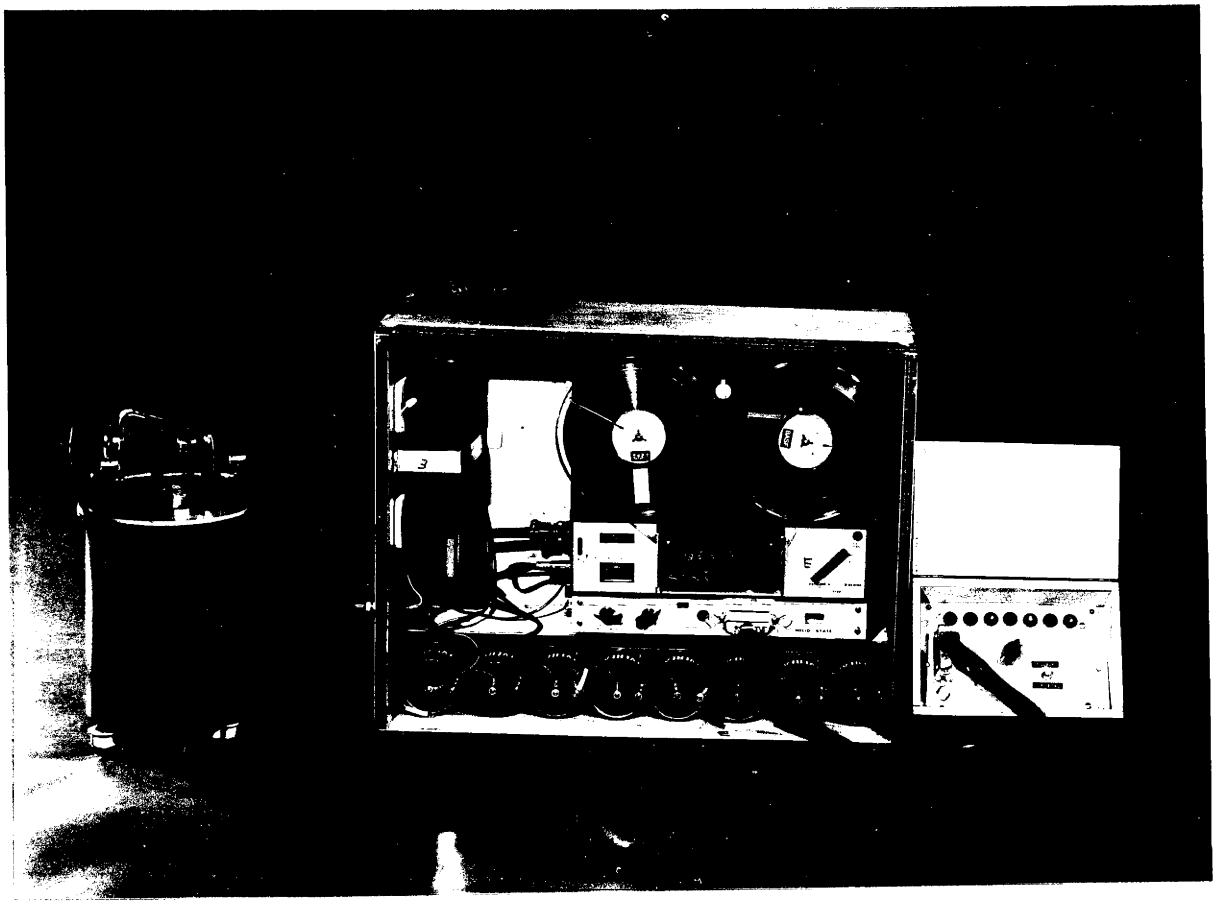

Figure 3-3. The complete field recording system with clock set-up box at right.

down to 20 Hz, are used to replay all four channels simultaneously on a multichannel "jet pen" recorder which has a maximum frequency response of 800 Hz. The difference in offset between the two tape heads on the recording and playback instruments is checked using a calibration pulse which is recorded simultaneously on all four channels at the start of each recording period. Events are located aurally using a high playback speed and are then transcribed to paper using a playback speed which brings the signals within the frequency band (20-800 Hz) of the playback system. If desired, the signals can be band-pass filtered on playback. The signals may also be digitized using the multiplexed analogue to digital converter system shown in Figure 5-2b.

3.3.3 Cost

The approximate cost of major components for each recording system (excluding the seismometer) is summarized in Table 3-1. Approximately two to three weeks of technical time are required for complete assembly.

3.4 Application and Performance

In the two studies to be described in the next chapter three instruments were used to record the Ord River explosions in June, 1971 (Figure 3-4a) and ten were used to record the American nuclear explosion Cannikin in November, 1971 (Figure 3-4b).

TABLE 3-1 Component Cost

	$ Australian
Field Recorder	
Tape transport	
Sony TC 105 tape recorder	80
Slow speed clock motor and gearbox	15
Second two track record head	25
Clock	
Crystal oscillator (4.194304 MHz)	20
RCA COS-MOS integrated circuits, dividers etc.	250
Radio	
Sony TR 1010 receiver	40
Crystal	10
Electronics	
Amplifiers, radio filter, bias oscillator etc.	100
Miscellaneous	
Plugs and sockets	15
Printed circuit boards and sockets	40
Fiberglassed box and lid	30
Interconnecting cables	10
Hardware	15
TOTAL	$A650
Ancillary Equipment	
Seismometer	600
Clock setting device	50
Playback deck	200
"Jet-pen" recorder	2000

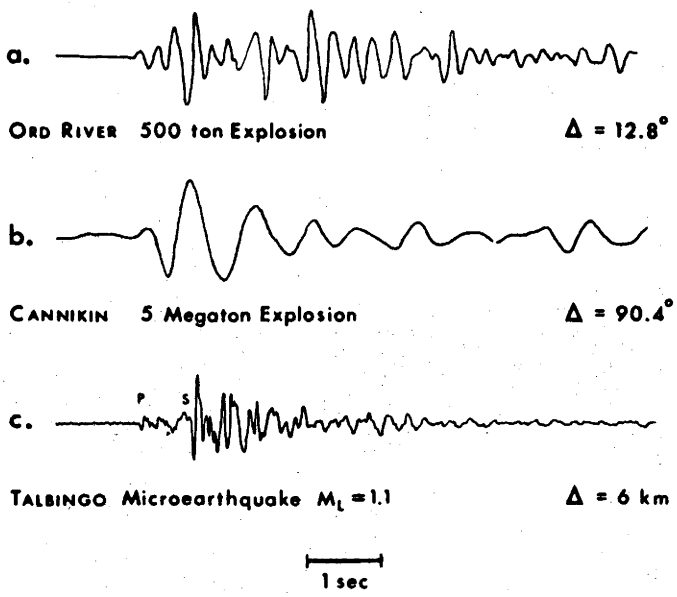

Figure 3-4. Sample records.
(from Muirhead and Simpson, 1972)

The three original instruments have been used for a total of ten months recording of microseismic activity associated with the filling of Talbingo Resevoir (Figure 3-4c) (Timmel and Simpson, 1972). During that time only one interruption to recording occurred, due to a minor mechanical failure on one instrument. The instruments have also been used to investigate the seismic effects of large dams on the Serpentine River in Tasmania and the Ord River in Western Australia, and to record 10 t explosions in the Flinders Ranges of South Australia and Bass Strait.

Figure 3-4 indicates the quality of records obtained from the instruments. Tape speed variation is about 2% and onset times can be measured to better than 0.1 s. The stability of the clock has been higher

than expected. Random drift amounts to less than 0.1 s over a month's recording.

CHAPTER 4

THE UPPERMOST MANTLE

OBSERVATIONS OF THE ORD RIVER AND CANNIKIN EXPLOSIONS

4.1 Introduction

During the decade of the Upper Mantle Project, the velocity structure of the uppermost mantle was the subject of extensive investigation. Travel times and attenuation of body waves, body wave station residuals and the dispersion characteristics of surface waves have revealed extensive regional variations in structure which are closely related to tectonic setting (Nuttli, 1963; Toksoz et al., 1967; Hales et al., 1968; Kanamori, 1970). The existence of a pronounced low velocity zone for both P and S waves in tectonic regions is now well established. Although surface wave studies indicate that a shear wave low velocity zone exists beneath stable continental regions (Brune and Dorman, 1963; Wickens, 1971), there is less support for a similar zone for compressional waves. P wave station residuals are lower for stations in stable areas (Cleary and Hales, 1966), suggesting that any low velocity layer for P waves, if it exists in these areas, is less pronounced than in more active regions.

The most extensive studies of P wave travel times in a stable continental area resulted from Project Early Rise, a series of large explosions in Lake Superior in 1966. The structures derived for the upper 200 km of

the mantle for various profiles from these and related shots (Barr, 1967; Green and Hales, 1968; Lewis and Meyer, 1968; Mereu and Hunter, 1969) have been summarized by Hales (1969). Although there was no conclusive evidence for a pronounced low velocity layer for P waves, all of the profiles revealed the presence of a sudden velocity increase at a depth between 80 and 130 km, which Hales attributed to a phase transition from spinel to garnet peridotite.

The Australian shield represents a tectonic region similar to that sampled by the Early Rise profiles, and observations of the Ord River explosions described in this chapter provided an opportunity to compare the structures beneath these two areas.

In contrast to the Australian shield, the eastern region of the continent is an area of Cenozoic uplift and volcanism. P wave residuals and refraction surveys have indicated lower crustal and upper mantle velocities and the possibility of a well developed low velocity layer in this region (Sutton and White, 1966; Cleary, 1973). The latter portion of this chapter describes observations of the nuclear explosion Cannikin along a line crossing the boundary between the Precambrian shield and the Eastern Highlands, which enabled a study to be made of the transition in upper mantle structure between the two areas.

A. THE ORD RIVER EXPERIMENT

4.2 The Ord River Explosions

The Ord River explosions, along with a preliminary investigation of travel times and amplitudes, have been described in the appended publication by Denham et al. (1972). The explosions were part of quarrying operations to provide fill for a large irrigation reservoir dam, and the method used in blasting made them exceptionally efficient seismic sources. The details of the shot configurations are shown in Figure 4-1.

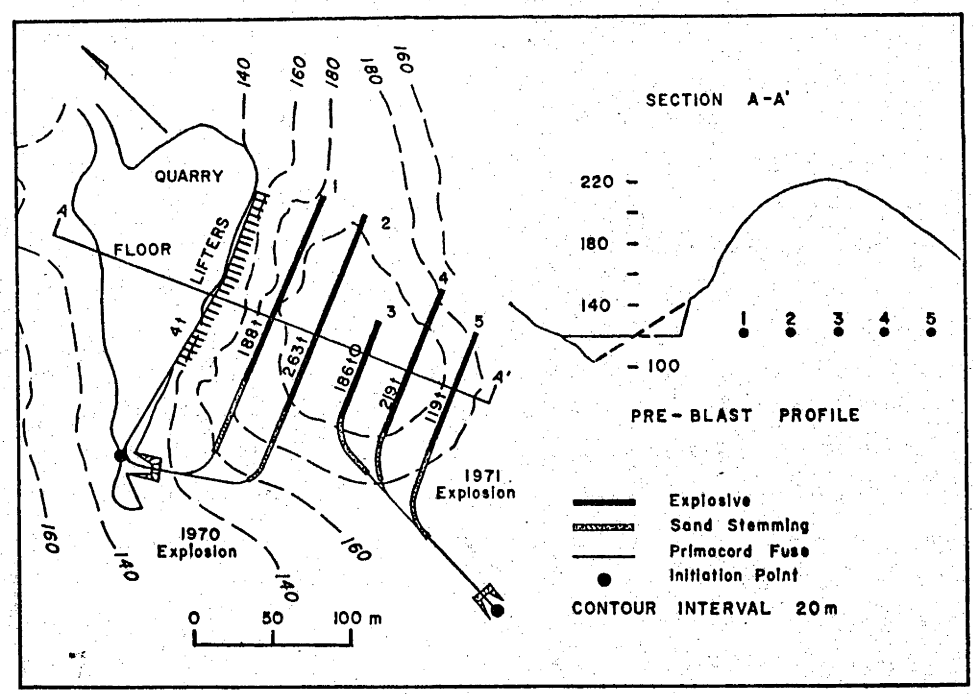

Figure 4-1. Shot details for the Ord River explosions.
(from Denham et al., 1972)

For each blast, tunnels at the base of a 100 m high hill of massive quartzite were filled with approximately 500 t of explosive. There was no delay between charge groups, producing a large, well contained, almost instantaneous explosion. The shot instants (02h 58m 48.4s on 21 June, 1970 and 03h 00m 07.6s on 2 May 1971) were determined with recording instruments placed within 0.5 km of the shot point and are accurate to within 0.05 s. The location of the shot point and the stations which recorded one or both of the explosions are given in Figure 4-2 and Table 4-1. The stations fall into three groups: those along lines to the south and east of the shot point and a series of stations in Western Australia.

Observed travel times and amplitudes of the first arrival mantle phases and later crustal phases are given in Table 4-2 and the P and S travel times are shown in Figures 4-3 and 4-4. On the basis of these first arrival times, Denham et al. reported a least squares analysis of apparent velocities and intercept times which is summarized in Table 4-3.

4.3 The Ord River - Adelaide line

4.3.1 P wave data

The seventeen stations from GRA to ADE provide the most complete set of data for a detailed interpretation of velocities in the uppermost mantle. Because a variety of instruments were used along this line, a direct comparison of original records is difficult. In order to overcome this problem, a record section was prepared

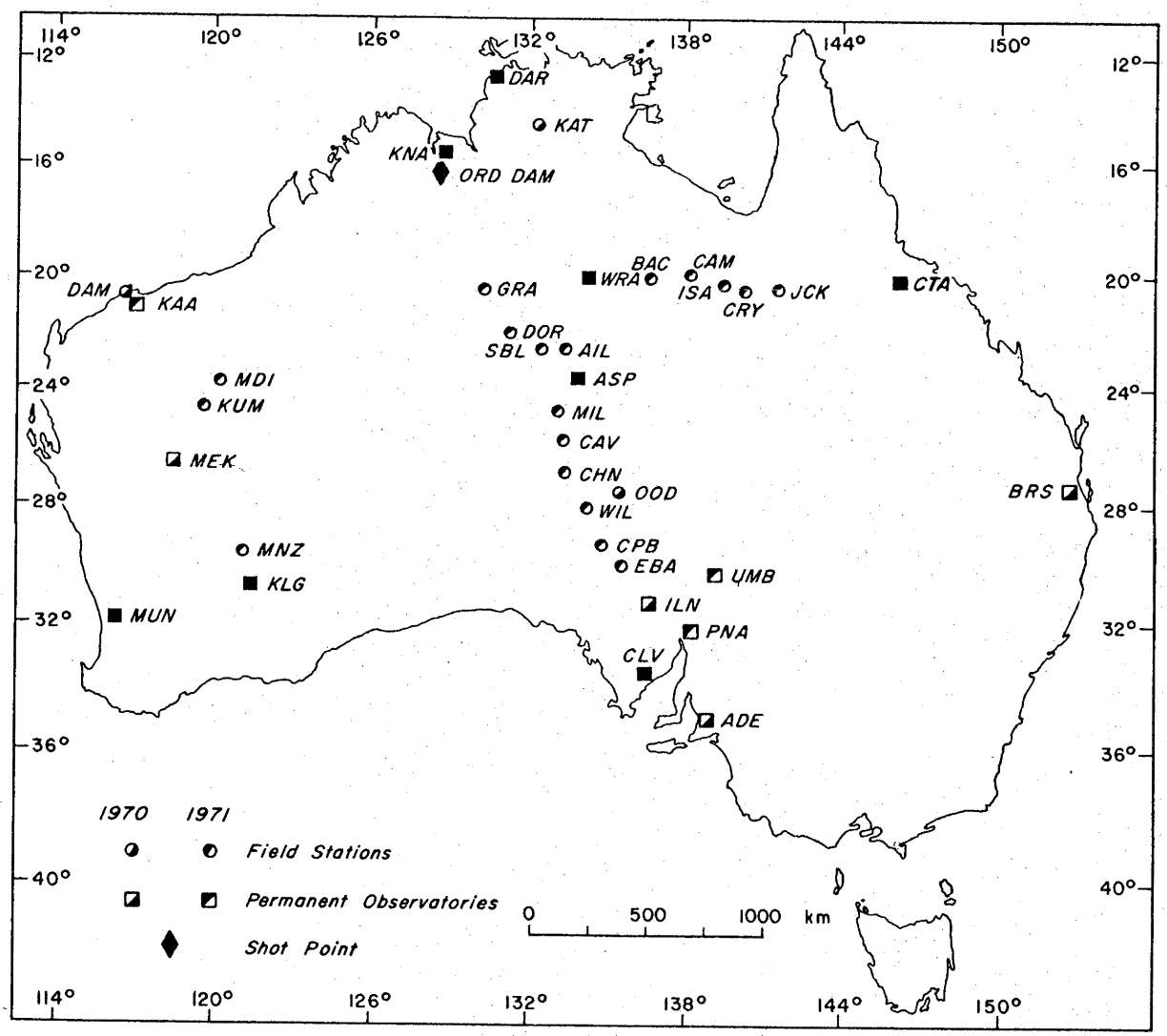

Figure 4-2. Shot point and station locations for the Ord River explosions (from Denham et al., 1972).

Table 4-1. Station information - Ord River explosions

Station information

Station	Code*	Lat, S deg min	Long, E deg min	Elevation (m)	Operator**
Kununurra	KNA ⊕	15 45·0	128 46·0	60	PWD
Katherine	KAT ○	14 29·6	132 21·1	50	BMR
Darwin	DAR ⊕	12 24·5	130 49·1	5	BMR
The Granites	GRA +	20 34·3	130 21·2	430	BMR
Mount Doreen	DOR +	22 02·6	131 19·7	520	BMR
Warramunga array	WRA ⊕	19 56·7	134 20·5	365	ANU
Stuart Bluff	SBL +	22 45·6	132 29·0	610	BMR
Aileron	AIL +	22 37·2	133 18·5	685	BMR
Barry Caves	BAC +	20 02·9	136 40·2	290	BMR
Alice Springs	ASP ⊕	23 41·0	133 53·8	600	BMR
Mill Ridge	MIL +	24 52·0	133 09·2	410	ANU
Camooweal	CAM +	19 53·4	138 09·4	260	BMR
Mount Cavenagh	CAV +	25 54·6	133 07·9	550	ANU
Mount Isa	ISA +	20 26·3	139 25·5	400	BMR
Mundiwindi	MDI +	23 47·1	120 14·8	570	BMR
Mount Chandler	CHN +	26 59·8	133 19·4	380	ANU
Kumarina	KUM +	24 42·7	119 36·9	610	BMR
Cloncurry	CRY +	20 41·7	140 32·6	300	BMR
Karratha	KAA +	20 46·6	116 51·5	15	BMR
Dampier	DAM ○	20 42·6	116 45·6	30	BMR
Mount Willoughby	WIL +	28 00·2	134 09·2	280	ANU
Oodnadatta	OOD ○	27 37·8	135 35·0	135	UA
Julia Creek	JCK +	20 38·6	141 43·3	115	BMR
Meekatharra	MEK ○	26 36·8	118 32·7	515	BMR
Coober Pedy	CPB +	29 15·7	134 58·4	205	UA
Menzies	MNZ +	29 40·9	121 01·5	435	BMR
Mount Eba	EBA +	30 03·6	135 37·7	200	UA
Kalgoorlie	KLG ⊕	30 47·0	121 27·5	360	BMR
Island Lagoon	ILN ○	31 23·6	136 52·2	135	UA
Umberatana	UMB +	30 14·4	139 07·7	610	UA
Charters Towers	CTA ⊕	20 05·3	146 15·3	355	QLD
Partacoona	PNA +	32 00·4	138 09·9	200	UA
Cleve	CLV ⊕	33 41·5	136 29·7	240	UA
Mundaring	MUN ⊕	31 58·7	116 12·5	255	BMR
Adelaide	ADE ○	34 58·0	138 42·5	655	UA
Brisbane	BRS ○	27 23·5	152 46·5	525	QLD

*Permanent seismograph station underlined, (○ Recorded 1970 explosion; + recorded 1971 explosion)

**BMR, Bureau of Mineral Resources; ANU, Australian National University; UA, University of Adelaide; QLD, Queensland University; PWD, Public Works Department, Western Australia.

(from Denham et al., 1972)

Table 4-2. Travel times and distances - Ord River explosions.

Station code and year		Distance degrees	Distance km	Travel times, seconds *P*	Travel times, seconds *S*
KNA	70	0·38	41·8	7·0B	11·7C
KNA	71			6·8A	10·8C
KAT	70	3·85	428·4	59·6A	
DAR	70	4·21	468·8	65·0B	111·5C
				76·5C(P_1)	
DAR	71			65·6B	111·6B
				77·5B(P_1)	127·1C(S_1)
GRA	71	4·68	520·8	71·59A	121·2B
DOR	71	6·38	709·4	94·65A	161·5B
WRA	70	6·55	728·6	95·10A	167·6B
WRA	71			95·10A	167·6B
SBL	71	7·49	832·9	109·62A	188·3B
AIL	71	7·77	864·5	113·5A	193·4B
BAC	71	8·49	945·1	121·7B	215·2C
ASP	70	8·95	995·7	129·2A	226·6B
ASP	71			129·3B	225·4B
MIL	71	9·63	1071·5	138·7A	240·7C
CAM	71	9·71	1080·8	138·1B	243·5C
CAV	71	10·56	1175·3	151·0A	263·2D
ISA	71	11·02	1226·4	155·9D	
MDI	71	11·03	1227·4	157·4B	276·2B
CHN	71	11·63	1293·6	165·1A	289·6B
KUM	71	12·08	1344·1	171·0B	299·9C
CRY	71	12·09	1345·6	170·8C	298·5C
KAA	71	12·18	1355·4	171·6B	300·6C
DAM	70	12·24	1362·5	172·4B	302·2C
WIL	71	12·84	1428·5	181·4A	320·0C
OOD	70	13·09	1456·3	185·1C	325·6D
JCK	71	13·12	1459·9	182·8D	
MEK	70	14·10	1568·5	197·4B	348·6D
CPB	71	14·28	1588·7	198·5A	350·8C
MNZ	71	15·24	1695·5	212·7B	374·1C
EBA	71	15·24	1695·9	212·2C	373·5B
KLG	70	16·04	1784·1	220·3C	390·5C
KLG	71			220·3B	390·5B
ILN	70	16·91	1881·6	232·6B	
UMB	71	16·97	1888·4	234·2C	415·4D
CTA	70	17·11	1904·3	237·9D	
CTA	71			237·6D	
PNA	71	17·98	2000·9	245·4C	
CLV	70	18·84	2095·8	256·1C	
CLV	71			256·1C	456·1D
MUN	70	19·46	2165·3	264·8C	
MUN	71			264·8C	
ADE	70	20·78	2312·0	281·6C	
BRS	70	24·93	2774·3	325·0B	

Uncertainty in travel time is assessed as follows: A $\leq$ 0·1 sec; B, 0·1 $\leq$ 0·5 sec; C, 0·5 $\leq$ 1 sec and D > 1 sec.

(from Denham et al., 1972)

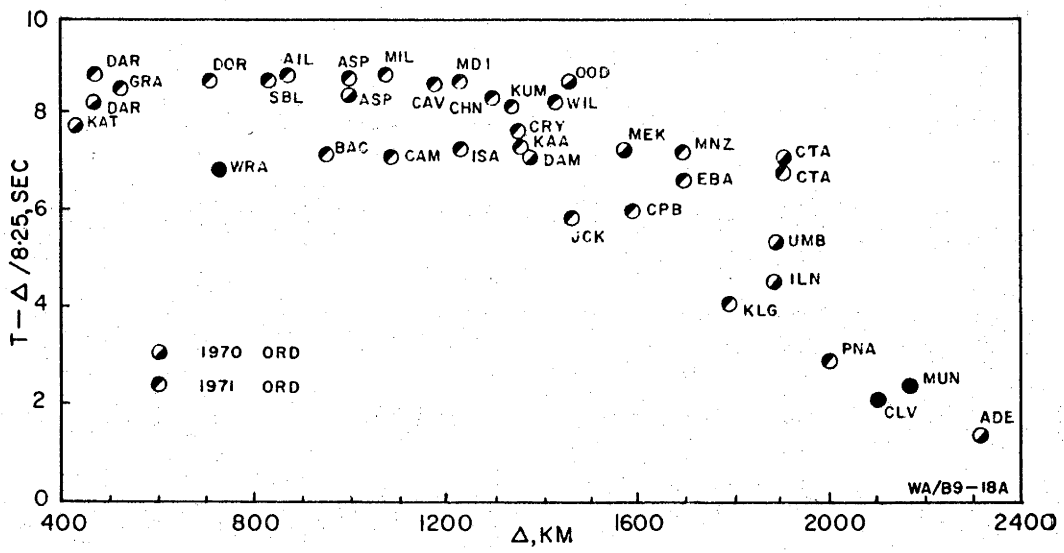

Figure 4-3. P travel times - Ord River explosions (from Denham et al., 1972).

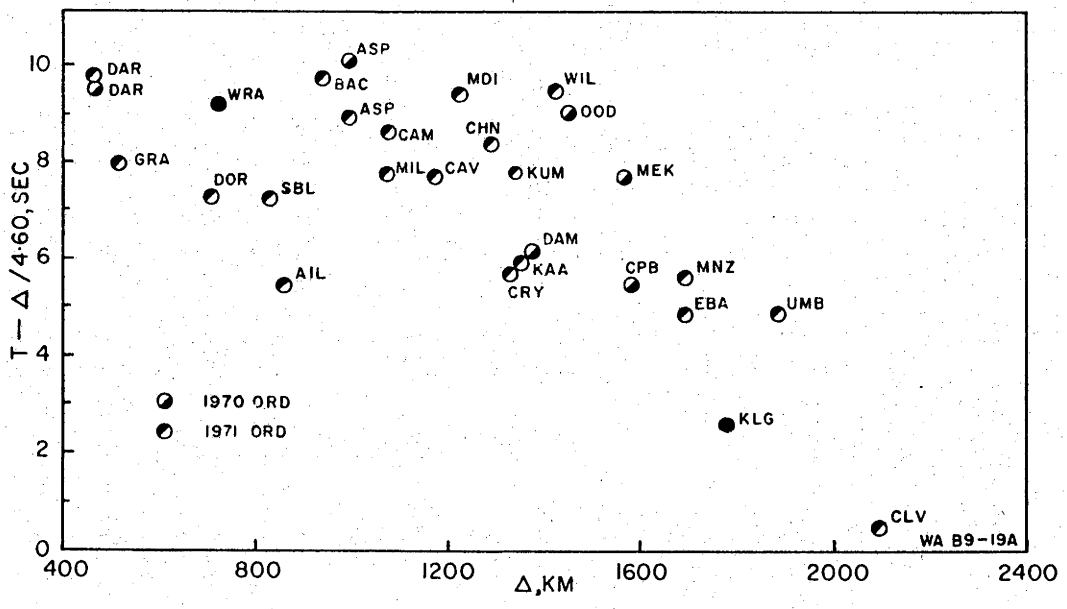

Figure 4-4. S travel times - Ord River explosions (from Denham et al., 1972).

TABLE 4-3

Least squares analysis - all Ord River data

Velocity (km/s)	Intercept time (s)	Range (km)	Line
P wave data			
8.27±0.01	8.79±0.20	400-1500	south
8.27±0.01	8.85±0.21	400-1500	south & west
8.82±0.10	19.13±2.53	1400-2400	south
8.85±0.08	19.90±2.03	1400-2400	south & west
8.17±0.02	5.92±0.30	700-1400	east
S wave data			
4.75±0.07	12.52±2.29	400- 900	all lines
4.49±0.02	7.84±1.04	400-1450	all lines
4.84±0.06	23.33±4.94	1500-2100	south & west

(from Denham et al., 1972)

and is shown in Figure 4-5. The ANU tape recording stations (MIL, CAV, CHN, WIL) were digitized using the A/D converter and computer system shown in Figure 5-2b. The remaining traces shown in Figure 4-5 were digitized from paper records. The records from AIL, OOD, UMB, PNA and ADE were not of sufficient quality to allow digitization, and the travel times of first and obvious later arrivals at these stations are indicated by points in Figure 4-5. Examples of the original records from most of the stations on this line are shown in Figure 4-6.

Although variations in instrument response and the distortion resulting from scale expansion are obvious on some of the records in Figure 4-5, it is possible to distinguish a number of later arrival branches. The phase marked A' in Figure 4-5 is a first arrival at GRA, DOR and SBL, and can be followed as a second arrival from ASP to WIL. The phase C' appears as a second arrival on GRA, DOR and SBL, and becomes the first arrival from ASP to WIL.

The most interesting record is that from CPB at 1588.7 km (see original record in Figure 4-6). The clear first arrival, E', is followed 1.3 s later by a very large amplitude arrival, C". The record from EBA at 1695.9 km shows an arrival similar to the C" arrival at CPB and, although no earlier arrival can be positively identified, the higher noise level at this site could easily mask a low amplitude earlier arrival. Both C" and E' can be identified at PNA and possibly ILN, and

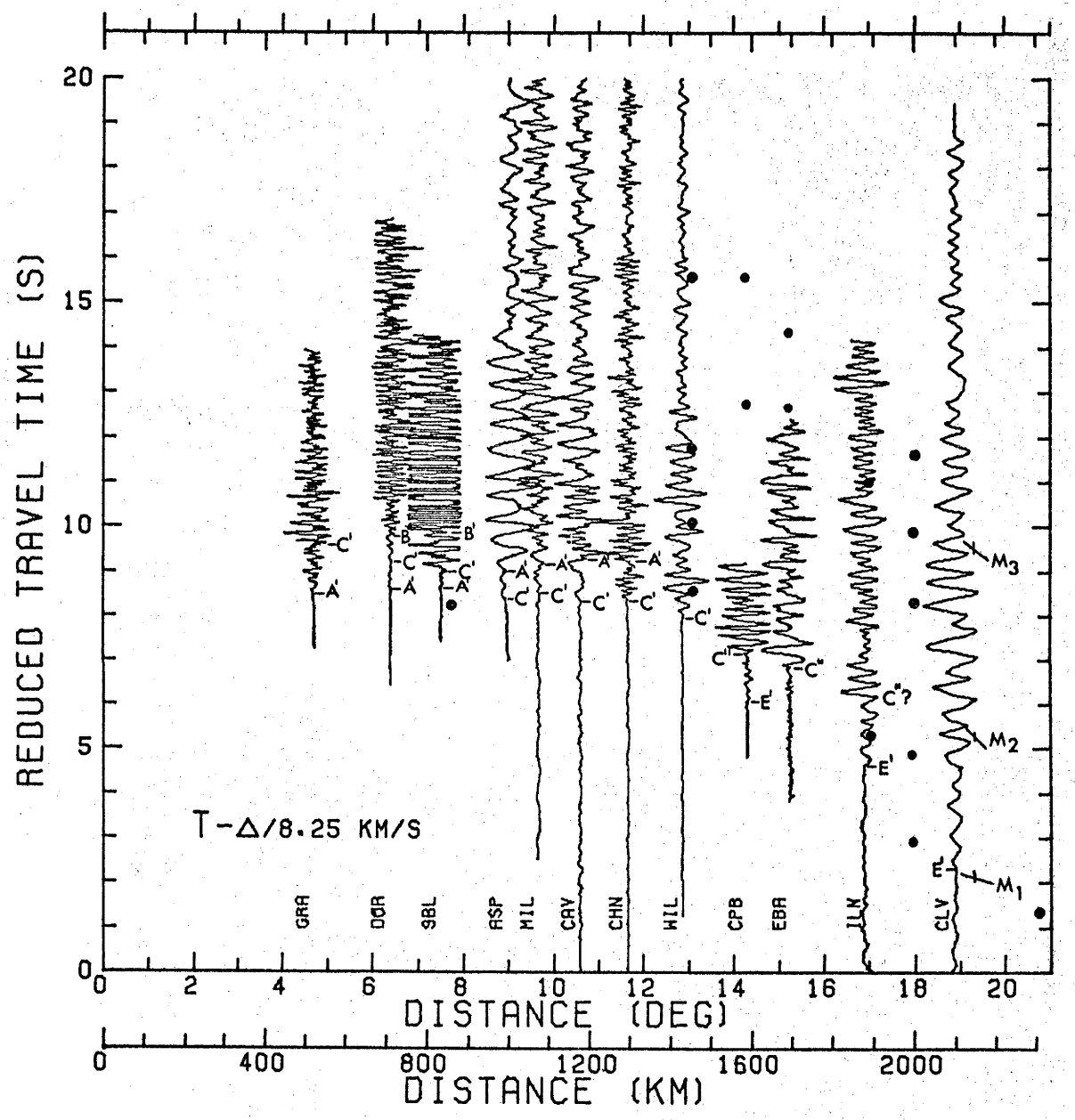

Figure 4-5. Record section, Ord River - Adelaide line. All amplitudes normalized to maximum in each trace. Solid points indicate arrivals at AIL (864.5 km), OOD (1456.3 km), UMB (1888.4 km), PNA (2000.9 km) and ADE (2312.0 km) and later arrivals at CPB and EBA. M_1-M_3 arrivals are from the Meckering aftershock (see text).

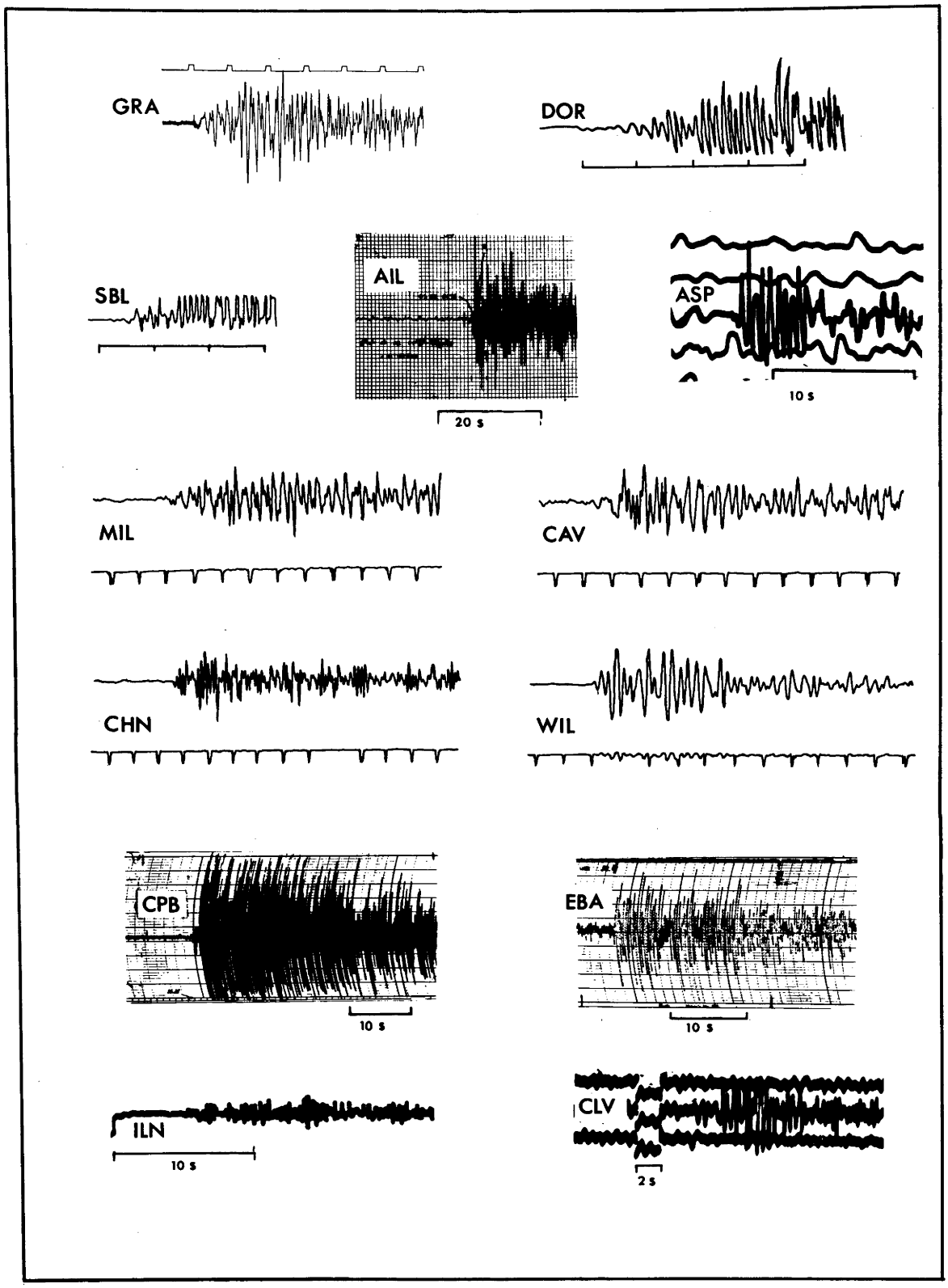

Figure 4-6. Sample records, Ord River - Adelaide line. Except where indicated, time marks are 1 s.

the higher amplitude phase C" is the first arrival identified at UMB. Least squares straight line fits to the arrivals A', C', C", and E' are given in Table 4-4.

TABLE 4-4

Least squares analysis - Ord River - Adelaide line

Branch	Velocity (km/s)	Intercept time (s)	Distance range (km)
A'	8.15±0.02	7.74±0.26	500-1300
C'	8.35±0.01	10.20±0.19	500-1500
C"	8.66±0.04	16.44±0.87	1500-2000
E'	8.74±0.07	16.76±1.79	1500-2400

4.3.2 P Velocity Structure

There is not sufficient data at short distances to derive a crustal structure from the Ord River observations. In a review of Australian crustal structure, Cleary (1973) finds that the average P_1 velocity for the upper crust of the western part of Australia is 6.2 km/s and that there is evidence for an intermediate layer in all parts of the continent with a P_2 velocity of approximately 6.5 km/s below 20 km. These values have been adopted as typical of the crust along the Ord River - Adelaide line.

Using the method outlined by Mereu (1968), velocities and layer thicknesses, corrected for a curved earth model,

have been determined from the apparent velocities and intercept times of the straight line fits to branches A' and C' given in Table 4-4. A layer of velocity 8.10 km/s is found to extend from the base of the crust at 39.4 km to a depth of 85.0 km where the velocity increases to 8.24 km/s. If the first arrival branch, E', is included in this analysis, a discontinuity from 8.24 to 8.52 km/s occurs at 156.4 km. The high amplitude arrivals C" in Figure 4-5 suggest, however, that the C' branch does not continue as a straight line beyond 1400 km, but that a strong curvature of the branch occurs near 1500 km, making the C" arrivals an extension of the C' branch and producing the high amplitudes associated with the focusing of energy related to such a rapid change in slope of the travel time curve. If the times for the C' branch beyond 1100 km are grouped with the C" arrivals, a smooth curve through these points can then be used as the basis of a Herglotz-Wiechert inversion to determine velocities below the 85.0 km discontinuity. The Ord P model resulting from such an inversion is tabulated in Table 4-5. Figure 4-7 shows the velocity model and the travel time curve derived from it superimposed on the record section.

Later arrivals at the stations beyond 1500 km may be related to structure below 250 km and these will be mentioned in Section 4.3.4 and Chapter 6. At shorter distances the only obvious arrivals unexplained by the model are those labelled B' in Figure 4-5 at DOR and SBL

TABLE 4-5. The Ord P Model

Ord P Model

Velocity (km/s)	Depth (km)
6.20	0.
6.20	20.
6.50	20.
6.50	39.
8.10	39.
8.10	85.
8.24	85.
8.2441	95.
8.2497	100.
8.2562	105.
8.2629	110.
8.2792	120.
8.3173	140.
8.3563	160.
8.3749	170.
8.3830	175.
8.5320	175.
8.6000	350.

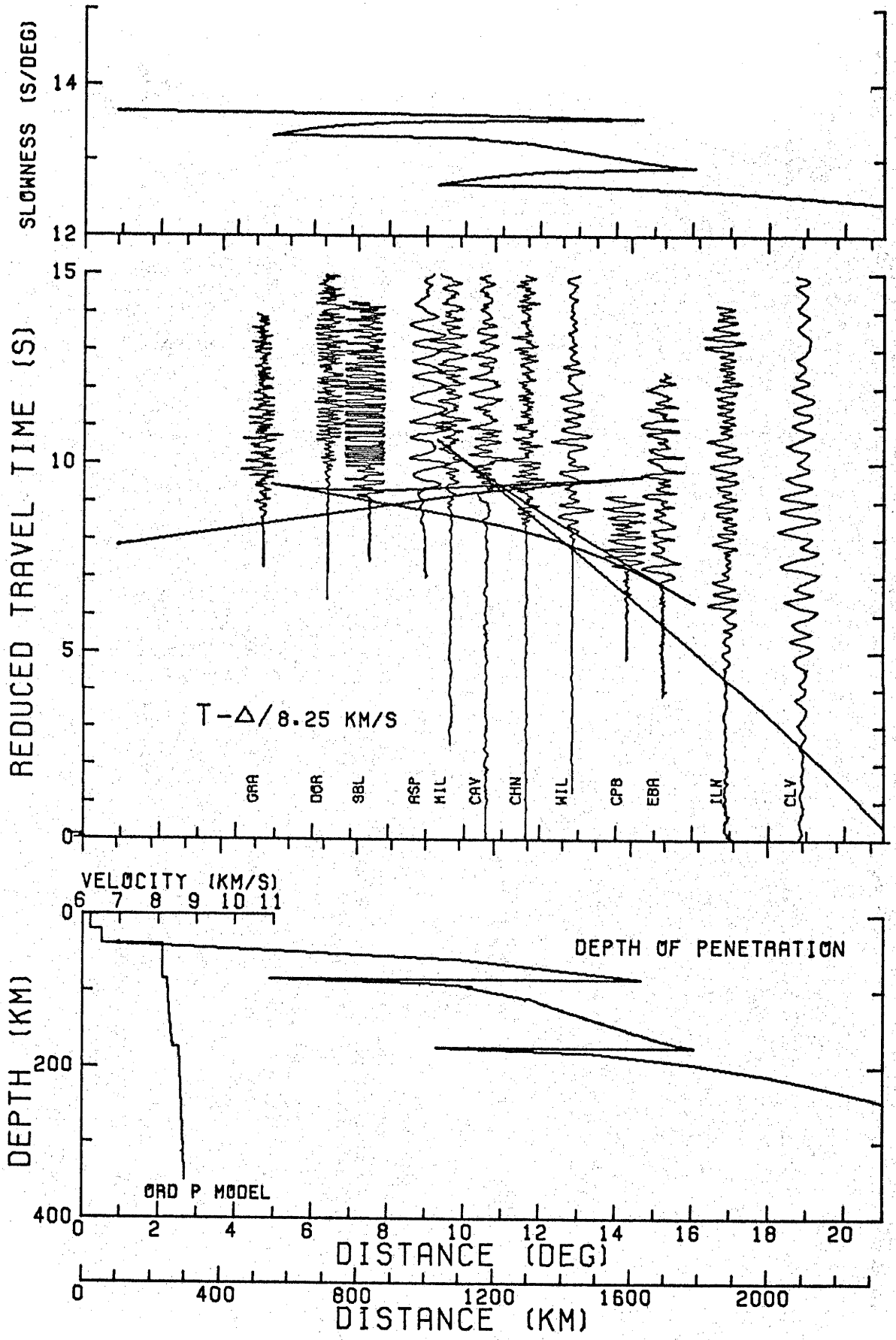

Figure 4-7. The Ord P model.

and a later arrival at DOR. Overloading of the instrument at SBL makes the identification of the B' arrival suspect, but the onset of a similar arrival at DOR suggests that it may be real. A minor low velocity layer starting near 65 km and a slight adjustment of the depth of the 85 km discontinuity in the Ord P model would produce the delay required to satisfy the B' arrivals without significantly altering the times for the C' branch in Figure 4-7.

4.3.3 Additional evidence supporting the Ord P model

Amplitudes - Although no absolute calibrations were available for most of the stations along the profile, it is possible to make some comparisons of relative amplitudes which, while based on rather tenuous assumptions, provide at least qualitative support for the high amplitudes associated with the curvature of the C'' branch near 1400 km. The fortuitous occurrence of an earthquake north of Australia (probably in the Banda Sea region), approximately five minutes after the 1971 Ord River explosion, provided the opportunity to compare the amplitudes from the explosion with those from a second source. Figure 4-8 shows the analogue records for the explosion and earthquake from the tape recorder stations MIL, CAV, CHN and WIL played back at the same gain and with a highly compressed time scale. The instruments are all similar and were set to the same gain for recording, but the apparent gain at WIL appears higher than the other stations, perhaps due to a local amplitude anomaly at this site. In spite of this, the overall

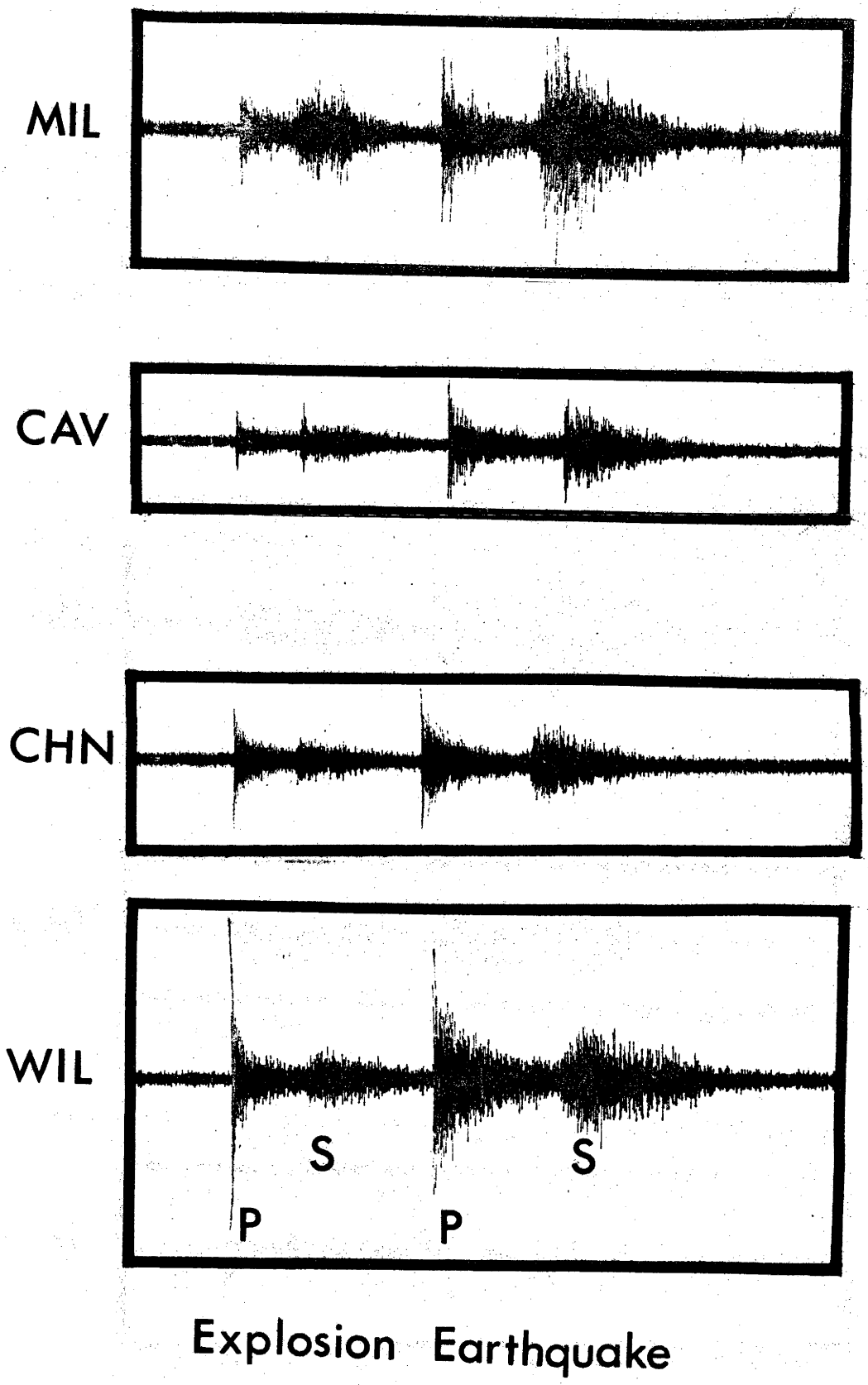

Figure 4-8. Comparison of the 1971 Ord River explosion and an earthquake recorded on the ANU tape recording stations.

character of the records, a comparison of the P amplitude from the explosions at each station, and the ratio of the P arrivals from the explosion and earthquake all suggest an increase in the initial P explosion amplitude from CAV to WIL. The first few cycles of the WIL record are especially strong. Comparisons of the explosion and earthquake at CPB and EBA indicate that the relative amplitudes of the C" arrival remain large at these stations.

The Meckering earthquakes - In the Ord P model the E' arrivals have been ascribed to the same branch with an apparent velocity of 8.74 km/s. As the recent models in Chapter 2 indicate, a higher velocity branch should emerge as a first arrival near 20° and it is important to determine whether the first arrivals beyond 18° on the Ord River profile could belong to the higher velocity branch.

The large Meckering earthquake near Perth in Western Australia on October 14, 1968 (Everingham et al., 1969) and a smaller aftershock on October 15, 1968 are at a distance of 19.4° from the WRA array and the travel path to the array is entirely within the Australian shield. Although the main shock saturated the recording system at WRA, the aftershock was well recorded and an adaptive processing solution (see section 5-3) for the apparent velocity from this event is shown in Figure 4-9. In the first ten seconds, six arrivals are obvious on the time averaged product (TAP) trace. Each of the M arrivals is followed approximately 2 s later by a higher amplitude

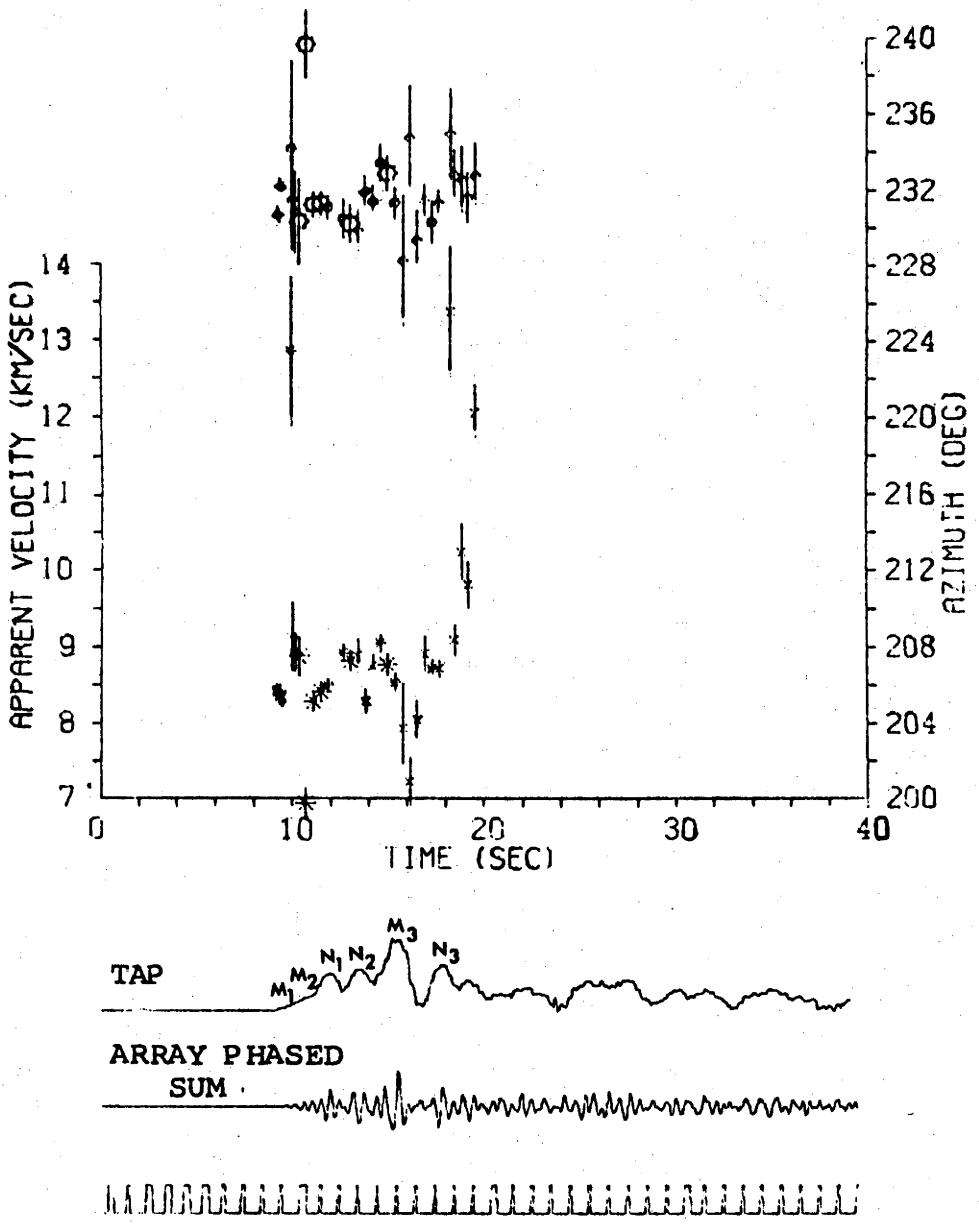

Figure 4-9. Adaptive processing solution for the October 15, 1968 Meckering aftershock.

N arrival with the same apparent velocity as the corresponding M phase. The N arrivals may be of the pP type, or due to a second shock. The M arrivals, however, show that at 19.4° there are three arrivals (M_1, M_2, M_3) separated by 3.2 and 4.2 s with measured apparent velocities of 8.5, 8.9 and 8.75 km/s. These apparent velocities should be corrected for array structure (see Chapter 6), but corrections for this azimuth and distance range have not been determined. The apparent velocity solutions do show, however, that the lower velocity phase is still the first arrival at 19.4° for a travel path similar to that for the Ord River - Adelaide line. Using the origin time determined from local stations for the main Meckering shock (Everingham et al., 1969), the travel time to WRA is approximately 3 s earlier than that expected for the E' branch in the Ord P model, which may be due to an error in origin time or higher velocities in the western part of the Australian shield. In Figure 4-5, lines with slopes corresponding to the measured apparent velocities are shown for the M_{1-3} arrivals, with the times adjusted so that the M_1 arrival falls on the E' branch. The arrivals approximately 3 s after the first arrivals at CLV and ILN may be related to the M_2 Meckering arrival and later arrivals at a number of the stations beyond 1400 km may correspond to the M_3 arrivals. The M_2 and M_3 arrivals result from structure below 250 km and will be discussed in Chapter 6.

4.3.4 S wave arrivals

Because of their emergent nature, the S arrivals are more difficult to identify than the P phases. Denham et al. (1972) noted that the S times in Figure 4-4 suggested a break in the travel time curve near 900 km which might be related to a low velocity layer. The records from the Ord River - Adelaide line have been searched for multiple arrivals and the revised times are shown in Figure 4-10. The delay in arrival times beyond 900 km is obvious in this figure and is supported by the identification of later arrivals, at the stations from GRA to SBL, which lie close to an extension of a line through the first arrivals at the more distant stations.

Using a notation similar to that for the P arrivals in Figure 4-5, a tentative interpretation of the data is shown in Figure 4-10. Because of the scatter in the data, the paucity of points on the S_n (A_S') line, and the difficulty in correlating arrivals from stations to station, no velocity model based on the observed data will be presented. A model with a low velocity layer from 60 to 85 km, similar to that suggested in Section 4.3.2 for P waves, would satisfy the A_S', B_S' and C_S' branches in Figure 4-10. The arrivals beyond 1200 km are weak and little confidence can be given to the identification of the E_S' branch, which may be related to a second low velocity layer below 85 km, or a discontinuity near 175 km similar to that shown in the Ord P model.

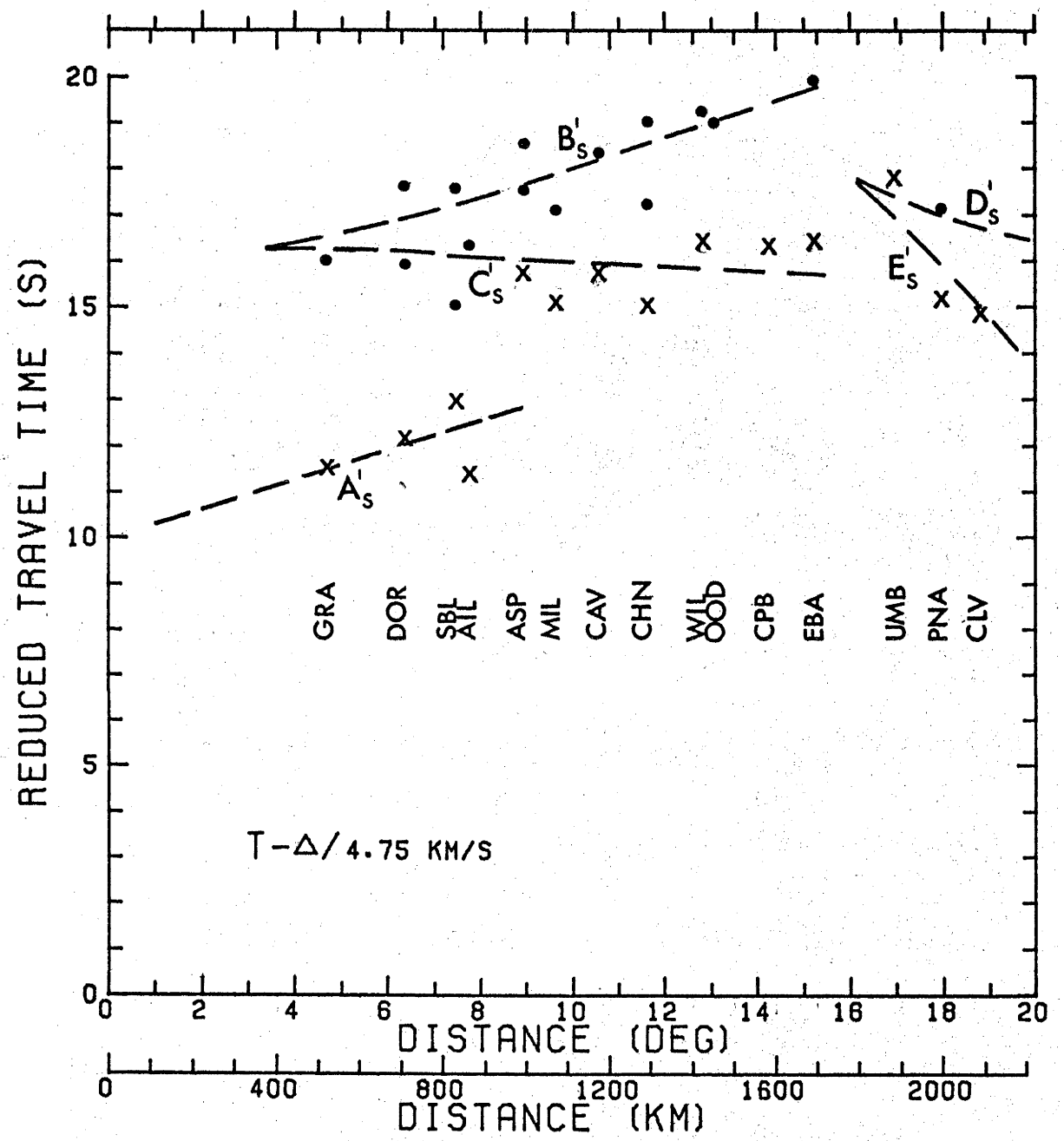

Figure 4-10. S travel times, Ord River - Adelaide line, with tentative interpretation. First arrivals denoted (X).

4.3.5 Comparison with other studies in shield areas

Australian shield - Bolt, Doyle and Sutton (1958) observed travel times to 10.7° from atomic explosions at Maralinga in South Australia on a line to the west along the southern part of the Australian shield. The average P_n velocity determined from first arrivals at four stations from 350 to 970 km was 8.21 km/s with the crustal thickness of 32.2 km. As shown by Denham et al. (1972), these values are consistent with the average values found using first arrival Ord River data. The most distant station to observe the Maralinga explosions, at 10.7°, showed an arrival 1.9 s earlier than the time expected from the apparent velocity of 8.21 km/s, which Doyle (1957) suggested as evidence for an increase in velocity with depth.

White (1971), using observations of first arrivals from earthquakes with travel time paths through the Australian shield, derived the velocity model shown in Figure 4-11a, which has a low velocity layer from 200 to 300 km. The low velocity layer in this model is not directly related to the present discussion of uppermost mantle. It was introduced to account for arrivals of the M_2, M_3 type (Figure 4-5) which are more likely explained by structure near 400 km (Chapter 7). White's data at less than 15° was limited and the model is presented here only to show a comparison of the average times for this model with those from the Ord P model. Up to a distance of 1400 km, the times from the White

model are approximately 0.5 s earlier than the first arrivals for the Ord P model. Beyond 1400 km the times are closer to the higher amplitude C" arrivals in Figure 4-5.

Canadian shield - The uppermost mantle P velocity models determined for the Canadian shield and central United States from Lake Superior and Hudson Bay explosions (Barr, 1967; Green and Hales, 1968; Lewis and Meyer, 1968; Weichert, 1968; Mereu and Hunter, 1969; and Mereu, personal communication) are compared with the Ord P and White models in Figure 4-11. Those studies which have the most continuous station coverage (Green and Hales, Lewis and Meyer, Mereu and Hunter, and the Ord River study) all show a change in slope in the travel time curve near 700 km and a change in slope or offset in the travel times near 1300 km. The offset near 1300 km is especially clear in the profiles shown by Green and Hales, Mereu and Hunter, and Weichert. Weichert had no data available in the distance range 500 to 1300 km and it is impossible to determine whether the A'B'C' triplication near 700 km (corresponding to a discontinuity near 85 km) exists along the profile to the east of the Yellowknife array. If such a structure did exist, the depth to the low velocity layer in Weichert's model would be shallower.

Dowling and Nuttli (1964) have studied the effect on travel time of various types of low velocity layers. In Figure 4-12 are shown a number of models similar to those discussed by Dowling and Nuttli. Above 120 km

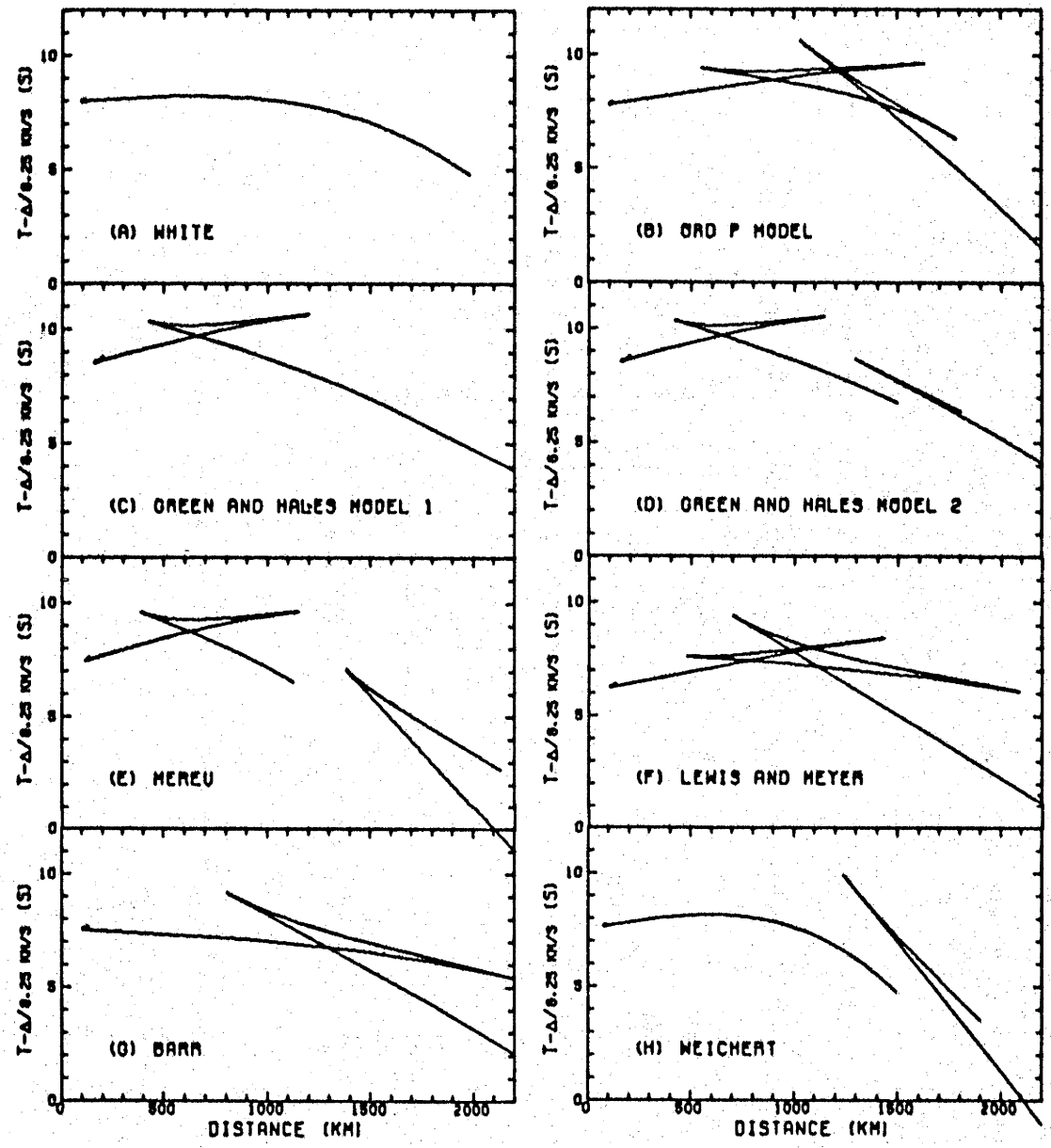

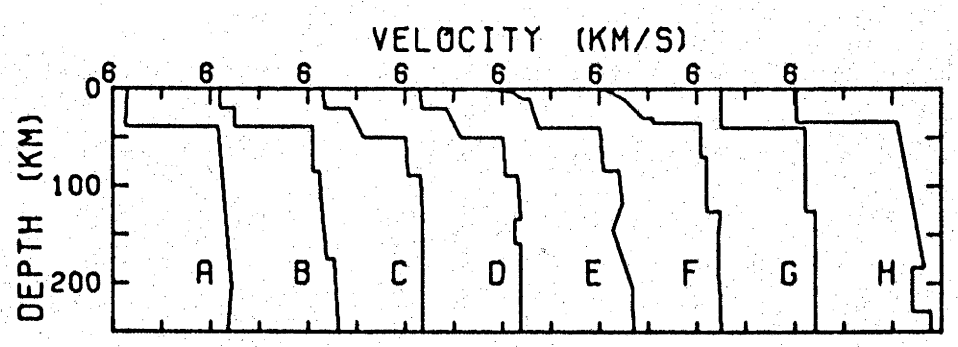

Figure 4-11. Comparison of Australian and Canadian shield P velocity models.

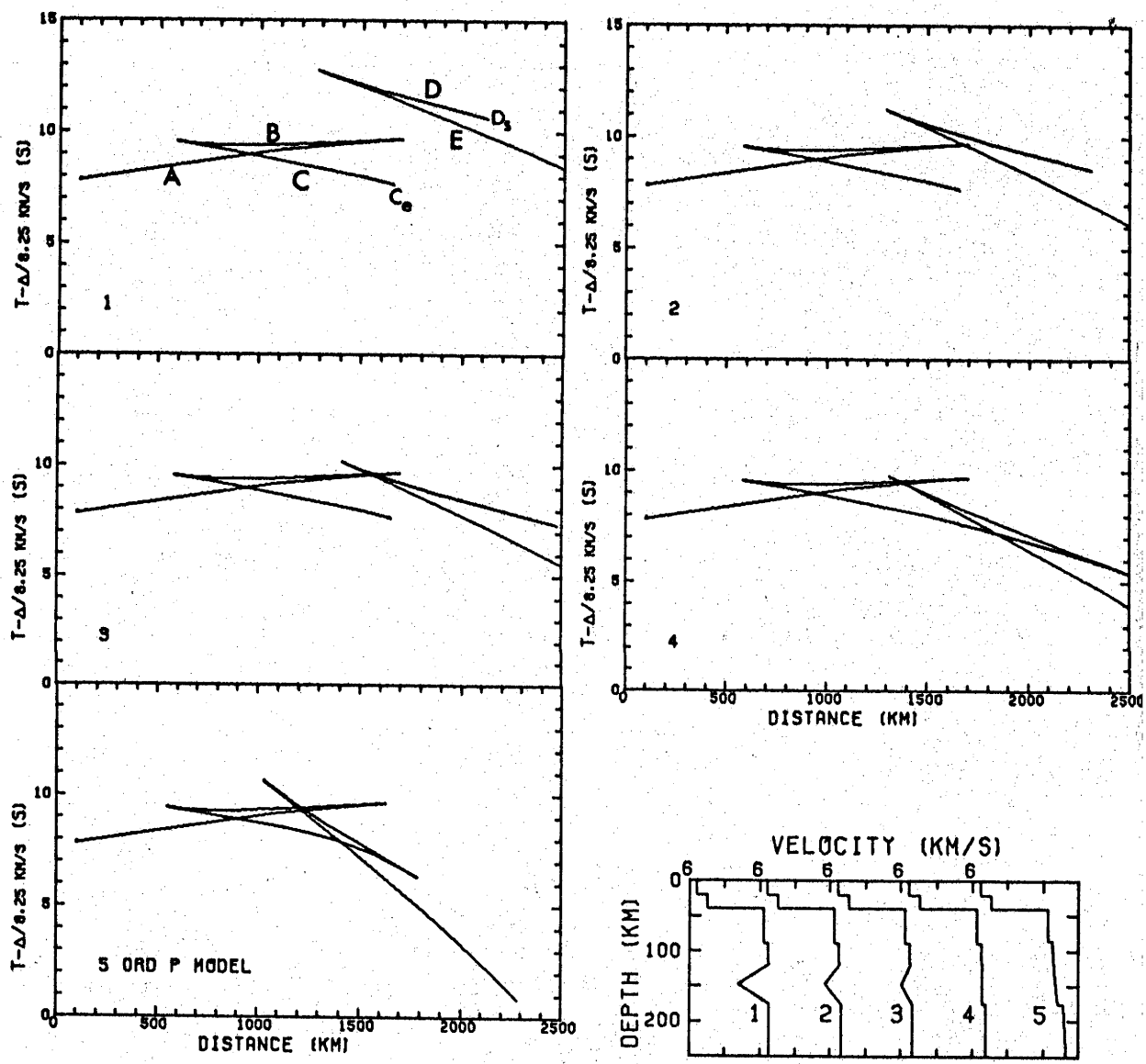

Figure 4-12. Examples of the effects of low velocity layers.

these models are the same as the Ord P model. Between 120 and 175 km low velocity layers are included in models 1 to 3. Model 4 has a constant velocity between 120 and 175 km and model 5 is the Ord P model. As Dowling and Nuttli have shown, the effect of the low velocity layer is to cut off the C branch at C_e and produce the delayed branch D. The first arrival from below the low velocity layer (D_S) emerges with the same apparent velocity as the end of the C branch and is offset above an extension of the C branch, the offset decreasing as the extent of the low velocity layer decreases until the situation such as that in model 4 is reached, when the travel time curve becomes continuous. Increasing the velocity gradient in the interval 120 to 175 km, as shown in the Ord P model, increases the curvature along the C branch.

The offset in travel times near 1300 km observed in the Canadian shield data is best explained by models similar to case 3 in Figure 4-12 with a minor low velocity layer near 150 km (e.g. models D (Green and Hales) and E (Mereu) in Figure 4-11). The high amplitude C" arrivals in the Ord River profile (Figure 4-5) occur at approximately the same distance as the offsets observed in the Early Rise profiles. The C" arrivals however, fall earlier than a continuation of the C' branch and do not show the offset characteristic of the presence of a low velocity layer. It thus appears that a minor low velocity layer for P waves near 150 km may be present

beneath the Canadian shield, but is absent beneath the Australian shield. The significance of this difference and the presence of a discontinuity near 85 km, which appears in both the Canadian and Australian shield models, will be discussed in Chapter 8.

4.4 The Cannikin Experiment

A study of the variations in P station anomalies across the eastern boundary of the Australian shield, using the nuclear explosion Cannikin on Amchitka Island as a signal source, is described in the appended publication by Cleary, Simpson and Muirhead (1972). Ten of the portable instruments described in Chapter 3 were installed along a 1700 km traverse approximately 90.5^{o} from the explosion site (Figure 4-13a). The P onset at one of these stations is shown in Figure 3-4b. Travel times and distances to the ten portable stations and four permanent stations along the same traverse are given in Table 4-6 along with station anomalies calculated from the 1968 P Tables (Herrin et al., 1968) and the P table of Hales, Cleary and Roberts (1968b). In Figure 4-13b the two sets of anomalies are shown reduced to a common baseline. Cleary, Simpson and Muirhead showed that the effects of structural irregularities near the source, changes in crustal structure along the traverse, onset timing errors and differences in distance from the source to receivers are minor, and concluded that the scatter in the data of Figure 4-13b may be due to local

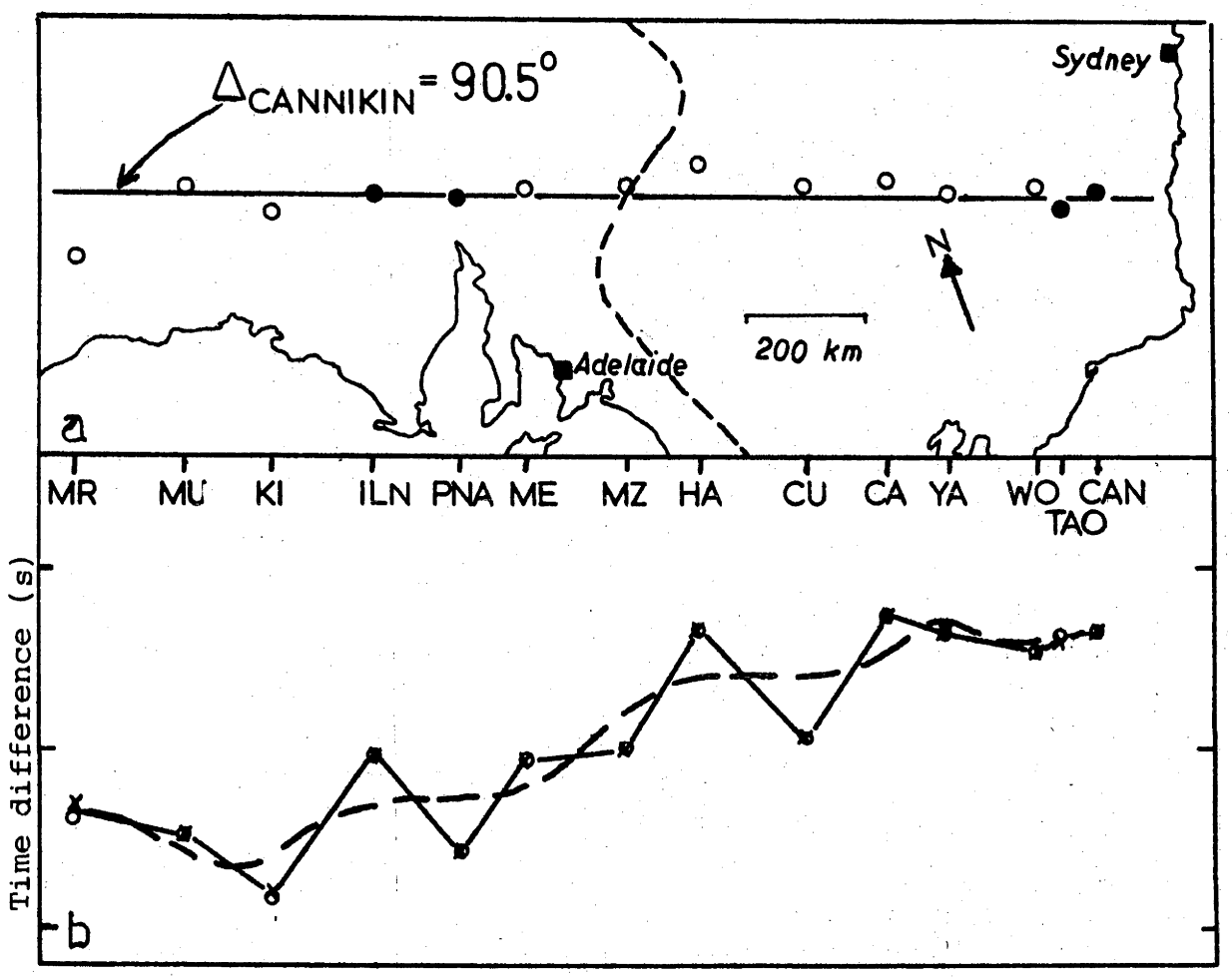

Figure 4-13. The Cannikin traverse.

a) Station locations. Shaded and unshaded circles represent permanent and portable stations. The dashed line indicates the eastern extent of exposed Precambrian rocks.

b) Differences in P station anomalies along the traverse, calculated from the Herrin et al. (1968) P tables (O) and the P table of Hales, Cleary and Roberts (1968b) (X). The smooth curve has been derived by taking means of adjacent points.

(after Cleary, Simpson and Muirhead, 1972)

TABLE 4-6. Cannikin traverse station data

Station	Distance[1] (deg)	Travel time[1] (s)	Station anomaly[2] (s) (a)	(b)
Maralinga (MR)	91.34	786.13	-0.58	-0.92
Mulgathing (MU)	90.47	781.99	-0.70	-1.10
Kingoonya (KI)	90.77	782.97	-1.02	-1.40
Island Lagoon (ILN)	90.45	782.30	-0.23	-0.63
Partacoona (PNA)	90.55	782.20	-0.78	-1.18
Melton (ME)	90.44	782.17	-0.27	-0.67
Mazar (MZ)	90.30	781.62	-0.20	-0.61
Harcourt (HA)	90.01	780.90	+0.47	+0.05
Curragh (CU)	90.36	781.90	-0.12	-0.53
Carrathool (CA)	90.21	781.86	+0.54	+0.13
Yanco (YA)	90.38	782.59	+0.45	+0.05
Woodstock (WO)	90.36	782.39	+0.37	-0.04
Talbingo (TAO)	90.79	784.40	+0.37	-0.01
Canberra (CAN)	90.34	782.40	+0.45	+0.04

[1]Calculated from the shot coordinates and origin time given by NOAA.

[2]Difference between observed time and time calculated from (a) Herrin et al. (1968) P tables, (b) P table of Hales, Cleary and Roberts (1968b), with ellipticity correction applied.

(from Cleary, Simpson and Muirhead, 1972)

variations in upper mantle structure beneath the stations or minor irregularities in velocity along the entire path. In spite of this scatter, there is an obvious trend towards earlier arrivals in a westerly direction along the Cannikin profile in Figure 4-13b. The trend appears most pronounced near the center of the traverse close to the eastern limit of exposed Precambrian rocks (see Figure 1-1).

Hales et al. (1968) investigated the origin of P station anomalies and concluded that they are related to variations in the extent of the upper mantle low velocity layer. They showed that the wedging out of a pronounced low velocity layer between the tectonically active western United States (the Nevada model, Figure 2-17) and the stable eastern region (the Early Rise model, Figure 2-16) was sufficient to account for observed differences in station anomalies for these two areas. A similar explanation is proposed for the gradual decrease in station anomalies across the boundary of the Australian shield.

Although there has been no detailed study of velocities in the uppermost mantle beneath eastern Australia, there are limited data which indicate that a low velocity layer for P wave exists beneath this region. Sutton and White (1966) suggested that a low velocity layer below 60 km was responsible for delayed P arrivals and prominent later arrivals observed near 13° from earthquakes in southeastern Australia.

In Figure 4-14, two hypothetical models for southeastern Australia are presented in an attempt to determine the extent of a low velocity layer required to satisfy the difference in P station anomalies observed along the Cannikin traverse. Cleary (1973) has reviewed the available data on crustal structure in eastern Australia, which indicate an upper crustal velocity of 6.0 km/s with a velocity of 6.5 km/s below 20 km, a P_n velocity of 7.95 km/s and a crustal thickness of 30 km. These values have been used in the models A and B (Figure 4-14) for the eastern end of the Cannikin traverse. The Ord P model has been used for the western end of the traverse. All three models, shown in Figure 4-14b, are assumed to be the same below 350 km, where the velocity is 8.7 km/s. In the A model the velocity at 85 km is decreased from 7.95 km/s to V_{min} and then increased linearly to 8.7 km/s at 350 km. In model B the velocity is held constant at V_{min} in a low velocity layer extending from 85 to 125 km. In Figure 4-14a the time (T), required for a ray from 90.5° (slowness 4.63 s/deg) to travel from a depth of 350 km to the surface, is shown as function of V_{min} for models A and B. Also shown in Figure 4-14a is the difference in time (ΔT) between the times for the two eastern models and the time (46.0 s) required for a ray at the same distance to pass through the Ord P model. The A and B models in Figure 4-14b show the values of V_{min} (7.72 km/s in case A and 7.53 km/s in case B) required to give the observed difference in station anomalies (1.3 s) along the Cannikin

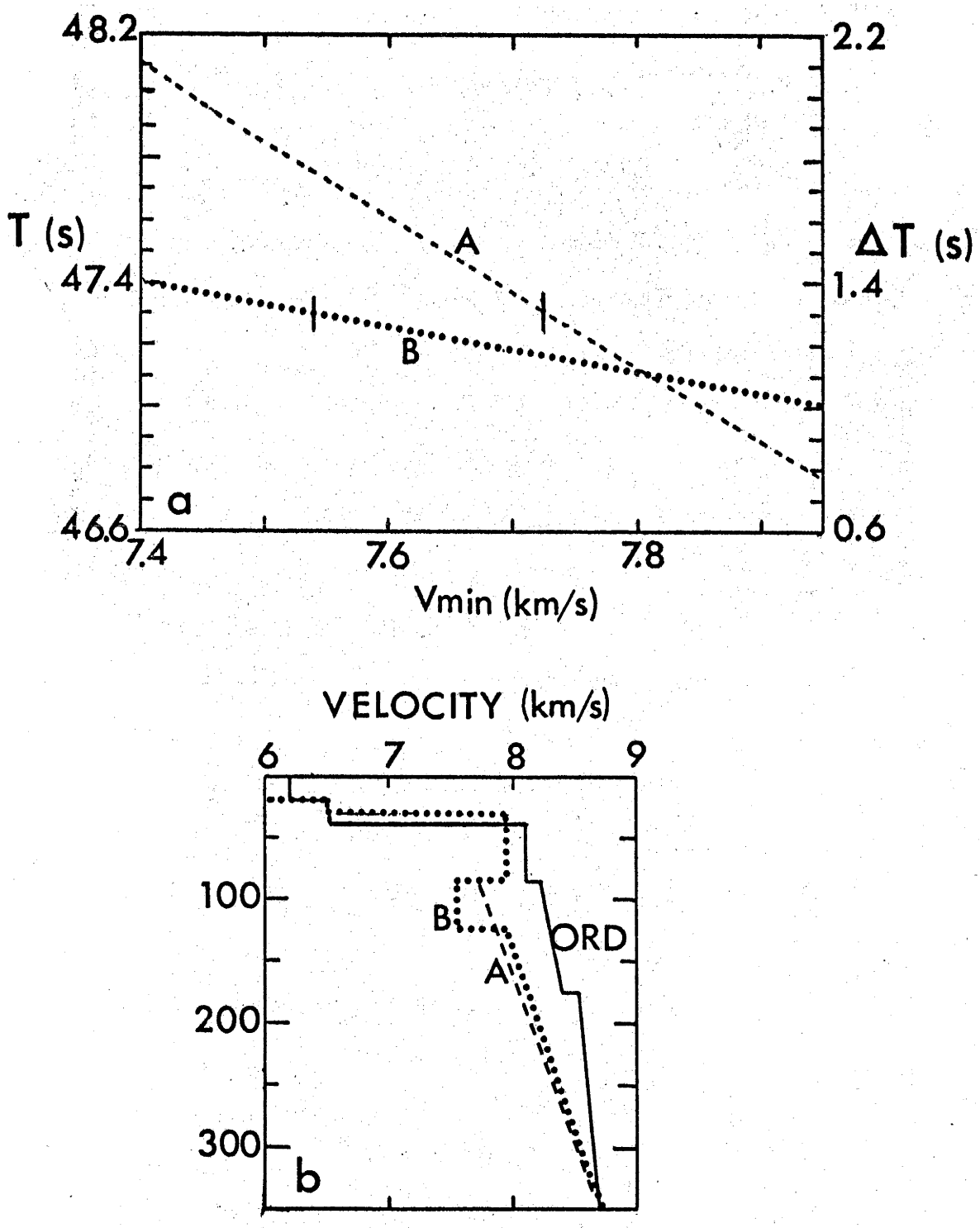

Figure 4-14. Hypothetical models for southeastern Australia (for explanation see text).

traverse.

There is, of course, an infinity of models for eastern Australia that will satisfy the constraints imposed by the station anomaly difference and the models A and B are only presented to indicate the approximate extent of possible low velocity layers in this region. A decrease in the thickness of the low velocity layer in model B, for instance, would decrease the required value of V_{min}; a decrease in the velocity contrast between the Ord P model and models A or B below 125 km would increase the extent of the low velocity required in either model. The B model is similar to the Nevada 2 model used by Hales et al. (1968), although the difference in station anomalies between the western and central U.S. (1.5 s) is greater than that observed on the Cannikin traverse and the minimum velocity of 7.5 km/s in the Nevada 2 model is slightly less than in model B. A more complete knowledge of the extent of a low velocity layer in eastern Australia must await detailed studies of travel times and velocities in this region.

CHAPTER 5

SEISMIC ARRAYS

5.1 Introduction

Phased seismic arrays, in the sense of spatial arrangements of seismometers which are recorded with a common time base on magnetic tape, were initially introduced as a tool for the detection and identification of nuclear explosions. The early "Geneva arrays" (SIPRI, 1968) were small in dimension compared to the wavelengths of recorded signals and were intended to provide signal to noise ratio (S/N) improvement, on the assumptions that the signals were coherent, and the noise incoherent, over the dimensions of the array. A S/N improvement of $\sqrt{n}$ (where n is the number of seismometers) can then be achieved by straight summation. The results from an early group of these small arrays in the United States did not substantiate the assumption of incoherent noise over a limited range (less than 5 km) (SIPRI, 1968) and the next generation of arrays was developed with wider aperture. The specially designed arrays (in contrast to regional networks recording with a common time base) have developed along two lines: 1) the medium aperture (20 km) United Kingdom Atomic Energy Authority (UKAEA) arrays (EKA - Scotland, YKA - Canada, WRA - Australia and GBA - India); and 2) the large aperture (200 km) American arrays (LASA - Montana and NORSAR - Norway). Since the extent of these arrays is comparable with or

larger than the signal wavelengths of interest in body wave seismology, it becomes possible, by inserting appropriate delays between the sensors, to use the array as a three dimensional directional filter in a manner analogous to that used in radio and radar arrays. In the seismological application the direction of approach of a signal is usually specified by the azimuth (the horizontal angle) and the apparent velocity or slowness (defining the vertical angle of incidence).

Seismic arrays can be considered in three modes of operation:

1) S/N improvement. The insertion of delays between sensors creates an azimuth and slowness filter. Since, for the Earth, distance is a unique function of slowness, this process enhances signals originating in one location with respect to those from another. The appropriate delays can be determined directly by the array, or, for a specific source location, they can be approximated from the calculated azimuth and standard tables of slowness as a function of distance.

2) Determination of seismic parameters. Using signals from events in known locations, values of azimuth deviations and of slowness as a function of distance can be determined.

3) Event location. If a table of slowness as a function of distance is available, either from 2) above or from standard tables, measured values of slowness and azimuth can be used to specify the azimuth and distance to, and hence the location of, the source of the recorded

signal.

Modes 1) and 3) are most directly related to the detection and identification of nuclear explosions. As well as making it possible to observe events which might otherwise go undetected, the S/N improvement obtained from 1) provides a low noise environment in which it is then possible to carry out more sophisticated processing. Mode 3) provides a means of real-time location of events so that those from areas of interest can be immediately processed in detail.

It is in the second mode of operation that arrays are able to provide the most useful information about the internal structure of the Earth. The purpose of the remainder of this chapter is to describe the operation of one particular array and the method used to determine slowness from array data. The following chapters will describe how such data has been used in the determination of Earth structure.

5.2 The WRA Array

The Warramunga array (WRA), located near Tennant Creek in north central Australia, is one of the UKAEA medium aperture arrays and is operated jointly by the UKAEA and the Australian National University (ANU). The array consists of twenty 1 Hz Willmore Mk II vertical seismometers at approximately 2.5 km spacing along two arms of an asymmetrical cross (Figure 5-1). The array installation facilities are shown schematically in Figure 5-2a. The recording, data storage and analogue

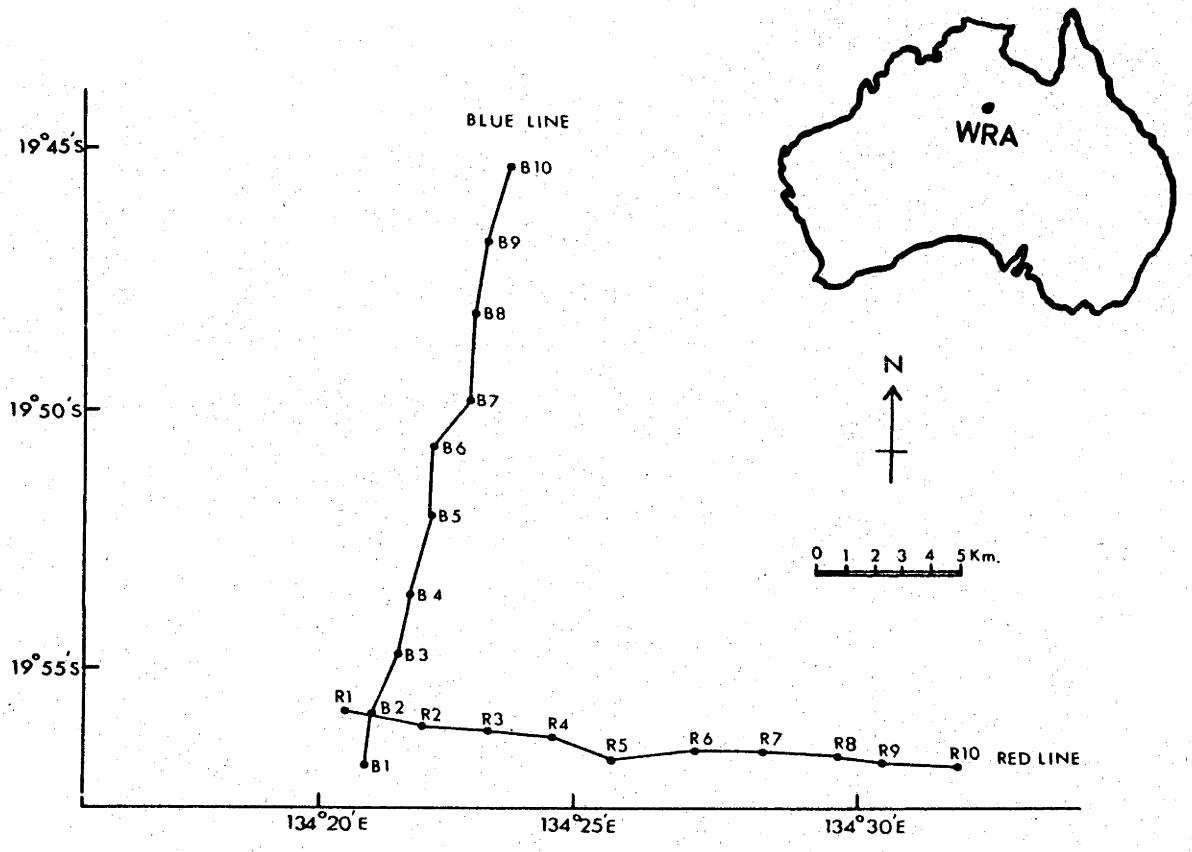

Figure 5-1. The WRA array.

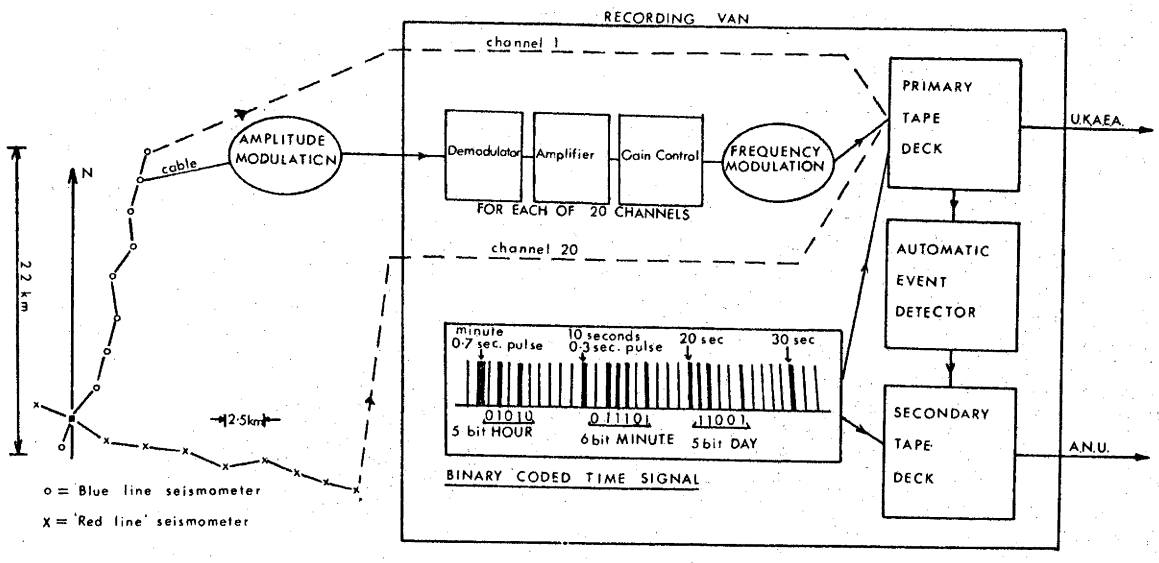

Figure 5-2a. Schematic diagram of the WRA recording system. (from King, 1971)

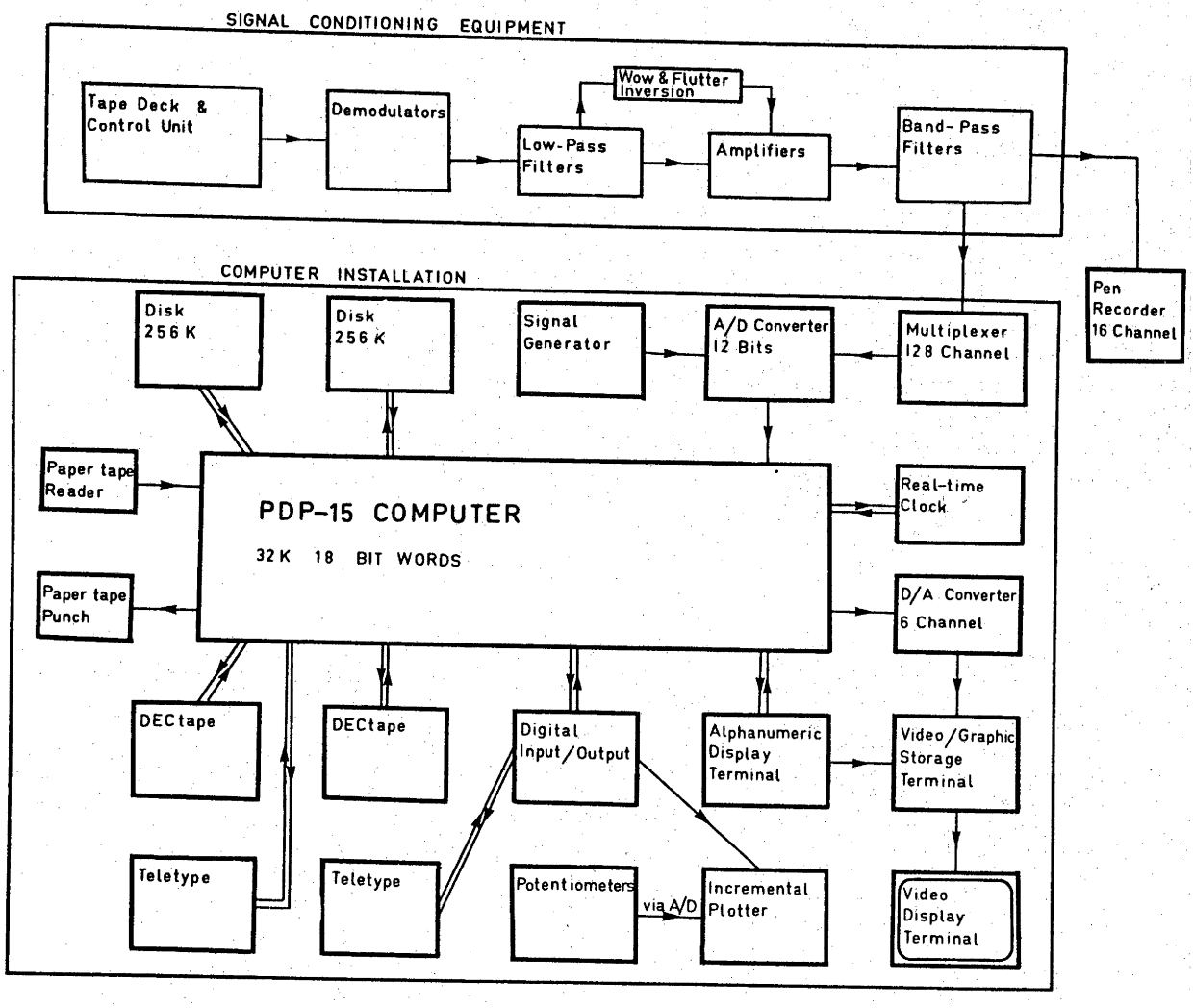

Figure 5-2b. Schematic diagram of the ANU processing system for WRA data. (from King et al., 1973)

processing equipment have been described, for the UKAEA arrays in general, by Keen et al. (1965) and, for the WRA system in particular, by Muirhead (1968). The seismic and timing information are recorded in frequency modulation (fm) form, along with a reference frequency channel, on two 24 track magnetic tape recorders. One tape (which goes to the UKAEA) records continuously and the other (retained by the ANU) is an edited version containing only events detected by an on-line automatic event detector at the array.

A schematic diagram of the playback facilities at ANU is shown in Figure 5-2b. The analogue equipment is described by Muirhead (1968). Playback is carried out with a speed-up factor of 12.5. The fm signals from the tape are demodulated, corrected for tape speed variations and band-pass filtered before being fed to a 16 channel pen recorder or to the computer installation.

A PDP15 computer forms the basis of the digital processing part of the system, which is described by King et al. (1973). After being digitized by a multiplexed analogue-to-digital (A/D) converter, the seismic and timing information is analysed using an adaptive processing technique (King et al., 1973) which will be briefly described below. The processed data can be presented graphically on a Calcomp incremental plotter or listed on a teletype printer.

5.3 Slowness and Apparent Azimuth Determination

Various methods can be used to determine the slowness and apparent azimuth of a signal crossing an array; either directly by measuring the delays between onset time at the sensors, or indirectly by inserting delays corresponding to various azimuths and slownesses and searching for an absolute maximum in the array response. Wright (1970) and King et al. (1973) have discussed a number of these methods, with particular reference to the processing of WRA data.

Early methods - A detailed analysis is given by Wright (1970) of a least squares method of determining slowness and apparent azimuth from onset times used in the first WRA study of mantle velocities (Wright, 1970, Wright and Cleary, 1972). The technique used to determine relative onset times (Cleary et al., 1968) involves visually matching all or part of the first few cycles of an arrival at each seismometer location. With a time scale of 40 mm/s, it is possible to determine onset times to approximately 0.015 s. These times are then used to determine, in a least squares sense, the best azimuth and slowness of a plane wavefront crossing the array, using the method described by Kelly (1964) and Otsuka (1966). Although it is possible to determine slowness and azimuth of a clear arrival to a precision of 2%, the procedure is tedious and does not provide reliable determinations for later arrivals. Because of interference between arrivals and changes in waveform it is difficult to determine the onset of a later phase as

it crosses the array unless the arrival is clear and well separated from the initial arrival. Wright and Muirhead (1969) and Wright (1970) have also used a correlation method, described by Birtill and Whiteway (1965), which they found to be useful in enhancing the arrival of later phases, but unsuitable for the precise determination of slowness and azimuth.

Adaptive processing - In an array study of upper mantle velocities, the multiplicity of arrivals in the distance range 10^{o} to 30^{o} makes it important that a method of slowness determination be available that can cope with multiple arrivals in the first 10 s after the initial onset. The method must also be fast enough to allow the processing of a sufficient quantity of data to define the nature of the complete travel time curve. This is especially important in earthquake studies, where scatter in the data caused by epicenter mislocation must be averaged out on the basis of a large number of observations. The adaptive processing procedure described by Gangi and Fariborn (1968), which has been implemented on the ANU processing system by King et al. (1973), satisfies these requirements. This was the method used in a study of upper mantle phases to be described in the next chapter. The following is a brief description of the method, based on the paper by King et al.

Initial estimates of the expected azimuth and apparent velocity for the event to be processed (determined from the NOAA epicenter location and the JB tables, and

reported for WRA in the monthly GEDESS listings (Young and Gibbs, 1968)) are used to calculate the steering delays:

$$t_i = \frac{R_i \cos (\Phi_e - \theta_i)}{v_e}$$

where

(R_i, θ_i) are the polar coordinates of the i^{th} seismometer

and

Φ_e, v_e are the expected azimuth and apparent velocity.

After the signals from all operating array channels are filtered (0.4 - 3.0 Hz) and digitized at approximately 24 samples/recorded s, the delays (t_i) are used to form the array beam:

$$\Sigma R + \Sigma B$$

and the time averaged product (TAP, loosely termed the correlogram):

$$(\Sigma R \times \Sigma B)^{\frac{1}{2}}$$

(see Figure 5-3b), where ΣR and ΣB refer to the appropriately delayed sums of the signals from the Red (E-W) and Blue (N-S) array arms.

For each portion of the signal to be analysed, the adaptive processing method is used to determine refinements to the steering delays (t_i) by subtracting the selected portion of each channel from the array beam, cross-correlating the channel with the depleted

beam, and finding the delay corresponding to a correlation maximum. The re-aligned channel is then added back into the beam and the process repeated for the remaining channels. The refined time delays are used to find revised values for the apparent azimuth and velocity from the normal equations given by Kelly (1964):

$$\sum_{i=1}^{n} x_i (t_i - x_i P - y_i Q) = 0$$

$$\sum_{i=1}^{n} y_i (t_i - x_i P - y_i Q) = 0$$

$$\sum_{i=1}^{n} t_i - x_i P - y_i Q = 0$$

where

$$P = \frac{\sin \Phi}{v}$$

$$Q = \frac{\cos \Phi}{v}$$

$t_i = T_o - T_i$ = delay for i^{th} seismometer with coordinates (x_i, y_i) and arrival time T_i

Then

T_o = arrival time at the origin of seismometer coordinates

$v = (P^2 + Q^2)^{-\frac{1}{2}}$

and $\Phi = \tan^{-1} (P/Q)$

An updated array beam is formed from the new estimates of apparent velocity (v) and azimuth (Φ), the steering delays are again revised and the process repeated until convergence is reached. The method is "adaptive" in that the time delays resulting from each iteration are used to provide a refined reference signal (array beam) for the subsequent iteration.

The portions of the signal to be analysed can be selected manually, or automatically determined by allowing the computer to select significant peaks in the TAP trace. The apparent velocity and azimuth determinations are normally formed with a window length of 0.75 s which is moved 0.333 s between each determination.

The number of iterations required for well-defined signals is, in general, less than five. When convergence is reached, results are printed and/or plotted as required. The sizes of the symbols plotted are indicative of the average maximum correlation between the beam and the channels, no symbols being plotted when the correlation average falls below a pre-set level.

Figure 5-3a shows the array channels for a particularly clear event from New Britain and the resulting adaptive processing solution is shown in Figure 5-3b. The result for two less clear events from New Guinea are shown in Figure 5-4a,b and Figure 5-5.

The complete solution shown for these events, including the digitization and plotting, takes less than 15 minutes, depending on the length of records to be analysed. Each determination of slowness and azimuth

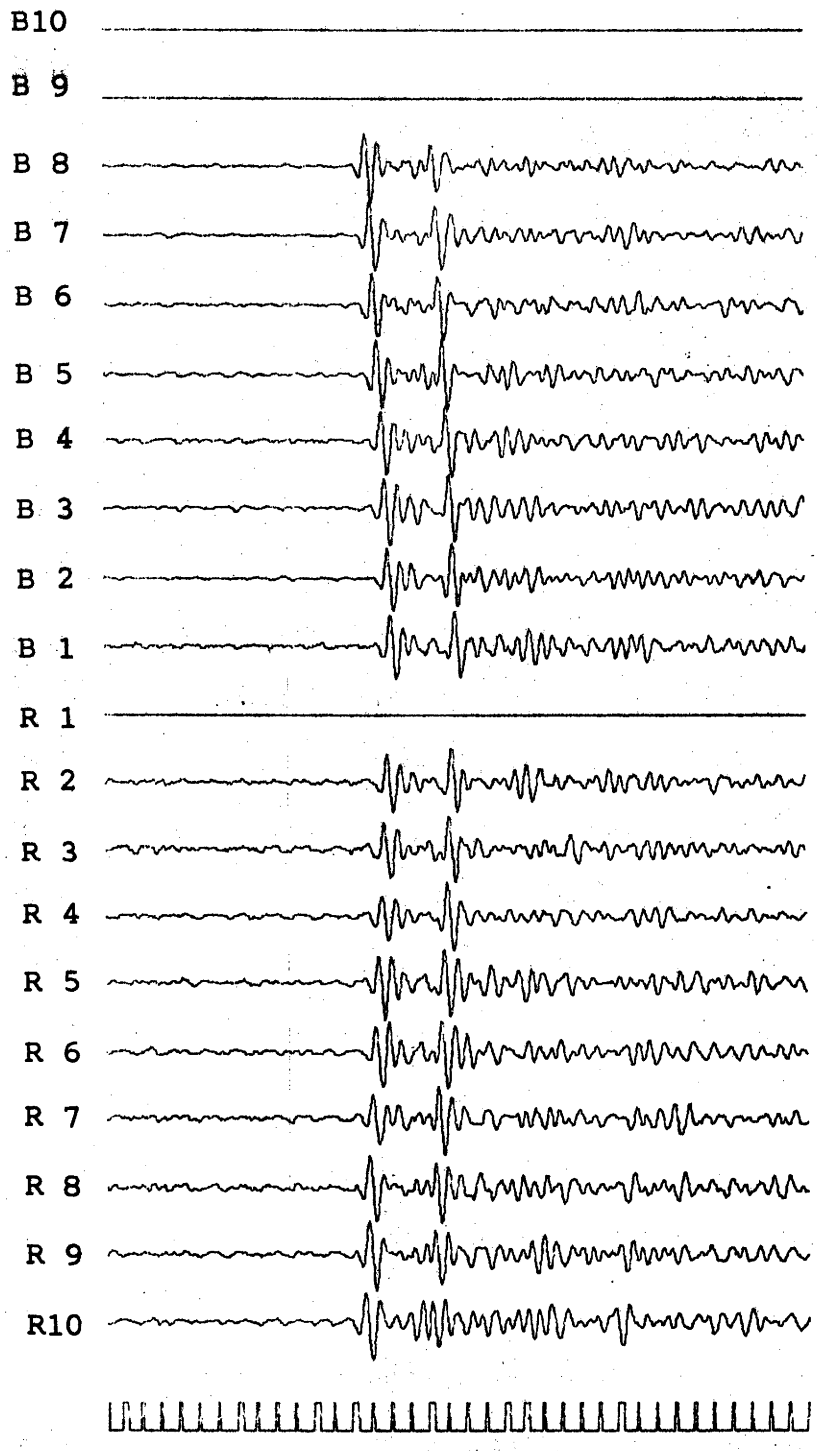

Figure 5-3a. Array channels for event 89 (Appendix B) Faulty channels have been blanked out. Amplitudes are normalized to the maximum in each channel.

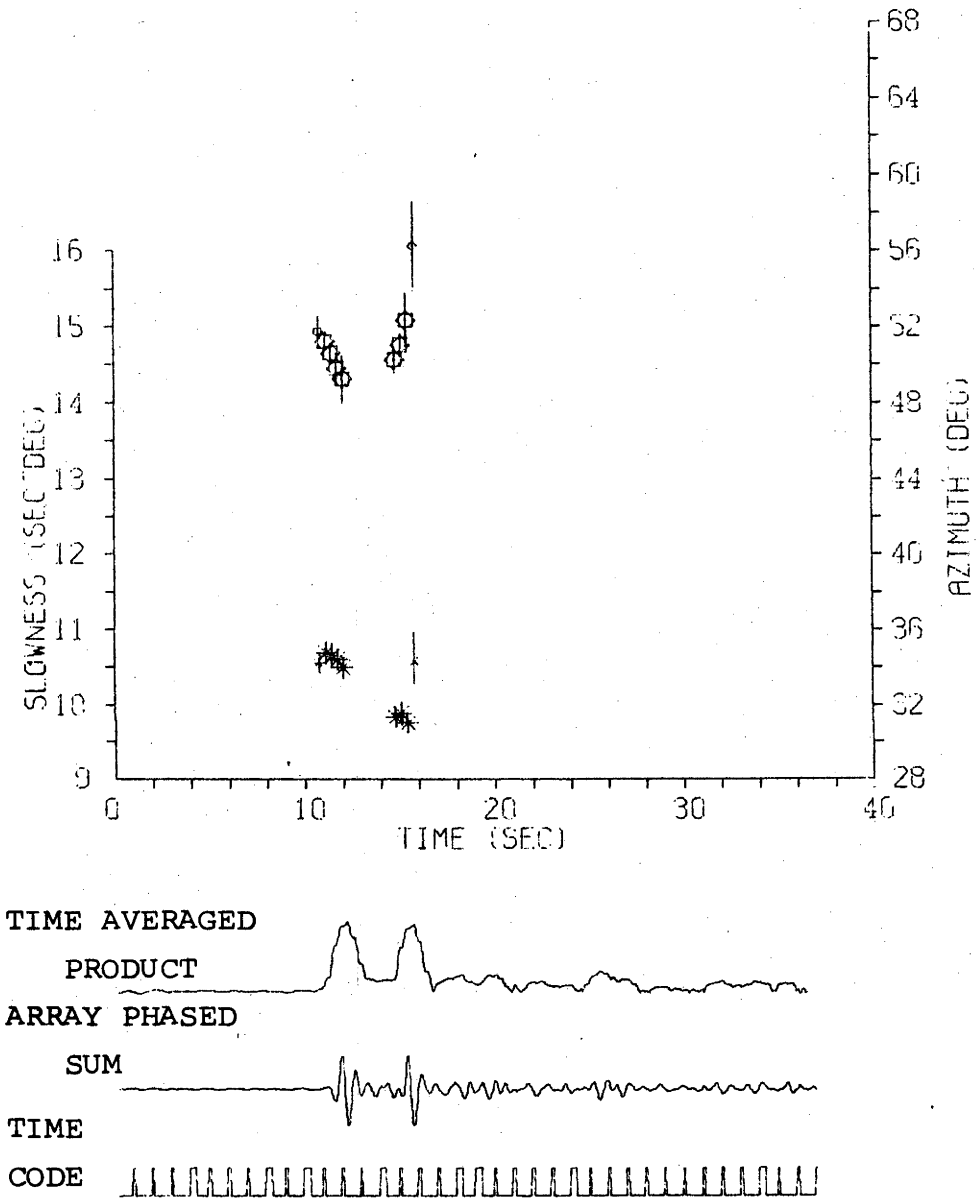

Figure 5-3b. Adaptive processing solution for event 89 (Δ_c = 21.4°). *'s are slowness determinations (left scale) and 0's are apparent azimuth determinations (right scale).

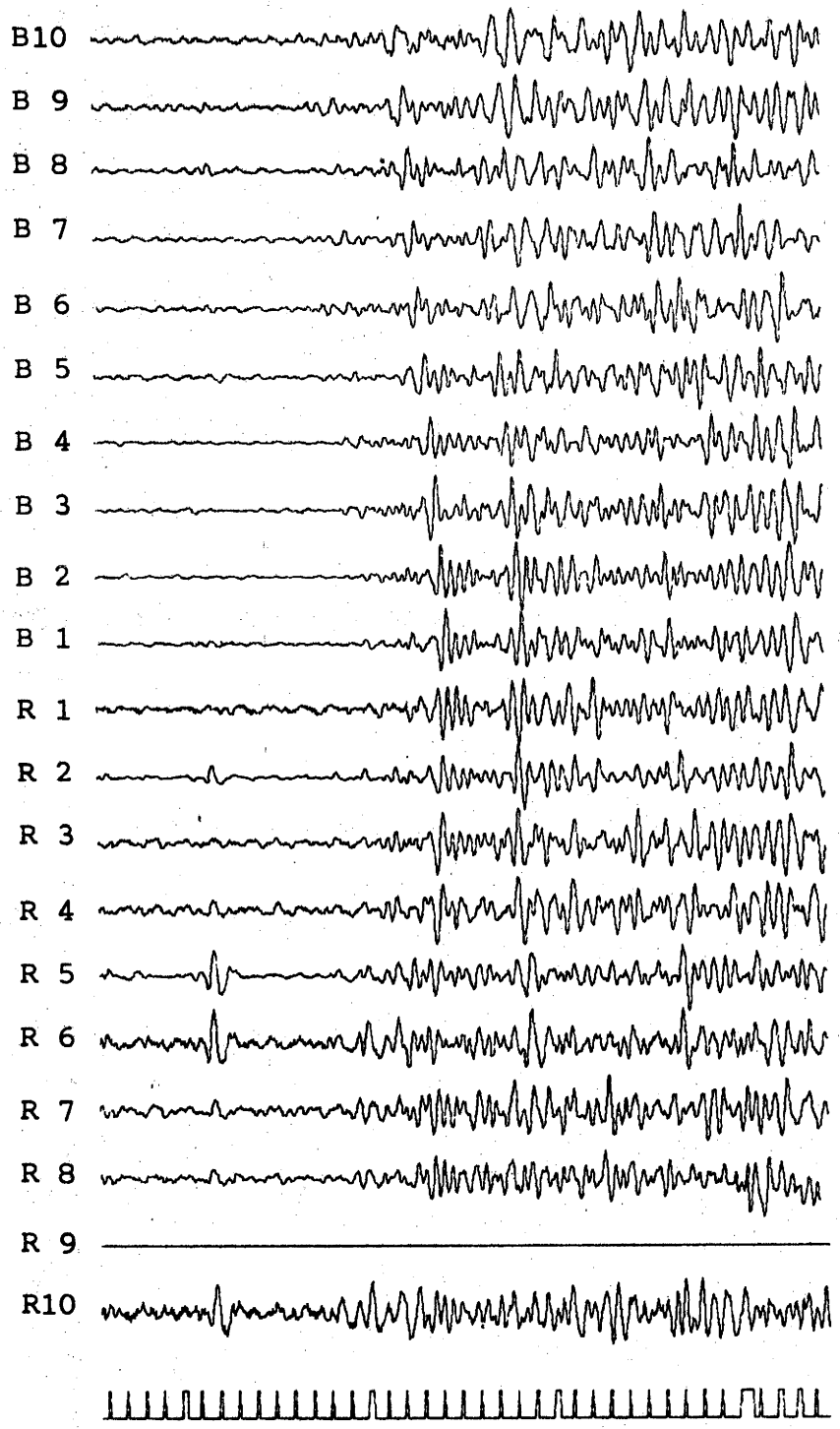

Figure 5-4a. Array channels for event 20 (Appendix B). The signal at 6 s on the Red line is a noise spike.

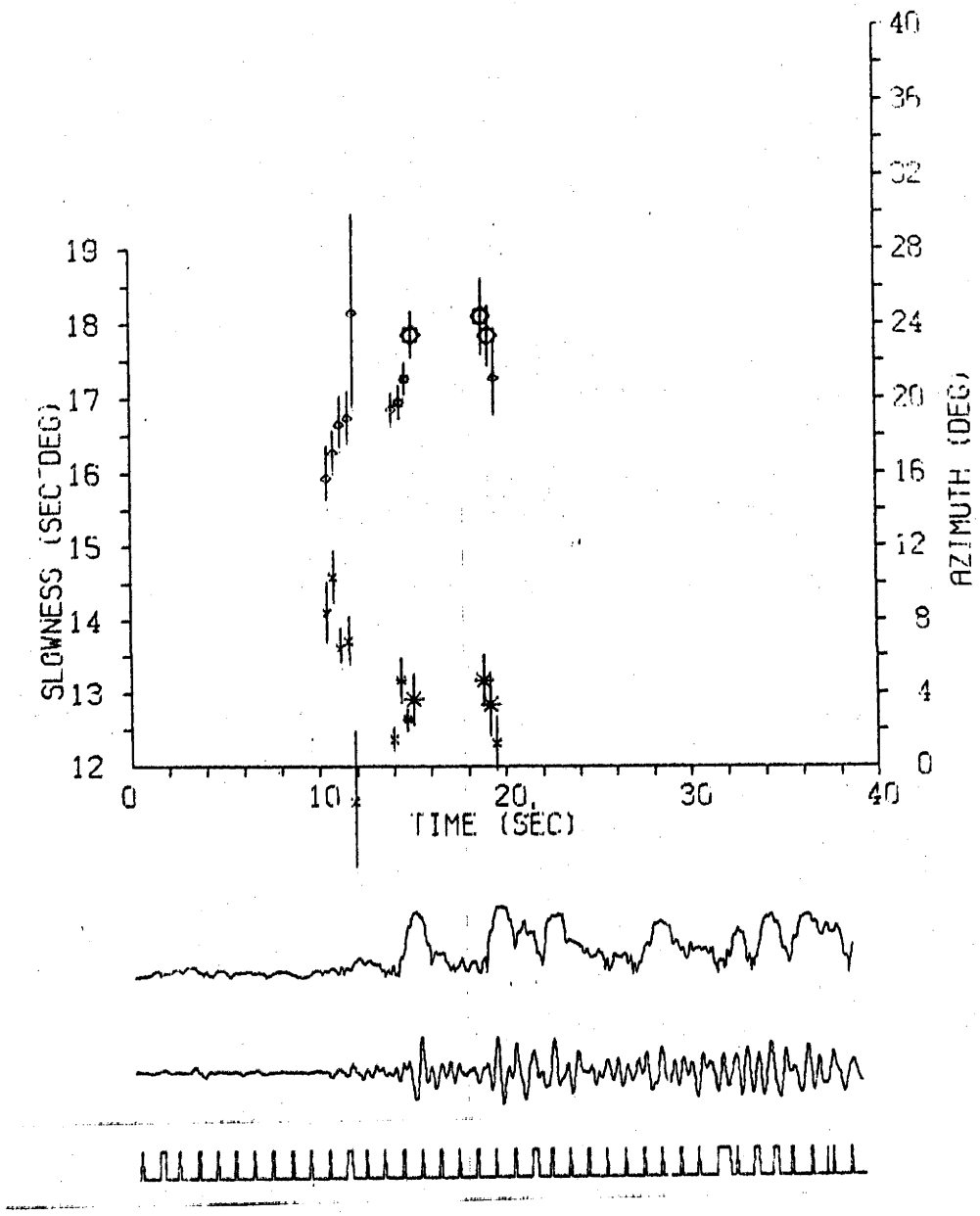

Figure 5-4b. Adaptive processing solution for event 20 (Δ_c = 17.7°).

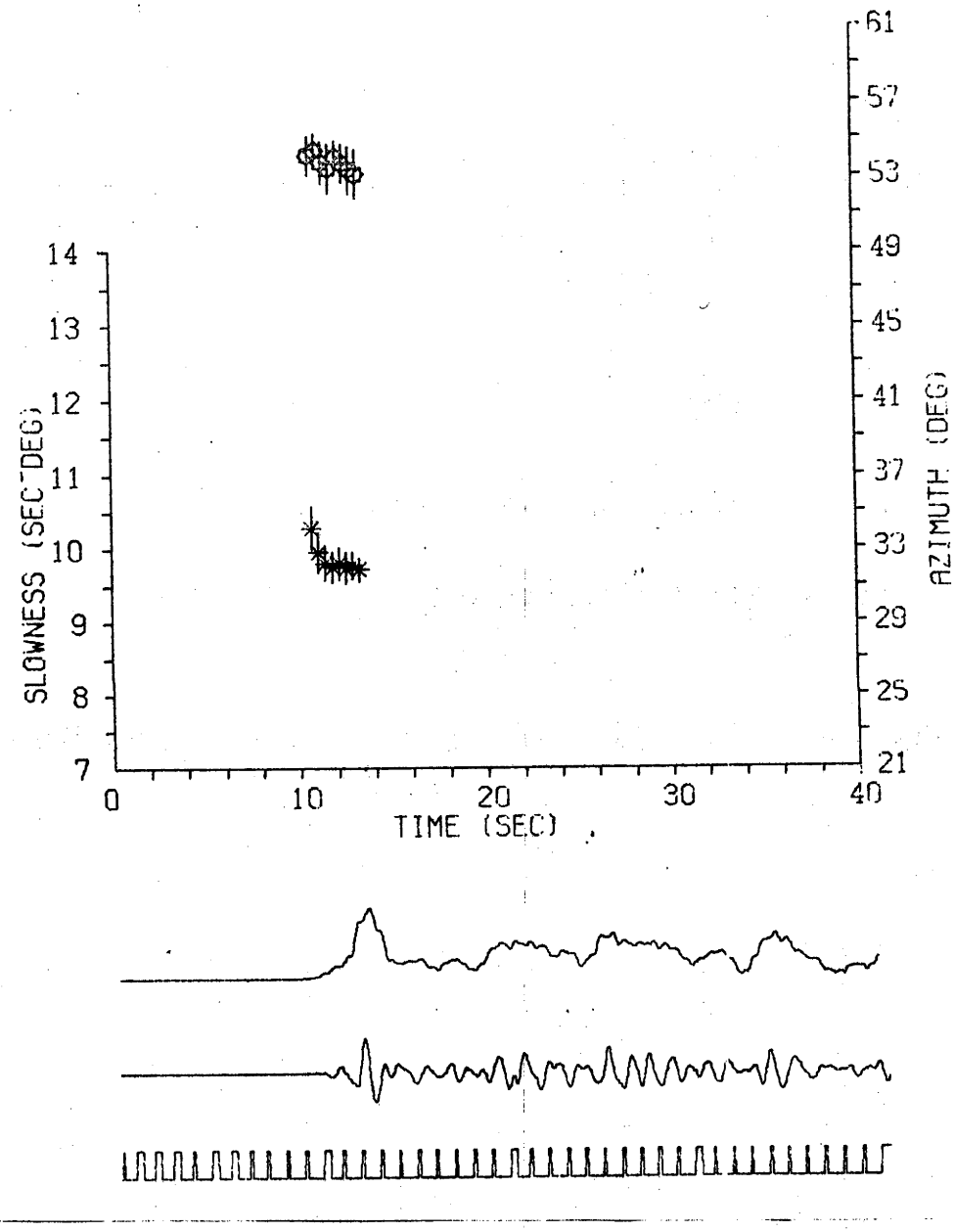

Figure 5-5. Adaptive processing solution for event 128 ($\Delta_c = 23.6^{\circ}$).

takes approximately 10 to 25 s depending on the rate of convergence. The improvement in S/N for many events is substantial (e.g. (Figure 5-4b) and this, along with the resolution provided by the TAP trace, greatly improves the identification of the onset of later arrivals.

The accuracy of the slowness determinations depends strongly on the nature of the signal. For clear and well separated arrivals (e.g. Figure 5-3b) the measurements of slowness are very consistent and can be determined with a precision of better than 0.1 s/deg. In many cases, however, interference between closely spaced arrivals causes drift in the measured values of slowness (e.g. Figure 5-5). King et al. have investigated this effect using real and synthetic data and, in general, it is found that, when two well defined phases interfere, the slowness values drift systematically between the correct values for the first and second arrivals (e.g. Figure 5-5). The effect of local structure near the array, which introduces a bias in the observed values of slowness, will be discussed in the next chapter. Significant differences in the apparent azimuths for different arrivals from the same event may result from the effect of lateral variations in structure along the ray paths but this has not been investigated in detail.

CHAPTER 6

UPPER MANTLE DATA FROM WRA

6.1 Tectonic Setting

The location of WRA in relation to the general tectonic pattern of Australia and surrounding regions was sketched in Figure 1-1. The Ord River project described in Chapter 4, and a small scale refraction study at WRA by Underwood (1967), indicate that the crustal and sub-crustal structure of central Australia is typical of stable shields in other continental regions, with a crustal thickness of approximately 40 km and P_n velocity near 8.1 km/s. The array itself is situated on upper Precambrian granitic outcrop which intrudes the lower Proterozoic Warramunga geosyncline. There is evidence that the local structure beneath the array may be quite complex, but a discussion of this will be delayed until later in this chapter.

The region to the north of Australia is one of the most complex areas of present day tectonic activity. The seismicity and tectonics of the region have recently been discussed in detail by a number of authors including Denham (1969), Dewey and Bird (1970), Fitch (1970, 1972), Fitch and Molnar (1970), Katili (1971a,b) and Johnson and Molnar (1972). Seismic and volcanic activity in this region is an expression of the complex interaction between the Pacific, Indian-Australian, Asian and Philippine Sea

plates (see Figures 1-1 and 6-1). Although the intricacies of the plate motions do not concern us here, there are two aspects of the seismicity which bear directly on the collection and interpretation of WRA upper mantle data. Firstly, the distribution of epicenters determines the distance ranges in which data are available; and secondly, the presence of deep zones of activity along descending plate margins, indicating anomalous zones within the upper mantle, limits the lateral homogeneity along ray paths from source region to WRA.

The closest events to the north of WRA occur beneath the Banda Sea at a distance of approximately 12^{o}. Activity to the north and northwest then extends to beyond 30^{o} within two azimuth groups: along the Philippine Sea plate margin, and along the Sunda arc. To the northeast of WRA, diffuse activity along the northern coast and central part of the main island of New Guinea begins at a distance of approximately 15^{o}, with more concentrated regions of major activity extending to beyond 30^{o} along the New Britain, New Ireland and Solomon Island arcs.

Because of structural complexities near the array, it is desirable to use events confined to a narrow azimuth range. The line of epicenters north of WRA through the Philippine Sea most readily meets this requirement; but early work, described in the next section, indicated that complexities in structure encountered by rays passing beneath the Banda Sea and Philippine Trench introduce major uncertainties into the

interpretation of travel time and slowness data from events in this region. Although the azimuth range covered by events at distances of 15^{o} to 30^{o} from New Guinea is larger than that to the north, the azimuth range is still narrow for distances from 18^{o} to 25^{o}. The New Guinea region has the added advantage that upper mantle structure between this region and WRA is not disturbed by anomalous zones of descending plates. The stable platform of the Australian continent extends into the main island of New Guinea. Thus for events out to 30^{o}, the critical region between the array and the point where rays bottom (i.e. out to about 15^{o}) lies mainly beneath the stable Australian continent. Even in the source region itself, the trend of the Benioff zones in the New Britain and New Ireland regions is generally away from the continent, so that energy travelling toward WRA spends only a small portion of its total path in the anomalous zone near the source.

6.2 Early WRA Upper Mantle Studies

As part of an investigation of lower mantle structure, Wright (1970) carried out a preliminary slowness study of upper mantle velocities using data from earthquakes in both the Indonesia-Philippines and New Guinea regions. Even with a limited amount of data, it was obvious that differences in travel time, slowness and slowness bias existed between these two regions. It was suggested by Wright that the best method to correct for the slowness

bias, caused by structure beneath the array (see Section 6.4.2), was on the basis of observed travel times. Thus, one of the first steps in the present study was to construct first arrival travel time curves for WRA.

6.2.1 Travel times to WRA, 0°-30°

The UKAEA provides a monthly report, GEDESS (Young and Gibbs, 1968), containing a chronological listing of all NOAA epicenter information, along with azimuths, distances and expected JB arrival times and apparent velocities, at each of the UKAEA arrays. Using these reports, arrival times at WRA are routinely converted to JB residuals and filed on cards. The GEDESS lists were used to find all events within 30° of WRA which occurred during the period September 1968 to December 1969. The JB residuals for all of these events which were recorded at WRA (Figure 6-1) are shown in Figure 6-2 and in Figure 6-3 the residuals have been converted back to travel times using the times from the JB tables.

The magnitudes of the JB residuals will be discussed later in this chapter. At this stage it is sufficient to note that the residuals appear to be independent of distance beyond about 22° and that the scatter also reduces beyond this distance. These diagrams also indicate the extent of differences in the travel times from the New Guinea and Indonesia-Philippines regions. The times from the Indonesia-Philippines group are generally earlier, which may reflect the presence of higher velocity slabs of descending lithosphere along the ray paths from the Philippine Sea region to WRA.

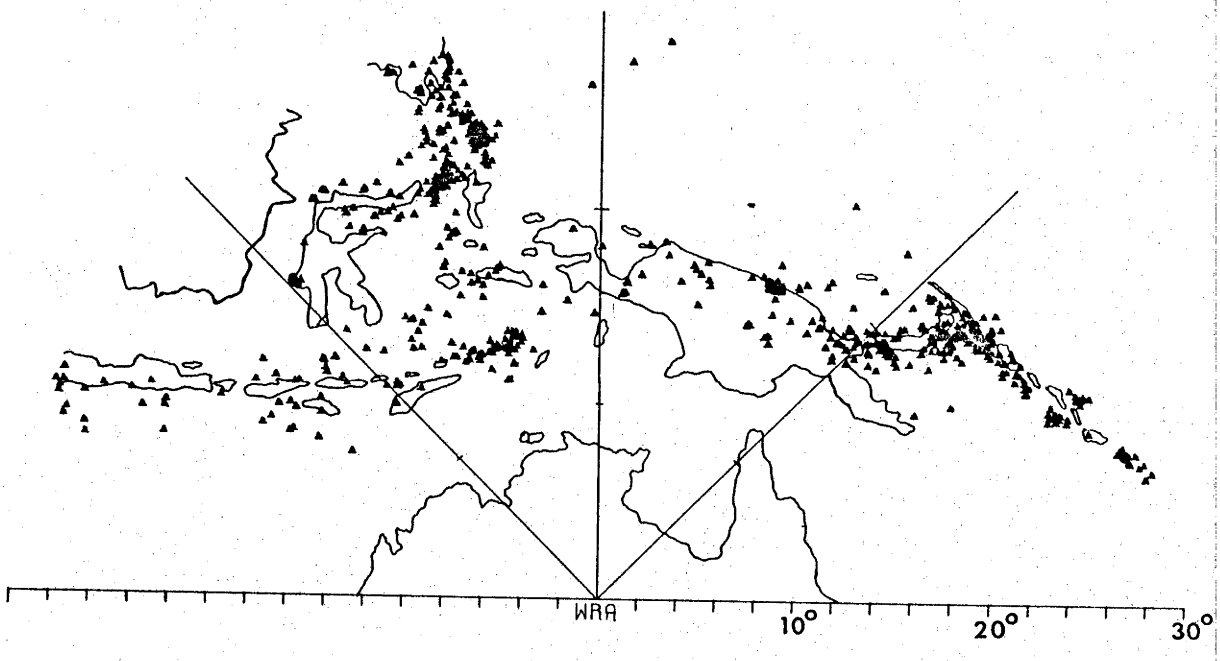

Figure 6-1. NOAA epicenters for events within 30° of WRA recorded during the period September 1968 to December 1969.

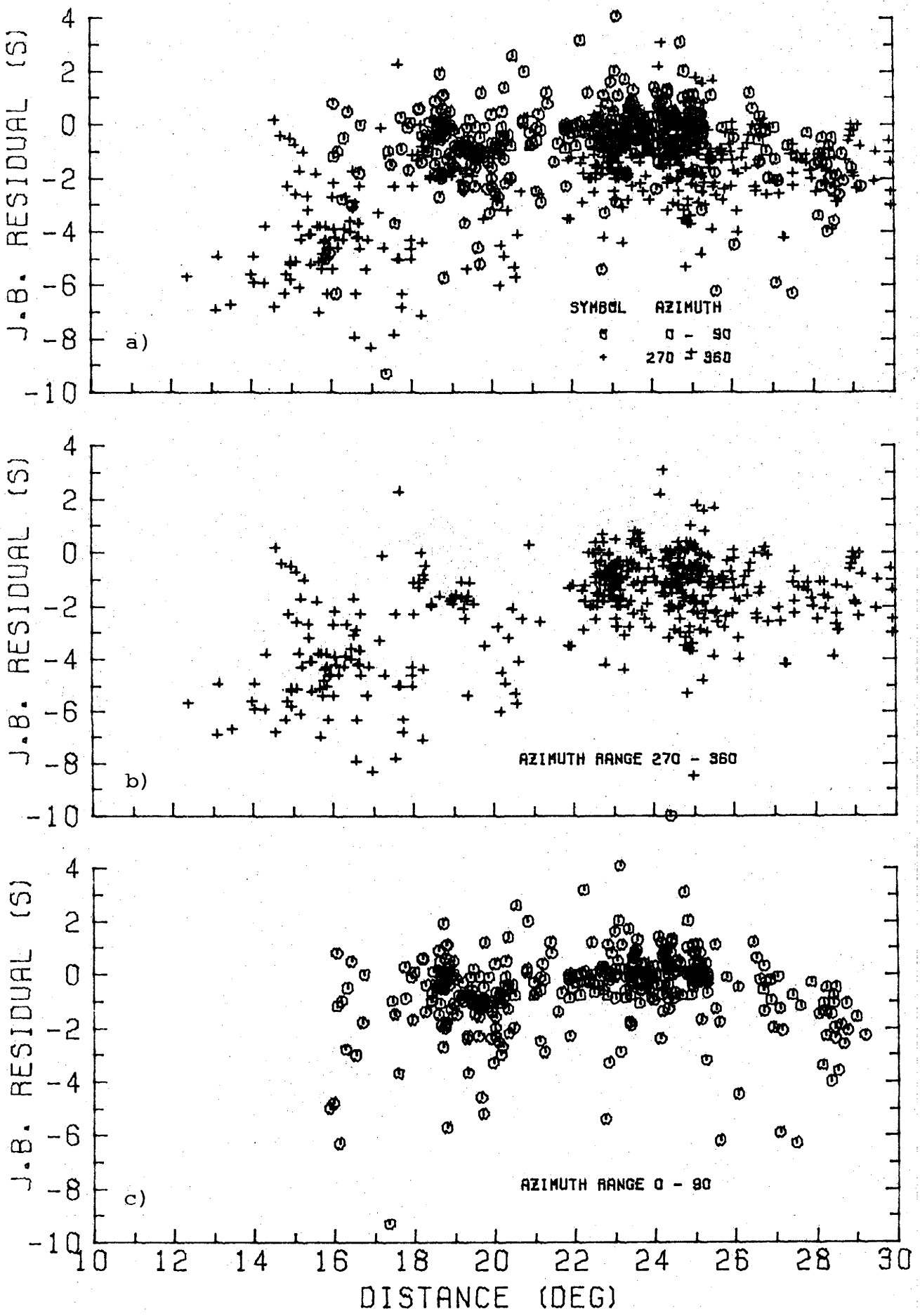

Figure 6-2. JB residuals at WRA for the events shown in Figure 6-1. a) azimuth range 270° to 90°, b) azimuth range 270° - 360°, c) azimuth range 0° - 90°.

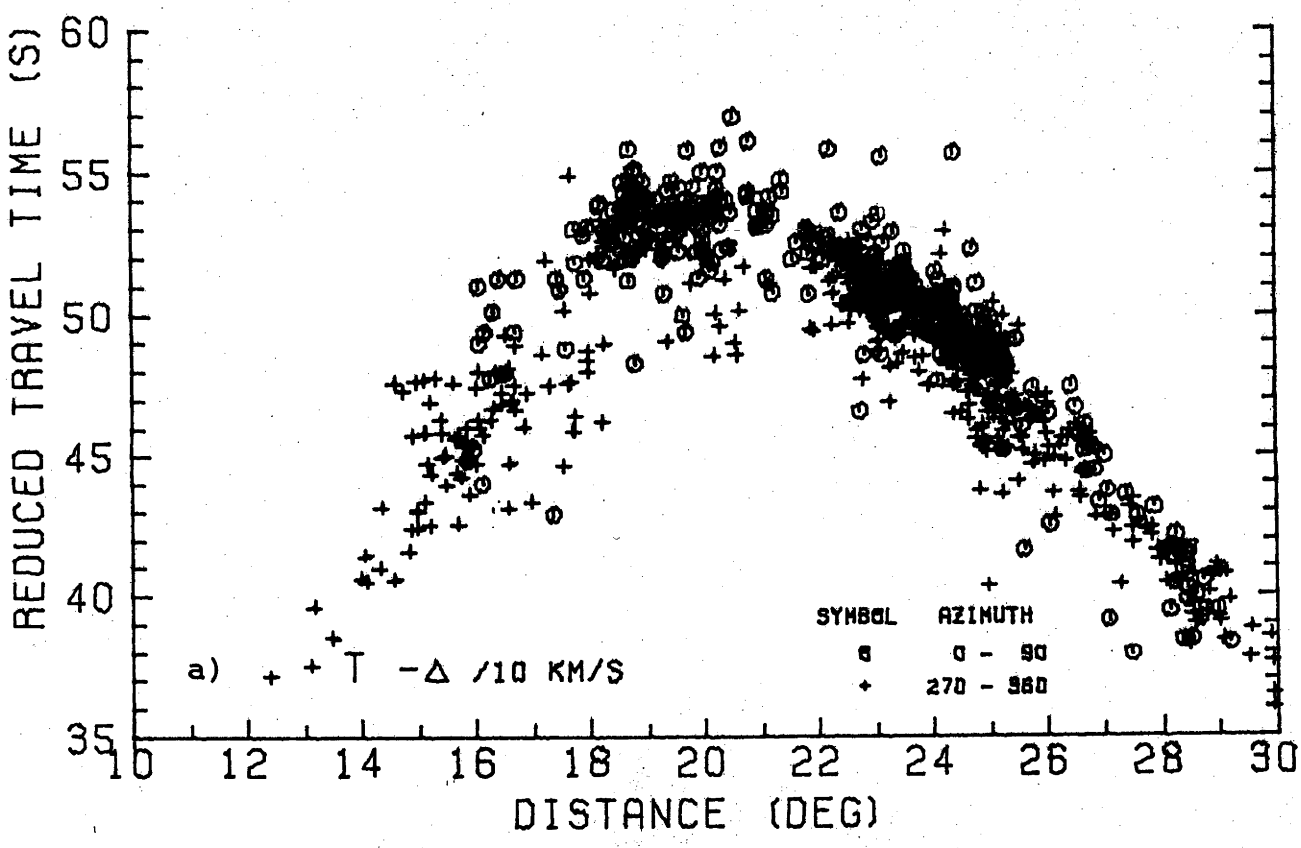

Figure 6-3 a) Reduced travel times to WRA for all events shown in Figure 6-1.

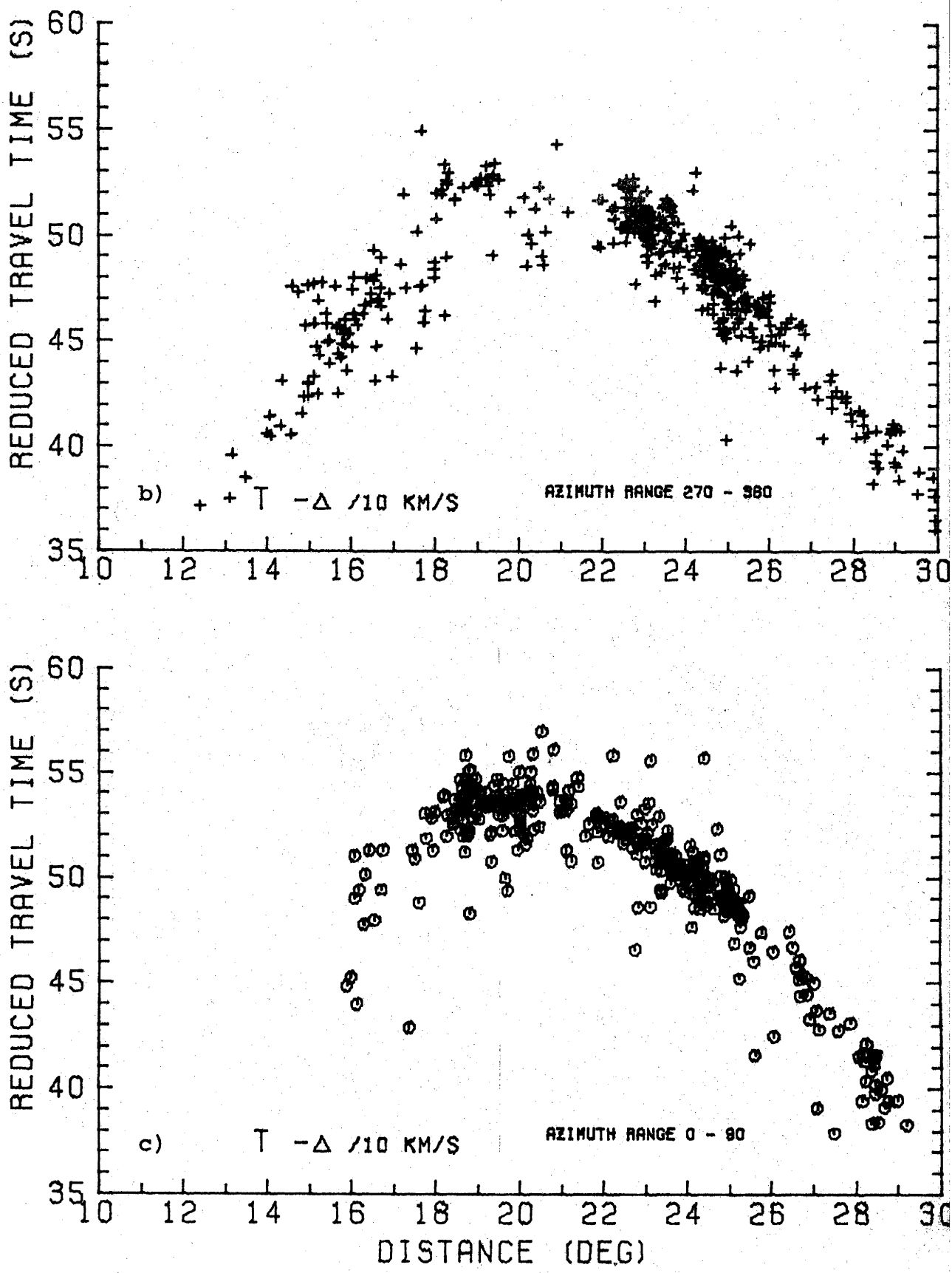

Figure 6-3 (continued). Reduced travel times to WRA for events in Figure 6-1.
b) azimuth range 270° to 360°.
c) azimuth range 0° - 90°.

Figures 6-1, 6-2 and 6-3 also give a general impression of the frequency of events at various distance and azimuth ranges from WRA. The presence of some anomalously large residuals indicates that there may be gross mislocations (either in time or in space) of a few of the events.

In a preliminary upper mantle velocity study (Simpson et al., 1971), the travel times in Figure 6-3 were combined with slowness data, derived using the onset time method of Cleary et al. (1968), for events in the Indonesia-Philippines region. The interpretation of these data will be discussed in the next chapter. The Indonesia-Philippines region was chosen for this initial study because of the more complete distance coverage and the narrow azimuth range. It soon became apparent, however, that a number of ambiguities in the data, caused by the interference of complicated subduction zones along the ray paths to WRA, greatly limited the interpretation of the data. Thus for a more detailed study, it was decided to use events from the New Guinea region which, for the reasons given above, was expected to be less contaminated by structural complexities than the area to the north.

6.3 The New Guinea Study

The occurrence of a magnitude 7.9 earthquake in New Ireland on July 14, 1971, and its many aftershocks, provided an excellent opportunity to study in detail the nature of the travel time curve in this region. Fifty four events from this series, which extended from

21.6° to 24.5° distance from WRA, along with an additional 142 events chosen to cover the rest of the distance range from 15° to 30°, form the basis for the velocity inversion which will be described in the next chapter.

The 196 events which were selected are listed in Table B-1 (Appendix B) and the locations of epicenters are shown in Figure 6-4. Where possible, events were chosen which lay within the azimuth range 30° to 60°, but at distances less than 18° and greater than 28° it was necessary to go to regions outside this range. The hypocenter data in Table B-1 are from the NOAA locations, and distances and azimuths are taken from the GEDESS lists. Using the adaptive processing technique of King et al. (1973) described in the last chapter, slowness and travel times have been determined for 494 initial P onsets and significant later arrivals and these are also listed in Table B-1. A weight has been ascribed to each determination of slowness in Table B-1, which reflects both the error in the slowness measurement (as determined from the standard deviation) and the effect of interfering signals (i.e., arrivals with consistent slowness values are given higher weight than those showing systematic drift between two separate phases).

Before these data can be used to determine velocity structure at depth, it is necessary to apply a number of corrections in order to produce a set of consistent data. The remainder of this chapter will discuss the nature of the necessary corrections and summarize the

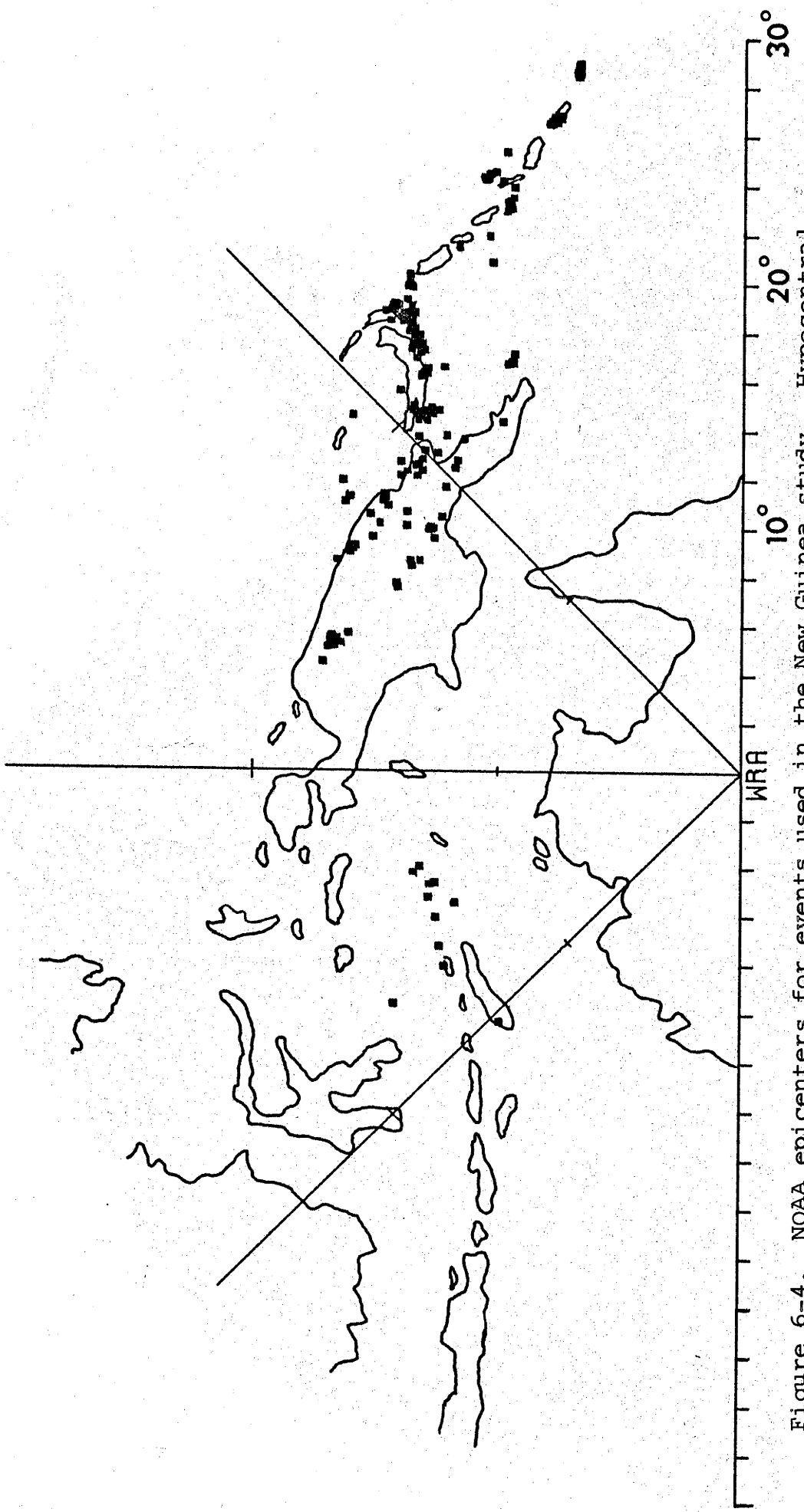

Figure 6-4. NOAA epicenters for events used in the New Guinea study. Hypocentral information given in Table B-1.

main features of the corrected travel time and slowness data.

6.4 Data Corrections

6.4.1 Focal depth correction

The method used to convert the raw time and distance data in Table B-1 to surface focus is discussed in Appendix A. The magnitudes of the corrections are a function of the focal depth, the velocity above the focus, and the ray path taken to reach the surface. Arrivals from the same event which have different slownesses, and hence follow different ray paths, will require separate corrections; and therefore the measured value of slowness for each arrival is used in determining the time and distance corrections. For the sake of consistency with the model used in determining the hypocenter, the Jeffreys (1939) velocity model has been used.

The times and distances corrected for focal depth are included in Table B-1 and are shown along with the slowness data, in Figure 6-5. When they are presented separately, as in Figure 6-5, the relationship between travel times and slownesses is not readily apparent, and resolution of finer features is lost in the scatter of the data. In Figure 6-6, a substantial improvement has been achieved by the incorporation of the travel time and slowness data in a single presentation. At each travel time point a line is drawn with slope

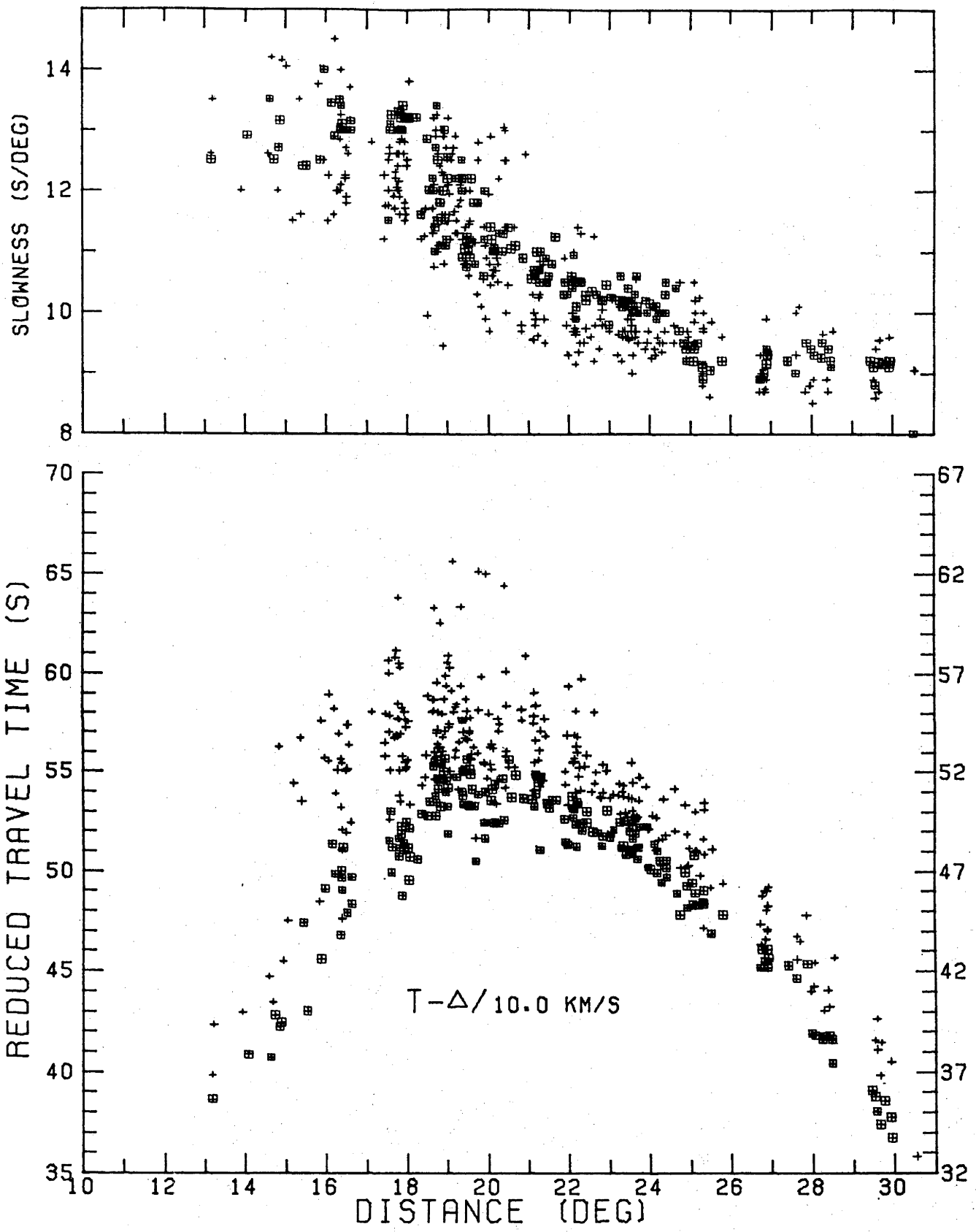

Figure 6-5. Travel times and slownesses, corrected for focal depth. Squares indicate first arrivals. Right hand scale includes -3 s JB origin time correction.

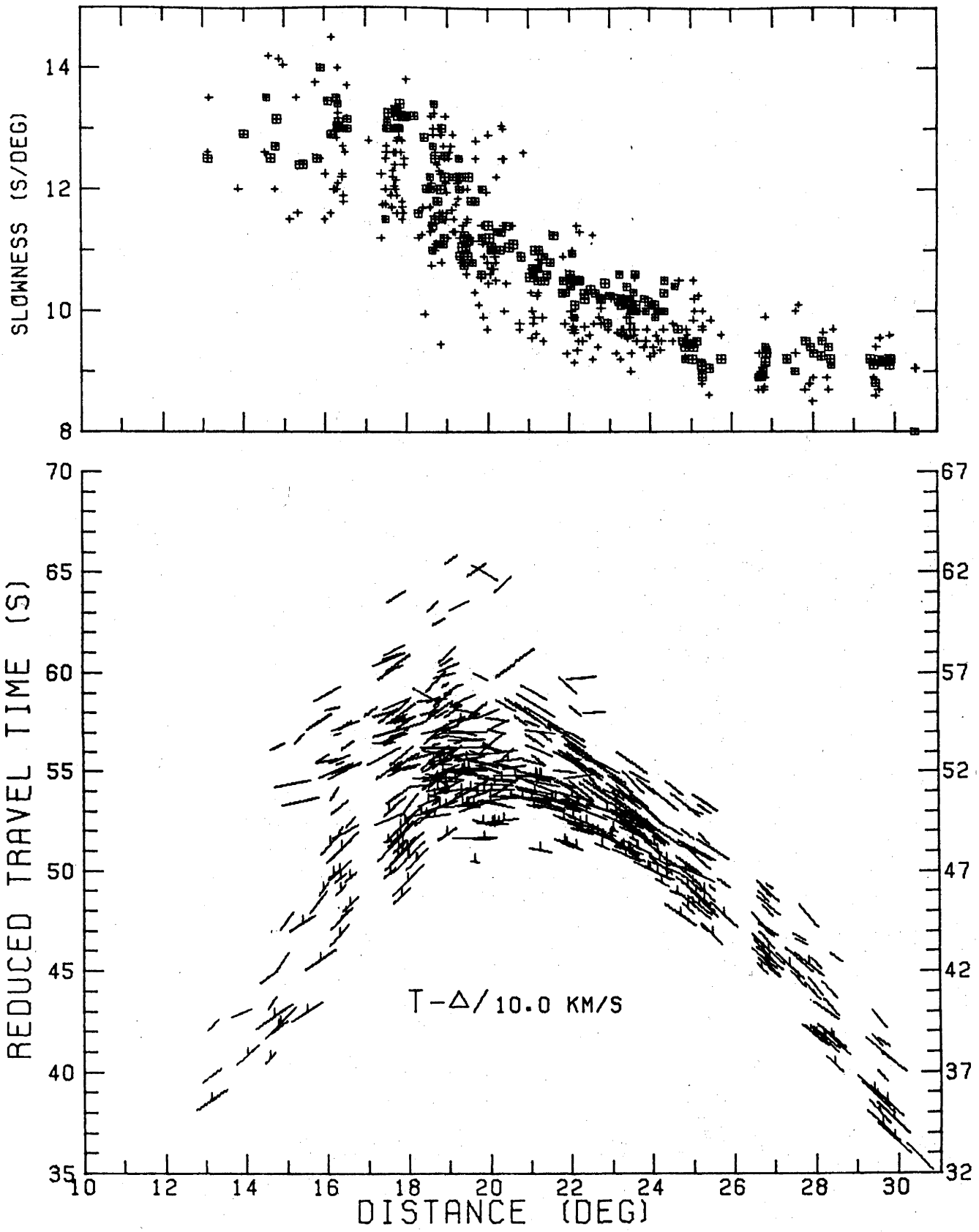

Figure 6-6. Travel times, slope lines and slownesses corrected for focal depth. Slope lines drawn with slope of measured slowness and length corresponding to weight. Vertical tics indicate first arrivals.

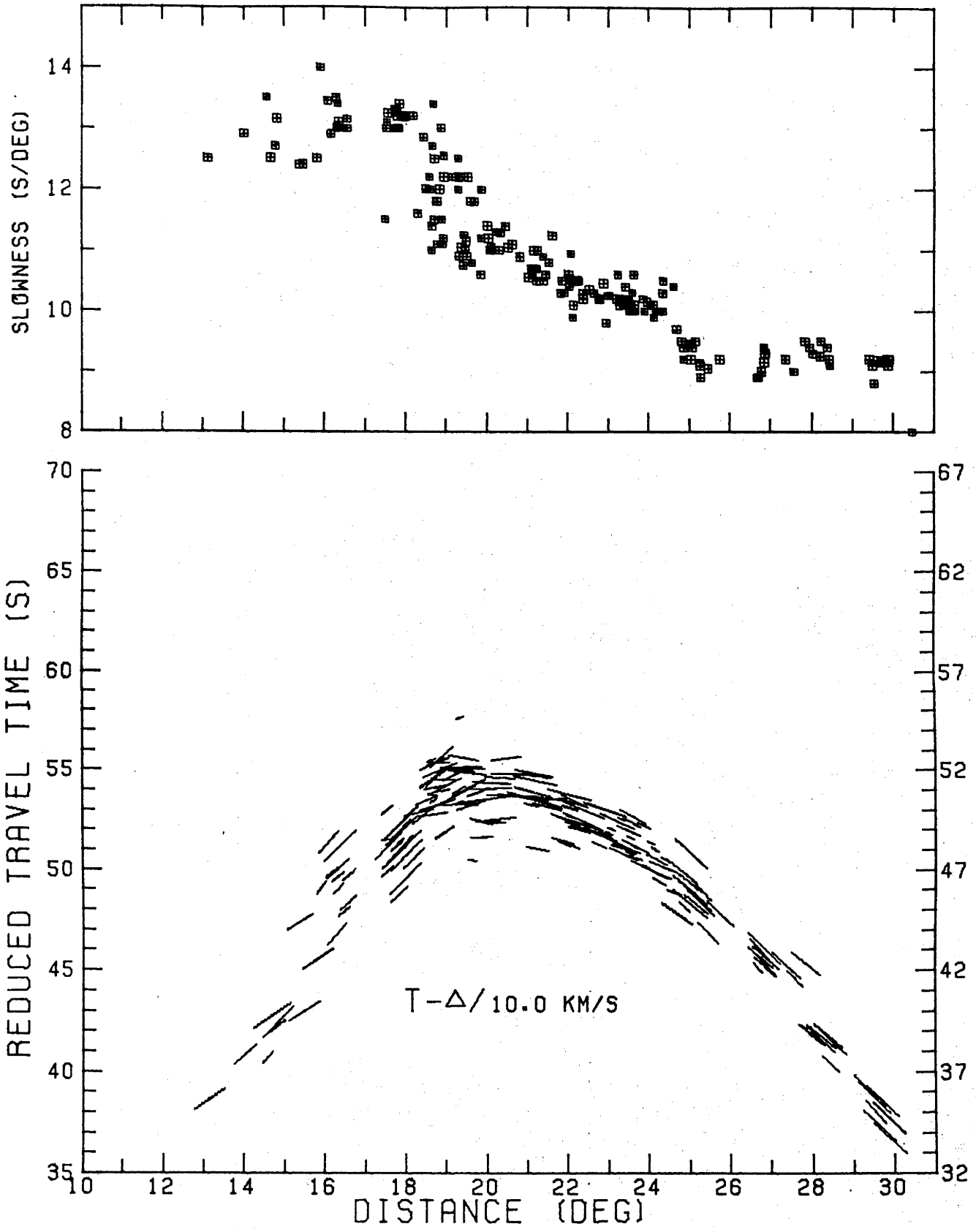

Figure 6-7. First arrival data from Figure 6-6.

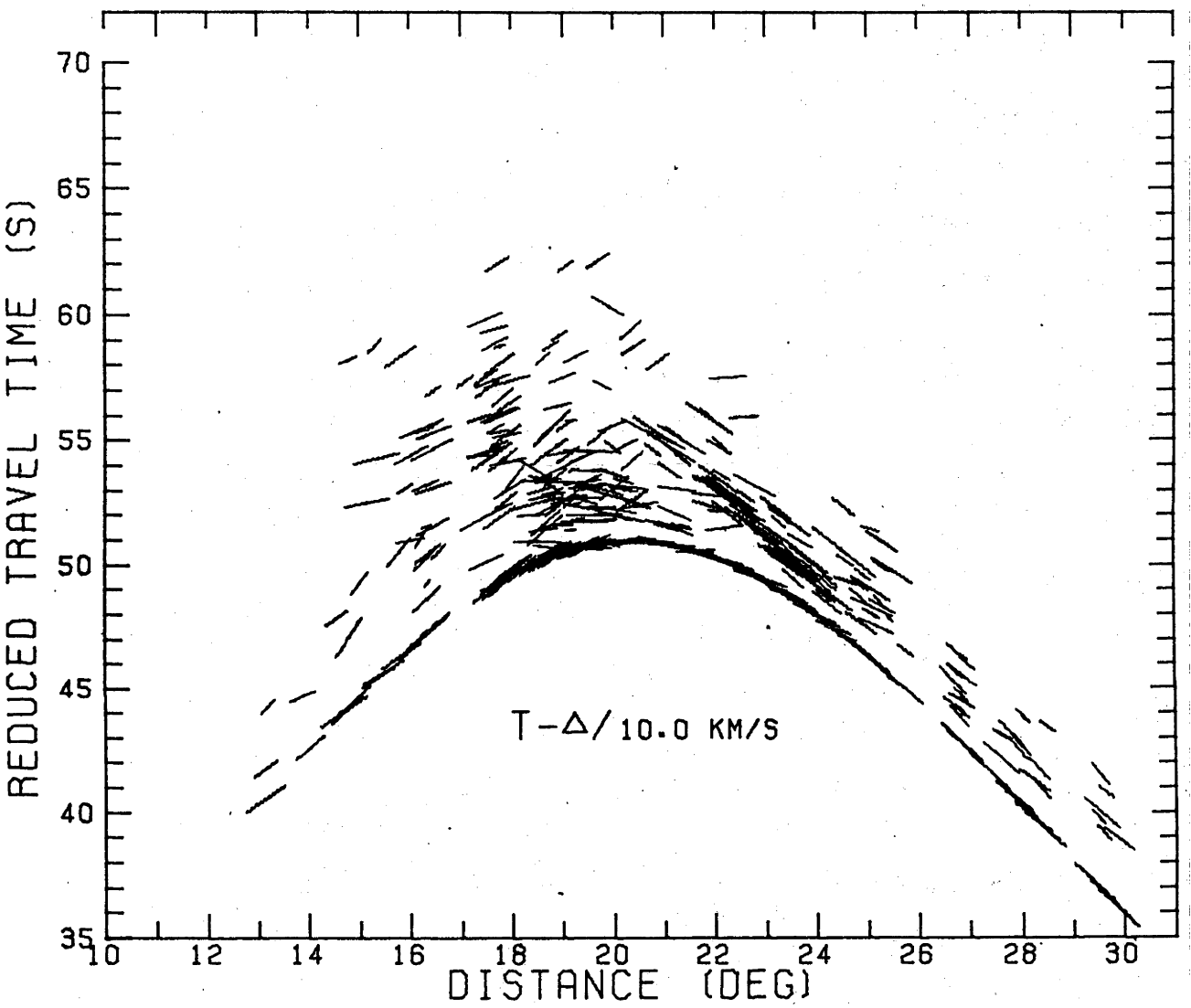

Figure 6-8. Data of Figure 6-6 with times adjusted so that first arrivals fall on Herrin et al. (1968) travel time curve.

corresponding to the measured value of slowness and a length corresponding to the weight given to the slowness determination.

In Figure 6-7 only the first arrival points from Figure 6-5 are shown, and in Figure 6-8 the second arrival branches are clarified by adjusting the times so that the first arrivals are constrained to fall on the Herrin et al. (1968) travel time curve.

6.4.2 Local structure correction

A careful inspection of Figures 6-5 to 6-8 reveals that the slope lines, which should lie tangent to the trend of the travel times at each point, show a bias away from the average curve. This bias is due to a shift in the measured values of slowness caused by local structure near the array. If a knowledge of the structure causing these variations is available, it is possible to compute corrections to the measured slowness values (Niazi, 1966; Zengeni, 1970). Niazi has shown that the effect of dipping layers beneath an array is to change the measured values of slowness by a factor which remains essentially constant over limited ranges of azimuth and slowness. Since we have no detailed knowledge of the structure under WRA and since the data is confined to a narrow azimuth range and should thus be affected by the same structure, it is possible to use an empirical approach to determine the corrections to the slowness measurements.

The first arrival times in Figure 6-7 between 18° and 30° have been combined with the times from the same

region in Figure 6-3c and smoothed using a fifth order polynomial. At each distance where a slowness determination was available the slope of the smoothed curve was compared with the measured value of slowness. The RMS residual was computed and the procedure repeated with the measured slowness values multiplied by factors ranging from 1.1 to 0.9. At each stage depth corrections were applied using the revised slowness values. The results are shown in Figure 6-9. A minimum in the RMS residual occurs with a correction factor of .97, indicating that the observed slowness values, within the azimuth range considered here, are high by approximately 3%.

Cleary et al. (1968) studied the effects of local structure beneath WRA, using events at distances near 80° and azimuths near 27° and 216°. From the equations given by Niazi (1966) they determined the best solution for a dipping interface below the array required to satisfy the observed residuals in azimuth and slowness. With a velocity contrast of 0.7 across the interface, the structure they reported dips at an angle of 6.5° in a direction of 235°. For events near a distance of 25° (angle of incidence 30°) and azimuth of 30° (155° from the direction of dip) the Niazi tables give a correction factor of 0.92 for this structure. Although the Cleary et al. structure was determined from events at greater distance and slightly different azimuths than the data presented here, the correction is at least in the right sense (i.e. a decrease, rather than an increase in

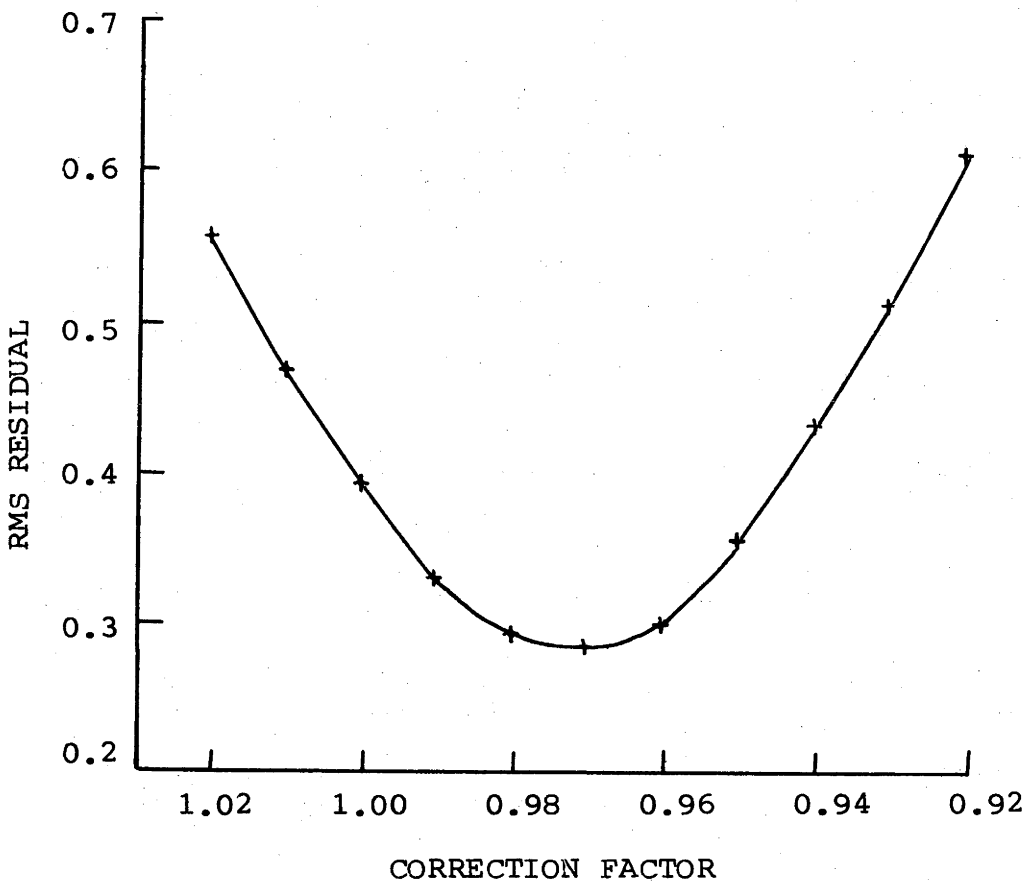

Figure 6-9 WRA structure correction factor. RMS residual is the root mean square of the difference between the slope of a fifth order polynomial through first arrival travel times and the observed slowness values multiplied by the structure correction factor.

slowness) indicating that the direction of dip of the reported structure is approximately correct. Decreasing the angle of dip, increasing the velocity ratio, or increasing the dip angle in the Cleary et al. structure brings the correction factor closer to that determined above from the New Guinea data.

The slowness values, corrected for structure, are included in Table B-1 along with the corresponding corrected times and distances. These corrected data are plotted in Figure 6-10. A comparison of Figure 6-10 with Figure 6-6, especially between 20^{o} and 25^{o}, shows the improvement in the trend of the slope lines with respect to the travel time data.

6.4.3 JB origin time bias

Although it is now well established that the JB times are in error, especially at shorter distances, by as much as 3 s (e.g., Cleary and Hales, 1966), the errors introduced into hypocenter determinations based on these times are difficult to assess. Even with a good distribution of stations, azimuth-dependent variations in station and source terms (Bolt and Nuttli, 1966; Cleary, 1967a) will introduce bias in hypocenter determination. Errors in focal depth and origin time are especially difficult to determine because of the inter-relationship in the determination of these two parameters. They depend to a large extent on the distance range covered by stations used in locating an event.

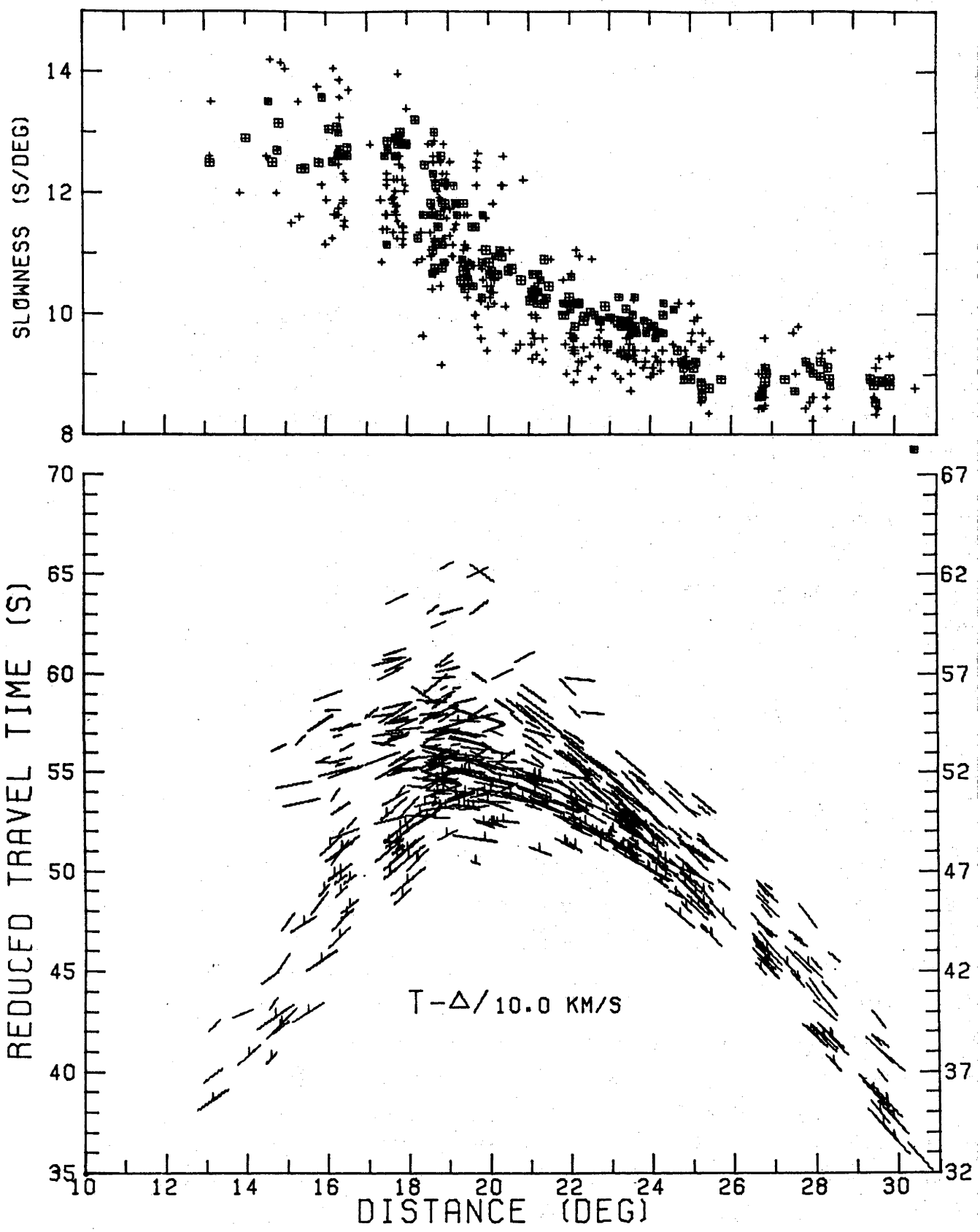

Figure 6-10. Travel times and slownesses corrected for focal depth and local array structure. Slowness values multiplied by correction factor of 0.970.

From 22° to 30°, the times in Figures 6-3c and 6-7 lie approximately 1 s earlier than the JB times (Figure 2-5) and 2 s later than the Herrin et al. times (Figure 2-10). Although a station anomaly for WRA based on the Herrin et al. times is not available, Cleary (1967b) has reported a value of -1.3 s based on the Cleary and Hales (1966) times. For Australian stations, the station anomalies calculated using the Cleary and Hales times are on the average 0.3 s less than those found from the Herrin et al. times (Hales et al., 1968). A correction of -1.0 s for WRA should therefore be in reasonable conformity with the Herrin et al. times, and the times in Figures 6-3c and 6-7 are thus approximately 3 s later than would be expected on the basis of the Herrin et al. tables (corrected for WRA). The Herrin et al. times are an average of 3 s earlier than the JB times and a -3 s correction to the observed WRA travel times is consistent with the error in origin time expected from the use of the JB tables to locate the events. The right hand scale on the time axis in the WRA data diagrams presented in this chapter is shifted by 3 s to incorporate this correction.

6.5 Main Features of the Data

6.5.1 Histograms and Sample Records

To facilitate discussion, the data have been divided

into groups corresponding to the various branches of the travel time curve. Histograms of first and later arrival slowness values are shown in Figure 6-11. The clustering in the histograms and the abrupt changes in slowness in the first arrival data of Figure 6-7 indicate that there are at least three major first arrival branches with cross-over points at 19° and 24.5°. In anticipation of the model to be discussed in the next chapter, the major divisions A to E have been used to describe the most obvious branches of the travel time curve, as indicated by the inset to Figure 6-12. In Figure 6-12 are shown a number of records, selected to indicate the main characteristics of each group, and these characteristics are summarized in Table 6-1.

6.5.2 General comments; the A and B branches

One of the dominant features of the travel time plots and the sample records in Figure 6-12 is the later branch D extending from 20° to 24.5°. At shorter distances, individual records show prominent later arrivals (e.g., Figure 6-12 a,e) but these do not fall on consistent later arrival branches as do the D arrivals. There are a number of factors which may have contributed to the greater scatter in the data at shorter distances compared to those beyond 22°.

(a) Azimuth range: Most of the events used in the distance range 22° to 25° are aftershocks of the New Britain earthquake of 14 July 1971, and the narrow azimuth range to which these events are confined may be partly responsible

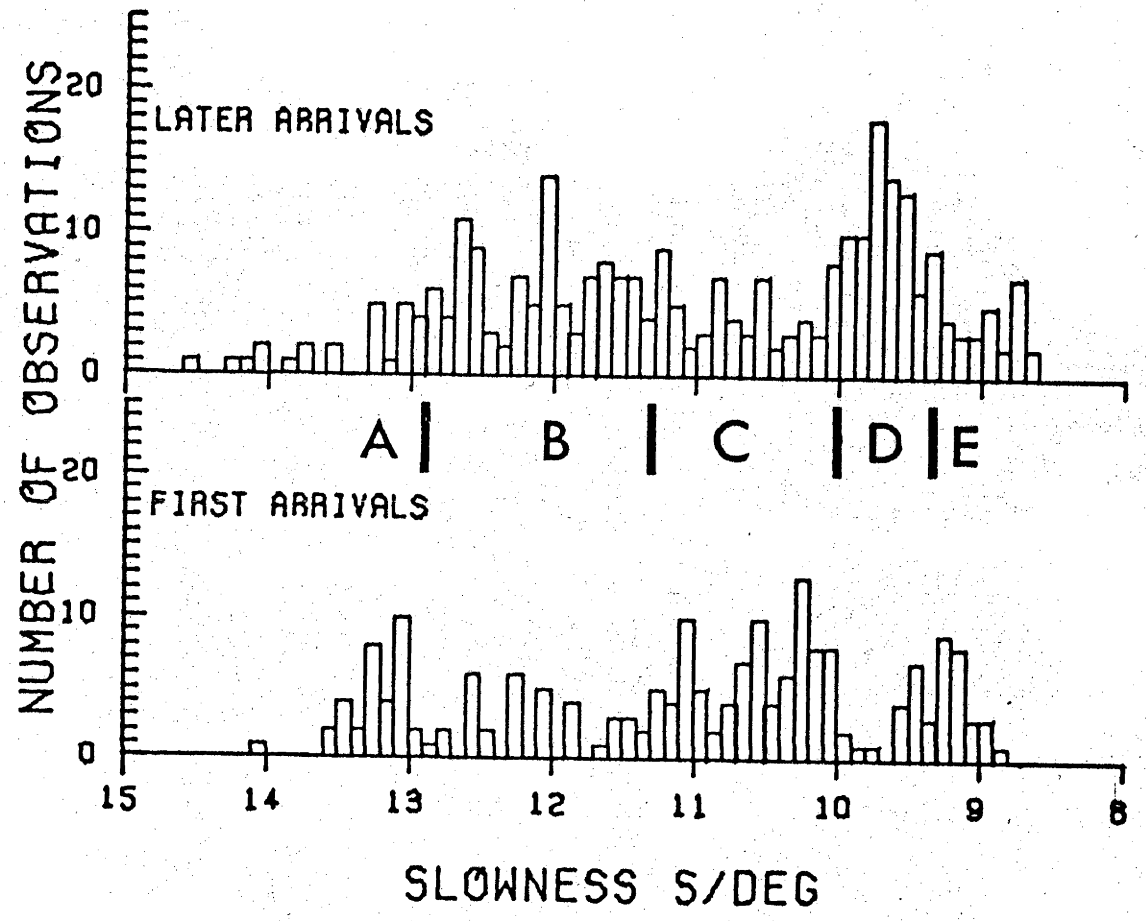

Figure 6-11 Slowness histograms, uncorrected for local array structure.

Figure 6-12 (opposite). Sample records. Event numbers refer to Table B-1.
Numbers over array phased sum trace are observed slowness values (s/deg) uncorrected for local structure and Δ_c values are average distances, corrected for focal depth.

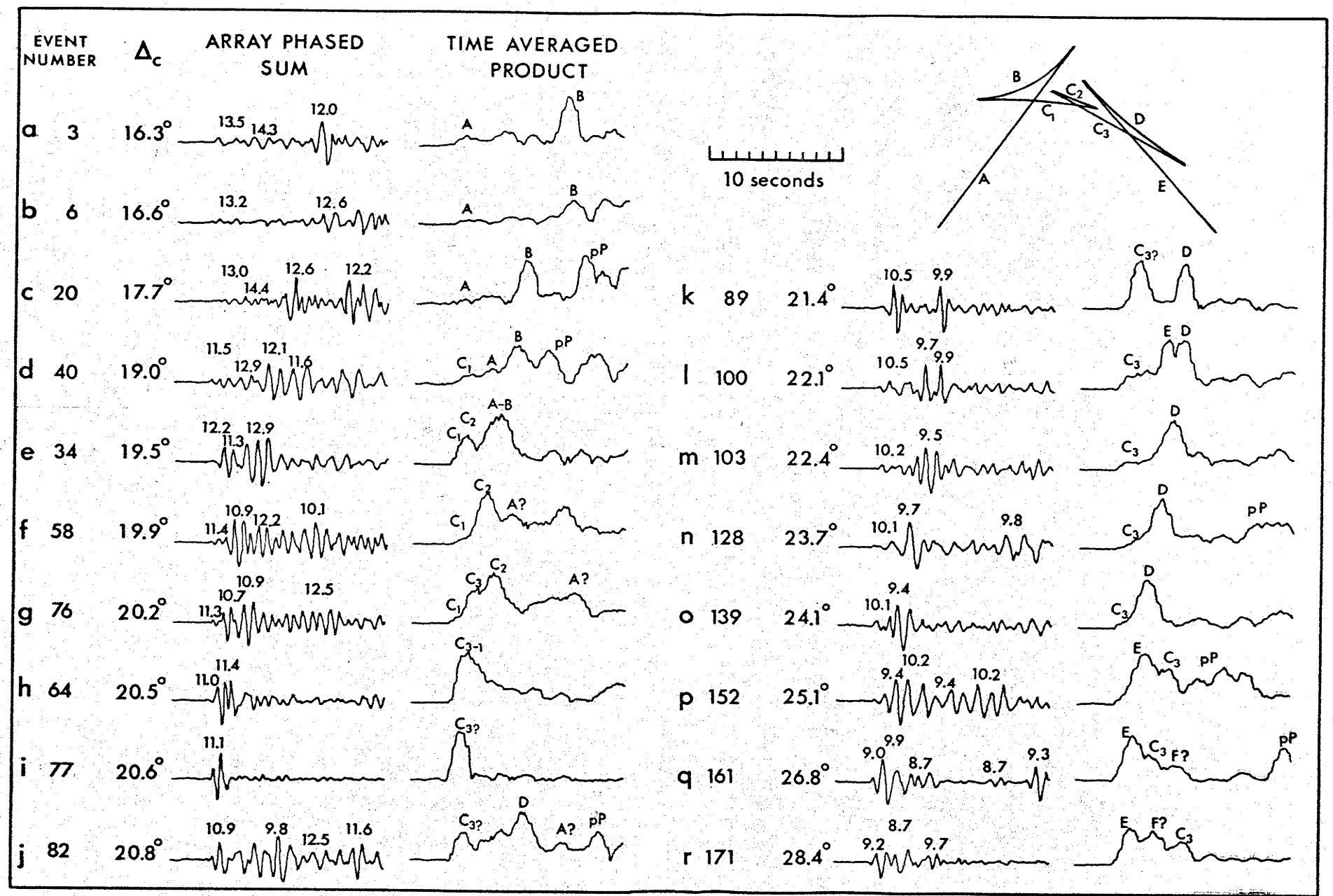
EVENT NUMBER
Δ_c
ARRAY PHASED SUM
TIME AVERAGED PRODUCT
10 seconds
a 3 16.3° 13.5 14.3 12.0 A B
b 6 16.6° 13.2 12.6 A B
c 20 17.7° 13.0 14.4 12.6 12.2 A B pP
d 40 19.0° 11.5 12.9 12.1 11.6 C1 A B pP
e 34 19.5° 12.2 11.3 12.9 C1 C2 A-B
f 58 19.9° 10.9 11.4 12.2 10.1 C1 C2 A?
g 76 20.2° 10.7 11.3 10.9 12.5 C1 C3 C2 A?
h 64 20.5° 11.0 11.4 C3-1
i 77 20.6° 11.1 C3?
j 82 20.8° 10.9 9.8 12.5 11.6 C3? D A? pP
k 89 21.4° 10.5 9.9 C3? D
l 100 22.1° 9.7 10.5 9.9 C3 E D
m 103 22.4° 10.2 9.5 C3 D
n 128 23.7° 10.1 9.7 9.8 C3 D pP
o 139 24.1° 9.4 10.1 C3 D
p 152 25.1° 9.4 10.2 9.4 10.2 E C3 pP
q 161 26.8° 9.0 9.9 8.7 8.7 9.3 E C3 F? pP
r 171 28.4° 8.7 9.2 9.7 E F? C3
A B C1 C2 C3 D E

TABLE 6-1. Main Feature of WRA data

GROUP	SLOWNESS RANGE (s/deg, uncorrected)	DISTANCE RANGE		EXAMPLE (Figure 6-12)	COMMENTS
		as first arrival	as later arrival		
A	13.5-12.8	13° -19.5°	19.5°-20.5°	a-e	Low amplitude except for region near 17°. Slowness and travel times scattered. Usually followed by large amplitude arrival of Group B. Sometimes also followed by arrival with slowness near 14 s/deg.
B	12.8-11.2		15° -21°	a-d	Large amplitude later arrival. Especially clear 14°-17°. Scattered slowness.
C1,C2	11.2-10.5	19.5°-22°	19.5°-22°	d-g	A number of events with multiple arrivals separated by 1-2 s with slownesses of 10.8 and 11.2 s/deg.
C3	10.5-10.0	21.5°-24.5°	24.5°-27.5°	i-k	A number of events near 21° with large amplitude first arrival followed by large amplitude arrival of Group D.
				l-o	From 22° to 24.5° low amplitude compared to later arrival D.
				p-r	Beyond 24.5° masked by E arrival.
D	9.9- 9.2		20° -26°	j-o	Large amplitude especially near 21°. Very consistent travel times. Slownesses scattered possibly due to interference with E group.
E	9.3- 8.9	24.5°-30°	?	p-r	Well determined as first arrival. Sometimes followed by C_3 arrival.
F	8.9- 8.5		28° -30°	q,r	A number of well determined later arrivals.

for the consistency of the D arrivals. For events at shorter distances, the azimuth range is from 320° to 60° and lateral variations in structure may be responsible for scatter in both the travel time and slowness data for these events.

(b) Focal depth corrections: Changing the focal depth from 30 km to 60 km for an arrival with slowness of 13 s/deg results in a change in distance correction of 0.9°; whereas the same change for an arrival with slowness of 10 s/deg produces a change in distance of only 0.3°. Thus the shorter distance, higher slowness branches are more sensitive to errors in focal depth determination.

(c) Surface reflections: The pP arrival was excluded from the data used in the study whenever it could be identified. Identification was based on the time expected for its arrival for the given focal depth and on the observed value of slowness. Because of the rapid decrease in slowness near 20°, the time of pP - P increases rapidly for events in this range. For example, the Herrin et al. (1968) tables show the pP - P time for a focal depth of 50 km at 23° to be 12 s, while at 16° the corresponding time is only 9 s. The D arrivals occur at a maximum of only 6 s after the first arrival and it is unlikely that pP has contaminated the data for this branch. At shorter distances, however, later arrival branches may extend up to 10 s or more after the first arrival, and for shallow events at less than 20° it is possible that pP has interfered with, or been misinterpreted as, arrivals on

later branches.

(d) Multiple branching: It is possible that more than one set of later arrival branches occurs in the B slowness range (Figure 6-11) as suggested by Simpson et al. (1971) and Massé et al. (1972). The first arrival slowness values near 12.0 s/deg at 18^{o} to 19^{o} (Figure 6-7) may result from the appearance of an intermediate branch as the first arrival over a very limited distance interval. It is possible, however, that these intermediate values of slowness are caused by interference between the close arrival of the low amplitude, high slowness phase A with the higher amplitude, lower slowness phase C. This effect has been duplicated in synthetic data by King et al. (1973).

(e) Lateral variations in velocity: The A and B branches correspond to rays which have penetrated to depths of less than 400 km, and it is in this depth range (especially above 250 km) that lateral variations in structure are likely to be most extensive. The travel paths for events at close distances will be mainly through the high velocity continental structure of the stable Australian platform. As the distance increases and the source end of the ray path includes a greater portion of the lower velocity New Guinea tectonic region structure, the times will be progressively delayed. This effect decreases at greater distances (i.e., on the C branch and beyond) as the portion of the total ray path spent in the laterally varying uppermost mantle decreases. Because of the

delay with increasing distance, the apparent slope of the A branch travel times will be greater than expected for a homogeneous structure. The observed values of slowness, however, depend only on the structure on the upgoing (receiver) end of the ray path, and will reflect the structure beneath the continental region. The resulting conflict between the travel times and slownesses can be seen in Figure 6-10 where the average slope of the travel time curve is near 14 s/deg, while the measured values of slowness are closer to 13 s/deg.

6.5.3 The C branch triplication

In Figure 6-12 and Table 6-1 the C branch has been divided into three groups. Many of the events near 20^{o} (e.g., Figure 6-12 f,g) show multiple arrivals in the first 5 s with uncorrected slownesses of 10.5 to 11.4 s/deg. As the histograms in Figure 6-11 show, the first arrivals tend to cluster near 11.1 and 10.6 s/deg, while the later arrivals show a minor peak at 10.8 s/deg. The triplication extends over a distance range of only 2 or 3 deg and scatter in the data due to errors in distance makes it difficult to identify the cross-over point between the C_1 and C_3 branches. However, multiple arrivals are consistently observed on enough records to consider the triplication of a real feature of the data. The relative amplitudes of arrivals in this range provide additional support for the presence of multiple branches and these will be discussed in Section 6.5.5.

6.5.4 The D, E and F branches

Possible reasons for the consistency of the D arrivals have been discussed in Section 6.5.2. The branch first appears near 20.5° and a number of records near 21°, of which Figure 6-12k is a typical example, show the D arrival as a simple, clear phase, well separated from the earlier C arrival. At greater distances (Figure 6-12 m-o) the C and D arrivals merge, with the D phase dominant, and the existence of two separate arrivals is obvious only on the array-processed records. On a few records (e.g., Figure 6-12 l) it is possible that both the retrograde (D) and prograde (E) branches can be distinguished. It is assumed that the higher amplitude later arrival corresponds to the retrograde branch, although interference between the two closely spaced arrivals (D and E) may be present and would account for the scatter in slowness determinations for the D branch.

Beyond 26° a number of records show arrivals with slownesses near 8.7 s/deg (the F arrivals in Figure 6-12 q,r). These may be related to structure below the discontinuity causing the D branch, but there is not sufficient data available in the study to comment on the depth of the structure required to produce these arrivals.

6.5.5 Amplitudes

The use of absolute amplitudes in earthquake studies is difficult even when a number of calibrated stations and earthquakes with well determined magnitudes are

available. Since only one recording location was used in this study and many of the earthquakes used have poor magnitude determination (or none), absolute amplitudes can only be considered in a qualitative manner (e.g., for events of similar magnitudes, arrivals on the A branch appear to be of lower amplitude and give less reliable slowness determination than arrivals on the C or D branches). Nevertheless, important information can be gained from a comparison of the relative amplitudes of multiple arrivals from the same event. Figure 6-13 shows a comparison of the amplitude ratios for the C and D branch arrivals between 20^{o} and 25^{o}. The ratio is determined from the maximum peak to peak amplitude of each arrival on the array phased sum trace of the adaptive processing records (see Figure 5-3b).

Although it cannot be determined from these data alone which arrival is responsible for the variation in amplitude ratio, the obvious features of Figure 6-13 are consistent with other characteristics of the travel time and slowness data and it is possible to suggest the underlying structure of the amplitude changes along the C and D branches. The sample records in Figure 6-12 h-m, and the rapid decrease in slowness for first arrivals on the C branch near 22^{o}, indicate that the increase in amplitude ratio at 22^{o} results from a sudden drop in amplitude of the C arrivals at this distance. This adds support to the identification of the C branch triplication (Section 6.5.3). The arrivals denoted $C_{3?}$ in Figure 6-12

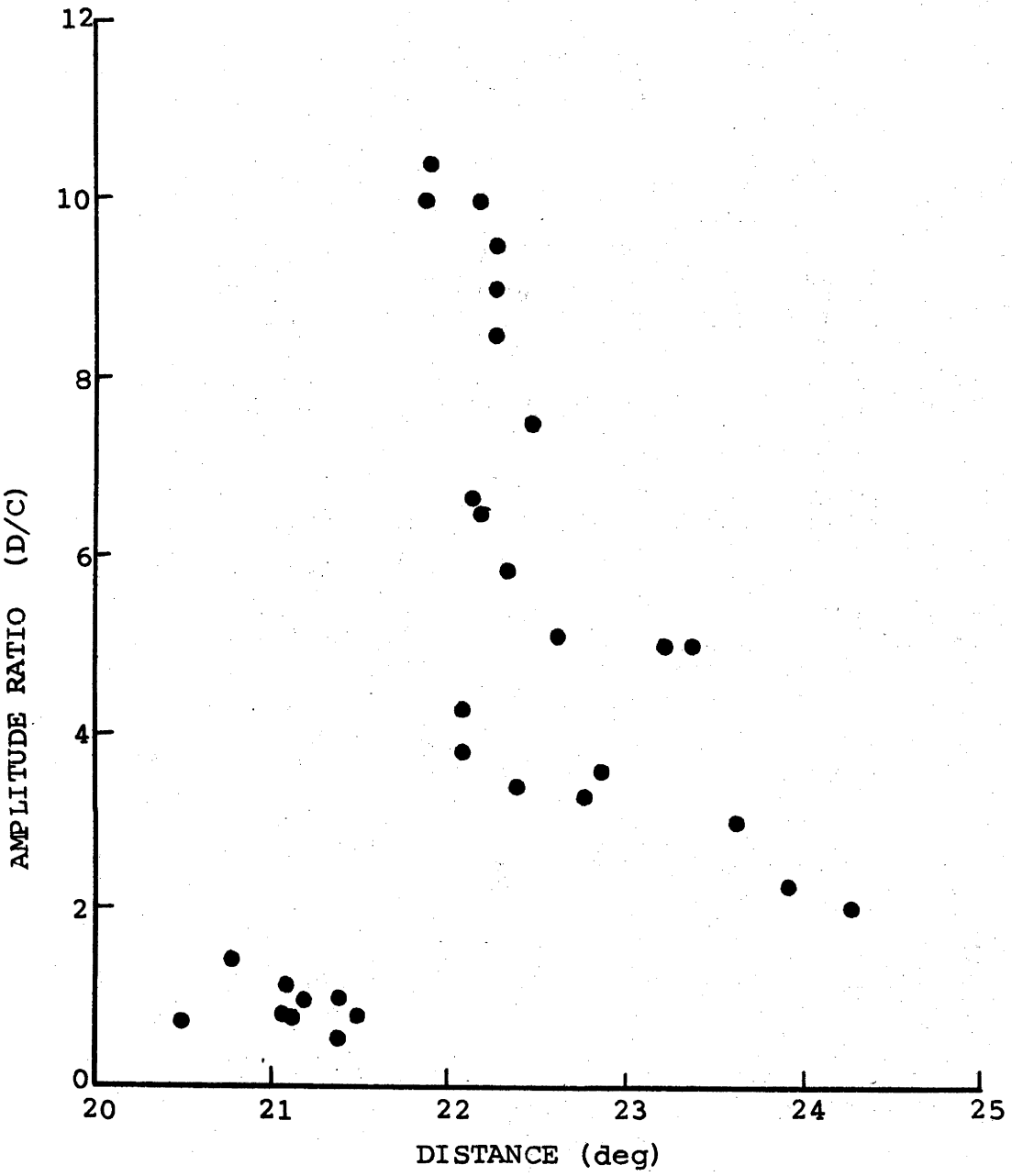

Figure 6-13 Amplitude ratios for C and D branches. Ratio of D branch amplitude over C branch amplitude. Amplitudes taken from maximum peak to peak in array phased sum.

may result from the interference of the C_1 and C_3 arrivals at the prograde end of this triplication, or they may correspond to arrivals from a zone of high velocity gradient just below the structure causing the triplication.

The gradual decrease in the amplitude ratio from 22° to 24° in Figure 6-13 is interpreted as corresponding to a gradual decrease in the D branch amplitude. As will be shown in the next chapter, an increase in amplitude towards the retrograde end of the D branch would be expected from the sudden velocity increase near 700 km required to give travel times corresponding to the D branch arrivals.

One general feature of the amplitudes which has an important bearing on the nature of the velocity discontinuities is that the ends of the major prograde branches (i.e. the extension of A beyond 19° and C beyond 24.5°) terminate with low amplitude, whereas high amplitudes are associated with the ends of the retrograde branches B and D. This makes it difficult to identify the ends of the prograde branches, but a search of the data has shown no indication of observable extensions of branch A beyond 21° or of branch C beyond 29°.

CHAPTER 7

THE UPPER MANTLE TRANSITION ZONE

7.1 Introduction

Because of the scatter in the slowness data presented in Chapter 6, a direct inversion of these data alone does not appear warranted. Instead, the combined travel time and slowness data, as summarized in Table 6-1, have been used as a basis for the determination of velocity models which satisfy the main features of these data and which do not produce features which are not warranted by the observed data (e.g., high amplitude extensions to the A and C branches). From the discussion of the main features of the data in Section 6.5, it is obvious that much greater confidence can be placed on the interpretation of the C, D, and E branches than on the data at shorter distances. It is possible, however, to suggest the type of structure most consistent with the A and B branch data and to indicate those types of models which produce features that are in conflict with the data.

7.2 Velocity Models

7.2.1 WRA-UM1

The model WRA-UM1 is tabulated in Table 7-1 and shown in Figure 7-1. The times and slownesses calculated from this model are compared with the observed data in Figure 7-2. Above 320 km a simple stripping model,

TABLE 7-1 The WRA-UM Models

WRA-UM1		WRA-UM2	
Velocity (km/s)	Depth (km)	Velocity (km/s)	Depth (km)
6.20	0.	6.20	0.
6.50	20.	6.20	20.
6.50	30.	6.50	20.
8.05	30.	6.50	35.
8.05	70.	8.10	35.
8.20	70.	8.10	85.
8.20	320.	8.25	85.
8.3672	321.	8.32	175.
8.4353	330	8.40	175.
8.5137	340.	8.40	320.
8.5910	350.	8.5130	330.
8.6851	360.	8.5652	340.
8.8152	370.	8.6288	350.
8.9814	380.	8.7063	360.
9.1836	390.	8.8029	370.
9.3003	400.	8.9409	380.
9.3508	410.	9.1452	390.
9.3918	420.	9.3063	400.
9.4272	430.	9.3641	410.
9.4591	440.	9.4097	420.
9.4885	450.	9.4491	430.
9.5145	460.	9.4847	440.
9.5415	470.	9.5174	450.
9.5790	480.	9.5480	460.
9.6382	490.	9.5755	470.
9.7192	500.	9.6197	480.
9.8326	510.	9.6880	490.
9.9370	520.	9.8116	500.
9.9982	530.	9.9015	510.
10.0500	540.	9.9581	520.
10.0974	550.	10.0071	530.
10.1400	560.	10.0515	540.
10.1696	570.	10.0933	550.
10.1901	580.	10.1322	560.
10.3200	680.	10.1632	570.
10.9500	695.	10.1808	580.
11.2000	800.	10.3200	680.
		10.9500	695.
		11.2000	800.

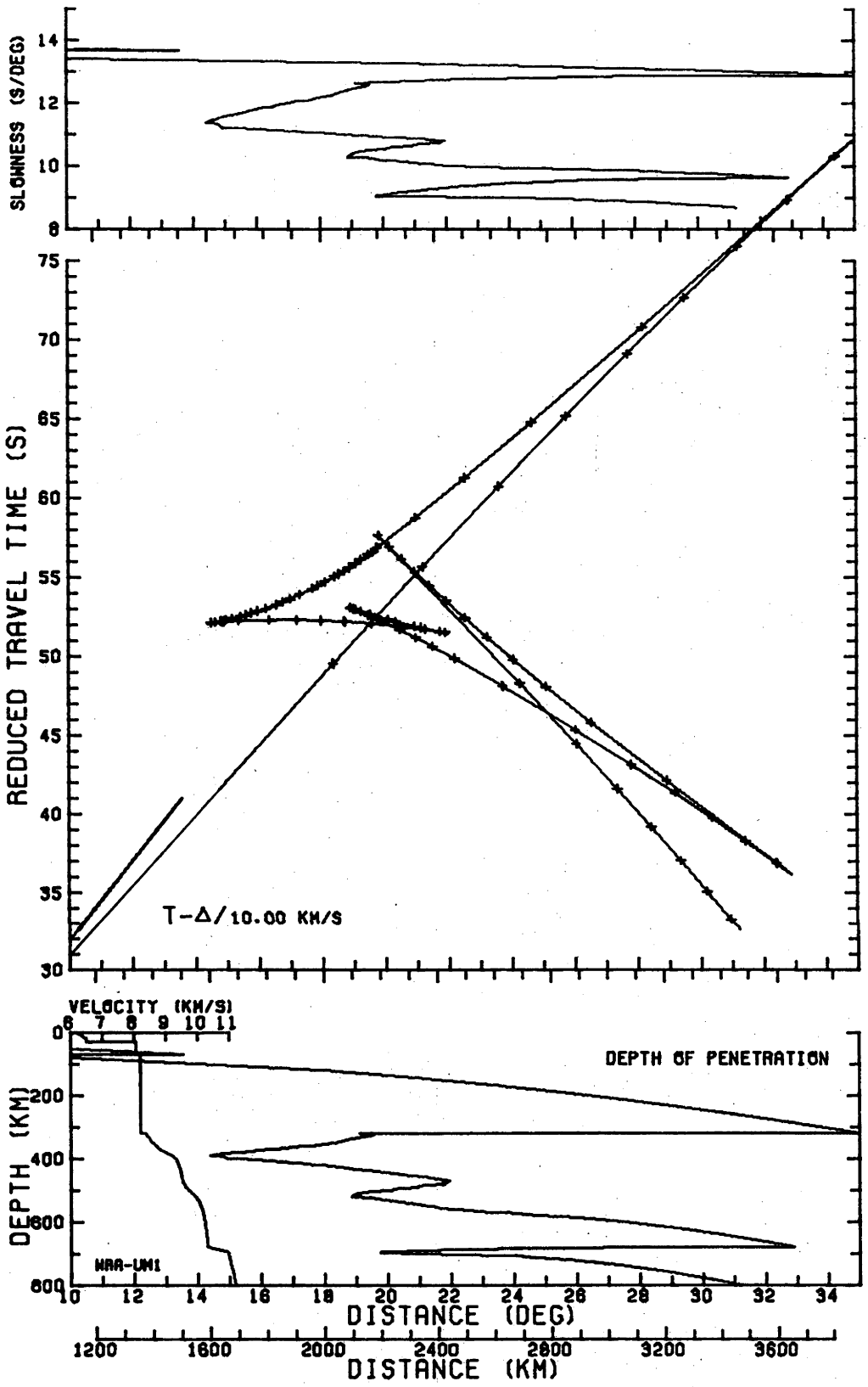

Figure 7-1. The WRA-UM1 model.

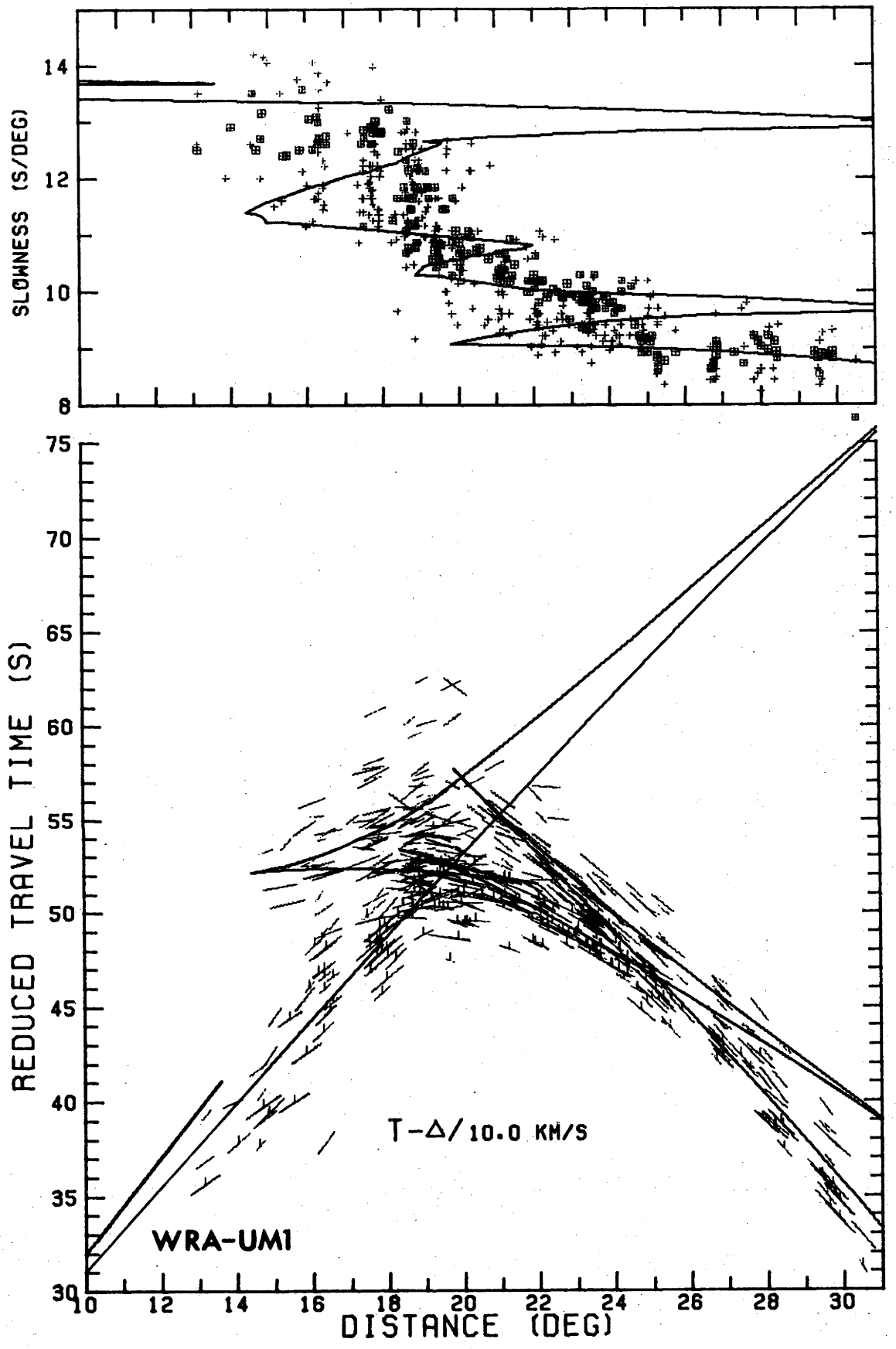

Figure 7-2. Comparison of the WRA-UM1 model with the WRA data corrected for focal depth, local array structure and JB origin time bias.

intermediate between the high velocities under the Australian shield and the lower velocities beneath New Guinea, has been used. No attempt has been made to delineate a low velocity layer in the upper 200 km, although it is likely that one exists for part of the path at least. For the reasons discussed in Section 6.5.2, the observed travel time and slowness values for the A branch are at variance with those from the model; but because of the low velocity gradient from 100 km to 300 km the amplitudes are low, as observed for the A branch below 19°, and remain low on the extension of the A branch as a second arrival. The sharp increase in velocity at 300 km produces a retrograde branch B which extends with low amplitude back to 20°, where the gradual increase in velocity below 300 km causes the amplitudes to increase over the range 20° to 14.5°.

The branch B is terminated at 14.5° by a decrease in velocity gradient near 400 km. An increase in velocity gradient below 500 km produces the C branch triplication near 20°. Below 520 km the velocity gradient decreases, producing the nearly linear, low amplitude section of the travel time and slowness curves between 22° and 24.5°. The C_3 branch is extended as a second arrival from $25.^{\circ}$ to 35°, where a discontinuity at 680 km produces the retrograde branch D extending back to 20°. The low velocity gradient below 700 km corresponds to the nearly constant slowness values for the E branch.

7.2.2 WRA-UM2

In order to remove the conflict between the observed and calculated slownesses for the A branch in the WRA-UM1 model, an attempt has been made in Figure 7-3 to compensate for lateral variations in uppermost mantle structure. The Ord P model above 250 km has been assumed to represent the receiver region and a model of type A in Figure 4-14 (with V_{min} = 7.8 km/s) has been assumed for the source area. For each arrival, the distances and times through these structures have been calculated and used to determine the changes which would result from replacing the upper 250 km beneath the source region with the Ord P structure:

$$(\Delta,T)_{corrected} = (\Delta,T)_{observed} - (\Delta,T)_{source} + (\Delta,T)_{Ord}$$

where $(\Delta,T)_{observed}$ are the observed values of distance and time corrected for focal depth, array structure and JB origin time bias (see Section 6.4); and $(\Delta,T)_{source}$ and $(\Delta,T)_{Ord}$ are the distances and times for the ray segments from a depth of 250 km to the surface, calculated using the structure corrected value of slowness for each arrival.

As shown by a comparison of Figures 7-3 and 6-10, this correction reduces the travel time and increases the distance for each arrival, the magnitudes of these effects decreasing for the more distant events. Since a gradual change in structure between the source and receiver has

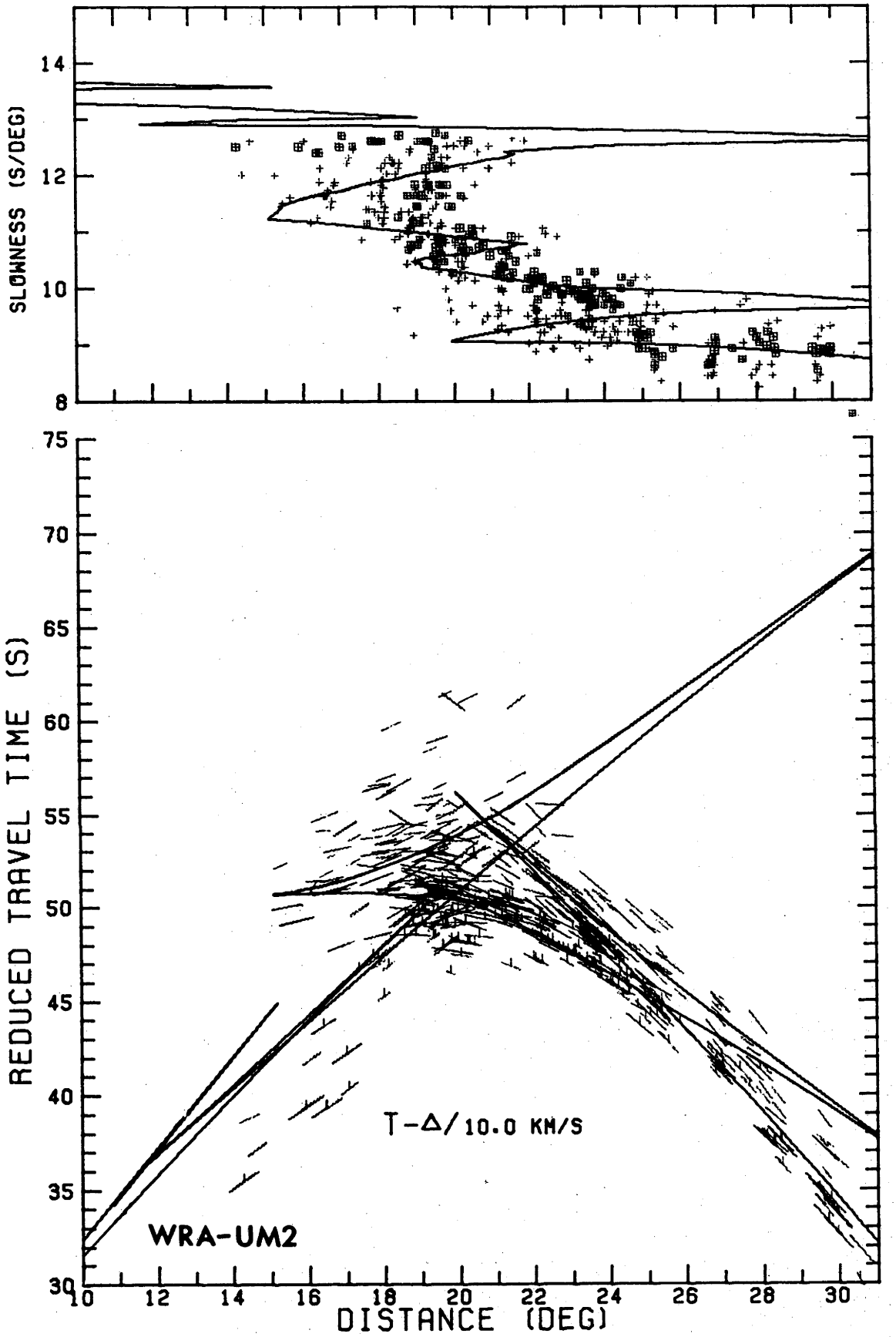

Figure 7-3. The WRA data (corrected for focal depth, local array structure, JB origin time bias and lateral velocity variation) compared with the WRA-UM2 model.

not been incorporated, this method has overcompensated for the shorter distance events, where differences in structure between the source and receiver ends of the ray paths may not be as extreme as assumed. Arrivals corresponding to rays which have bottomed above 250 km have been excluded from Figure 7-3.

Above 300 km, the velocities in the WRA-UM2 model in Figures 7-3 and 7-4 and Table 7-1 are a slightly modified version of the Ord P model, and the slownesses calculated for the A branch are in closer agreement with the observed values than those calculated from WRA-UM1. Below 300 km the velocities are similar to those in WRA-UM1.

7.3 Comparison With Other Studies

7.3.1 Refraction models

The rapid increases in velocity near 400 and 700 km in the WRA-UM models are similar to zones of high velocity gradient in most of the recent models discussed in Chapter 2. Below 400 km the WRA-UM models are especially similar to the Helmberger and Wiggins model HWNE (Figure 2-22). In order to satisfy their amplitude observations, Helmberger and Wiggins included an increased velocity gradient near 520 km and a decreased gradient below this depth. This produces only a minor high amplitude region near 21^{o} in their model, whereas the WRA data indicate that a more pronounced triplication may be present. The observed times at WRA for the C_3, D and E branches are almost identical with the HWNE times, although the high

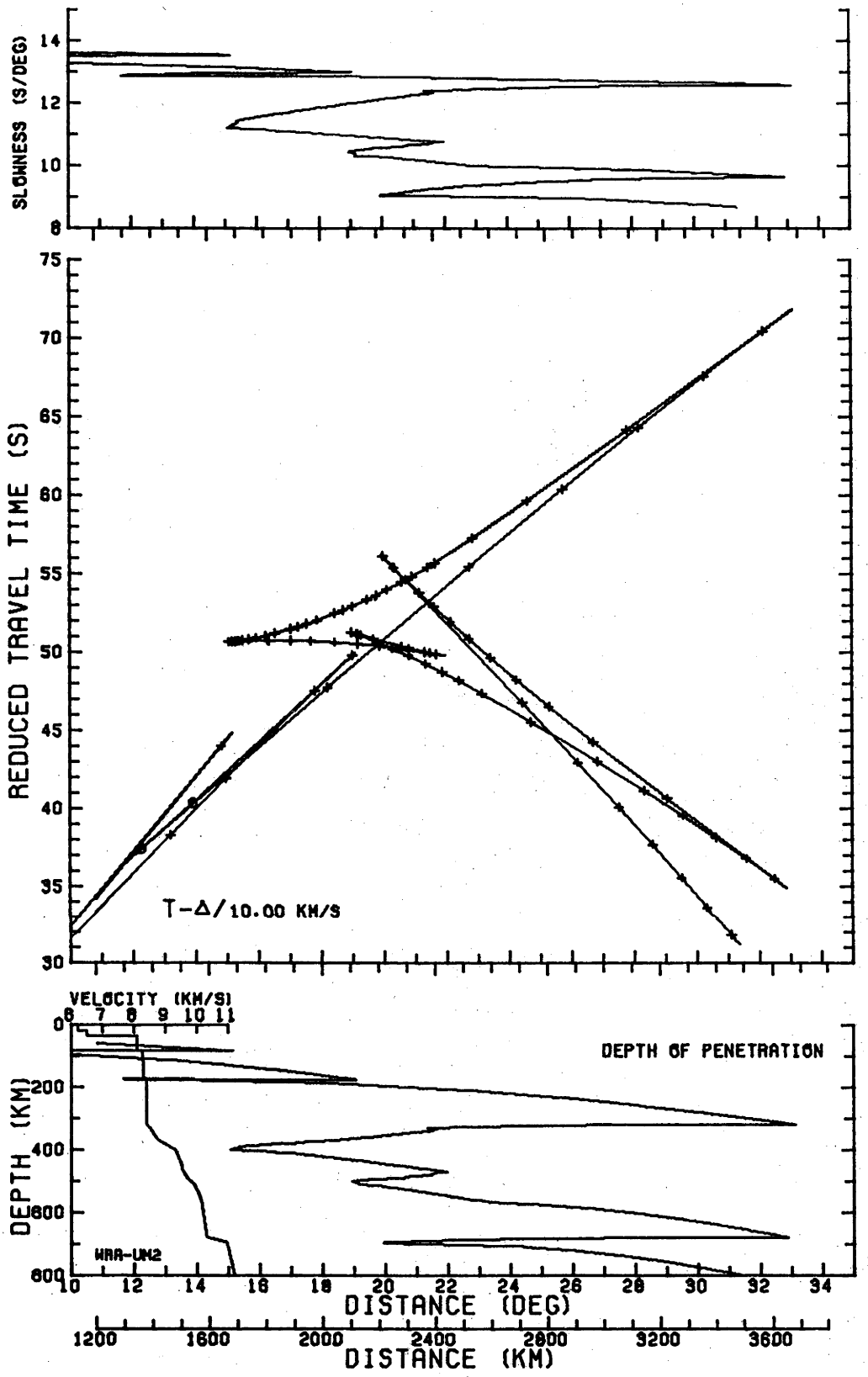

Figure 7-4. The WRA-UM2 model.

amplitudes at the forward end of the C_3 branch in their model are inconsistent with the absence of pronounced arrivals for this range in the WRA data.

In the region above 400 km, the constant velocity zone near 250 km in the WRA-UM models (required to give the low amplitude extension to the A branch) and the gradual increase in velocity between 300 and 400 km (required to give times and higher amplitudes corresponding to the retrograde end of the B branch) are similar to the structure in this region in the Green and Hales models (Figures 2-16, 2-17). In the WRA-UM models the velocity increase between 300 and 400 km has been made gradual to prevent a minor high amplitude caustic along the B branch such at that at 25° in the Green and Hales models which was caused by a sudden increase in velocity gradient between 200 km and 400 km.

Models with an increase in velocity from the base of the low velocity layer to a single discontinuity near 400 km produce a major later arrival branch which extends to distances beyond 22° (c.f. Figures 2-13, 2-14, 2-18 to 2-25). In Johnson's model (Figure 2-13) the sharp decrease in slowness just after the A branch becomes a second arrival should be associated with an increased amplitude, later arrival from 17° to 21°, but no obvious high amplitude phase is present over this distance range on his published record section. The synthetic seismograms presented by Helmberger and Wiggins (1971) and Wiggins and Helmberger (1972) show that, for the HW

series models, the amplitude of the A branch extension at 23^{o} should be at least twice that of the first arrival. Later arrivals are present on their record sections in this region, but the inconsistency of these arrivals makes it difficult to be confident of the branch to which they belong. As shown in Figure 6-12 the D branch arrivals at WRA are obvious as a clear later arrival only at the end of the branch near 21^{o} (Figure 6-12 i, j) and in the absence of slowness measurements it is possible for D branch arrivals in this region to be misinterpreted as extensions to the A branch.

In an earlier investigation of events to the north of WRA (Simpson et al., 1971) observations of a low amplitude early arrival near 20^{o} were attributed to a discontinuity at 280 km. With the increased data available in this study, it now appears that these arrivals correspond to the C_{1-3} arrivals in Figure 6-12, related to the deeper structure near 500 km, and thus the earlier arguments for a discontinuity at 280 km are no longer applicable. Massé et al. have recently presented a similar model for the Basin and Range region (Figure 2-26). Although it is possible that a model of this type could explain the first arrival slownesses near 11.5 s/deg at 19^{o} in Figure 6-10 (see section 6.5), there is no evidence in the travel time plots of later arrival branches corresponding to those in the Massé et al. model.

7.3.2 P'dP' results

Precursors, P'dP' to the core phase P'P', which have been attributed to underside reflections from discontinuities in the upper mantle (Gutenberg, 1960; Adams, 1968, 1971; Engdahl and Flinn, 1969; Whitcomb and Anderson, 1970), provide an independent source of information on velocity structure in the upper mantle. The most detailed study, by Whitcomb and Anderson, indicated a number of features that are in reasonable agreement with the WRA-UM models. They showed a pronounced discontinuity at 630 km, with other reflectors at 280 km and 520 km and possibly 410 km. In general, the arrivals for "P'650P'" are more prominent than for "P'400P'" (Whitcomb and Anderson, 1970; Adams, 1971) especially on short period records, suggesting, in agreement with the WRA-UM models, that the deeper structure is more abrupt. Richards (1972) has shown that the amplitudes of "P'650P'" require a discontinuity less than 4 km thick, and the observations of "P'650P'" also indicate that the depth to this reflector does not vary greatly beneath different tectonic regions.

7.4 Regional Variations in Velocity

Observations of a prominent later arrival phase in the distance range 12° - 18° in the western United States (cf. Julian and Anderson, 1968; Helmberger and Wiggins, 1971) show an average slowness of 10.8 s/deg.

Johnson's (1967) slowness values for a similar arrival, however, lie between 11 and 11.5 s/deg , and the WRA B branch arrivals have corrected values closer to 12 s/deg (see Figure 7-5a). In the western United States the arrival extends with very large amplitude back to at least 12^{o}, where it arrives almost 20 s after the first arrival (see record section in Julian and Anderson, 1968). In the WRA data, B branch arrivals can be seen at 14^{o}, but, although the data is sparse at shorter distances, they nevertheless are not as prominent on records below this distance. In the Ord River record section (Figure 4-5) arrivals of the M_2 and M_3 type can be observed beyond 12^{o} but the amplitude and delay after the first arrival are far less than observed in the western United States. If these arrivals all arise from the same depth range, they may indicate an appreciable regional variation in velocities to depths greater than 200 km. Lehmann (1970), in a review of observations of this arrival, has also suggested that variations in velocity down to 400 km are responsible for the observation of the B type arrival in the western United States and its apparent absence in other regions (e.g., eastern United States and Europe).

McMechan and Wiggins (1972) have used slowness and travel time data from the western United States to define extremal limits to velocity models for that region. The bounds on slowness, which they based on the Johnson

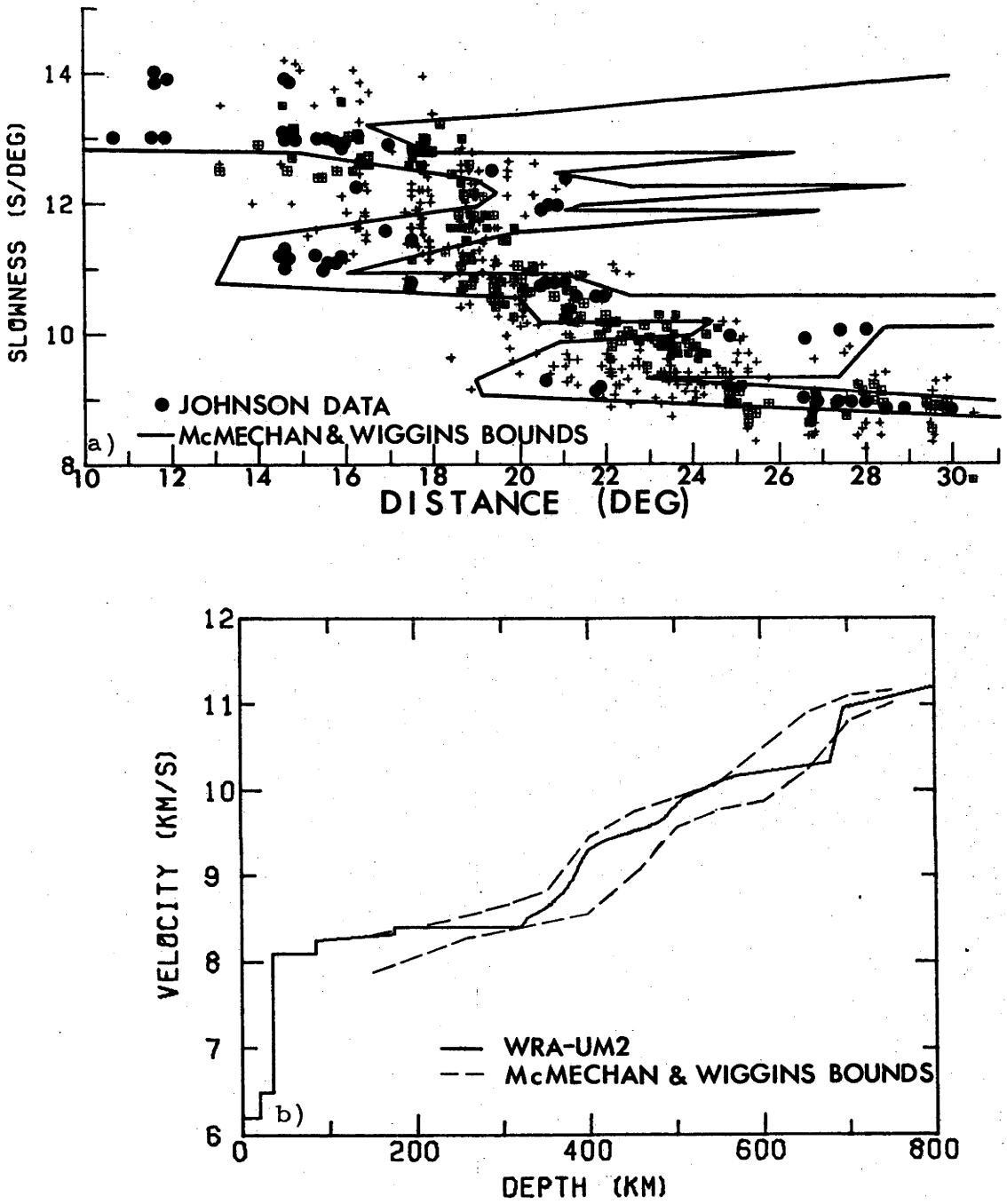

Figure 7-5. a) Comparison of the WRA and Johnson (1967) slowness data with the McMechan and Wiggins (1972) bounds.
b) Comparison of the WRA-UM2 model with the McMechan and Wiggins (1972) extremal bounds.

(1967) data, are compared with the WRA and Johnson data in Figure 7-5a, and their velocity bounds are shown with the WRA-UM models in Figure 7-5b. It appears from the similarity in the Johnson and WRA slowness data for the C, D and E branches and the close agreement of the WRA travel time data with the times from the Helmberger and Wiggins model HWNE that the structure below 400 km is very similar beneath the western United States and Australia. If this is the case, then some major changes are necessary to the McMechan and Wiggins bounds for the C branch slownesses. In the range 18° - 22° (corresponding to the C branch triplication) the bounds should be widened and the median value along the C_3 branch should be lowered to 10 s/deg. Worthington et al. (1973) have shown that the depth range which they find for the "650 km" discontinuity (690 $\pm$ 25 km), from a Monte Carlo inversion of S wave travel time and slowness data, indicates a deeper discontinuity than do the bounds for P waves (650 $\pm$ 25 km) given by Wiggins (1969) and McMechan and Wiggins (1972). The Worthington et al. result is constrained by the observation of S arrivals (corresponding to an extension of the C_3 branch) at distances up to 35° (Nuttli, 1969). The depth to the discontinuity in the McMechan and Wiggins bounds appears to be constrained by the abrupt decrease in the width of the slowness bounds beyond 28°, which (following Johnson's interpretation) constrains the Johnson slowness observations of 10 s/deg from 24° to 28° to lie on the retrograde branch D. This

interpretation is opposite to that given by Helmberger and Wiggins (1971) where they choose to confine these Johnson data to the C_3 branch. The WRA data confirms that these arrivals fall on the C_3 branch and show the McMechan and Wiggins slowness bounds to be over-constrained in this range.

As Figure 7-5b shows, it is possible for the depth to the deep discontinuity for P waves to fall outside the McMechan and Wiggins bounds and extend into a range more compatible with the Worthington et al. S wave results. Unfortunately, from the available WRA data it is not possible to determine whether a low amplitude extension to the C_3 branch (similar to that observed for S by Nuttli) extends beyond 30°. The WRA data are, however, the most detailed data available for the D branch, and a Monte Carlo or extremal technique inversion of the observed data on the C, D and E branches should greatly improve the resolution of bounds for the structure from 400 to below 700 km.

7.5 Conclusions

No uniqueness, of course, can be claimed for the WRA-UM models. In particular, the inability to detect the ends of the A and C branches greatly limits the resolution of the depths to the rapid velocity increases near 300 km and 680 km. However, from the general features of the data it is possible to specify at least

approximate depths and velocity increases, and the following features are considered to be characteristic of a model which would satisfy the WRA slowness and travel time data without producing any features that are not observed:

1. a low velocity gradient between 150 km and 300 km,
2. a total increase in velocity of about 10% between 300 km and 400 km, which starts abruptly near 300 km and increases most rapidly near 400 km,
3. an increase in velocity of about 2% in a narrow zone near 520 km,
4. a low velocity gradient from 550 km to 650 km,
5. an abrupt velocity increase of about 6% at a depth between 650 and 700 km,
6. possible additional rapid increases in velocity below 700 km (cf. Section 6.5.4).

CHAPTER 8

DISCUSSION

8.1 Introduction

Ringwood (1962, 1969) has argued in favour of an upper mantle of predominantly peridotitic composition, and has proposed a model composition, pyrolite, which Green and Ringwood (1967), Ringwood (1970) and Green (1973) have used as a basis for determining possible mineralogical variation in the uppermost mantle and mantle transition zone. Although the pyrolite composition originally arose from petrological considerations, the fine structure in physical properties of the upper mantle, which would result from mineralogical variations within this composition, is in substantial agreement with that found by geophysical methods. It is the purpose of this chapter to compare the geochemical results with the P wave models presented in Chapter 4 and 7.

8.2 The Uppermost Mantle

Ringwood and Green have presented a series of papers on the composition, mineralogy and evolution of the crust and uppermost mantle (Ringwood, 1962, 1969; Green and Ringwood, 1967, 1967b, 1970; Green, 1972a, 1973). They have pointed out four factors which influence the seismic velocity in the mantle:

1. pressure and temperature
2. mineralogical zoning
3. chemical zoning
4. partial melting

Although the absolute determination of seismic velocities based on the effects of temperature and pressure on a particular mantle composition (Wang, 1972; Graham, 1970) is limited by uncertainties in temperature and thermal gradient at depth, it is possible to qualitatively discuss the differences in velocity to be expected from gross differences in temperature beneath active and stable tectonic regions. Within a specific tectonic setting, relative changes in velocity (either velocity jumps caused by phase transitions, or changes in velocity gradient due to variations in mineral assemblage or chemical composition) can also be compared with observed velocity profiles.

Green and Ringwood (1967, 1970) have discussed the mineralogy of a pyrolite upper mantle along an oceanic geotherm, and in the 1967 paper (from which Figure 8-1 is reproduced) they suggest the effects on shear velocity produced by the experimentally observed P,T-dependent mineralogical variations. In a homogeneous upper mantle, increasing temperature (acting to decrease velocity) dominates over increasing pressure (acting to increase velocity) at shallow depths, and the first order effect on velocity in the region shown in Figure 8-1c is a gradual decrease in velocity, which (assuming a critical

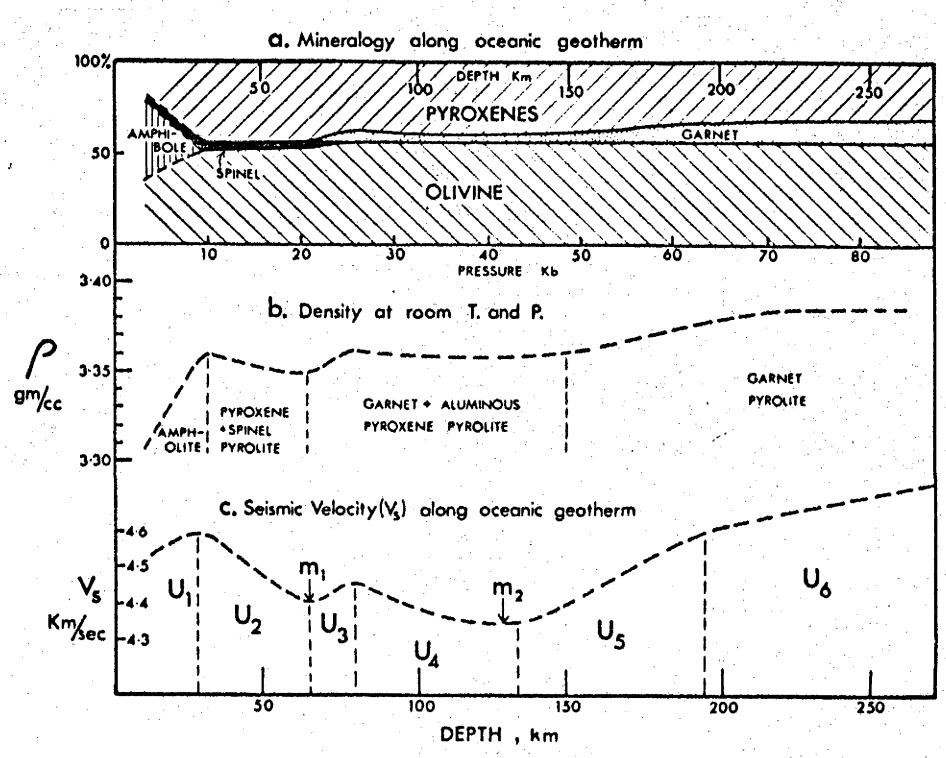

Figure 8-1. Changes in (a) mineralogy, (b) density (room T and P) and (c) relative changes in shear velocity along an oceanic geotherm for a pyrolite upper mantle (from Green and Ringwood, 1967).

gradient of $(\partial T/\partial P)V_S = 4.5^{\circ}C/km$) extends to approximately 140 km (m_2 in Figure 8-1c), and then an increase with depth. Superimposed on this broad minimum are a number of secondary features caused by changes in mineralogy. In the zone U_1, a slight velocity increase may be caused by a decrease in amphibole content which counteracts the temperature effect. The sudden velocity increase in U_3 is associated with a large density change due to the formation of garnet at the expense of spinel. In U_5, the velocity increase produced by the effect of pressure is augmented by an increase in garnet content.

This model does not consider the effect of partial melting, which may play an important role in the nature of the low velocity zone near 150 km. Anderson and Sammis (1970) have shown that, in the presence of a small percentage of partial melt, the minimum in velocity will be enhanced and the boundaries of the zone of low velocity may be more abrupt. The extent of partial melting depends on the proximity of the geotherm to the melting curve and is also sensitive to the amount of water in the bulk composition (Green, 1972a, 1973).

Chemical zoning may be a significant factor in stable continental shield regions, where a high degree of fractional melting, associated with the formation of primitive crustal material, has resulted in a residual zone of refractory dunite and peridotite in the uppermost mantle overlying a region of more primitive mantle

(Ringwood, 1969). Green (1972b) has pointed out that the characteristic ultramafic and basaltic volcanism of the oldest Archean greenstone belts requires very high degrees of melting in the upper mantle source region and suggested that the unique ultramafic volcanism of some Archean provinces may have been triggered by impact processes similar to those which formed the lunar maria. The effects of this postulated process, yielding very refractory residues, may have extended to depths of 150 to 300 km. If chemical zoning does occur, then the upper mantle beneath regions such as the Canadian and Australian shields will be depleted in the low melting point elements, and lower concentrations of radioactive heat sources will result in lower temperatures beneath these regions (Hyndman et al., 1968).

The general character of the travel times observed from the Project Early Rise and Ord River explosions suggest that the gross structure beneath the Canadian and Australian shields is similar. It is interesting, however, to investigate minor differences in the structures derived for these regions and compare these structures with that suggested by Green and Ringwood for a pyrolite upper mantle.

8.2.1 The 85 km discontinuity

Hales (1969) has suggested that a discontinuity at a depth near 85 km in the Early Rise models (D, E and F in Figure 4-11) resulted from the transition of spinel to garnet peridotite (zone U_3, in Figure 8-1c). The

discontinuity at a similar depth in the Ord P model adds weight to the postulated presence of the structure as a common feature of shield areas. The spinel-garnet transition is sensitive to the amount of aluminium in the bulk composition, the amount of aluminium present determining the amount of garnet produced (Green and Ringwood, 1967). The velocity above 85 km in the Ord P model (8.1 km/s) is higher and the velocity increase across the discontinuity (0.14 km/s) is smaller than in the Canadian shield models, where the velocities above the discontinuity are closer to 8.05 km/s and the velocity increases are 0.18 to 0.31 km/s. These differences may reflect a higher degree of fractionation beneath the Australian shield; the lower temperatures and lower concentrations of less refractory elements (more abundant and more Mg-rich olivine) resulting in a higher velocity zone above the discontinuity, and the lower aluminium content decreasing the amount of the higher velocity garnet phase produced across the discontinuity.

Under the oceanic conditions shown in Figure 8-1c the spinel-garnet transition occurs near 80 km. The depth of the transition should decrease at lower temperatures but is increased at lower aluminium concentrations. It is possible that these two effects almost cancel one another in the colder, more refractory mantle beneath the Australian shield. If a minor low velocity layer exists above the 85 km discontinuity (corresponding to m_1 in Figure 8-1c), as suggested in Section 4.3.3 to

explain the B' Ord River arrivals, the depth of the discontinuity may be slightly shallower.

8.2.2 The region between 85 and 175 km

In this zone, the effect of small portions of partial melt may be the dominant control on seismic velocities. The gradual increase of velocity through the zone in the Ord P model, contrasted with the presence of a minor low velocity layer near 150 km in the Green and Hales and Mereu models (D and E, Figure 4-11) again suggests that the temperatures are lower beneath the Australian shield. Variations in composition (especially water content) may enhance this difference.

8.2.3 The 175 km discontinuity

The zone of increasing velocity below 85 km in the Ord P model is terminated by a sudden velocity jump at 175 km. This discontinuity may be related to the bottom of the low velocity layers in the Green and Hales and Mereu models. A very small fraction of partial melt between 85 and 175 km beneath the Australian shield may be sufficient to depress the velocity gradient in this zone without producing a decrease in velocity. An alternative explanation for the 175 km discontinuity is that it represents the base of the depleted upper mantle being carried along by the Australian plate (i.e. the base of the asthenosphere).

8.2.4 The region between 175 and 300 km

Because of the low temperatures at shallow depths beneath shields, the thermal gradients at depths of

150 km to 300 km in these regions may be higher than beneath oceans (Clark and Ringwood, 1964) and it is possible that the low velocity gradient from 175 to 300 km in the WRA-UM2 model is the result of a high temperature gradient at these depths beneath Australia. The effect of temperature on S waves is more pronounced than for P waves (Liebermann and Schreiber, 1969) and deep low velocity zones for S waves beneath other shield areas (Brune and Dorman, 1963; Wickens, 1971) also suggest the existence of high temperature gradients below 200 km. The critical thermal gradient required to keep velocity constant with depth can be found from ultrasonic data, and Liebermann and Schreiber (1969) show the critical gradient for typical upper-mantle minerals to be in the range 5-8° C/km. These values, which are based on low temperature determinations of the temperature derivative, decrease for higher temperatures. Soga et al. have studied the effect of temperature on velocities in forsterite (Mg_2SiO_4) and using their data, the critical gradient for this mineral drops from 8.4° C/km at room temperature to 6.0° C/km at 1200°C. If decreases of the same magnitude occur for the other minerals used by Liebermann and Schreiber, then values of 3.5 to 6.0° C/km may be typical critical gradients for P waves at depths near 250 km. The gradient of the Clark and Ringwood (1964) shield temperature model is slightly less than 3° C/km at 250 km, and Herrin (1972) finds a similar

value for a model of the Canadian shield. The velocity gradient between 175 and 300 km need not be exactly zero as shown in the WRA-UM2 model, but if the low velocity gradient in this region is controlled by temperature alone, a temperature gradient of at least 3^{o} C/km (which corresponds to a velocity gradient of approximately 0.15 km/s/100 km in forsterite) would appear necessary to satisfy the low amplitude requirement for the A branch in the WRA data.

8.3 The Transition Zone

The probable changes in mineralogy of a pyrolite mantle between 300 and 800 km are shown in Figure 8-2 (Ringwood, 1972). The transition which has been studied in most detail is the conversion of $(Mg,Fe)_2SiO_4$ olivine to the spinel structure. Ringwood and Major (1970) show that the transition takes place over an extended pressure range, the magnesium-rich olivine first forming a solid solution of olivine and spinel components before transforming at higher pressure to a spinel-like material which they call the beta phase (Figure 8-3). Using their experimental data and assuming a mantle composition of Fo_{89} (i.e., $((Mg_{0.89},Fe_{0.11})_2SiO_4)$) and a temperature of 1600^{o}C at 400 km, Ringwood and Major (1970) indicate that the transition occurs over a range of 27 km centered about an average depth of 397 km. The interval over which it begins depends strongly on the iron content of the olivine and the temperature at the transition

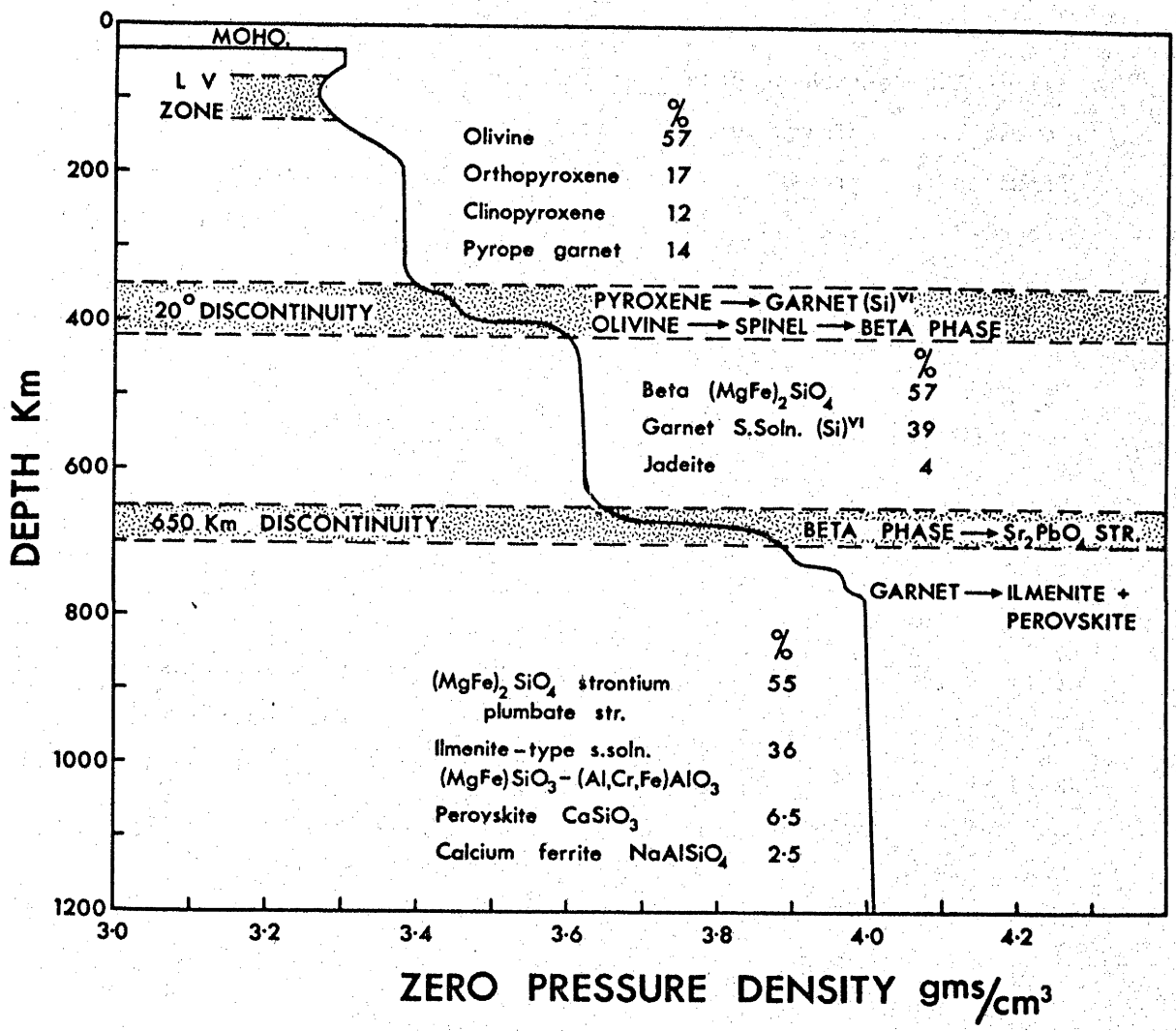

Figure 8-2. Probable mineral assemblages in a pyrolite upper mantle (from Ringwood, 1972).

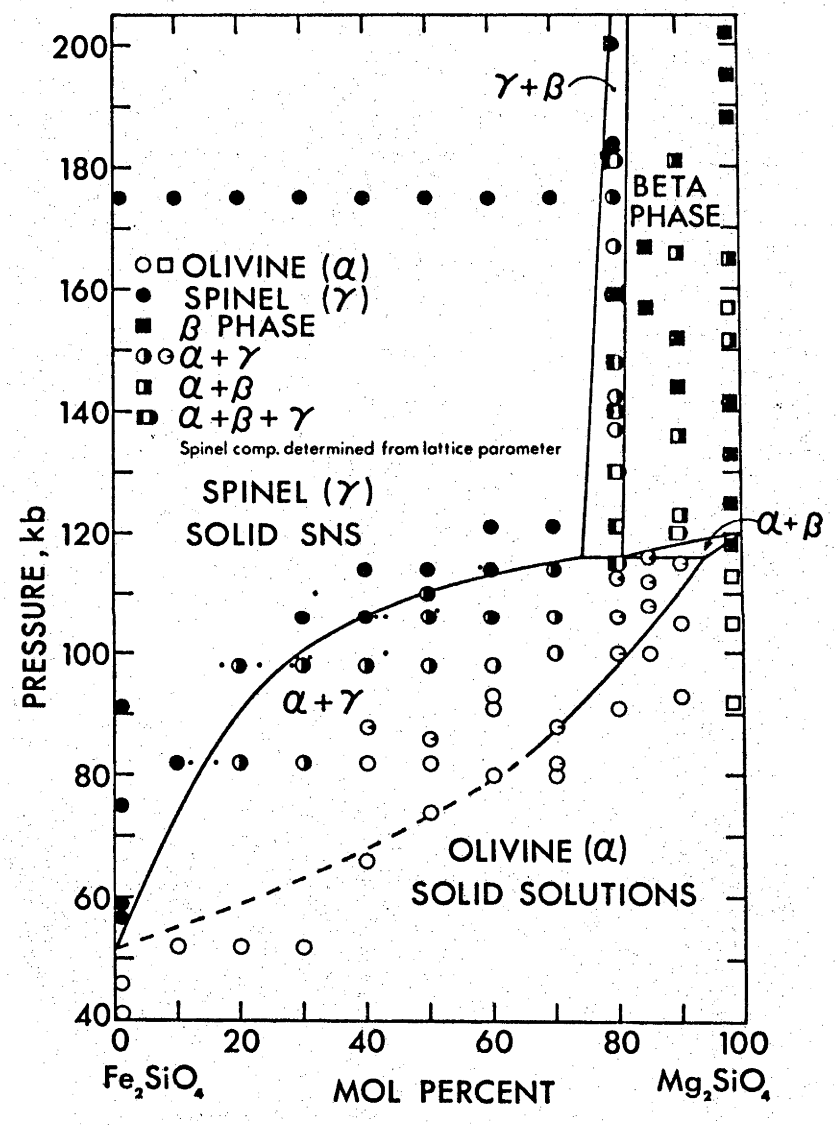

Figure 8-3. Phase diagram for the system $(Mg,Fe)_2SiO_4$ at 1000°C (from Ringwood and Major, 1970).

depth. The depth of the decrease in velocity gradient near 400 km in WRA-UM2 agrees with the depth expected for the end of the transition, when all of the olivine will have been converted to the beta phase. Above 400 km, the gradual increase in velocity in WRA-UM2 suggests that the onset of the transition, corresponding to the solid solution region of the olivine phase diagram, may extend over a depth range of up to 50 km.

The boundary between the beta phase and true spinel at higher pressure is uncertain and it is possible that as pressure increases the stability field for spinel is entered, where the beta phase would convert to the true spinel structure (Akimoto and Aramaki, 1972). This has been invoked by Whitcomb and Anderson (1970) to explain the discontinuity they observe at 520 km in their P'dP' study and it may also account for the high velocity gradient near 500 km in WRA-UM2. Ringwood (personal communication) has also suggested that the transformation of the calcium-rich garnet component into a perovskite structure should occur at a comparable depth.

The pyroxene-garnet transformation occurs at a lower pressure than that required for the olivine-spinel transition. As mentioned in Section 7.5, the depth to the 300 km discontinuity in WRA-UM2 is not well defined by the data, but it is possible that it corresponds to this transition. Ringwood (1967) has shown that near 1000^{o}C the transition should take place at 100 kbar (300 km). The temperature near 300 km is from 1200^{o}-

1400°C (Clark and Ringwood, 1964), and thus if the 300 km discontinuity in WRA-UM2 corresponds to the pyroxene-garnet transition, the temperature derivative of the transition pressure (which is unknown) must be close to zero (Ringwood, personal communication).

Controlled experimental studies at pressures and temperatures corresponding to depths near 700 km are beyond the range of present apparatus, but information on transitions in this region has been inferred from studies of germanate analogues (Ringwood, 1970). Rapid increases in velocity below 650 km have been attributed to the transformation of the spinel and garnet phases into more densely packed states (see Figure 8-2), and the beta phase to strontium plumbate transition appears the most likely candidate for the major discontinuity near 680 km in WRA-UM2. As discussed in the last chapter, all the available seismic evidence suggests that this transition must be very abrupt. Minor velocity increases below this depth could correspond to the other transitions shown in Figure 8-2 and would give rise to the WRA F-branch arrivals (Table 6-1) and the minor precursors to "P'650P'" observed by Bolt and Qamar (1972).

The low velocity gradients above 300 km and 680 km in the WRA-UM models were introduced to satisfy the requirements of low amplitudes along the A and C_3 branches. Although not pursued here, an interesting alternative would be to terminate these branches by introducing slight low velocity layers above the

discontinuities near 300 and 680 km, such as those shown in the S wave models of Ibrahim and Nuttli (1967) and Anderson and Julian (1969). A decrease in shear velocity, resulting from crystal lattice instability, may be associated with the onset of phase transitions (Liebermann and Schreiber, 1969; Anderson and Julian, 1969) and a similar but less pronounced effect on P velocity has been observed in certain types of phase changes (Wang, 1966).

The above discussion has shown that the main features of a velocity model such as WRA-UM2 are comparible with an upper mantle of pyrolite composition. A more detailed comparison of the finer variations in velocity, especially near the major phase transitions, should be possible as ultrasonic data on the behaviour of the physical properties of upper mantle minerals at high temperatures and pressures become available.

APPENDIX A

SEISMIC RAY THEORY

A.1 Basic Ray Theory Equations

The ray theory calculations used in this thesis are based on the presentations by Bullen (1961, 1965 chapter 7) from which the following equations have been adapted.

Given a velocity model for a spherically symmetrical earth, tabulated as a series of velocity - depth pairs (v_e, d_i); for each layer boundary,

$$r_i = R_E - d_i, \quad x_i = \frac{r_i}{R_E}$$

$$\eta_i = r_i/v_i \quad , \quad \mu_i = \eta_i/\eta_1 \qquad \text{A.1}$$

where R_E is the radius of the Earth; and within each layer L_i,

$$\zeta_i = \frac{r}{v}\frac{dv}{dr} = \frac{d \ln v}{d \ln r} = \ln\left(\frac{v_{i+1}}{v_i}\right)/\ln\left(\frac{r_{i+1}}{r_i}\right)$$

$$\alpha_i = 2/(1-\zeta_i) = 2\,\frac{d \ln r}{d \ln \eta} = 2 \ln\left(\frac{v_{i+1}}{v_i}\right)/\ln\left(\frac{\eta_{i+1}}{\eta_i}\right) \qquad \text{A.2}$$

For a particular ray P_j, with seismic ray parameter p_j, passing through this velocity structure,

$$P_j = \frac{r \sin i}{v} = dT/d\Delta = \frac{r_p}{v_p} = \text{constant along ray } P_j \qquad \text{A.3}$$

$$\lambda_j = P_j/\eta_1 \ , \qquad t_j = T_j/\eta_1$$

where the subscript p refers to the deepest point along the ray and T_j and Δ_j are the time and distance along the ray.

When α = constant, the integral equations for time and distance along a ray as a function of p (Bullen, 1961, p 94) have a direct analytical solution and the time and distance through a layer, L_i, can be expressed as:

$$t_i = \tfrac{1}{2}\ \alpha_i\ \left|(\mu_i-\lambda_j^{\,2})^{\frac{1}{2}}-(\mu_{i+1}-\lambda_j^{\,2})^{\frac{1}{2}}\right| \qquad \text{A.4}$$

$$\Delta_i = \tfrac{1}{2}\ \alpha_i\ \left|\cos^{-1}\ (\lambda_j/\mu_i) - \cos^{-1}\ (\lambda_j/\mu_{i+1})\right| \qquad \text{A.5}$$

A.2 The Power Low Interpolation for v

The case discussed above for α = constant corresponds to a velocity law of the form

$$v = v_o\ x^{\zeta_o}$$

$$v_r = v_i\ \left(\frac{r}{r_i}\right)^{\zeta_i} \qquad r_{i+1} < r < r_i \qquad \text{A.6}$$

This relation can be used to find the depth d_p at which the ray bottoms:

$$p_j = r_p / v_p$$

$$\text{but } v_p = v_i \left(\frac{r_p}{r_i}\right)^{\zeta_i}$$

$$\therefore \quad r_p = (p_j v_i / r_i^{\zeta_i})^{\alpha_i/2} \qquad \text{A.7}$$

$$\text{and } d_p = R_E - r_p$$

where L_i is the layer in which the ray bottoms ($\mu_{i+1} < p_j < \mu_i$).

This form of velocity law is slightly different than that given by Engdahl et al. (1968) who used $v = a.r^b$. In this form the constant b can become very large in regions of high velocity gradient.

A.3 Applications

A.3.1 Travel time curves

The total time and distance along a given ray path are (from equations A.4 and A.5):

$$\Delta_j = \sum_{i=1}^{n-1} \left[\alpha_i \{\cos^{-1}(\lambda_j/\lambda_i) - \cos^{-1}(\lambda_j/\mu_{i+1})\}\right] + \alpha_n \cos^{-1}(\lambda_j/\mu_n) \qquad \text{A.8}$$

$$t_j = \sum_{i=1}^{n-1} \left[\alpha_i \{(\mu^2_i - \lambda_j^2)^{\frac{1}{2}} - (\mu^2_{i+1} - \lambda_j^2)^{\frac{1}{2}}\}\right] + \alpha_n (\mu^2_n - \lambda^2_j)^{\frac{1}{2}} \qquad \text{A.9}$$

where n refers to the layer in which the ray bottoms.

Note that if a first order disconintuity exists at r_i then $r_i = r_{i+1}$ and no layer L_i exists and is therefore excluded from the summation in equations A.8 and A.9.

To form a complete travel time curve, it is necessary to determine the times and distances for a suite of rays covering the distance range of interest. In the program used to determine the various curves derived from the velocity models presented in Chapter 2, values of $dT/d\Delta$ separated by .05 s/deg were used; and to ensure that the end points of branches were reached, values of $dT/d\Delta$ corresponding to rays grazing each interface were inserted at the appropriate places. Use of $dT/d\Delta$ (p) as the independent variable enables the curves ($T-\Delta$, $p-\Delta$, $d_p-\Delta$) to be constructed in a continuous fashion, special steps being taken when the curves become segmented due to the effect of a low velocity layer.

A.3.2 Focal depth corrections

The time and distance along the extension of a ray path from focus back to the surface can be found using equations A.4 and A.5 and summing through the layers above the focus.

As pointed out in Chapter 6, this method allows separate corrections to be made for different arrivals from a single event, the value of slowness for each arrival (which determines λ_j in equations A.4 and A.5) specifying the magnitude of the correction for that arrival.

This method can also be used to find the travel time and distance corresponding to segments of ray paths between specific depths, such as in the Cannikin models of Section 4-4 or in "stripping the Earth" (see next section).

A.3.3 Velocity inversion - the Herglotz-Wiechert technique

The integral equations for T and Δ can be solved to determine η as a function of r. The solution (Bullen, 1961, p 97) is:

$$\int_{\Delta_p}^{o} \cosh^{-1}(\lambda/\mu_p)\, d\Delta = \pi \ln x_p = \pi \ln (r_p/R_E) \qquad \text{A.10}$$

where Δ_p, μ_p, x_p refer to the values of these parameters for a ray with deepest point corresponding to r_p. Given λ (from $dT/d\Delta$) as a function of distance, the left hand side of A.10 can be evaluated. The right hand side gives a value of r_p and from equations A.6 and A.7 the corresponding value of v_p can be found. As the distance increases along any branch of the travel time curve, r_p decreases, allowing (v,d) pairs to be determined for the depth range covered by that branch. If complete (p,Δ) data is available the procedure can be applied directly, noting that $d\Delta$ is negative along retrograde portions of the travel time curve. If data are available only in limited distance intervals, a velocity model from the

surface to the depth corresponding to the first data point, must be assumed. The layers above this depth can then be "stripped" off (section A.3.2) so that the first data point corresponds to zero stripped distance. The inversion technique can then be used to determine the velocities below the stripped depth.

APPENDIX B

WRA TRAVEL TIME AND SLOWNESS DATA

TABLE B-1 WRA SLOWNESS AND TRAVEL TIME DATA

EV NO	DATE	ORIGIN TIME	DELTA	AZIMUTH	FOCAL DEPTH	SLOWNESS	WT	TRAVEL TIME	DELTA (FDC)	T (FDC)	T-Δ/10 (FDC)	SLOWNESS (SC)	DELTA (FDSC)	T (FDSC)	T-Δ/10 (FDSC)
	DA-MO-YR	HR:MIN:S	DEG	DEG	KM	S/DEG		S	DEG	S	S	S/DEG	DEG	S	S
1	15- 4-69	17:50:20.8	15.8	33.2	31.	13.4	3	222.7	16.1	230.4	51.3	13.0	16.1	230.1	51.3
						11.5	2	227.0	16.0	233.6	55.5	11.2	16.0	233.5	55.5
						12.3	3	230.4	16.0	237.4	58.9	11.9	16.0	237.2	58.9
2	30- 8-70	21:57:55.1	15.8	37.1	10.	14.0	1	223.7	15.9	226.2	49.1	13.6	15.9	226.1	49.1
						12.5	1	230.3	15.9	232.6	55.7	12.1	15.9	232.6	55.7
3	5- 9-68	17: 2:49.8	16.0	31.9	33.	13.5	3	220.0	16.3	228.2	46.8	13.1	16.3	227.9	46.7
						14.3	3	224.0	16.0	233.0	55.1	13.9	16.3	232.5	55.8
						12.0	4	228.4	16.2	235.7	55.1	11.6	16.2	235.5	55.1
4	23-12-68	20:13:46.9	16.0	28.1	33.	13.4	1	222.7	16.3	230.8	49.0	13.0	16.3	230.5	49.0
						12.0	0	230.7	16.3	238.0	56.9	11.6	16.3	237.8	56.9
5	15- 4-69	21: 8:12.8	16.1	32.4	11.	12.9	1	227.3	16.2	229.8	49.9	12.5	16.2	229.8	49.9
						14.5	1	231.3	16.2	234.1	53.9	14.1	16.2	234.0	53.9
						11.6	1	235.6	16.2	238.1	58.2	11.3	16.2	238.0	58.2
6	10-11-69	15:42:34.5	16.1	28.5	40.	13.1	2	222.5	16.6	232.8	48.3	12.8	16.5	232.2	48.3
						12.6	1	230.6	16.5	240.1	56.3	12.2	16.5	239.7	56.3
7	3- 8-71	4:41:38.4	16.1	40.2	41.	13.0	1	223.8	16.6	234.2	49.7	12.6	16.5	233.6	49.6
						11.8	3	229.4	16.5	238.4	55.1	11.4	16.5	238.2	55.1
						11.9	3	231.6	16.5	240.7	57.4	11.5	16.5	240.4	57.3
8	8-10-71	18: 5:21.6	16.1	38.2	28.	13.1	5	226.6	16.4	233.3	51.2	12.7	16.4	233.1	51.1
						12.1	0	230.9	16.3	237.1	55.4	11.7	16.3	237.0	55.4
9	8-10-71	14:15:35.9	16.2	37.8	18.	13.0	3	227.3	16.3	231.6	50.0	12.6	16.3	231.5	50.0
						14.0	0	229.3	16.4	233.9	52.1	13.6	16.3	233.7	52.0
						12.8	2	230.5	16.3	234.7	53.2	12.5	16.3	234.6	53.2
10	9- 8-71	12:47:29.4	16.2	37.6	14.	13.0	1	228.0	16.3	231.3	49.6	12.6	16.3	231.2	49.6
						13.1	3	229.4	16.3	232.7	51.0	12.7	16.3	232.7	51.0
						12.0	2	234.0	16.3	237.1	55.6	11.6	16.3	237.1	55.6
11	9-10-71	2:36:34.4	16.3	38.1	26.	13.0	1	225.0	16.5	231.2	47.9	12.6	16.5	231.0	47.9
						12.3	3	229.1	16.5	234.9	51.9	11.9	16.4	234.8	51.9
						12.2	4	232.2	16.5	238.0	55.0	11.8	16.4	237.9	55.0
						12.7	1	234.5	16.5	240.5	57.4	12.3	16.5	240.4	57.3
12	21- 9-67	12:17:42.7	16.8	43.8	53.	13.0	1	233.9	17.6	248.2	53.0	12.6	17.5	247.1	52.8
						12.3	4	236.9	17.4	249.4	55.8	11.9	17.4	248.8	55.7
13	27- 6-71	2:37:20.8	17.0	36.2	58.	13.0	0	234.2	17.9	250.1	51.4	12.6	17.8	248.8	51.2
						12.6	3	236.8	17.8	251.4	53.8	12.2	17.7	250.5	53.7
14	28-12-68	6:27:23.1	17.1	19.4	41.	13.3	4	235.9	17.6	246.7	51.2	12.9	17.5	246.0	51.1
						11.2	2	241.4	17.4	250.0	56.5	10.9	17.4	249.8	56.5
						11.8	2	242.9	17.4	251.9	58.0	11.4	17.4	251.6	58.0
15	12- 9-67	7:31:34.9	17.1	46.5	137.	12.2	2	232.8	19.2	267.9	54.7	11.8	19.0	265.3	54.5
						11.6	1	235.1	18.8	266.2	56.8	11.3	18.7	264.6	56.7

NOTE:

Hypocenter data from NOAA locations.

Distances and azimuths from GEDESS lists.

FDC - Focal depth corrected.

SC - Structure corrected - slowness values multiplied by correction factor of 0.97.

FDSC - Focal depth corrections using structure corrected slowness values.

EV NO	DATE	ORIGIN TIME	DELTA	AZIMUTH	FOCAL DEPTH	SLOWNESS	WT	TRAVEL TIME	DELTA (FDC)	T (FDC)	T-Δ/10 (FDC)	SLOWNESS (SC)	DELTA (FDSC)	T (FDSC)	T-Δ/10 (FDSC)
	DA-MO-YR	HR:MIN:S	DEG	DEG	KM	S/DEG		S	DEG	S	S	S/DEG	DEG	S	S
16	15- 1-71	7:46: 5.9	17.3	17.8	33.	13.1	1	237.3	17.6	245.2	49.9	12.7	17.5	245.0	49.9
						12.6	3	242.5	17.5	250.1	55.1	12.2	17.5	249.9	55.0
						12.7	2	245.3	17.5	252.9	57.9	12.3	17.5	252.7	57.9
						12.0	3	248.1	17.5	255.4	60.6	11.6	17.5	255.2	60.6
17	3- 9-67	1:23:19.6	17.3	47.4	139.	11.1	2	235.2	18.8	264.5	55.4	10.8	18.7	263.3	55.4
						9.9	3	238.5	18.5	264.3	58.9	9.7	18.4	263.6	59.0
						13.0	2	242.3	20.4	290.9	64.4	12.7	19.8	283.1	63.4
						12.1	2	242.9	19.3	277.8	63.3	11.7	19.1	275.3	63.2
18	20-12-68	20: 0:30.7	17.4	37.7	91.	12.0	2	237.9	18.5	259.4	53.5	11.6	18.4	258.2	53.4
						11.2	2	238.8	18.3	258.0	54.3	10.9	18.3	257.3	54.3
						11.7	4	240.3	18.4	260.8	55.8	11.3	18.4	259.9	55.8
19	8-10-67	16:59:34.4	17.4	55.4	17.	11.5	0	242.5	17.5	246.2	51.5	11.2	17.5	246.2	51.5
						12.0	3	243.6	17.5	247.4	52.6	11.6	17.5	247.3	52.6
						11.8	3	248.0	17.5	251.8	57.0	11.4	17.5	251.7	57.0
						12.5	2	251.0	17.5	254.9	60.0	12.1	17.5	254.8	60.0
20	14- 1-71	11:39:37.2	17.4	17.2	33.	13.0	0	241.0	17.7	248.8	51.6	12.6	17.7	248.6	51.6
						14.4	1	242.3	17.4	252.4	58.4	14.0	17.8	251.9	54.0
						12.6	3	246.2	17.7	253.8	56.8	12.2	17.7	253.6	56.7
						12.2	2	250.6	17.7	258.0	61.1	11.8	17.7	257.8	61.1
21	14- 1-71	15:57:44.9	17.4	18.3	33.	13.3	4	240.1	17.8	248.1	50.7	12.9	17.7	247.9	50.7
						12.3	1	246.3	17.7	253.7	56.8	11.9	17.7	253.5	56.8
						11.7	2	250.3	17.7	257.4	60.8	11.3	17.7	257.3	60.8
22	15- 1-71	4: 2:50.3	17.5	17.6	33.	13.0	1	241.0	17.8	248.8	51.2	12.6	17.8	248.6	51.1
						12.0	2	247.6	17.7	254.9	57.7	11.7	17.7	254.7	57.7
						12.4	2	253.7	17.7	261.2	63.8	12.0	17.7	261.0	63.8
23	6- 1-69	17:25:41.8	17.5	17.3	33.	13.3	4	241.9	17.8	249.9	51.9	12.9	17.8	249.7	51.8
						12.0	3	248.6	17.8	255.9	58.5	11.6	17.7	255.7	58.5
						12.6	3	250.6	17.8	258.2	60.5	12.2	17.8	258.0	60.5
24	14- 1-71	9: 4:45.9	17.5	17.1	33.	13.2	5	242.5	17.8	250.5	52.2	12.8	17.8	250.2	52.2
						12.1	2	245.4	17.8	252.7	55.1	11.8	17.8	252.6	55.0
						12.0	1	248.0	17.8	255.3	57.6	11.6	17.8	255.1	57.6
25	15- 1-71	7:28:38.4	17.5	17.2	33.	13.4	4	241.6	17.9	249.7	51.0	13.0	17.8	249.4	51.0
						12.8	3	246.4	17.8	254.1	55.8	12.5	17.8	253.9	55.7
						11.6	1	247.6	17.8	254.7	56.9	11.3	17.8	254.6	56.9
						13.0	2	248.9	17.8	256.7	58.3	12.6	17.8	256.5	58.2
						11.9	0	251.0	17.8	258.2	60.3	11.5	17.8	258.1	60.3
26	15- 1-71	22:16:55.5	17.6	17.4	33.	13.2	5	243.9	17.9	251.8	52.4	12.8	17.9	251.6	52.3
						12.8	2	247.0	17.9	254.7	55.5	12.4	17.9	254.5	55.4
						12.6	3	249.6	17.9	257.2	58.0	12.2	17.9	256.9	58.0
27	14- 1-71	18: 7:22.1	17.7	18.0	33.	13.2	5	243.2	18.0	251.2	51.1	12.8	18.0	250.9	51.1
						11.8	2	249.8	17.9	257.0	57.7	11.4	17.9	256.8	57.7
28	14- 1-71	10:23:45.5	17.7	16.8	33.	13.2	5	241.7	18.0	249.7	49.5	12.8	18.0	249.4	49.5
						13.8	3	245.4	18.0	253.8	53.3	13.4	18.0	253.5	53.3
						11.5	2	247.4	17.9	254.4	55.1	11.2	17.9	254.3	55.1
						11.7	4	249.5	17.9	256.6	57.2	11.3	17.9	256.5	57.2
29	15- 1-71	13: 4:30.1	17.7	18.3	33.	13.2	3	244.4	18.0	252.4	52.1	12.8	18.0	252.1	52.1
						12.4	3	247.9	18.0	255.4	55.6	12.0	18.0	255.2	55.5
30	10- 8-71	0:57:38.3	17.7	14.6	33.	13.2	5	243.1	18.0	251.1	50.7	12.8	18.0	250.8	50.7
						11.6	3	247.7	17.9	254.8	55.2	11.3	17.9	254.6	55.2
						12.5	2	250.0	18.0	257.5	57.6	12.1	18.0	257.3	57.5
31	6-10-67	23: 2:44.0	17.8	50.0	57.	11.6	3	244.2	18.3	256.6	52.8	11.3	18.3	256.2	52.8
						13.2	1	249.0	18.6	265.5	58.1	12.8	18.5	263.9	57.9
32	10-10-67	8:23:25.0	17.9	32.4	94.	12.5	1	244.2	19.3	268.9	54.0	12.1	19.2	267.0	53.8
						11.6	4	245.5	19.0	266.4	55.0	11.3	18.9	265.5	55.0
33	26- 6-71	8:34:44.0	18.0	34.4	77.	12.2	4	246.4	19.0	265.0	54.2	11.8	18.9	264.0	54.1
						12.7	2	250.1	19.1	270.7	58.1	12.3	19.0	269.1	57.9
						12.6	1	257.7	19.1	277.9	65.6	12.2	19.0	276.4	65.5

EV NO	DATE	ORIGIN TIME	DELTA	AZIMUTH	FOCAL DEPTH	SLOWNESS	WT	TRAVEL TIME	DELTA (FDC)	T (FDC)	T-Δ/10 (FDC)	SLOWNESS (SC)	DELTA (FDSC)	T (FDSC)	T-Δ/10 (FDSC)
	DA-MO-YR	HR:MIN:S	DEG	DEG	KM	S/DEG		S	DEG	S	S	S/DEG	DEG	S	S
34	15- 9-68	3: 9:29.6	18.0	43.2	111.	12.2	4	243.8	19.6	271.6	54.1	11.8	19.4	269.7	54.0
						11.3	3	244.0	19.2	267.8	54.1	11.0	19.1	266.8	54.1
						12.9	3	245.4	20.0	279.2	56.4	12.5	19.7	275.3	55.9
35	7- 1-69	1:14:14.1	18.0	42.3	97.	12.2	4	244.8	19.3	268.7	53.8	11.8	19.2	267.2	53.7
						11.2	1	245.9	19.0	266.4	54.7	10.9	19.0	265.6	54.7
						11.6	3	246.9	19.1	268.7	55.8	11.3	19.1	267.7	55.7
36	19-10-68	21:51:45.9	18.1	46.2	87.	11.1	2	246.9	18.9	265.0	54.5	10.8	18.9	264.4	54.5
						10.8	4	247.1	18.9	264.7	54.8	10.5	18.8	264.1	54.8
37	4-11-70	4: 3:54.1	18.1	36.9	34.	12.8	3	250.1	18.5	258.1	52.8	12.5	18.4	257.9	52.7
						11.3	2	252.1	18.4	259.3	54.7	10.9	18.4	259.1	54.7
38	30- 4-70	10:30: 6.1	18.3	44.2	108.	11.3	2	246.7	19.5	269.7	53.3	10.9	19.4	268.8	53.3
						11.5	2	249.0	19.5	272.8	55.6	11.2	19.4	271.7	55.6
39	24- 9-67	7:48:36.4	18.3	43.4	84.	12.0	0	252.8	19.3	272.6	57.6	11.6	19.2	271.5	57.6
						11.3	0	253.6	19.2	271.5	58.3	11.0	19.1	270.8	58.3
						11.8	0	254.6	19.3	273.9	59.4	11.5	19.2	272.9	59.3
40	21- 9-67	3:31:33.3	18.3	43.0	60.	11.5	1	251.3	18.9	264.3	54.0	11.2	18.9	263.8	54.0
						12.9	1	253.1	19.2	269.3	56.1	12.5	19.1	268.0	55.9
						12.1	4	254.7	19.0	268.7	57.4	11.7	18.9	268.0	57.4
						12.5	1	256.3	19.1	271.2	59.1	12.1	19.0	270.3	59.0
						11.6	2	257.2	18.9	270.3	59.9	11.3	18.9	269.9	59.9
41	24- 8-69	12:39:30.1	18.4	48.6	39.	11.4	3	252.1	18.7	260.4	52.8	11.1	18.7	260.2	52.8
						10.8	2	255.3	18.6	263.2	56.0	10.4	18.6	263.1	56.0
42	29- 9-68	17:18:23.8	18.4	29.8	38.	11.0	0	253.3	18.7	261.2	53.8	10.7	18.6	261.0	53.8
						12.0	0	255.9	18.7	264.4	56.4	11.6	18.7	264.1	56.4
						12.6	4	257.5	18.7	266.5	58.0	12.2	18.7	266.1	58.0
43	29- 9-68	17:37:46.8	18.4	30.3	46.	11.8	2	254.3	18.8	264.5	55.4	11.4	18.8	264.1	55.4
						12.3	1	256.8	18.8	267.6	58.0	11.9	18.8	267.1	57.9
						13.2	2	259.5	19.0	272.0	60.9	12.8	18.9	271.1	60.8
44	28- 9-68	7:38:25.5	18.4	29.2	33.	13.4	2	254.5	18.7	262.6	54.6	13.0	18.7	262.3	54.5
						12.9	4	255.7	18.7	263.5	55.7	12.5	18.7	263.2	55.7
						13.3	3	259.5	18.7	267.5	59.6	12.9	18.7	267.2	59.5
45	29-10-68	22:42: 6.0	18.4	29.9	43.	13.0	3	254.7	18.9	265.7	55.6	12.6	18.8	265.1	55.5
						12.0	2	255.0	18.8	264.7	55.8	11.6	18.8	264.3	55.8
						11.0	3	255.4	18.7	264.3	56.1	10.7	18.7	264.1	56.1
						12.9	2	257.8	18.9	268.6	58.7	12.5	18.8	268.0	58.6
46	30-10-68	8:13:36.1	18.4	29.8	33.	12.0	0	255.5	18.6	262.8	55.5	11.6	18.6	262.6	55.5
						13.0	3	256.9	18.7	264.7	56.9	12.6	18.7	264.5	56.9
						11.3	3	258.7	18.6	265.7	58.7	11.0	18.6	265.5	58.7
						12.1	1	258.7	18.6	266.0	58.7	11.7	18.6	265.9	58.7
47	17-10-68	15:40:16.0	18.4	41.8	73.	12.2	0	250.8	19.3	268.4	53.4	11.8	19.3	267.4	53.3
						11.8	0	254.0	19.2	270.4	56.5	11.4	19.2	269.7	56.4
						11.5	0	256.0	19.2	271.9	58.5	11.2	19.1	271.3	58.4
48	29-10-68	21:54:35.2	18.4	30.1	44.	12.0	4	254.8	18.9	264.7	55.0	11.6	18.8	264.4	55.0
						12.3	4	256.8	18.9	267.0	57.0	11.9	18.8	266.6	57.0
						12.7	0	259.1	18.9	269.9	59.4	12.3	18.9	269.3	59.3
49	31-10-70	6:19:40.7	18.4	37.6	37.	11.5	2	254.5	18.7	262.4	54.1	11.2	18.7	262.2	54.1
						13.0	1	256.3	18.8	265.4	56.0	12.6	18.8	265.0	56.0
						12.4	1	262.9	18.8	271.4	62.6	12.0	18.8	271.1	62.5
50	3-11-70	4: 8:31.6	18.4	37.5	28.	12.7	0	254.7	18.7	261.2	53.4	12.3	18.7	261.0	53.4
						11.4	2	255.9	18.6	261.9	54.6	11.1	18.6	261.8	54.6
51	1-11-70	1:33: 4.3	18.5	37.0	20.	12.2	2	257.7	18.6	262.2	55.3	11.8	18.6	262.1	55.3
						11.7	2	260.5	18.6	264.9	58.1	11.3	18.6	264.8	58.1
						13.2	1	265.7	18.6	270.5	63.3	12.8	18.6	270.4	63.3
52	5- 9-67	3:39:55.9	18.5	34.7	27.	12.5	4	256.8	18.7	263.0	54.6	12.1	18.7	262.8	54.6
						11.5	3	259.3	18.7	265.1	57.1	11.2	18.7	265.0	57.1
53	29- 4-70	2:45:22.9	18.5	45.3	51.	11.2	1	253.3	19.0	264.0	53.2	10.9	18.9	263.7	53.3
						11.5	2	257.3	19.0	268.3	57.3	11.2	18.9	268.0	57.2
						11.9	2	260.3	19.0	271.8	60.3	11.6	19.0	271.4	60.3

EV NO	DATE	ORIGIN TIME	DELTA	AZIMUTH	FOCAL DEPTH	SLOWNESS	WT	TRAVEL TIME	DELTA (FDC)	T (FDC)	T-Δ/10 (FDC)	SLOWNESS (SC)	DELTA (FDSC)	T (FDSC)	T-Δ/10 (FDSC)
	DA-MO-YR	HR:MIN:S	DEG	DEG	KM	S/DEG		S	DEG	S	S	S/DEG	DEG	S	S
54	15-10-70	11:19:20.2	18.5	40.8	159.	11.4	3	247.9	20.5	283.2	55.6	11.1	20.3	281.4	55.6
						10.8	2	250.0	20.2	282.3	57.7	10.5	20.1	281.1	57.7
						9.9	3	257.1	19.9	286.4	65.0	9.6	19.8	285.6	65.1
55	2-11-70	14: 3:13.4	18.5	37.7	31.	11.8	4	255.4	18.8	262.2	53.2	11.4	18.8	262.0	53.2
						11.1	4	258.4	18.8	264.9	56.2	10.8	18.8	264.8	56.2
56	7- 5-70	12: 8:21.1	18.7	27.6	33.	12.5	2	255.2	19.0	262.8	51.9	12.2	18.9	262.6	51.8
						9.4	1	257.8	18.9	264.2	54.5	9.2	18.9	264.1	54.5
57	14- 9-68	18: 5:30.8	18.9	42.1	216.	12.5	1	263.9	19.0	271.4	60.6	12.1	18.9	271.2	60.5
						11.3	3	246.2	21.6	294.1	53.6	10.9	21.4	291.5	53.6
						10.8	1	247.2	21.3	291.7	54.6	10.5	21.1	289.8	54.7
						9.7	1	249.8	20.8	288.9	57.6	9.4	20.7	287.8	57.8
58	26- 8-69	19:13:13.1	19.1	45.9	88.	11.4	5	257.2	20.0	276.2	53.5	11.1	20.0	275.4	53.5
						10.9	1	258.3	19.9	276.3	54.7	10.6	19.9	275.7	54.7
						12.2	2	260.9	20.2	282.5	57.4	11.8	20.1	281.2	57.4
						10.1	1	263.4	19.8	280.1	59.9	9.8	19.8	279.7	59.9
59	9- 5-70	9:19:54.4	19.2	60.5	35.	10.8	3	264.6	19.4	271.8	55.6	10.4	19.4	271.6	55.6
						11.1	4	265.6	19.5	272.9	56.6	10.8	19.4	272.8	56.6
						10.8	2	267.1	19.4	274.3	58.1	10.5	19.4	274.2	58.1
60	8- 5-70	9:18:27.2	19.2	60.3	40.	10.9	4	263.8	19.5	272.0	54.9	10.6	19.5	271.9	54.9
61	8- 5-70	12:39:53.4	19.2	60.1	16.	11.2	5	264.8	19.5	273.2	55.9	10.9	19.5	273.0	55.9
						10.9	3	266.6	19.3	270.0	55.0	10.6	19.3	270.0	55.0
62	8- 5-70	1: 0:41.9	19.3	59.9	34.	11.2	4	268.6	19.3	272.1	57.0	10.9	19.3	272.0	57.0
						11.0	2	262.9	19.5	270.0	53.3	10.7	19.5	269.8	53.3
						11.4	3	265.3	19.5	272.5	55.7	11.1	19.5	272.4	55.7
						11.1	4	266.7	19.5	273.8	57.1	10.8	19.5	273.7	57.1
63	8- 5-70	13: 6:56.7	19.3	60.5	22.	11.0	5	266.2	19.4	270.8	55.1	10.7	19.4	270.8	55.1
						10.8	3	267.8	19.4	272.4	56.7	10.5	19.4	272.3	56.7
						11.4	3	268.8	19.4	273.5	57.7	11.1	19.4	273.5	57.7
						12.0	2	269.8	19.4	274.7	58.7	11.6	19.4	274.6	58.7
64	16- 9-68	14:55:24.0	19.3	49.9	99.	11.0	3	260.1	20.3	280.5	54.6	10.7	20.3	279.8	54.6
						11.4	2	261.5	20.4	283.0	56.0	11.1	20.3	282.1	56.0
						10.5	1	262.5	20.2	281.9	57.0	10.2	20.2	281.3	57.1
65	17- 9-68	7:30:51.9	19.3	47.9	36.	11.8	3	263.6	19.6	271.5	53.2	11.4	19.6	271.3	53.2
66	18- 9-68	9:11:52.7	19.4	49.0	57.	11.2	2	266.6	19.6	274.2	56.2	10.9	19.6	274.0	56.2
						11.1	1	261.8	19.9	273.6	52.4	10.8	19.9	273.3	52.4
						10.5	3	264.8	19.8	276.1	55.4	10.2	19.8	275.9	55.5
						11.9	2	267.3	20.0	280.3	58.0	11.6	19.9	279.7	57.9
67	16- 9-68	15: 0:44.2	19.4	48.1	66.	11.2	5	263.3	20.1	277.2	54.1	10.9	20.0	276.7	54.1
						10.8	4	264.6	20.0	277.9	55.4	10.5	20.0	277.6	55.4
68	8- 5-70	13:13: 5.2	19.5	61.2	5.	11.1	3	271.0	19.5	272.1	55.1	10.8	19.5	272.1	55.1
						10.6	1	272.8	19.5	273.9	56.9	10.3	19.5	273.8	56.9
						12.0	2	273.6	19.5	274.7	57.7	11.6	19.5	274.7	57.7
69	18- 9-68	14:10:57.8	19.5	48.0	68.	11.0	1	262.4	20.1	276.4	52.4	10.7	20.1	276.0	52.5
						10.7	2	263.4	20.1	277.0	53.5	10.4	20.1	276.7	53.5
						9.7	1	266.1	20.0	278.7	56.2	9.4	20.0	278.5	56.3
70	4- 1-69	10:28:34.9	19.6	48.0	58.	11.0	3	263.8	20.1	275.7	52.4	10.7	20.1	275.4	52.4
71	16- 9-68	13:55:36.1	19.6	47.2	59.	10.4	2	266.5	20.0	277.9	55.1	10.1	20.0	277.7	55.1
						11.0	4	265.9	20.1	278.1	54.4	10.7	20.1	277.8	54.4
						10.6	2	267.7	20.1	279.4	56.2	10.3	20.1	279.2	56.2
72	27- 6-71	20:50:22.6	19.6	35.1	17.	11.8	1	269.3	19.7	273.1	53.8	11.4	19.7	273.0	53.8
						10.3	1	271.4	19.7	275.0	56.0	10.0	19.7	274.9	56.0
						12.8	2	273.6	19.7	277.6	58.2	12.4	19.7	277.5	58.2
						12.5	2	280.6	19.7	284.5	65.2	12.1	19.7	284.5	65.2
73	16- 9-68	16:31:45.9	19.6	49.3	3.	10.8	0	268.3	19.6	268.9	50.5	10.5	19.6	268.9	50.5
74	27- 6-71	17:50:50.7	19.6	34.9	33.	11.1	5	269.5	19.6	270.1	51.7	10.8	19.6	270.1	51.7
						12.0	1	267.9	19.9	275.2	54.0	11.6	19.9	275.0	54.0
						11.4	1	269.3	19.9	276.3	55.4	11.1	19.9	276.2	55.4

EV NO	DATE	ORIGIN TIME	DELTA	AZIMUTH	FOCAL DEPTH	SLOWNESS	WT	TRAVEL TIME	DELTA (FDC)	T (FDC)	T-A/10 (FDC)	SLOWNESS (SC)	DELTA (FDSC)	T (FDSC)	T-A/10 (FDSC)
	DA-MO-YR	HR:MIN:S	DEG	DEG	KM	S/DEG		S	DEG	S	S	S/DEG	DEG	S	S
75	3- 5-70	18:22:56.7	19.6	34.1	33.	11.2	2	265.8	19.9	272.7	51.6	10.9	19.9	272.6	51.6
						10.6	2	266.6	19.9	273.3	52.4	10.3	19.9	273.2	52.4
76	16- 9-68	15:45: 4.6	19.7	48.7	59.	11.3	0	264.8	20.2	277.3	52.4	11.0	20.2	276.9	52.4
						10.7	4	265.8	20.2	277.6	53.4	10.4	20.1	277.3	53.4
						10.9	4	267.0	20.2	279.0	54.6	10.6	20.2	278.7	54.6
						12.5	2	272.4	20.4	287.0	60.1	12.1	20.3	286.2	60.0
77	6-10-68	12:28: 7.3	19.8	48.0	86.	11.1	5	266.5	20.6	284.4	54.8	10.8	20.6	283.8	54.8
78	16- 9-68	17:50:31.5	19.8	47.5	76.	11.0	5	266.5	20.6	282.2	53.7	10.7	20.5	281.7	53.7
						10.4	2	268.0	20.5	282.9	55.2	10.1	20.4	282.5	55.3
						11.4	2	268.0	20.6	284.4	55.2	11.1	20.6	283.7	55.2
						10.0	2	271.1	20.4	285.4	58.4	9.7	20.4	285.1	58.4
79	1- 5-70	5:12:59.7	20.1	47.5	129.	10.9	0	265.0	21.4	291.4	53.5	10.6	21.3	290.4	53.5
						10.3	3	265.7	21.2	290.4	54.2	10.0	21.2	289.7	54.3
						9.8	2	267.9	21.1	291.5	56.6	9.5	21.1	291.0	56.6
80	28- 8-69	15:10:29.3	20.2	48.0	100.	11.0	4	269.6	21.2	290.2	54.7	10.7	21.1	289.5	54.8
						10.6	2	270.3	21.1	290.1	55.5	10.3	21.0	289.5	55.5
81	7-10-68	0:24:13.0	20.2	36.0	19.	11.3	3	274.8	20.4	278.9	52.6	11.0	20.3	278.8	52.6
						12.5	3	276.4	20.4	280.8	54.2	12.1	20.4	280.7	54.2
						13.0	2	278.0	20.4	282.5	55.8	12.6	20.4	282.4	55.8
82	14-10-70	12: 3:56.7	20.6	53.4	33.	10.9	5	278.5	20.8	285.3	53.7	10.6	20.8	285.2	53.7
						9.8	4	283.0	20.8	289.5	58.2	9.5	20.8	289.4	58.2
						12.6	2	285.7	20.9	293.3	60.9	12.2	20.9	293.1	60.9
83	4-10-70	8:13:37.1	20.8	51.4	43.	10.6	4	281.2	21.1	289.9	54.8	10.3	21.1	289.7	54.8
						10.0	3	285.4	21.1	293.7	59.1	9.7	21.1	293.6	59.1
84	28- 8-69	11:55:17.5	20.9	51.0	49.	10.5	2	281.2	21.2	290.9	54.8	10.2	21.2	290.7	54.8
						11.0	2	281.2	21.3	291.3	54.7	10.7	21.3	291.1	54.8
						10.3	3	282.5	21.2	292.1	56.1	9.9	21.2	291.9	56.1
85	4-10-70	1:58: 5.8	20.9	50.8	33.	10.8	3	283.5	21.3	293.5	57.1	10.5	21.2	293.3	57.1
						10.7	1	281.1	21.1	287.9	53.3	10.4	21.1	287.7	53.3
						10.7	4	281.9	21.1	288.7	54.1	10.4	21.1	288.5	54.1
86	4-10-70	3:16:59.5	20.9	51.1	43.	10.3	1	285.3	21.1	291.9	57.5	10.0	21.1	291.8	57.5
						10.7	5	281.5	21.2	290.2	54.5	10.4	21.2	290.0	54.5
						9.9	5	285.4	21.2	293.7	58.4	9.6	21.1	293.6	58.4
87	3-10-70	10:34: 9.8	20.9	50.8	23.	10.5	5	282.8	21.0	287.5	53.6	10.2	21.0	287.5	53.6
88	4-10-70	17:40:51.3	20.9	51.3	35.	10.6	4	281.8	21.1	288.9	53.9	10.3	21.1	288.8	53.9
						9.5	5	285.7	21.1	292.5	57.8	9.3	21.1	292.4	57.9
89	3-10-70	14: 0:37.0	20.9	51.7	58.	10.5	4	280.0	21.4	291.5	53.4	10.2	21.4	291.2	53.4
						9.9	5	284.3	21.4	295.3	57.7	9.6	21.3	295.1	57.8
90	5-10-70	7:34:22.8	21.0	51.9	67.	10.8	4	279.6	21.5	293.1	53.6	10.5	21.5	292.8	53.6
						11.3	1	282.4	21.6	296.5	56.4	10.9	21.6	296.1	56.4
91	3-10-70	21:11:45.7	21.0	51.8	61.	10.6	3	279.8	21.5	291.9	53.2	10.3	21.4	291.7	53.2
						9.5	1	283.3	21.4	294.6	56.8	9.2	21.4	294.4	56.8
92	5- 1-69	11: 3:28.1	21.0	48.0	37.	10.7	2	279.8	21.2	287.3	51.1	10.4	21.2	287.2	51.1
						9.6	1	284.3	21.2	291.4	55.6	9.3	21.2	291.3	55.6
93	26- 8-69	16:58: 2.3	21.6	51.6	59.	10.6	5	287.2	22.0	298.9	53.8	10.3	22.0	298.7	53.8
						11.0	1	285.1	22.1	301.3	55.7	10.7	22.1	300.9	55.7
						9.3	2	292.7	22.0	303.5	59.4	9.0	21.9	303.3	59.4
94	27- 7-71	3: 1:34.0	21.6	52.8	38.	10.5	2	287.0	21.9	294.6	51.5	10.2	21.9	294.5	51.5
						10.5	2	289.9	21.9	297.5	54.3	10.2	21.9	297.4	54.4
95	22-12-68	15:27:18.9	21.6	42.4	33.	10.3	2	288.9	21.8	295.5	52.6	10.0	21.8	295.4	52.6
						10.9	2	291.3	21.9	298.1	55.0	10.6	21.9	298.0	55.0
96	26- 8-69	7:53:55.7	21.7	52.3	52.	10.9	1	288.1	22.1	298.8	53.1	10.6	22.1	298.5	53.1
						10.4	1	288.1	22.1	298.3	53.1	10.1	22.0	298.1	53.1
97	27- 7-71	5:33:58.7	21.7	52.7	33.	10.3	1	288.5	21.9	295.1	51.3	10.0	21.9	295.0	51.3
						10.5	3	290.5	21.9	297.2	53.3	10.2	21.9	297.1	53.3
						9.8	5	294.0	21.9	300.5	56.8	9.5	21.9	300.4	56.9
98	26- 7-71	12:56:42.8	21.9	52.8	33.	10.5	0	291.4	22.1	298.1	52.7	10.2	22.1	298.0	52.7
						10.0	5	294.2	22.1	300.7	55.5	9.7	22.0	300.7	55.5

EV NO	DATE	ORIGIN TIME	DELTA	AZIMUTH	FOCAL DEPTH	SLOWNESS	WT	TRAVEL TIME	DELTA (PDC)	T (PDC)	T-A/10 (PDC)	SLOWNESS (SC)	DELTA (PDSC)	T (PDSC)	T-A/10 (PDSC)
	DA-MO-YR	HR:MIN:S	DEG	DEG	KM	S/DEG		S	DEG	S	S	S/DEG	DEG	S	S
99	27- 7-71	7:55:48.4	21.9	52.8	41.	9.9	1	289.4	22.1	297.3	51.2	9.6	22.1	297.2	51.2
						9.8	5	292.1	22.1	300.0	53.9	9.5	22.1	299.9	54.0
100	27- 7-71	12:42:54.9	21.9	53.0	33.	10.5	1	291.5	22.1	298.2	52.2	10.2	22.1	298.1	52.3
						9.7	4	294.7	22.1	301.1	55.5	9.4	22.1	301.1	55.6
						9.9	2	296.0	22.1	302.5	56.8	9.6	22.1	302.4	56.8
101	27- 7-71	6:31:45.4	22.0	52.8	33.	10.1	3	293.3	22.2	299.9	53.5	9.8	22.2	299.8	53.5
						11.4	3	294.6	22.2	301.6	54.8	11.1	22.2	301.5	54.8
						9.6	4	296.1	22.1	302.5	56.3	9.4	22.1	302.5	56.3
						9.1	1	297.9	22.1	304.2	58.1	8.9	22.1	304.1	58.1
102	26- 7-71	3:26:27.7	22.0	52.6	33.	10.5	2	293.3	22.2	300.0	53.9	10.2	22.2	299.9	53.9
						9.7	3	295.9	22.2	302.3	56.0	9.4	22.1	302.3	56.0
						9.9	1	296.7	22.2	303.2	56.8	9.6	22.2	303.1	56.8
103	27- 7-71	4: 4: 7.3	22.0	51.8	54.	10.2	5	290.9	22.4	301.4	52.4	9.5	22.4	301.2	52.4
						9.5	5	293.7	22.3	303.7	55.3	9.2	22.3	303.6	55.3
104	27- 7-71	13:18:42.9	22.0	52.6	33.	10.5	5	292.1	22.3	299.8	52.4	10.2	22.2	299.7	52.4
						9.3	4	295.9	22.2	302.3	55.2	9.1	22.2	302.2	55.2
						11.3	3	300.5	22.3	307.5	59.8	11.0	22.3	307.3	59.8
105	26- 7-71	3:17:14.7	22.1	52.2	33.	10.5	2	293.1	22.3	299.8	52.0	10.2	22.3	299.7	52.0
						9.5	3	295.1	22.3	301.5	54.1	9.2	22.2	301.4	54.1
106	27- 7-71	14:56:49.0	22.2	52.9	33.	10.3	5	295.5	22.4	302.1	53.0	10.0	22.4	302.0	53.0
						9.8	5	298.3	22.4	304.8	55.8	9.5	22.4	304.7	55.8
107	27- 7-71	7:49:13.8	22.3	52.7	53.	10.3	2	293.6	22.7	304.0	51.9	10.0	22.6	303.8	51.9
						9.2	1	296.0	22.6	305.7	54.4	8.9	22.6	305.6	54.4
						9.8	1	296.6	22.6	306.6	55.0	9.5	22.6	306.5	55.0
108	27- 7-71	11:30:25.8	22.3	53.3	41.	10.3	4	294.6	22.6	302.7	52.0	10.0	22.5	302.6	52.0
						9.6	3	296.6	22.5	304.4	54.0	9.3	22.5	304.3	54.0
						11.3	2	300.7	22.6	309.3	58.0	10.9	22.6	309.1	58.0
109	27- 7-71	3:16:45.5	22.4	53.0	47.	10.2	1	295.3	22.8	304.5	51.3	9.9	22.8	304.3	51.3
						9.9	2	297.7	22.8	306.7	53.7	9.6	22.7	306.6	53.7
						9.4	1	297.7	22.7	306.5	53.7	9.1	22.7	306.4	53.7
110	26- 7-71	7:13:52.1	22.8	53.3	33.	10.2	4	298.7	22.8	305.3	51.7	9.9	22.8	305.2	51.8
						9.8	5	300.9	22.8	307.4	54.0	9.5	22.8	307.3	54.0
						10.0	4	302.3	22.8	308.8	55.4	9.7	22.8	308.8	55.4
111	27- 7-71	4:26: 2.4	22.6	52.7	52.	10.3	0	297.6	23.0	307.7	51.8	9.9	23.0	307.5	51.9
						9.7	2	299.4	23.0	309.2	53.7	9.4	23.0	309.0	53.7
112	27- 7-71	3:22:25.3	22.7	53.0	33.	10.4	5	301.1	22.9	307.8	53.0	10.1	22.9	307.7	53.0
						9.8	5	303.1	22.9	309.6	55.0	9.5	22.9	309.5	55.1
113	27- 7-71	9:23:58.6	22.7	53.1	39.	9.8	2	299.6	23.0	307.1	51.7	9.5	23.0	307.0	51.7
114	26- 7-71	23:33:32.1	22.8	53.3	42.	10.3	0	300.3	23.1	308.6	52.1	9.9	23.1	308.4	52.1
						10.2	2	302.1	23.1	310.4	53.9	9.9	23.1	310.2	53.9
115	27- 7-71	11:40:59.3	22.9	53.3	49.	10.2	4	301.1	23.2	310.6	52.4	9.9	23.2	310.5	52.5
						9.3	1	302.4	23.2	311.5	53.6	9.0	23.2	311.3	53.6
116	27- 7-71	9: 7:57.9	22.9	53.6	44.	10.6	1	301.0	23.3	309.8	51.1	10.3	23.2	309.7	51.2
						10.1	2	302.7	23.2	311.3	52.9	9.8	23.2	311.1	52.9
						9.6	3	304.2	23.2	312.6	54.4	9.4	23.2	312.4	54.4
117	25- 7-71	16:44:36.5	23.1	54.2	49.	10.4	3	302.1	23.4	311.8	51.1	10.1	23.4	311.6	51.1
						9.6	3	303.7	23.4	312.9	52.7	9.3	23.4	312.8	52.8
118	26- 7-71	9: 7: 7.3	23.1	52.8	33.	10.1	3	303.9	23.3	310.5	51.3	9.8	23.3	310.4	51.3
						9.4	1	306.6	23.3	312.9	54.0	8.9	23.3	312.9	54.0
						9.7	2	306.9	23.3	313.4	54.3	9.4	23.3	313.3	54.3
119	27- 7-71	6:45:20.4	23.1	53.7	34.	10.2	2	305.2	23.3	312.0	52.5	9.9	23.3	311.9	52.6
						9.6	5	306.4	23.3	313.0	53.8	9.3	23.3	312.9	53.8
120	26- 7-71	20:35: 3.8	23.1	54.3	46.	10.2	2	303.9	23.5	312.9	52.0	9.9	23.4	312.8	52.0
						9.9	5	305.6	23.4	314.5	53.7	9.6	23.4	314.3	53.8
121	27- 7-71	16: 3:13.7	23.1	53.9	54.	10.2	1	303.7	23.5	314.2	52.4	9.9	23.5	314.0	52.5
						9.9	4	304.9	23.5	315.2	53.7	9.6	23.5	315.0	53.7
						9.7	4	306.7	23.5	316.8	55.5	9.4	23.5	316.7	55.5
122	22- 7-71	23:10: 6.4	23.2	54.1	33.	10.2	3	304.1	23.4	310.7	50.8	9.9	23.4	310.6	50.8
						9.7	4	306.2	23.4	312.6	52.9	9.4	23.3	312.6	52.9

EV NO	DATE	ORIGIN TIME	DELTA	AZIMUTH	FOCAL DEPTH	SLOWNESS	WT	TRAVEL TIME	DELTA (FDC)	T (FDC)	T-A/1C (FDC)	SLOWNESS (SC)	DELTA (FDSC)	T (FDSC)	T-A/1C (FDSC)
	DA-MO-YR	HR:MIN:S	DEG	DEG	KM	S/DEG		S	DEG	S	S	S/DEG	DEG	S	S
123	2-12-70	10:15: 2.6	23.2	63.6	53.	10.0	3	305.0	23.6	315.2	52.7	9.7	23.6	315.0	52.7
						9.0	3	306.7	23.5	316.3	54.5	8.7	23.5	316.2	54.5
124	27- 7-71	11:38:42.4	23.2	53.1	52.	10.3	1	304.3	23.6	314.5	51.9	10.0	23.6	314.3	51.9
						9.3	2	305.1	23.6	314.7	52.7	9.0	23.6	314.5	52.8
125	27- 7-71	11:21: 6.1	23.3	54.0	44.	10.1	0	304.9	23.5	313.5	51.6	9.8	23.5	313.3	51.6
						9.6	5	306.3	23.5	314.6	53.0	9.3	23.5	314.4	53.1
126	27- 7-71	19:16:26.5	23.3	53.5	33.	10.1	2	305.2	23.4	311.7	51.0	9.8	23.4	311.7	51.0
						9.6	5	306.5	23.4	312.9	52.3	9.3	23.4	312.9	52.4
127	27- 7-71	13:31:46.8	23.3	52.9	33.	10.2	0	305.7	23.5	312.3	51.1	9.9	23.5	312.2	51.1
						9.5	4	307.0	23.5	313.4	52.4	9.2	23.5	313.3	52.4
128	27- 7-71	14: 2:25.3	23.3	53.1	53.	10.1	3	304.2	23.7	314.4	51.2	9.8	23.7	314.2	51.2
						9.7	5	305.7	23.6	315.7	52.7	9.4	23.6	315.5	52.8
129	26- 7-71	22:50: 1.1	23.3	53.6	47.	10.0	0	305.0	23.6	314.1	51.2	9.7	23.6	313.9	51.2
						9.6	3	306.4	23.6	315.3	52.6	9.3	23.6	315.2	52.7
130	27- 7-71	20:47:5e.5	23.3	53.4	43.	10.6	1	305.0	23.7	313.6	50.6	10.3	23.6	313.5	50.6
						9.7	4	306.4	23.6	314.6	52.0	9.4	23.5	314.5	52.0
131	27- 7-71	21:32:37.4	23.3	53.3	33.	10.0	0	306.0	23.5	312.5	50.8	9.7	23.5	312.5	50.8
						9.8	5	307.2	23.5	313.7	52.0	9.5	23.5	313.6	52.0
132	27- 7-71	0: 6:58.4	23.4	54.4	45.	10.0	2	307.1	23.7	315.8	52.2	9.7	23.7	315.7	52.3
						9.5	2	308.4	23.7	316.9	53.6	9.2	23.7	316.8	53.6
						10.0	2	309.6	23.7	318.3	54.7	9.7	23.7	318.2	54.8
133	27- 7-71	16:14:52.4	23.4	51.9	70.	10.1	4	303.3	24.0	316.7	50.1	9.8	23.9	316.4	50.1
						9.7	3	305.3	23.9	318.3	52.1	9.4	23.9	318.0	52.2
134	26- 7-71	15: 9:13.1	23.7	52.8	33.	10.2	1	311.2	23.9	317.8	52.2	9.9	23.9	317.7	52.2
						9.4	2	313.2	23.9	319.6	54.3	9.1	23.9	319.5	54.3
135	25- 7-71	22:24:26.0	23.7	54.4	35.	10.0	0	309.3	23.9	316.1	50.1	9.7	23.9	316.1	50.1
						9.5	5	311.2	23.9	317.9	52.1	9.2	23.9	317.9	52.1
136	22- 7-71	23:55:25.0	23.8	52.7	61.	10.0	2	308.0	24.2	319.6	50.5	9.7	24.2	319.4	50.5
						9.6	1	309.0	24.2	320.3	51.6	9.3	24.1	320.1	51.6
137	26- 7-71	14:49:44.0	23.8	53.2	43.	10.1	0	310.5	24.1	318.9	51.4	9.8	24.0	318.8	51.4
						9.8	3	311.9	24.0	319.9	52.8	9.5	24.0	319.8	52.8
138	27- 7-71	2: 3:20.4	23.8	53.4	55.	9.9	0	309.2	24.2	319.6	51.0	9.6	24.1	319.5	51.0
						9.3	3	310.8	24.1	320.9	52.7	9.0	24.1	320.7	52.7
139	27- 7-71	11:58:25.6	23.8	52.7	49.	10.1	3	308.8	24.1	318.3	49.9	9.8	24.1	318.1	49.9
						9.4	2	309.9	24.1	319.0	51.1	9.1	24.1	318.9	51.1
140	25- 7-71	9: 9:59.5	23.9	53.0	64.	10.5	1	308.2	24.4	320.8	49.7	10.2	24.4	320.5	49.7
						9.3	1	310.0	24.3	321.7	51.6	9.1	24.3	321.5	51.6
141	25- 7-71	11:23: 4.0	23.9	53.3	53.	10.0	1	309.0	24.3	319.2	49.4	9.7	24.2	319.0	49.5
						9.5	3	309.8	24.2	319.7	50.3	9.2	24.2	319.5	50.3
142	25- 7-71	21: 0:41.0	23.9	52.1	66.	10.0	0	309.1	24.4	321.6	50.5	9.7	24.3	321.3	50.6
						9.7	4	310.3	24.3	322.5	51.8	9.4	24.3	322.3	51.8
143	24- 7-71	12:51:50.2	23.9	53.2	60.	10.3	3	309.4	24.4	321.1	50.1	10.0	24.3	320.8	50.2
						9.5	4	312.8	24.3	323.9	52.6	9.2	24.3	323.7	50.7
144	23- 7-71	14:35:52.3	24.0	55.5	110.	9.5	4	306.3	24.8	326.0	49.9	9.2	24.8	325.7	50.0
						9.5	4	309.7	24.8	329.4	52.3	9.2	24.8	329.1	52.4
145	23- 7-71	17:58: 4.1	24.1	55.5	104.	9.4	3	307.3	24.9	325.9	49.3	9.1	24.9	325.5	49.3
						9.7	3	308.4	24.9	327.4	50.3	9.4	24.9	327.2	50.4
						9.5	1	309.9	24.9	328.6	51.8	9.2	24.8	328.2	51.9
146	23- 7-71	22:50:53.5	24.1	55.3	105.	9.2	2	306.4	24.9	324.9	48.1	8.9	24.9	324.5	48.2
						9.3	2	308.5	24.9	327.0	50.3	9.0	24.9	326.7	50.3
						9.6	1	309.5	24.9	328.5	51.2	9.3	24.9	328.1	51.2
						10.5	1	311.5	25.1	332.0	53.0	10.2	25.0	331.4	53.1
147	23- 7-71	15:27:13.9	24.2	55.3	113.	9.4	3	307.3	25.0	327.5	49.4	9.2	25.0	327.1	49.5
						10.0	1	309.1	25.1	330.2	51.1	9.7	25.1	329.7	51.1
148	23- 7-71	6:27:22.5	24.2	55.5	110.	9.4	5	306.9	25.0	326.6	48.3	9.2	25.0	326.2	48.4
						9.8	4	309.7	25.1	330.0	51.0	9.6	25.0	329.5	51.1

EV NO	DATE	ORIGIN TIME	DELTA	AZIMUTH	FOCAL DEPTH	SLOWNESS	WT	TRAVEL TIME	DELTA (FOC)	T (FOC)	T-Δ/10 (FOC)	SLOWNESS (SC)	DELTA (FOSC)	T (FOSC)	T-Δ/10 (FOSC)
	DA-MO-YR	HR:MIN:S	DEG	DEG	KM	S/DEG		S	DEG	S	S	S/DEG	DEG	S	S
149	3- 5-70	18: 7: 1.3	24.3	64.5	48.	10.4	1	313.2	24.6	322.7	48.9	10.1	24.6	322.5	48.9
						9.8	1	316.3	24.6	325.4	52.0	9.5	24.6	325.3	52.0
						9.5	2	318.4	24.6	327.4	54.1	9.2	24.6	327.3	54.2
150	26- 9-67	17: 5:55.0	24.4	61.4	94.	9.2	5	312.8	25.1	329.4	50.8	8.9	25.0	329.1	50.9
151	17- 7-71	6:50:44.7	24.5	56.0	33.	9.7	4	316.1	24.7	322.5	47.8	9.4	24.7	322.5	47.8
						10.5	3	318.5	24.7	325.2	50.2	10.2	24.7	325.1	50.2
152	6- 1-69	2: 5:39.9	24.9	67.0	33.	9.4	4	321.5	25.1	327.9	48.9	9.1	25.1	327.8	48.9
						10.2	4	323.6	25.1	330.2	51.0	9.9	25.1	330.1	51.0
153	6- 1-69	3: 6:10.9	24.9	67.5	43.	9.5	3	320.1	25.2	328.2	48.3	9.2	25.2	328.1	48.3
						10.3	3	321.6	25.2	330.1	49.8	9.9	25.2	329.9	49.8
154	7- 9-69	3: 6: 2.2	25.1	67.4	33.	9.1	4	323.3	25.3	329.6	48.4	8.8	25.3	329.5	48.4
						8.8	1	323.3	25.3	329.5	48.4	8.5	25.3	329.5	48.4
						10.0	2	325.8	25.3	332.3	50.8	9.7	25.3	332.3	50.8
						9.8	3	328.4	25.3	334.9	53.4	9.5	25.3	334.8	53.4
155	6- 9-69	14:49:55.9	25.2	67.4	15.	8.9	3	327.3	25.3	330.3	49.0	8.6	25.3	330.3	49.0
						9.0	1	329.9	25.3	332.9	51.6	8.7	25.3	332.9	51.6
						9.7	1	331.4	25.3	334.5	53.1	9.4	25.3	334.5	53.1
156	6- 9-69	17: 8: 3.2	25.2	67.6	10.	9.1	3	327.6	25.3	329.6	48.4	8.9	25.3	329.6	48.4
						9.1	0	326.3	25.3	328.3	47.1	8.9	25.3	328.3	47.2
						8.9	1	327.6	25.3	329.6	48.4	8.6	25.3	329.6	48.5
157	7- 9-69	6:21: 5.1	25.3	68.0	35.	9.0	3	329.6	25.5	330.2	46.8	8.8	25.5	330.2	46.9
						8.6	0	325.9	25.5	332.4	49.2	8.4	25.5	332.4	49.2
						9.8	4	327.9	25.5	334.8	51.1	9.6	25.5	334.7	51.1
158	18- 5-69	3:15:31.5	25.7	68.4	16.	9.2	4	331.2	25.8	334.4	47.8	8.9	25.8	334.4	47.8
						9.6	1	332.8	25.8	336.1	49.4	9.3	25.8	336.0	49.4
159	29- 5-70	4: 3:26.6	26.1	67.7	168.	9.2	4	320.6	27.4	349.8	45.3	8.9	27.3	349.2	45.4
						10.0	1	322.4	27.6	353.7	46.7	9.7	27.5	352.8	46.8
160	25- 6-70	5:13:58.6	26.4	66.5	69.	9.3	4	332.2	26.9	344.7	45.6	9.0	26.9	344.5	45.7
						8.9	1	333.5	26.9	345.7	47.0	8.6	26.8	345.5	47.0
						9.3	0	335.8	26.9	348.3	49.2	9.0	26.9	348.1	49.3
161	25- 6-70	13: 6:40.3	26.4	66.3	57.	9.0	4	333.2	26.8	343.5	45.5	8.7	26.8	343.3	45.5
						9.9	2	334.9	26.9	345.7	47.1	9.6	26.8	345.5	47.1
						8.7	1	336.7	26.8	346.8	49.0	8.4	26.8	346.7	49.1
162	25- 6-70	5:24:32.6	26.5	66.4	59.	9.4	2	333.4	26.9	344.2	45.5	9.1	26.9	344.1	45.5
						8.7	2	334.4	26.8	344.8	46.6	8.4	26.8	344.7	46.6
						9.4	3	336.2	26.9	347.0	48.3	9.1	26.9	346.9	48.3
						9.1	3	336.9	26.8	347.6	49.0	8.8	26.8	347.4	49.0
163	9- 1-69	16:32:51.7	26.5	66.3	31.	8.9	1	336.1	26.7	342.0	45.1	8.6	26.7	341.9	45.2
						9.3	2	337.3	26.7	343.3	46.3	9.0	26.7	343.2	46.3
						8.7	3	338.3	26.7	344.2	47.4	8.4	26.7	344.1	47.4
164	6- 1-69	1: 4:52.1	26.6	67.4	33.	8.9	3	337.1	26.7	343.4	46.1	8.6	26.7	343.3	46.1
						9.0	1	339.8	26.7	346.1	48.7	8.7	26.7	346.0	48.8
165	13- 1-69	8:55: 3.9	26.6	66.8	48.	9.1	5	335.9	26.9	344.7	46.1	8.9	26.8	344.6	46.1
						8.8	1	337.8	26.8	346.5	48.0	8.5	26.8	346.4	48.1
166	5- 1-69	13:26:39.9	26.6	66.9	47.	9.3	3	335.3	26.9	344.0	45.2	9.0	26.9	343.9	45.2
167	1- 5-70	23:32:37.6	27.2	68.9	67.	9.0	2	339.4	27.6	351.4	44.6	8.7	27.6	351.2	44.7
						9.3	4	340.4	27.6	352.6	45.6	9.0	27.6	352.4	45.6
						10.1	1	341.4	27.7	354.2	46.5	9.8	27.6	354.0	46.5
168	30- 4-70	9:25:23.1	27.6	73.8	85.	9.5	4	340.4	28.2	355.8	41.7	9.2	28.2	355.5	41.8
169	26-10-70	15: 5:47.4	27.7	73.4	82.	9.3	4	340.8	28.2	355.4	41.6	9.0	28.2	355.2	41.7
						9.6	3	342.3	28.3	357.3	43.0	9.4	28.2	357.0	43.1
170	16- 9-67	19:12:13.6	27.7	73.2	31.	9.5	4	349.0	27.9	355.0	45.3	9.2	27.8	354.8	45.4
						8.7	3	351.4	27.8	357.3	47.8	8.4	27.8	357.2	47.8
171	24- 5-69	16:27:39.4	27.8	73.4	96.	9.2	5	341.0	28.5	358.0	41.6	8.9	28.4	357.7	41.7
						8.7	2	342.5	28.4	358.9	43.2	8.4	28.4	358.7	43.3
						9.7	1	345.2	28.5	362.8	45.7	9.4	28.5	362.4	45.7
172	19- 6-70	2:11: 9.4	27.8	74.2	33.	9.4	3	346.4	28.0	352.8	41.9	9.1	28.0	352.7	41.9
						6.8	2	348.5	27.9	354.7	44.0	8.5	27.9	354.7	44.0

EV NO	DATE	ORIGIN TIME	DELTA	AZIMUTH	FOCAL DEPTH	SLOWNESS	WT	TRAVEL TIME	DELTA (FDC)	T (FDC)	T-A/10 (FDC)	SLOWNESS (SC)	DELTA (FDSC)	T (FDSC)	T-A/10 (FDSC)
	DA-MO-YR	HR:MIN:S	DEG	DEG	KM	S/DEG		S	DEG	S	S	S/DEG	DEG	S	S
173	9- 5-70	11:28:26.2	27.9	74.2	33.	9.3	3	347.2	28.0	353.5	41.8	9.0	28.0	353.5	41.8
						8.5	2	349.6	28.0	355.8	44.2	8.2	28.0	355.7	44.2
						8.9	1	350.8	28.0	357.1	45.4	8.6	28.0	357.0	45.4
174	26- 1-69	4:58:45.8	27.9	73.7	75.	9.4	4	344.0	28.4	357.6	41.8	9.1	28.4	357.3	41.8
						8.9	2	346.2	28.4	359.4	44.1	8.8	28.3	359.2	44.1
175	20- 9-69	0:12:17.6	27.9	74.2	87.	9.1	2	341.6	28.5	356.9	40.4	8.8	28.4	356.7	40.4
176	2-12-70	15:54:19.9	29.3	76.5	33.	9.2	5	359.9	29.4	366.2	39.0	8.9	29.4	366.2	39.1
177	1-12-70	18:14:36.6	29.3	76.6	33.	9.1	5	360.6	29.5	366.9	38.8	8.8	29.5	366.9	38.8
						8.9	1	363.4	29.5	369.7	41.6	8.6	29.5	369.6	41.6
178	1-12-70	18:51:18.7	29.4	76.7	26.	8.8	3	361.7	29.6	366.7	38.0	8.5	29.6	366.6	38.0
						9.4	4	364.8	29.6	369.9	41.1	9.1	29.6	369.8	41.1
						8.6	2	366.3	29.6	371.3	42.6	8.3	29.5	371.2	42.7
179	2-12-70	15:25:46.7	29.4	76.5	36.	9.2	5	360.1	29.6	366.9	37.4	8.9	29.6	366.9	37.4
						8.7	1	362.5	29.6	369.2	39.8	8.4	29.6	369.1	39.8
						9.5	1	364.2	29.6	371.1	41.5	9.2	29.6	371.0	41.5
180	2-12-70	15:17:22.2	29.5	76.7	39.	9.1	5	361.8	29.7	369.1	38.6	8.9	29.7	369.0	38.6
181	3-12-70	7:57:49.0	29.7	76.7	42.	9.2	5	361.4	29.9	369.2	38.7	8.9	29.9	369.1	38.8
182	3-12-70	11:54:32.1	29.7	76.8	33.	9.2	5	363.7	29.9	370.0	37.7	8.9	29.9	370.0	37.7
183	3-12-70	13:26:20.0	29.8	76.8	25.	9.1	5	365.2	29.9	370.0	37.7	8.8	29.9	370.0	37.7
						9.6	3	368.0	29.9	372.9	40.5	9.3	29.9	372.9	40.5
184	5- 1-69	17:33:40.5	30.3	76.8	33.	8.0	1	367.1	30.5	373.2	34.2	7.8	30.5	373.1	34.2
						9.0	4	368.8	30.5	375.1	35.8	8.8	30.5	375.0	35.8
185	5-12-70	23: 9:54.9	32.0	86.0	141.	9.0	3	372.1	33.0	396.4	29.5	8.8	33.0	396.0	29.6
						8.5	1	373.1	32.9	396.7	30.7	8.3	32.9	396.3	30.8
						7.9	1	374.1	32.8	396.8	32.0	7.7	32.8	396.5	32.1
186	18-11-68	1:39:22.4	12.9	334.9	28.	12.5	4	178.4	13.1	184.8	38.6				
						12.6	2	179.6	13.1	186.0	39.8				
						13.5	1	182.0	13.2	188.9	42.3				
187	4-10-68	6:50:50.9	13.4	339.7	52.	12.9	3	183.3	14.0	196.9	40.8				
						12.0	2	185.6	13.9	197.5	42.9				
						14.0	2	187.4	15.0	214.5	47.5				
188	27-10-68	19:59:13.8	13.6	339.7	91.	12.5	5	185.4	14.7	206.3	42.8				
189	11-11-68	9:33:30.1	13.7	343.1	75.	12.7	2	186.9	14.8	206.9	42.2				
						13.8	3	190.9	15.8	224.1	48.4				
						13.5	1	200.3	15.3	227.2	56.7				
190	9-11-68	2: 1:18.9	13.8	337.7	112.	12.4	4	186.0	15.5	215.4	43.0				
						13.3	3	189.1	16.4	229.5	47.6				
191	4- 9-68	20:41:57.0	13.9	334.0	124.	12.5	4	187.9	15.8	221.8	45.5				
						14.0	1	190.3	13.9	198.9	44.6				
						11.6	4	196.3	15.4	224.2	53.4				
192	1- 9-68	21:53:12.6	14.0	342.6	153.	12.5	3	199.9	15.8	233.8	57.5				
						13.2	3	190.0	18.2	253.1	50.6				
						12.8	1	195.6	17.1	248.4	58.1				
193	2- 9-68	19:29:13.0	14.3	313.6	33.	13.5	1	194.9	14.6	203.1	40.7				
						14.2	1	197.5	14.7	206.3	43.4				
						12.6	2	199.0	14.6	206.6	44.7				
194	9- 9-68	16: 1:22.1	14.3	329.5	82.	12.4	3	197.9	15.4	218.6	47.4				
						13.7	1	200.4	16.6	236.9	52.5				
						11.5	4	205.1	15.2	223.0	54.4				
195	4-10-68	7:27:16.3	14.5	326.4	32.	13.1	5	199.8	14.8	207.5	42.4				
						14.1	2	202.7	14.9	211.2	45.5				
						12.0	1	213.7	14.8	220.8	56.3				
196	1-11-68	13:18:47.1	17.1	325.9	53.	13.0	2	232.9	17.8	247.2	48.8				
						12.8	1	237.7	17.8	251.4	53.5				
						11.9	3	241.1	17.7	253.0	56.7				

No structure correction applied for events in the azimuth range 310° to 360°

REFERENCES

Adams, R.D., 1968. Early reflections of P'P' as an indication of upper mantle structure, Bull. Seism. Soc. Amer., 58, 1933-1947.

Adams, R.D., 1971. Reflections from discontinuities beneath Antarctica, Bull. Seism. Soc. Amer., 61, 1441-1451.

Akimoto, S. and S. Aramaki, 1972. Phase transformation and physical properties of the Earth's interior, in The Crust and Upper Mantle of the Japanese Area, 107-119, Earthquake Research Institute, Tokyo.

Anderson, D.L., 1967. Latest information from seismic observations, in The Earth's Mantle, (ed., T.F. Gaskell), 355-420, Academic Press, London, 509 pp.

Anderson, D.L., 1967b. Phase changes in the upper mantle, Science, 157, 1165-1173.

Anderson, D.L. and B.R. Julian, 1969. Shear velocities and elastic parameters of the mantle, J. Geophys. Res., 74, 3281-3286.

Anderson, D.L. and M.N. Toksoz, 1963. Surface waves on a spherical earth, I. Upper mantle structure from Love waves, J. Geophys. Res., 68, 3483-3500.

Anderson, D.L. and C. Sammis, 1970. Partial melting in the upper mantle, Phys. Earth Planet. Interiors 3, 41-50.

Angoran, Y. and D. Davis, 1972. Studies of PP and precursors to it, (abstract), Trans. Amer. Geophys. Union, 53, 447.

Archambeau, C.B., E.A. Flinn and D.G. Lambert, 1969. Fine structure of the upper mantle, J. Geophys. Res., 74, 5825-5865.

Barr, K.G., 1967. Upper mantle structure in Canada from seismic observations using chemical explosions, Can. J. Earth Sci., 4, 961-975.

Birtill, J.W. and F.E. Whiteway, 1965. The application of phased arrays to the analysis of seismic body waves, Phil. Trans. Roy. Soc. London, Ser. A, 258, 421-493.

Bolt, B.A., H.A. Doyle and D.J. Sutton, 1958. Seismic observations from the 1956 atomic explosions in Australia, Geophys. J. R. astr. Soc., 1, 135-145.

Bolt, B.A. and O.W. Nuttli, 1966. P wave residuals as a function of azimuth, J. Geophys. Res., 71, 5977-5985.

Bolt, B.A., M. O'Neill and A. Qamar, 1968. Seismic waves near 110°: is structure in core or upper mantle responsible?, Geophys. J. R. astr. Soc., 16, 475-481.

Bolt, B.A. and A. Qamar, 1972. Observations of pseudo-aftershocks from underground nuclear explosions, Phys. Earth Planet. Interiors, 5, 400-402.

Brune, J. and J. Dorman, 1963. Seismic waves and earth structure in the Canadian shield, Bull. Seism.

Soc. Amer., 53, 167-210.

Buchbinder, G.G.R., 1972. Travel times and velocities in the outer core from PmKP, Earth Planet. Sci. Letters, 14, 161-168.

Bullard, E.C., 1957. The density within the earth, Verhandelingen van het Koninklijk Nederlandsch Geologish-Mijnbouwkundig Genootschap, Geologische Serie, 18, 23-41.

Bullen, K.E., 1961. Seismic ray theory, Geophys. J. R. astr. Soc., 4, 93-105.

Bullen, K.E., 1963. An Introduction to the Theory of Seismology, 3rd Edition, Cambridge University Press, Cambridge, 381 pp.

Byerly, P., 1926. The Montana earthquake of June 28, 1925, Bull. Seism. Soc. Amer., 16, 209-265.

Carder, D.S., 1964. Travel times from central Pacific nuclear explosions and inferred mantle structure, Bull. Seism. Soc. Amer., 54, 2271-2294.

Chapman, C.H., 1971. On the computation of seismic ray travel times and amplitudes, Bull. Seism. Soc. Amer., 61, 1267-1274.

Clark, S.P. and A.E. Ringwood, 1964. Density distribution and constitution of the mantle, Rev. Geophys., 2, 35-88.

Cleary, J.R., 1967a. Azimuthal variations of the Longshot source term, Earth Planet. Sci. Letters, 3, 29-37.

Cleary, J.R., 1967b. P times to Australian stations from nuclear explosions, Bull. Seism. Soc. Amer., 57, 773-781.

Cleary, J.R., 1973. Australian crustal structure, Tectonophysics (in the press).

Cleary, J.R. and R.A.W. Haddon, 1972. Seismic wave scattering near the core-mantle boundary: a new interpretation of precursors to PKP, Nature, 240, 549-550.

Cleary, J.R. and A.L. Hales, 1966. An analysis of the travel times of P waves to North American stations, in the distance range 32^{o} to 100^{o}, Bull. Seism. Soc. Amer., 56, 467-489.

Cleary, J.R., D.W. Simpson and K.J. Muirhead, 1972. Variations in Australian upper mantle structure, from observations of the Cannikin explosion, Nature, 236, 111-112.

Cleary, J.R., C. Wright and K.J. Muirhead, 1968. The effects of local structure upon measurements of the travel time gradient at the Warramunga seismic array, Geophys. J. R. astr. Soc., 16, 21-29.

Denham, D., 1969. Distribution of earthquakes in the New Guinea-Solomon Islands region, J. Geophys. Res., 74, 4290-4299.

Denham, D., D.W. Simpson, P.J. Gregson and D.J. Sutton, 1972. Travel times and amplitudes from

explosions in Northern Australia, Geophys. J. R. astr. Soc., 28, 225-235.

Dewey, J.F. and J.M. Bird, 1970. Mountain belts and the new global tectonics, J. Geophys. Res., 75, 2625-2647.

Dibble, R.R., 1964. A portable slow motion magnetic tape recorder for geophysical purposes, N.Z. J. Geol. Geophys., 7, 445-465.

Douglas, A., P.D. Marshall and D.J. Corbishley, 1971. Absorption and complexity of P signals, Nature Phys. Sci., 233, 50-51.

Dowling, J.J. and O.W. Nuttli, 1964. Travel-time curves for a low velocity channel in the upper mantle, Bull. Seism. Soc. Amer., 54, 1981-1996.

Doyle, H.A., 1957. Seismic recordings of atomic explosions in Australia, Nature, 180, 132-134.

Doyle, H.A. and J.P. Webb, 1963. Travel times to Australian stations from Pacific nuclear explosions in 1958, J. Geophys. Res., 68, 1115-1120.

Engdahl, E.R. and E.A. Flinn, 1969. Seismic waves reflected from discontinuities within earth's upper mantle, Science, 163, 177-179.

Engdahl, E.R., J. Taggart, J.L. Lobdell, E.P. Arnold and G.E. Clawson, 1968. Computational methods, Bull. Seism. Soc. Amer., 58, 1339-1344.

Everingham, I.B., P.J. Gregson and H.A. Doyle, 1969. Thrust fault scarp in the Western Australian

shield, Nature, 223, 701-703.

Fitch, T.J., 1970. Earthquake mechanisms and island arc tectonics in the Indonesian-Philippine region, Bull. Seism. Soc. Amer., 60, 565-591.

Fitch, T.J., 1972. Plate convergence, transcurrent faults, and internal deformation adjacent to southeast Asia and the western Pacific, J. Geophys. Res., 77, 4432-4460.

Fitch, T.J. and P. Molnar, 1970. Focal mechanisms along inclined earthquake zones in the Indonesia-Philippine region, J. Geophys. Res., 75, 1431-1444.

Gangi, A.F. and J.W. Fairborn, 1968. Accurate determinations of seismic array steering delays by an adaptive computer program, Suppl. al Nuovo Cimento, 6, 105-115.

Graham, E.K., 1970. Elasticity and composition of the upper mantle, Geophys. J. R. astr. Soc., 20, 285-302.

Green, D.H., 1972a. Magmatic activity as the major process in the chemical evolution of the Earth's crust and mantle, Tectonophysics, 13, 47-71.

Green, D.H., 1972b. Archaean greenstone belts may include terrestial equivalents of lunar maria?, Earth Planet. Sci. Letters, 15, 263-270.

Green, D.H., 1973. Experimental melting studies on model upper mantle compositions at high pressure

under both water-saturated and water-undersaturated conditions, preprint.

Green, D.H. and A.E. Ringwood, 1967. The stability fields of aluminous pyroxene peridotite and garnet peridotite and their relevance in upper mantle structure, Earth Planet. Sci. Letters, 3, 151-160.

Green, D.H. and A.E. Ringwood, 1967b. An experimental investigation of the gabbro-eclogite transformation and some petrological applications, Geochim. Cosmochim. Acta., 71, 3589-3594.

Green, D.H. and A.E. Ringwood, 1970. Mineralogy of peridotitic compositions under upper mantle conditions, Phys. Earth Planet. Interiors, 3, 359-371.

Green, R.W.E. and A.L. Hales, 1968. The travel times of P waves to 30° in the central United States and upper mantle structure, Bull. Seism. Soc. Amer., 58, 267-289.

Gutenberg, B., 1959. Wave velocities below the Mohorovicic discontinuity, Geophys. J. Roy. astr. Soc., 4, 348-352.

Gutenberg, B., 1959b. Physics of the Earth's Interior, Academic Press, New York, 240 pp.

Gutenberg, B., 1960. Waves reflected at the "surface" of the Earth: P'P'P'P', Bull. Seism. Soc. Amer., 50, 71-79.

Gutenberg, B. and C.F. Richter, 1935. On seismic waves (second paper), Gerl. Beitr. Geophys., 45, 280-360.

Hales, A.L., 1969. A seismic discontinuity in the lithosphere, Earth Planet. Sci. Letters, 7, 44-46.

Hales, A.L., 1972. The travel times of P seismic waves and their relevance to the upper mantle velocity distribution, Tectonophysics, 13, 447-482.

Hales, A.L., J.R. Cleary, H.A. Doyle, R. Green and J. Roberts, 1968. P-wave station anomalies and the structure of the upper mantle, J. Geophys. Res., 73, 3885-3896.

Hales, A.L., J.R. Cleary and J.L. Roberts, 1968b. Velocity distribution in the lower mantle, Bull. Seism. Soc. Amer., 58, 1975-1989.

Helmberger, D. and R.A. Wiggins, 1971. Upper mantle structure of midwestern United States, J. Geophys. Res., 76, 3229-3245.

Herrin, E., 1972. A comparative study of upper mantle models: Canadian shield and Basin and Range provinces, in The Nature of the Solid Earth, (ed. E.C. Robertson), 216-231, McGraw-Hill, New York, 677 pp.

Herrin, E., W. Tucker, J.N. Taggart, D.W. Gordon and J.L. Lobdell, 1968. Estimation of surface-focus P travel times, in 1968 Seismological Tables for P Phases, (chairman, E. Herrin),

Bull. Seism. Soc. Amer., 58, 1273-1291.

Hyndman, R.D., I.B. Lambert, K.S. Heier, J.C. Jaeger and A.E. Ringwood, 1968. Heat flow and surface radioactivity measurements in the Precambrian shield of Western Australia, Phys. Earth Planet. Interiors, 1, 129-135.

Ibrahim, A.K. and O.W. Nuttli, 1967. Travel time curves and upper mantle structure from long period S waves. Bull. Seism. Soc. Amer., 57, 1063-1092.

Isacks, B., J. Oliver and L. Sykes, 1968. Seismology and the new global tectonics, J. Geophys. Res., 73, 5885-5899.

Iyer, H.M., L.C. Pakiser, D.J. Stuart and D.H. Warren, 1969. Project Early Rise: seismic probing of the upper mantle, J. Geophys. Res., 74, 4409-4441.

Jackson, D.D., 1972. Interpretation of inaccurate, insufficient and inconsistent data, Geophys. J. R. astr. Soc., 28, 97-110.

Jacob, K.H., 1970. Three-dimensional seismic ray tracing in a laterally heterogeneous spherical Earth, J. Geophys. Res., 75, 6675-6689.

Jeffreys, H., 1939. The times of P, S and SKS and the velocities of P and S, Mon. Not. R. astr. Soc., Geophys. Suppl., 4, 498-533.

Jeffreys, H., 1966. Revision of travel times, Geophys. J. R. astr. Soc., 11, 5-12.

Jeffreys, H., 1970. The Earth, (5th ed.), Cambridge University Press, Cambridge, 525 pp.

Jeffreys, H. and M. Shimshoni, 1966. The use of amplitudes in improving velocity distributions for Europe, Geophys. J. R. astr. Soc., 10, 515-524.

Johnson, L.R., 1967. Array measurements of P velocities in the upper mantle, J. Geophys. Res., 72, 6309-6325.

Johnson, L.R., 1969. Array measurements of P velocities in the lower mantle, Bull. Seism. Soc. Amer., 59, 973-1008.

Johnson, T. and P. Molnar, 1972. Focal mechanisms and plate tectonics of the Southwest Pacific, J. Geophys. Res., 77, 5000-5032.

Jordan, T.H., 1973. Estimation of the radial variation of seismic velocities and density in the Earth, Ph.D. thesis, California Institute of Technology, Pasadena.

Julian, B.R. and D.L. Anderson, 1968. Travel times, apparent velocities and amplitudes of body waves, Bull. Seism. Soc. Amer., 58, 339-366.

Kanamori, H., 1967. Upper mantle structure from apparent velocities of P waves recorded at Wakayama micro-earthquake observatory, Bull. Earthquake Res. Inst. Tokyo, 45, 657-678.

Kanamori, H., 1970. Seismological evidence for heterogeneity of the mantle, J. Geomag. Geoelectr. 22, 53-70.

Katili, J.A., 1971a. A review of the geotectonic theories

and tectonic maps of Indonesia, Earth Sci. Rev., 7, 143-163.

Katili, J.A. and R. Soetadi, 1971b. Neotectonics and seismic zones of the Indonesian Archipelago, Roy. Soc. N.Z. Bull., 9, 39-45.

Keen, C.G., J. Montgomery, W.M.H. Mowat, J.E. Mullard and D.C. Platt, 1965. British seismometer array recording systems, The Radio and Electronic Engineer, 30, 297-306.

Kelly, E.J., 1964. Limited network processing of seismic signals, Mass. Inst. Technol. Group Rept., 44.

King, D.W., 1971. A digital processing system for seismic array data, The Austral. Computer J., 3, 178-181.

King, D.W., R.E. Mereu and K.J. Muirhead, 1973. The measurement of apparent velocity and azimuth using adaptive processing techniques on data from the Warramunga seismic array, Geophys. J. R. astr. Soc. (submitted).

Lehmann, I., 1934. Transmission times for seismic waves for epicentral distances around 20°. Geod. Inst. Copenhagen, Medd. 5, 44 pp.

Lehmann, I., 1964. On the travel times of P as determined from nuclear explosions, Bull. Seism. Soc. Amer., 54, 123-139.

Lehmann, I., 1970. The 400-km discontinuity, Geophys. J. R. astr. Soc., 21, 359-372.

Lenham, I., 1967. Low velocity layers, in The Earth's Mantle (ed., T.F. Gashell), 41-61, Academic Press, London, 509 pp.

Lewis, B.T.R. and R.P. Meyer, 1968. A seismic investigation of the upper mantle to the west of Lake Superior, Bull. Seism. Soc. Amer., 58, 565-596.

Liebermann, R.C. and E. Schreiber, 1969. Critical thermal gradients in the mantle, Earth Planet. Sci. Letters, 7, 77-81.

Lukk, A.A. and I.L. Nersesov, 1965. Structure of the upper mantle as shown by observations of earthquakes of intermediate focal depth, Doklady Akad. Nauk SSSR. (Eng. trans.), 162, 14-16.

Massé, R.P., M. Landisman and J.B. Jenkins, 1972. An investigation of the upper mantle compressional velocity distribution beneath the Basin and Range province, Geophys. J. R. astr. Soc., 30, 19-36.

McMechan, G.A. and R.A. Wiggins, 1972. Depth limits in body wave inversions, Geophys. J. R. astr. Soc., 28, 459-473.

Mereu, R.F., 1968. Curvature corrections to upper mantle seismic refraction surveys, Earth Planet. Sci. Letters, 3, 469-475.

Mereu, R.F. and J.A. Hunter, 1969. Crustal and upper

mantle structure under the Canadian shield from Project Early Rise data, Bull. Seism. Soc. Amer., 59, 147-165.

Muirhead, K.J., 1968. The reduction and analysis of seismic data using digital computers, Ph.D. thesis, University of Tasmania, Hobart.

Muirhead, K.J. and L. Read, 1966. Slow-speed tape recordings of seismic signals, Nature, 210, 929-930.

Muirhead, K.J. and D.W. Simpson, 1972. A three-quarter watt seismic station, Bull. Seism. Soc. Amer., 62, 985-990.

Neumann, F., 1933. The transmission of seismic waves, Trans. Amer. Geophys. Union, 14, 329-335.

Niazi, M., 1966. Corrections to apparent azimuths and travel time gradients for a dipping Mohorovicic discontinuity, Bull. Seism. Soc. Amer., 56, 491-509.

Niazi, M. and D.L. Anderson, 1965. Upper mantle structure of western North America from apparent velocities of P waves, J. Geophys. Res., 70, 4633-4640.

Nuttli, O., 1963. Seismological evidence pertaining to the structure of the Earth's upper mantle, Rev. Geophys., 1, 351-400.

Nuttli, O.W., 1969. Travel times and amplitudes of S waves from nuclear explosions in Nevada, Bull. Seism. Soc. Amer., 59, 385-398.

Otsuka, M., 1966. Azimuth and slowness anomalies of seismic waves measured on the central California seismic array, Pt. II Interpretation Bull. Seism. Soc. Amer., 56, 655-675.

Press, F., 1968. Earth models obtained by Monte Carlo inversion, J. Geophys. Res., 73, 5223-5234.

Press, F., 1972. The Earth's interior as inferred from a family of models, in, The Nature of the Solid Earth, (ed. E.C. Robertson), 147-171, McGraw-Hill, New York, 677 pp.

Richards, P.G., 1972. Seismic waves reflected from velocity gradient anomalies within the Earth's upper mantle, Zeitschrift fur Geophysik, 38, 517-527.

Ringwood, A.E., 1962. A model for the upper mantle, J. Geophys. Res., 67, 857-867.

Ringwood, A.E., 1967. The pyroxene-garnet transformation in the Earth's mantle, Earth Planet. Sci. Letters, 2, 255-263.

Ringwood, A.E., 1969. Composition and evolution of the upper mantle, in The Earth's Crust and Upper Mantle, (ed. P.J. Hart), 1-17, Geophys. Monogph, 13, Amer. Geophys. Union, Washington, 735 pp.

Ringwood, A.E., 1970. Phase transformations and the constitution of the mantle, Phys. Earth Planet. Interiors, 3, 109-155.

Ringwood, A.E., 1972. Mineralogy of the deep mantle: current status and future developments, in

The Nature of the Solid Earth, (ed. E.C. Robertson), 67-92, McGraw-Hill, New York, 677 pp.

Ringwood, A.E. and A. Major, 1970. The system Mg_2SiO_4-Fe_2SiO_4 at high-pressures and temperatures, Phys. Earth Planet. Interiors, 3, 89-108.

Shimshoni, M. and A. Ben-Menahem, 1970. Computation of the divergence coefficient for seismic phases, Geophys. J. R. astr. Soc., 21, 285-294.

Simpson, D.W., C. Wright and J.R. Cleary, 1971. Double discontinuity in the upper mantle, Nature Phys. Sci., 231, 201-203.

SIPRI (International Institute for Peace and Conflict Research), 1968. Seismic Methods for Monitoring Underground Explosions, SIPIRI, Stockholm, 130 pp.

Smith, T.J., J.S. Steinhart and L.T. Aldrich, 1966. Lake Superior crustal structure, J. Geophys. Res., 71, 1141-1172.

Soga, N., E. Schreiber and O.L. Anderson, 1966. Estimation of bulk modulus and sound velocities of oxides at very high temperatures, J. Geophys. Res., 71, 5315-5320.

Sorrells, G.G., J.B. Crowley and K.F. Veith, 1971. Methods for computing ray paths in complex geological structures, Bull. Seism. Soc. Amer., 61, 27-53.

Sutton, D.J. and R.E. White, 1966. A study of P travel-times from some Australian earthquakes, Austral. J. Phys., 19, 157-166.

Timmel, K.E. and D.W. Simpson, 1972. Seismic events during filling of Talbingo Reservoir, ANCOLD Bull., 36, 27-33.

Toksoz, M.N., M.A. Chinnery and D.L. Anderson, 1967. Inhomogeneities in the Earth's mantle, Geophys. J. R. astr. Soc., 13, 31-59.

Underwood, R., 1967. The seismic network and its applications, Ph.D. thesis, Australian National University, Canberra.

Wang, C., 1966. Velocity of compressional waves in limestones, marbles and a single crystal of calcite to 20 kilobars, J. Geophys. Res., 71, 3543-3547.

Wang, C., 1972. A simple earth model, J. Geophys. Res., 77, 4318-4329.

Weber, P.C., 1963. The Tape Recorder as an Instrumentation Device, The Ampex Corporation, 74 pp.

Weichert, D.H., 1968. Upper mantle structure under the Churchill Province of the Canadian shield, east of the Yellowknife seismic array, J. Phys. Earth, 16, 93-101.

Wesson, R.L., 1970. A time integration method for computation of the intensities of seismic rays, Bull. Seism. Soc. Amer., 60, 307-316.

Whitcomb, J.H. and D.L. Anderson, 1970. Reflection of P'P' seismic waves from discontinuities in the mantle, J. Geophys. Res., 75, 5713-5728.

White, R.E., 1971. P-wave velocities in the upper mantle beneath the Australian shield from earthquake data, Geophys. J. R. astr. Soc., 24, 109-118.

Wickens, A.J., 1971. Variations in lithospheric thickness in Canada, Can. J. Earth Sci., 8, 1154-1162.

Wiggins, R.A., 1969. Monte Carlo inversion of body-wave observations, J. Geophys. Res., 74, 3171-3181.

Wiggins, R.A. and D.V. Helmberger, 1972. Upper mantle structure of Western United States, preprint.

Worthington, M.H., J.R. Cleary and R.S. Anderssen, 1972. Density modelling by Monte Carlo inversion - II Comparison of recent Earth models, Geophys. J. R. astr. Soc., 29, 445-457.

Worthington, M.H., J.R. Cleary and R.S. Anderssen, 1973. Upper and lower mantle shear velocity modelling by Monte Carlo inversion, Geophys. J. R. astr. Soc. (submitted).

Wright, C., 1970. P wave investigations of the Earth's structure using the Warramunga seismic array. Ph.D. thesis, Australian National University, Canberra.

Wright, C., 1972. Array studies of seismic waves arriving between P and PP in the distance range 90° to 115°, Bull. Seism. Soc. Amer., 62, 385-400.

Wright, C. and J.R. Cleary, 1972. P wave travel-time gradient measurements for the Warramunga seismic array and lower mantle structure, Phys. Earth Planet. Interiors, 5, 213-230.

Wright, C. and K.J. Muirhead, 1969. Longitudinal waves from the Novaya Zemlya nuclear explosion of October 27, 1966, recorded at the Warramunga seismic array, J. Geophys. Res., 74, 2034-2048.

Young, J.B. and P.G. Gibbs, 1968. GEDESS: a series of computer programs for deriving information at selected seismic recording sites, for signals of known hypocentres, AWRE report no. O 54168, United Kingdom Atomic Energy Authority, Aldermaston.

Zengeni, T.G., 1970. A note on an azimuthal correction for $dT/d\Delta$ for a single dipping plane interface, Bull. Seism. Soc. Amer., 60, 299-306.

LETTERS TO NATURE

PHYSICAL SCIENCES

Variations in Australian Upper Mantle Structure, from Observations of the Cannikin Explosion

It has been established that P and S times to stations in shield areas are significantly earlier than times to other continental regions at similar epicentral distances[1–4]. The observed differences, called "station anomalies", are largely produced by variations in the properties of the low velocity layer within the upper mantle[5,6], thus providing one of the few means available for estimating such variations. Except for some studies based on the dense seismic network in California[7–9], however, detailed investigations of upper mantle structure by this method have been precluded by the relatively sparse distribution of permanent stations.

Muirhead and Simpson[10] have recently developed portable seismic stations which can operate unattended for long periods. These instruments have enabled us to study the variation of P anomalies across the eastern boundary of the Australian shield, using the nuclear explosion Cannikin on Amchitka Island as a signal source. The position of the shield boundary is not accurately known, but a previous study of P times to Australian stations from Longshot[11] had indicated a significant change in the pattern of anomalies between stations of the Australian National University network in New South Wales and those of the Adelaide University network in South Australia. Although the firing date for Cannikin (2200 h on November 6, 1971) was not announced until a few days beforehand, the capability of the instruments for long term unattended operation allowed us to deploy them across a 1,700 km traverse about 3 weeks before the explosion took place. In conjunction with some of the permanent network stations, ten portable stations were set up at intervals of 100 to 150 km between Canberra and Maralinga, along a line approximately at right angles to the shot direction (Fig. 1*a*). The positions of some stations were chosen to coincide with those of a recent magnetic variometer experiment by Gough, McElhinny and Lilley (personal communication). The P signal from the explosion was well recorded at all stations: an example is shown in Fig. 2. Onset times were measurable to an accuracy of about 0.05 s at the portable stations, and to better than 0.2 s at the permanent stations. Epicentral distances and travel times were calculated from the official shot data, and details are given in Table 1, including station anomalies calculated both from the 1968 tables[12] and the P table of Hales *et al.*[13]. The two sets of anomalies, reduced to a common baseline, are plotted in Fig. 1*b*. Thus reduced, the difference between the two sets is 0.07 s at Maralinga and less than 0.05 s at all other stations. Errors introduced by the application of distance corrections appear therefore to be insignificant.

It is unlikely that the data have been contaminated to any significant extent by effects in the vicinity of the source. The azimuthal variation found for the Longshot source anomaly[14,15] corresponds to a change of less than 0.05 s between Canberra and Maralinga. There is no measurable difference between the relative times to Canberra and Adelaide from Longshot and Cannikin although the two explosion sites are 6 km apart, and we infer that any effect of structural irregularities near the source has been negligible. We believe also that the results have not been appreciably affected by variations in crustal structure beneath the stations. Estimates of crustal thickness beneath south-east Australia and the Maralinga-Adelaide region do not differ by more than a few km[16–18] and the observed differences in crustal velocity between the two regions are insufficient to account for a difference of more than about 0.2 s in the anomalies. As Hales *et al.*[6] pointed out, moreover, differences in crustal structure will not produce anomalies of

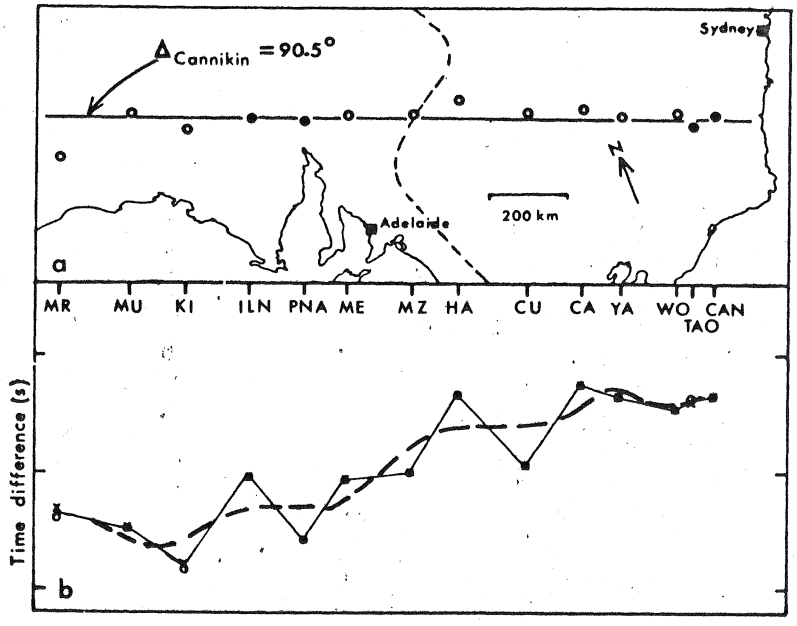

Fig. 1 *a*, The Cannikin traverse. Shaded and unshaded circles represent permanent and portable stations. The dashed line indicates the eastern boundary of Precambrian rocks[19]. *b*, Differences between P station anomalies along the traverse, calculated from the 1968 P tables[12] (○) and the P table of Hales *et al.*[13] (×). The smoothed curve has been derived by taking means of adjacent points.

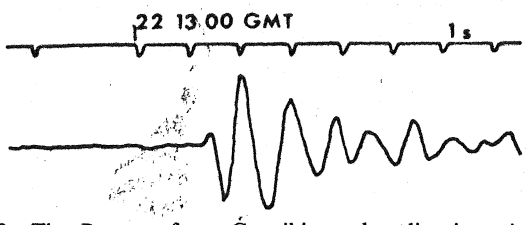

Fig. 2 The P onset from Cannikin and radio time signals recorded on magnetic tape by the portable station at Curragh.

this order without the accompaniment of disturbances in the gravity field much greater than those observed here.

Nevertheless, the scatter between anomalies at adjacent stations is quite large, with an average value of 0.4 s. It must be concluded that this is a consequence either of local inhomogeneities in the upper mantle beneath the stations or of minor irregularities in the velocity structure along the entire path (or a combination of the two). It should be possible to resolve this question by studying arrivals from a number of events at some of the stations. An interesting feature of the scatter is that it is least marked near the eastern end of the traverse, in a region that has been subjected to recent uplift.

In spite of the scatter, Fig. 1*b* clearly indicates a trend towards more negative anomalies (corresponding to earlier arrivals) in a westerly direction. The trend appears to be most pronounced near the centre of the traverse. This feature is emphasized when first-order smoothing is applied by taking means of adjacent points, as shown in the figure. Following Hales *et al.*[6], the change in gradient may be interpreted as a wedging out of the lower velocity layer in the upper mantle as the shield boundary is approached. Fig. 1*a* shows that this occurs close to the line indicating the eastern limit of exposed Precambrian rocks[19].

The western end of the presumed "wedge" happens to coincide with a NW–SE trending anomaly in the vertical component of the magnetic variation field, found by Gough, McElhinny and Lilley (personal communication). Although the magnetic variation data have not yet been fully interpreted, it may be noted that Hales *et al.*[6] found a similar coincidence between one end of their postulated "wedge" and a magnetic variation anomaly found by Schmucker[20] and subsequently mapped by Reitzel *et al.*[21] and Porath *et al.*[22].

Apart from this central feature of the anomaly pattern, the data of Fig. 1*b* also suggest a gradual decrease in the anomalies from east to west. The Longshot data suggest that an additional decrease of about 1 s takes place between Maralinga and Kalgoorlie, situated some 950 km further west in the Archaean portion of the shield. The possibility arises that the decrease is associated with an ageing process within the upper mantle, corresponding to a gradual disappearance with time of the low velocity layer. Other geophysical observations in Australia seem to have an association with the ages of basement rocks, notably the occurrence of very low heat-flow values in the Archaean shield, and very high values in south-east Australia[19]. Cleary[18] has also drawn attention to an east–west increase in P_n velocities across the continent (not in itself sufficient to account for the variation in P anomalies).

The apparent relationship between changes in the velocity structure of the upper mantle and the ages of crustal rocks has an important bearing on questions of continental growth. In particular, the implied change in the character of the low velocity layer across the shield boundary appears to be compatible with models of accretion such as that proposed recently for south-east Australia by Oversby[23].

We thank Dr David Sutton for providing records from stations of the Adelaide University network.

Table 1 Station Data

Station	Distance* (deg)	Travel time* (s)	Station anomaly† (s) (1)	(2)
Maralinga (MR)	91.34	786.13	−0.58	−0.92
Mulgathing (MU)	90.47	781.99	−0.70	−1.10
Kingoonya (KI)	90.77	782.97	−1.02	−1.40
Island Lagoon (ILN)	90.45	782.30	−0.23	−0.63
Partacoona (PNA)	90.55	782.20	−0.78	−1.18
Melton (ME)	90.44	782.17	−0.27	−0.67
Mazar (MZ)	90.30	781.62	−0.20	−0.61
Harcourt (HA)	90.01	780.90	+0.47	+0.05
Curragh (CU)	90.36	781.90	−0.12	−0.53
Carrathool (CA)	90.21	781.86	+0.54	+0.13
Yanco (YA)	90.38	782.59	+0.45	+0.05
Woodstock (WO)	90.36	782.39	+0.37	−0.04
Talbingo (TAO)	90.79	784.40	+0.37	−0.01
Canberra (CAN)	90.34	782.40	+0.45	+0.04

* Calculated from shot coordinates and origin time given for Cannikin by NOAA (PDE card 82–71).

† Difference between observed time and time calculated from (1) 1968 P tables[12], (2) P table of Hales *et al.*[13], with ellipticity correction applied.

J. R. Cleary
D. W. Simpson
Department of Geophysics and Geochemistry
K. J. Muirhead
Department of Engineering Physics, Australian National University, Canberra

Received January 11, 1972.

1 Cleary, J., and Hales, A. L., *Bull. Seismol. Soc. Amer.*, **56**, 467 (1966).
2 Doyle, H. A., and Hales, A. L., *Bull. Seismol. Soc. Amer.*, **57**, 761 (1967).
3 Herrin, E., and Taggart, J. N., *Bull. Seismol. Soc. Amer.*, **58**, 1325 (1968).
4 Lilwall, R. C., and Douglas, A., *Geophys. J. Roy. Astron. Soc.*, **19**, 165 (1970).
5 Hales, A. L., and Doyle, H. A., *Geophys. J. Roy. Astron. Soc.*, **13**, 403 (1967).
6 Hales, A. L., Cleary, J. R., Doyle, H. A., Green, R., and Roberts, J., *J. Geophys. Res.*, **73**, 3885 (1968).
7 Press, F., and Biehler, S., *J. Geophys. Res.*, **69**, 2979 (1964).
8 Bolt, B. A., and Nuttli, O. W., *J. Geophys. Res.*, **71**, 5977 (1966).
9 Nuttli, O. W., and Bolt, B. A., *J. Geophys. Res.*, **74**, 6594 (1969).
10 Muirhead, K. J., and Simpson, D. W., *Bull. Seismol. Soc. Amer.* (in the press).
11 Cleary, J., *Bull. Seismol. Soc. Amer.*, **57**, 773 (1967).
12 *Bull. Seismol. Soc. Amer.*, **58**, 1196 (1968).
13 Hales, A. L., Cleary, J. R., and Roberts, J. L., *Bull. Seismol. Soc. Amer.*, **58**, 1975 (1968).
14 Cleary, J., *Earth Planet. Sci. Lett.*, **3**, 29 (1967).
15 Herrin, E., and Taggart, J. N., *Bull. Seismol. Soc. Amer.*, **58**, 1791 (1968).
16 Doyle, H. A., Underwood, R., and Polak, E. J., *J. Geol. Soc. Austral.*, **13**, 355 (1966).
17 Doyle, H. A., and Everingham, I. B., *J. Geol. Soc. Aust.*, **11**, 141 (1964).
18 Cleary, J., *Tectonophysics* (in the press).
19 Howard, L. E., and Sass, J. H., *J. Geophys. Res.*, **69**, 1617 (1964).
20 Schmucker, U., *J. Geomagnet. Geoelect.*, **15**, 193 (1964).
21 Reitzel, J. S., Gough, D. I., Porath, H., and Anderson, C. W., *Geophys. J.*, **19**, 213 (1970).
22 Porath, H., Oldenburg, D. W., and Gough, D. I., *Geophys. J.*, **19**, 237 (1970).
23 Oversby, B., *Nature*, **234**, 45 (1971).

Are Quasars Local or Cosmological?

The debate about the distances of the quasars resembles in many ways the nineteenth century debate on the nebulae. One of the chief defining characteristics used, that of being stellar in appearance, is apparent rather than intrinsic. And rather compelling arguments have been advanced to show both that quasars are at the large distances implied by a cosmological interpretation of their redshifts (continuity with radio-galaxies[1,2], association with cluster of same redshift[3]) and that they are comparatively weak, nearby objects (continuity with Seyfert nuclei[4,5], associations with foreground galaxies[6], the anomalous 1.95 redshift[7], rapid lateral motions[8] in 3C 273 and 279, anisotropic distribution on the sky[9]).

SEISMIC EVENTS DURING FILLING OF TALBINGO RESERVOIR

by K. E. Timmel, D.Phil, F.I.E.Aust. and D. W. Simpson, M.Sc. *

Introduction

In 1957 the Snowy Mountains Hydro-Electric Authority established a network of four seismic recording stations in the Snowy Mountains area, to assess the seismicity of this area, to locate and measure any earthquakes, and to determine earthquake allowances to be made in the design of the major engineering structures of the Snowy Mountains Scheme. The layout and instrumentation of the network were designed to ensure detection and location of even small seismic events. Initially the system was operated manually, with a recorder installed at each station. In 1967 the procedure was changed to a telemetered operation, with a central recorder located in Cooma. The network was operated in close co-operation with the Department of Geophysics and Geochemistry of the Australian National University. The seismic film records were also analysed by this Department (Ref. 1). The Authority's network will shortly be transmitting directly to a recorder at the University.

Following reports on seismic events observed during and after filling of large reservoirs elsewhere (Refs. 2, 3, 5, 6, 8, 9, 11), the Authority decided to monitor carefully seismic events in relation to the filling of Talbingo Reservoir which has a maximum capacity of about 3/4 million acre feet, and a surface area of 4 800 acres. Talbingo was situated outside the quadrangle of the original network. Therefore an additional station was established about 2 miles north of Talbingo Dam in 1969, that is two years before filling of Talbingo Reservoir began. Although the original network was capable of locating seismic events in the Talbingo area of a magnitude of 2 or more on the Richter Scale (Ref. 4), the additional station at Talbingo made it possible to locate events of magnitudes less than 1, and to detect smaller micro-tremors in this area.

Talbingo Dam, a 530 feet high earth and rockfill structure with a crest length of 2 300 feet and containing 19 million cubic yards of material, has previously been described in this Bulletin (Ref. 7). See also Figure 1. Since the Snowy Mountains area had been established as only slightly seismically active, it was not considered necessary to include seismometers in the instrumentation for the dam to check the behaviour of the structure during earthquakes.

* Mr. Timmel is Head of the Physical Sciences Branch of the Snowy Mountains Hydro-Electric Authority, and Mr. Simpson is a Research Scholar with the Department of Geophysics and Geochemistry of the Australian National University.

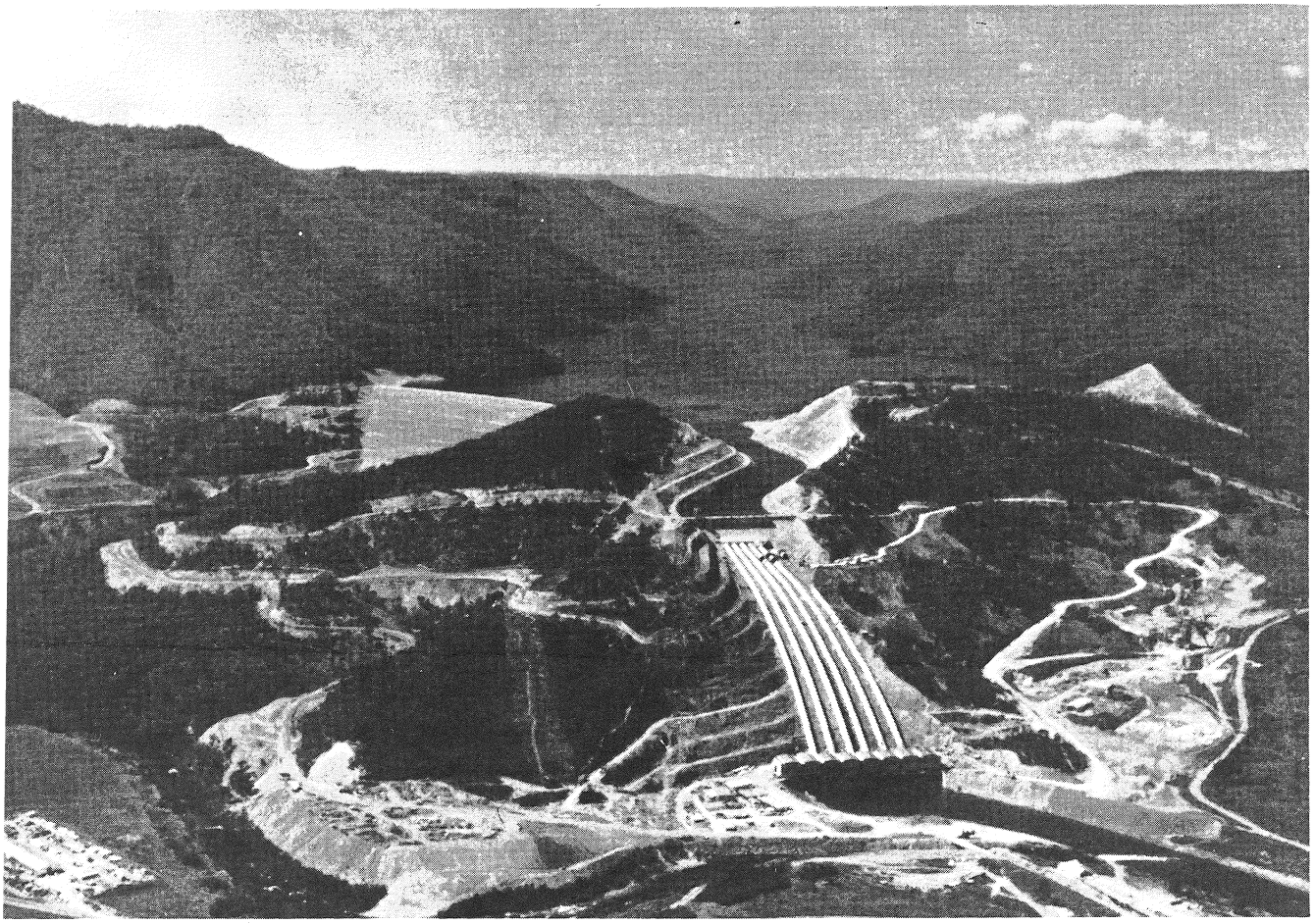

Figure 1. Tumut 3 Project, February 1972.

Seismic Observations during the Early Stages of Reservoir Filling

Prior to 1st May 1971, when the filling of Talbingo Reservoir began, seismic activity in the area had been monitored by the Authority's seismic network for a period of 13 years, including 2 years close monitoring from Talbingo Station. No tremors had been recorded, except for a minor one about 12 miles north of the damsite.

After 1st May 1971, seismic activity commenced on 19th May with a very small event, followed by two more in the same month. The level of activity increased in June to 39 recorded events, including 4 of sufficient magnitude to be located. A further increase in the seismic activity was noted in July and August with increasing water level in the reservoir. After August, when the rate of filling dropped sharply, there was a corresponding drop in recorded seismic events. The number of located events from May till December, together with the water levels in the reservoir during that period, are given in the following table:

TABLE 1

Month:	May	June	July	Aug	Sept	Oct	Nov	Dec
Water level (RL in feet) (at mid month)	1525	1637	1707	1745	1762	1766	1772	1783
Frequency (events per month)	0	4	21	19	5	5	3	3
Maximum magnitude (Richter Scale)		2.3	2.4	2.2	1.8	1.9	2.1	1.8

The number of events per month given in the table refers only to tremors large enough to be recorded not only by the Talbingo station but also by other stations in the network, so that they could be located. In addition there were more than 2000 very weak events during the period, recorded at Talbingo station only.

The strongest event recorded so far occurred in July 1971. This had a magnitude of 2.4 and its epicentre was close to the dam. An event of such low magnitude is generally not felt by persons in the area, and is unlikely to be of any engineering significance. However, a tremor of magnitude 1.8 in July was distinctly noticed by workmen on top of the Talbingo Outlet Works Tower, about 100 feet above ground. This is the only event reported by personnel during the May-December period in 1971.

Most of the tremors large enough to be located are concentrated in an area of about 5 miles radius, on the west bank of the reservoir and just upstream of the dam. Some events are located around the dam itself, while only a few isolated epicentres were located east of the reservoir (Figure 2).

Whilst the frequency of locateable tremors declined towards the end of the period covered by this report, the number of micro-tremors remained fairly constant initially at several hundred per month and showed an increase towards the end of the period.

At the time of writing this report, computer analysis of the records had proceeded only up to 31st December 1971. Talbingo Reservoir had risen to within a few feet of Full Supply Level during December 1971, and it remained fairly constant during the following months. Initial scanning of the seismometer records obtained early in 1972 indicated a generally low level of seismic activity.

In spite of the large number of events recorded during filling, the seismic activity is small in terms of total energy releases. A graphical

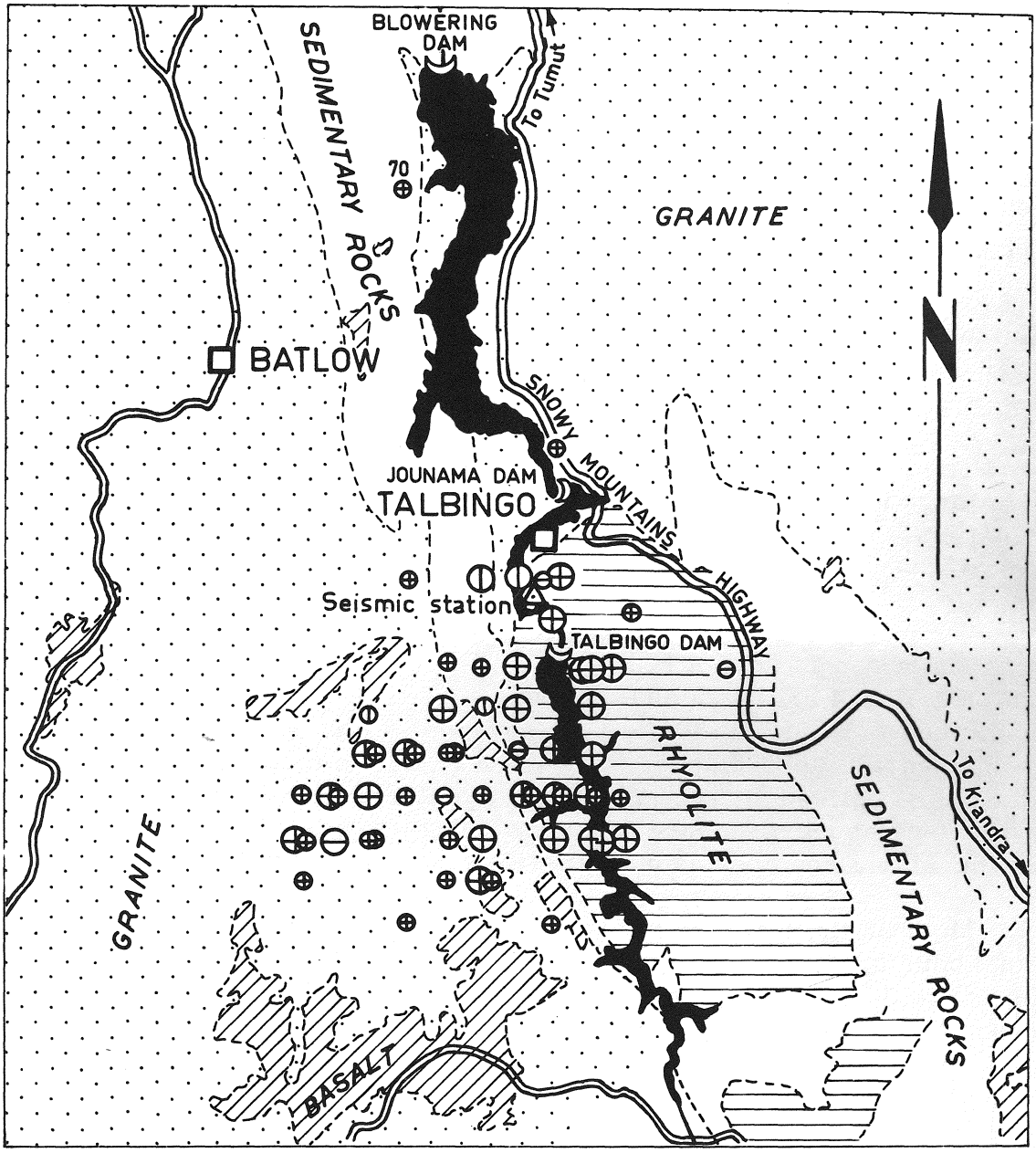
BLOWERING DAM
To Tumut
70
SEDIMENTARY ROCKS
GRANITE
BATLOW
SNOWY MOUNTAINS HIGHWAY
JOUNAMA DAM
TALBINGO
Seismic station
TALBINGO DAM
RHYOLITE
To Kiandra
SEDIMENTARY ROCKS
GRANITE
BASALT
N
SCALE OF MILES
5 0 5 10
MAGNITUDE
(Richter scale)
1 2
TIME
70
Year of event if prior to 1 May 1971.
ACCURACY OF LOCATION
Computer location
Good graphical location
Fair graphical location

Figure 2.

presentation (Figure 3) of water level, water load and frequency of locateable events suggests a causal relationship between rate of loading and level of seismic activity. However, no firm conclusions can be drawn before the records obtained during filling and a subsequent period of essentially constant water level are fully analysed. In particular it is too early to say whether a process of gradual adjustment of the earth's crust to the water load, which is implied in Figure 3, is complete.

To obtain a better knowledge of the seismic activities during filling of the reservoir, the A.N.U. has augmented the Authority's network by three temporary seismic stations (Ref. 10) arranged in roughly an equilateral triangle of $3\frac{1}{2}$ mile sides with its apex at the dam and its base crossing the reservoir. These stations commenced operation on 6th July 1971. At the time of writing this report, the tape records are still being evaluated. Their information will supplement the data given above, from the Authority's fixed stations, and will more accurately locate the epicentres shown on Figure 2.

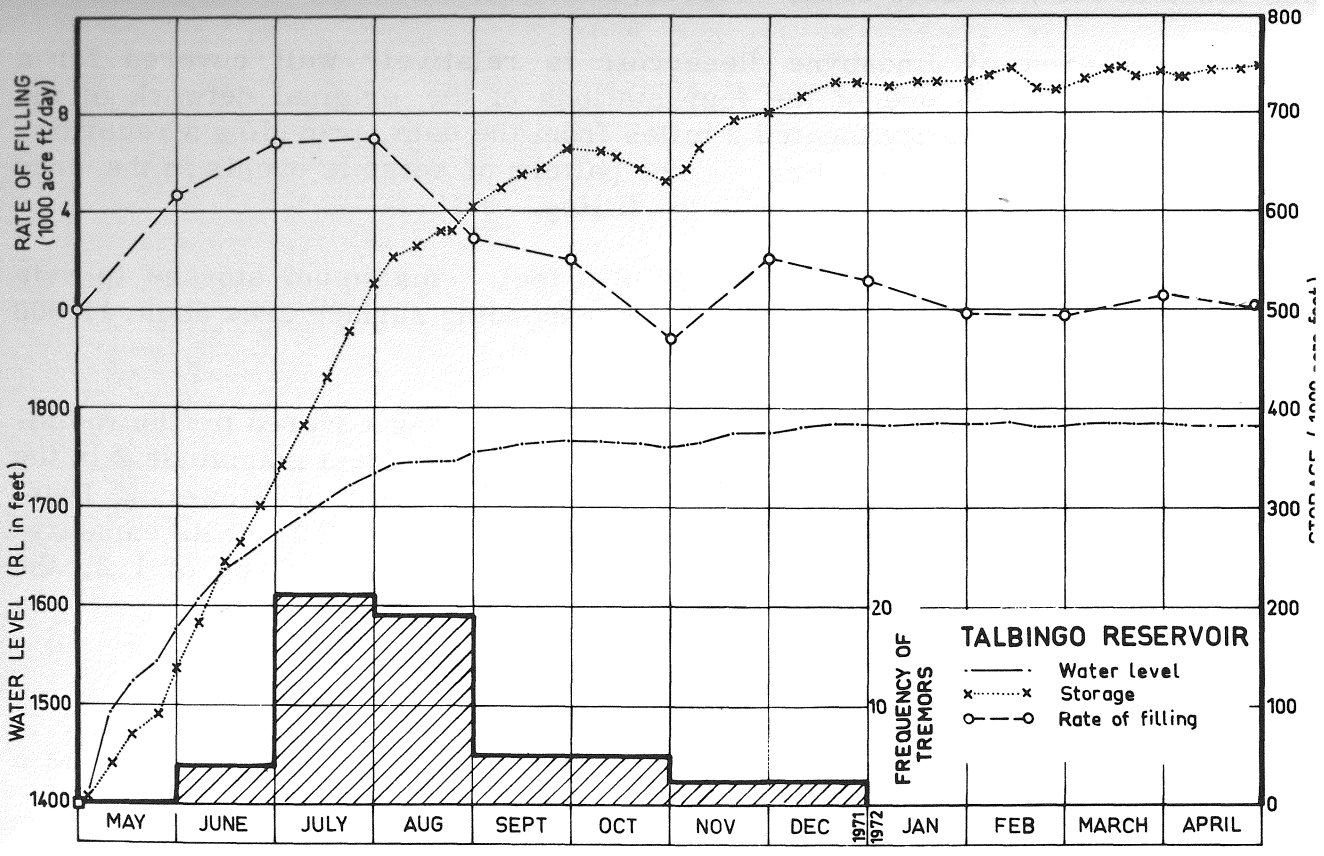

Figure 3.

NOTE: Seismic records analysed after completion of this article indicate a revival of activity in 1972. Also there was a noticeable drift of the epicentres towards the eastern side of the reservoir. Tremors in 1972 are not entered in Figures 2 and 3.

Observations made during Filling of other Reservoirs in the Snowy Mountains Area

Lake Eucumbene: Dam height 381 feet; maximum storage to date 3 345 000 acre feet, December 1970; corresponding surface area about 32 500 acres.

A number of tremors, including one of magnitude 5, was recorded during and after filling. Since the Authority's network did not come into operation until impounding had commenced, and thus relatively little was known about the seismicity in the area, it has not been established whether the water load increased the seismic activity in the area (Ref. 1 and 5).

Lake Jindabyne: Dam height 225 feet; maximum storage to date 502 000 acre feet, October 1970; corresponding surface area 7 100 acres.

The area of Jindabyne Reservoir is relatively well covered for a seismic survey, with one of the four stations of the original network of the Snowy Mountains Authority located 2 miles from the dam, providing a recording period of 9 years prior to filling. The pattern of seismic events in the area does not suggest any correlation with the filling.

Lake Blowering: Dam height 370 feet; maximum storage to date 1 378 000 acre feet, September 1970; corresponding surface area about 11 000 acres.

During the early period of filling, the area was covered by the Authority's original network which could detect events of at least magnitude 2 in the area. Talbingo seismic station, located 15 miles south of Blowering Dam, came into operation when the reservoir was filled to about 60% of its capacity. Only one event was recorded in the area. Having a magnitude of 1.3, the event occurred in November 1970.

REFERENCES

1. Cleary, J. R., Doyle, H. A. and Moye, D. G. 1964: 'Seismic Activity in the Snowy Mountains Region and its relationship to geological structures.' J. Geol. Soc. Aust. 11, 89-106.

2. Gough, D. I. and Gough, W. I. 1970: 'Stress and Deflection in the Lithosphere near Lake Kariba - I.' Geophys. J. R. Ast. Soc. 21, 65-78.

3. Gough, D. I. and Gough, W. I. 1970: 'Load-induced earthquakes at Lake Kariba - II.' Geophys. J. R. Ast. Soc. 21, 79-101.

4. Gutenberg, B. and Richter, C. F. 1956: 'Earthquake magnitude, intensity, energy and acceleration.' Bull. Seis. Soc. Amer. 46, 105-145.

5. Jaeger, J. C. 1969: 'Occurrence and effects of earthquakes.' ANCOLD Bulletin 29, 2-24.

6. Lane, R. G. T. 1971: 'Seismic activity at man-made reservoirs.' Institution of Civil Engineers 7416.

7. Snowy Mountains Hydro-Electric Authority 1970: 'Talbingo Dam, Construction Procedure and Progress.' ANCOLD Bulletin 31, 6-19.

8. Endersbee, L. A. 1969: 'Man-initiated earthquakes?' ANCOLD Bulletin 31, 25-27.

9. Housner, G. W. 1969: 'Seismic events at Koyna Dam.' Proc. 11th Symp. Rock Mech. Rock Mechanics, Theory and Practice, Berkeley 541-558.

10. Muirhead, K. J. and Simpson, D. W. 1972: 'A three-quarter watt seismic station.' Bull. Seism. Soc. Am. (in press).

11. Carder, D. S. 1968: 'Reservoir Loading and Local Earthquakes.' Proc. 6th Annual Engng. Geol. Sympos. Boise, Idaho. 225-241.

SEISMOTECTONICS OF THE AUSTRALIAN CONTINENT

By
J. R. CLEARY
and
D. W. SIMPSON

(*Reprinted from Nature, Vol.* 230, *No.* 5291, *pp.* 239–241, *March* 26, 1971)

(*Reprinted from Nature, Vol. 230, No. 5291, pp. 239–241, March 26, 1971*)

Seismotectonics of the Australian Continent

ONE of the successes of the seafloor spreading hypothesis has been the coherent explanation it provides of world seismicity. Isacks *et al.*[1] have given an account of seismic activity along mid-ocean ridges and island arcs in accordance with the concepts of plate tectonics, and McKenzie[2] has shown that these concepts can be applied also to instantaneous motions across continental plate boundaries. It seems reasonable, therefore, to attempt an analysis of continental seismicity within plates in terms of the same hypothesis. Morgan[3] and Le Pichon[4] have shown that the assumption of perfectly rigid plates gives results which are in approximate accord with observation. Nevertheless, their results are unlikely to be adversely affected—and may well be improved—if inhomogeneous stresses within plates are postulated to explain patterns of earthquake activity in continental regions.

Because of the relative infrequency of earthquakes in continental areas removed from plate boundaries, many years of monitoring by regional networks are usually required before specific patterns of seismicity emerge. Epicentral data for the Australian continent from the beginning of the century until the end of 1966 have been tabulated and discussed by Doyle *et al.*[5]. The quantity and quality of data improved considerably from about 1959, corresponding to increases in the number of Australian stations, and since 1966 the addition of more stations in central and western Australia has further improved the seismic monitoring of these regions.

In Fig. 1 the seismicity map of Doyle *et al.*[5], with the more recent epicentres added, has been superimposed on a portion of the ESSA 1961–1969 world seismicity map[6] showing events in the surrounding oceanic areas. Sykes[7] considers that the stepped shape of the ridge-fracture zone south of Tasmania reflects the shape of the south-east Australian continental slope. The orientations of transform faults in this zone also indicate a northward migration of Australia relative to the Antarctic plate, in approximate agreement with the differential movements calculated by Le Pichon[4].

Fig. 1 shows three major Australian seismic zones. In south-east Australia, the zone *a–b* probably represents a late stage of the post-middle Miocene Kosciusko uplift described by David[8]. From fault-plane studies, Cleary[9] and Underwood[10]

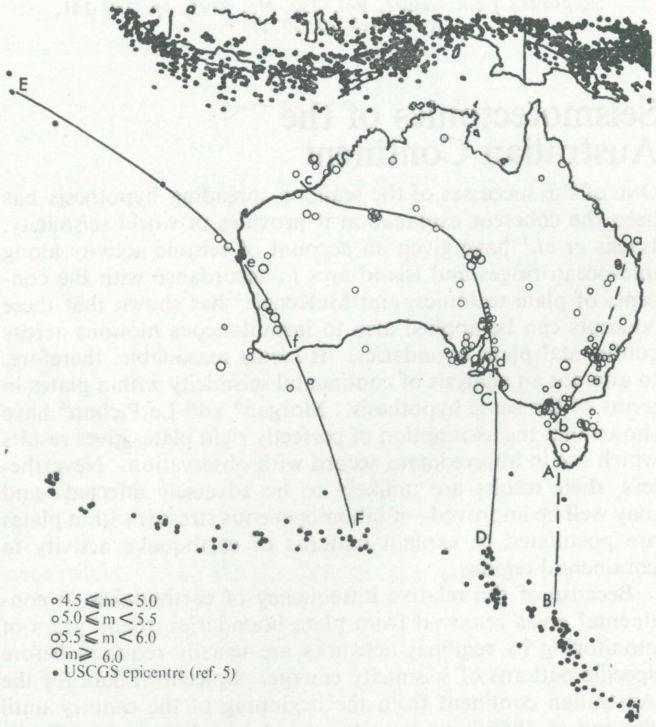

Fig. 1 Australian seismicity in relation to that of the Antarctic ridge and the Indonesian–New Guinea arc. The lettering is explained in the text.

have inferred a horizontal, principal compressive stress acting at right angles to the strike of *a–b*, with high-angle reverse movements typical of the larger shocks. In the middle of the continent, the apparently continuous zone *c–d* coincides with a feature postulated by Cook[11], Wilson[12] and Crawford[13] to be an ancient fracture zone. In the south-west corner is a zone *e–f*, first described by Everingham[14], within which large earthquakes have recently occurred at Meckering[15] and elsewhere.

Possible extensions of these zones beyond the continental shelf have also been indicated in Fig. 1. *A–B* and *C–D* are oceanic fracture zones depicted by Heirtzler *et al.*[16]. Wilson[17] has postulated that transform faults originate on lines of weakness within continents, and the coincidence of continental and oceanic fracture zones in these regions strongly suggests the operation of such a mechanism. The presence of epicentres close to these features may be indicative of minor seismic

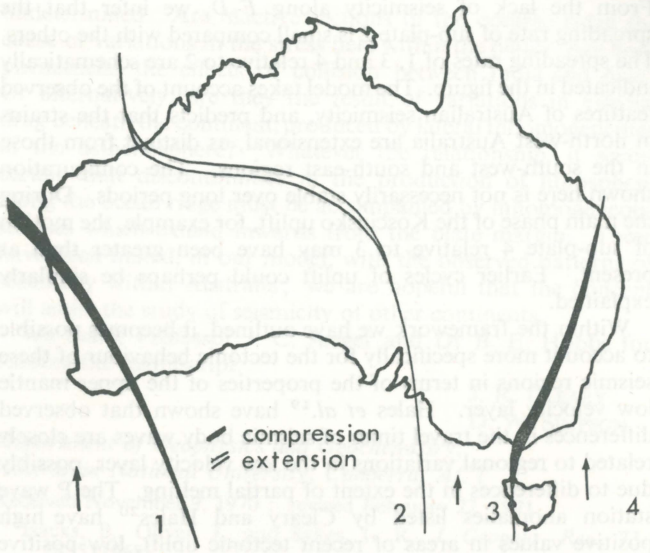

Fig. 2 Division of Australia into four sub-plates. Differences in spreading rate are represented schematically by the lengths of the arrows.

activity, difficult to detect by the existing network. Sykes[7] has suggested that the Indian Ocean epicentres along the line *E–F* may represent a nascent stage in the development of an island arc. Doyle also believes that this and other aspects of Australian seismicity may be due to second order effects within the plate. (Paper delivered at intern. conf. on recent crustal movements, Wellington, New Zealand, 1970.)

We now postulate that differences in spreading rate, indicated by discontinuities in seismic activity along the Antarctic ridge, are accompanied by the production of stress gradients within the plate, which are in turn responsible for the patterns of seismicity already described. In view of this, the section of the ridge marked *F–D* is interesting. Within *F–D*, which is about 1,000 km long, almost no seismic activity has been detected since Gutenberg and Richter's original study of world seismicity[18]. There is evidence also of a break in the seismicity of the ridge at *B*, with a change in activity west of this point. No corresponding variations in activity can be recognized along the arc to the north of Australia; it is not known, however, how much of this activity is caused by relative motion of the south-east Asian plate.

In Fig. 2, the continent has been divided into four sub-plates.

From the lack of seismicity along *F–D*, we infer that the spreading rate of sub-plate 2 is small compared with the others. The spreading rates of 1, 3 and 4 relative to 2 are schematically indicated in the figure. The model takes account of the observed features of Australian seismicity, and predicts that the strains in north-west Australia are extensional, as distinct from those in the south-west and south-east regions. The configuration shown here is not necessarily stable over long periods. During the main phase of the Kosciusko uplift, for example, the motion of sub-plate 4 relative to 3 may have been greater than at present. Earlier cycles of uplift could perhaps be similarly explained.

Within the framework we have outlined, it becomes possible to account more specifically for the tectonic behaviour of these seismic regions in terms of the properties of the upper mantle low velocity layer. Hales *et al.*[19] have shown that observed differences in the travel times of seismic body waves are closely related to regional variations in the low velocity layer, possibly due to differences in the extent of partial melting. The P wave station anomalies listed by Cleary and Hales[20] have high positive values in areas of recent tectonic uplift, low positive values at oceanic stations, and negative values in shield areas. These results imply that the low velocity zone is best developed beneath tectonically active areas and least developed under shields. A similar conclusion has been reached by Kanamori[21], based on a study of Love and Rayleigh wave phase velocities. Cleary[22] has confirmed that P wave station anomalies in Australia follow this trend. In particular, stations in south-east Australia have large positive anomalies, indicating a strongly developed low velocity layer and probably, therefore, a substantial zone of low strength in the upper mantle asthenosphere.

Presumably, portions of the asthenosphere which are intrinsic to particular tectonic provinces are carried along by the moving lithosphere, otherwise it is difficult to explain how such differences persist. In these circumstances, it is conceivable that the "soft" layer beneath south-east Australia (*a–b*) is being compressed by the more rigid upper mantles of the shield and oceanic regions on either side, resulting in uplift of the crustal block. In shield areas, on the other hand, the less strongly developed low velocity layer is less susceptible to deformation. Thus in the south-west Australian shield regions (*e–f*) no significant uplift has occurred and the fault motion may be predominantly strike-slip, while in the shield area of north-west Australia (*c–d*) the applied stresses are most easily relieved by rifting along ancient zones of weakness.

The casual sequence underlying the foregoing model remains

undetermined. Are inactive sections of the oceanic ridge the cause of variations in the stress field within the plate? Are both phenomena the effects of collision between India and Asia? Or alternatively, are they the result of variations in viscous drag beneath the continent, produced by lateral inhomogeneities in the asthenosphere? Whatever the relationship, it seems certain that discontinuities in the production of lithosphere along the ocean ridge must be accompanied by inhomogeneous stresses which extend inwards from the plate margin. These have been linked, in our model, with the observed patterns of seismicity within Australia; we are hopeful that the concept will assist the study of seismicity of other continents.

We thank Professor J. C. Jaeger and Dr B. E. Hobbs for reading the manuscript.

J. R. CLEARY
D. W. SIMPSON

Department of Geophysics and Geochemistry, Australian National University, Canberra, ACT

Received November 9, 1970 ; revised February 22, 1971.

[1] Isacks, B., Oliver, J., and Sykes, L. R., *J. Geophys. Res.*, **73**, 5855 (1968).
[2] McKenzie, D. P., *Nature*, **226**, 239 (1970).
[3] Morgan, W. J., *J. Geophys. Res.*, **73**, 1959 (1968).
[4] Le Pichon, X., *J. Geophys. Res.*, **73**, 3661 (1968).
[5] Doyle, H. A., Everingham, I. B., and Sutton, D. J., *J. Geol. Soc. Austral.*, **15**, 295 (1968).
[6] U.S. Department of Commerce, ESSA, *World Seismicity, 1961–1969*, Map NEIC—3005 (1970).
[7] Sykes, L. R., *J. Geophys. Res.*, **75**, 5041 (1970).
[8] David, T. W. E. (edit. by Browne, W. R.), *The Geology of the Commonwealth of Australia* (Arnold, London, 1950).
[9] Cleary, J. R., thesis, Australian National Univ. (1963).
[10] Underwood, R., thesis, Australian National Univ. (1967).
[11] Cook, P. J., *Rec. Bur. Min. Res. Geol. Geophys. Austral.*, **46** (1966).
[12] Wilson, J. T., *Science, History and Hudson Bay* (edit. by Beals, C. S.), **2** (Queen's Printer, Ottawa, 1968).
[13] Crawford, A. R., *Econ. Geol.*, **65**, 11 (1970).
[14] Everingham, I. B., *Rep. Bur. Min. Res. Geol. Geophys. Austral.*, **132** (1968).
[15] Everingham, I. B., Gregson, P. J., and Doyle, H. A., *Nature*, **223**, 701 (1969).
[16] Heirtzler, J. R., Dickson, G. O., Herron, E. M., Pitman, W. C., III, and Le Pichon, X., *J. Geophys. Res.*, **73**, 2119 (1968).
[17] Wilson, J. T., *Nature*, **207**, 343 (1965).
[18] Gutenberg, B., and Richter, C. F., *Seismicity of the Earth*, first ed. (Princeton Univ. Press, 1949).
[19] Hales, A. L., Cleary, J. R., Doyle, H. A., Green, R., and Roberts, J., *J. Geophys. Res.*, **73**, 3885 (1968).
[20] Cleary, J. R., and Hales, A. L., *Bull. Seism. Soc. Amer.*, **56**, 467 (1966).
[21] Kanamori, H., *Phys. Earth Planet. Interiors*, **2**, 259 (1970).
[22] Cleary, J. R., *Bull. Seism. Soc. Amer.*, **57**, 773 (1967).

Printed in Great Britain by Fisher, Knight & Co., Ltd., St. Albans.

(*Reprinted from Nature Physical Science, Vol.* 231, *No.* 26, *pp.* 201–203, *June* 28, 1971)

Double Discontinuity in the Upper Mantle

ALTHOUGH the use of seismic arrays for direct measurement of P wave travel time gradients ($dT/d\Delta$) has greatly improved the resolution of upper mantle structure[1–3], the technique is limited by the effects of local crustal structure beneath arrays and by the paucity of events giving arrivals of sufficient quality for $dT/d\Delta$ measurements. Using the Australian array WRA, we find that the combination of a large quantity of travel time data with selected $dT/d\Delta$ measurements provides a more powerful tool for the interpretation of P wave arrivals than either technique used in isolation.

WRA is well situated for the study of earthquakes in the Indonesia–Philippines and New Guinea–New Britain regions, in the distance range 12° to 30° (Fig. 1). P travel times have been computed for all events shown in Fig. 1 using USCGS PDE card data, and $dT/d\Delta$ has been derived from selected events using a method similar to that described by Cleary *et al.*[4]. Possible differences between the transmission paths from Indonesia and New Guinea to WRA are currently being investigated. The present study, however, is concerned with P wave signals recorded from 330 events in the former area (region 1 of Fig. 1).

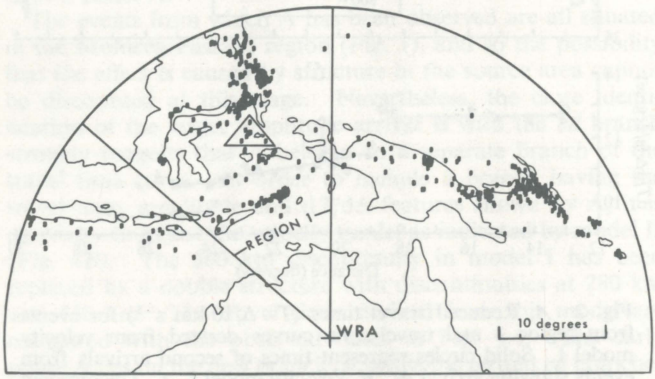

Fig. 1 USCGS epicentres for earthquakes less than 30° from WRA during September 1, 1968, to December 31, 1969. Events deeper than 150 km and those located using less than 10 stations are not included. Region 1 covers the azimuth range 310° to 360° from WRA. Events which show arrival A lie in the area enclosed by the triangle.

Travel times and uncorrected $dT/d\Delta$ measurements from region 1 are shown in Fig. 2. The $dT/d\Delta$ data clearly define three branches, *ab*, *cd*, *ef*. Velocity model I was constructed from these branches after correcting for structure beneath the array using a method described by Wright[5,6]. The model has discontinuities near 360 km and 650 km, in close agreement with the results of other investigators[1–3,7,8].

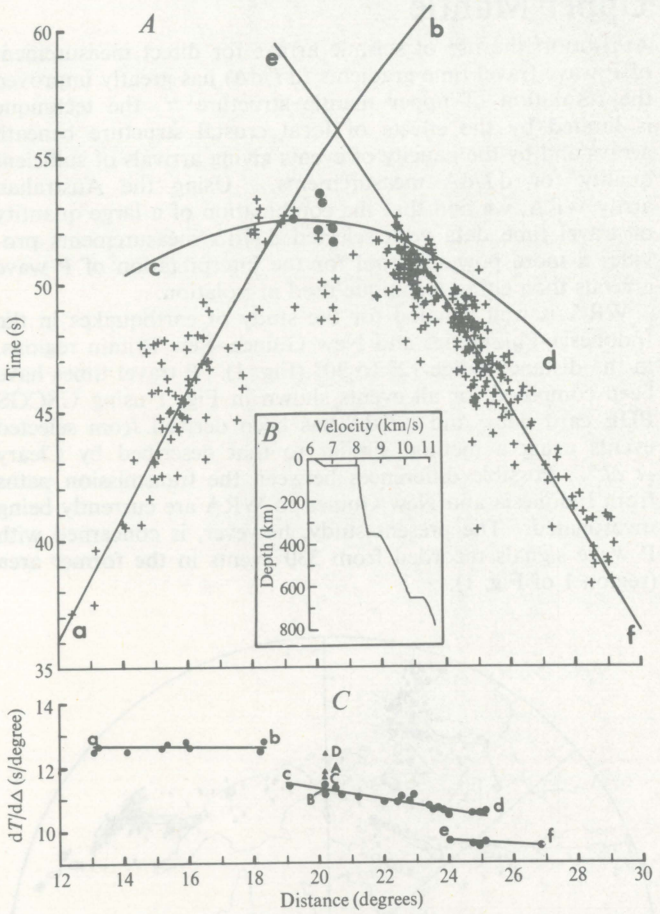

Fig. 2 *A*, Reduced travel times ($T-\Delta/10$ km s^{-1}) for events from region 1 and travel time curves derived from velocity model I. Solid circles represent times of second arrivals from events showing arrival A. *B*, Velocity model I. *C*, Uncorrected $dT/d\Delta$ values for selected events from region 1. Points A, B, C and D at 20.2° refer to the phases shown in Fig. 3.

Most of the observed travel times lie close to the branches derived from model I (Fig. 2*A*). Between 19.4° and 20.6°,

however, there are a number of low amplitude arrivals a few seconds earlier than the times predicted from the model. Fig. 3 is an example of such an arrival at 20.2°. Comparison of the observed $dT/d\Delta$ values for this event with the branches in Fig. 2*C* shows that the larger amplitude, second arrival B has the value expected for the *cd* branch at this distance. Furthermore, the travel time for this arrival and similar arrivals from the other events in the group agrees with the time expected for the *cd* branch. Arrival C in Fig. 3 may

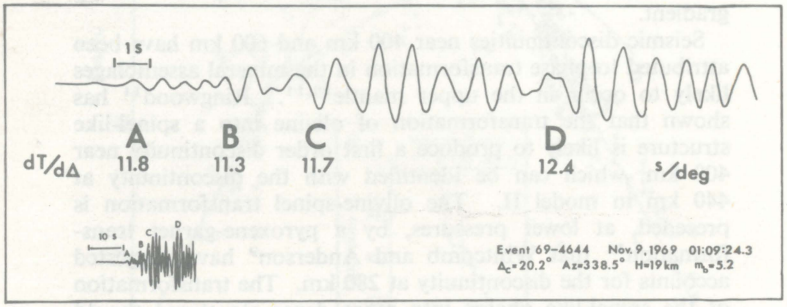

Fig. 3 An event at 20.2° showing arrival A. The upper record, with expanded time scale, is filtered 0.8–1.5 Hz and the lower one is filtered 0.4–2.0 Hz.

belong to the *ab* branch, while D is probably the reflected phase pP. It therefore appears that the second, higher amplitude arrival B corresponds to the main *cd* branch. The question arises as to the source of the earlier, low amplitude, high $dT/d\Delta$ phase A.

The events from which A has been observed are all situated in the Molucca Passage region (Fig. 1), and so the possibility that the effect is caused by structure in the source area cannot be discounted at this stage. Nevertheless, the close identification of the larger amplitude arrival B with the *cd* branch strongly suggests that A belongs to a separate branch of the travel time curve. In order to include a branch having the travel time, amplitude and $dT/d\Delta$ features shown by A, it is necessary to adjust the velocity model as indicated by model II (Fig. 4*B*). The 360 km discontinuity in model I has been replaced by a double structure with discontinuities at 280 km and 440 km. The travel times derived from this model are compared with the observed times in Fig. 4*A*. The early phase A lies on the new branch *pq*, while the *ab* and *cd* branches still satisfy the data used to derive model I.

It is interesting to compare velocity model II with a rather similar model recently presented by Whitcomb and Anderson[9] from the results of an entirely different study. They interpret precursors to the PKPPKP phase as underside reflexions

from upper mantle discontinuities at depths of 280 km, 520 km and 630 km. Unlike model II, however, they report no obvious indication of a discontinuity near 450 km. Instead of a sharp velocity change in this region, they propose a gradual velocity increase between 280 km and 520 km with perhaps a small discontinuity at 410 km. Their model gives a travel time branch similar to *pq*, but because of the high velocity gradient below 280 km the amplitudes along the branch are large. This is inconsistent with our findings. In order to produce the low amplitudes observed for the *pq* branch, the discontinuity at 280 km must be followed by a region of very low velocity gradient.

Seismic discontinuities near 400 km and 600 km have been attributed to phase transformation in the mineral assemblages likely to occur in the upper mantle[10,11]. Ringwood[11] has shown that the transformation of olivine into a spinel-like structure is likely to produce a first order discontinuity near 400 km, which can be identified with the discontinuity at 440 km in model II. The olivine-spinel transformation is preceded, at lower pressures, by a pyroxene-garnet transformation[11] that Whitcomb and Anderson[9] have suggested accounts for the discontinuity at 280 km. The transformation of the spinel-like phases into more dense structures should occur in a series of complex steps near 600 km[11] and the usual model of a single discontinuity at this depth[1,3,7,8] probably results from a lack of resolution in the techniques used. The discontinuity shown by Whitcomb and Anderson at 520 km may thus be more closely related to the 650 km discontinuity than to the one near 400 km. The data near 24° from WRA have not yet been closely analysed, but preliminary $dT/d\Delta$ measurements suggest the existence of complexities which may be related to another double structure near 650 km.

If a double structure related to radial distributions of pressure and temperature similar to that of model II is a widespread feature of the upper mantle, then it is surprising that the *pq* branch has not been reported earlier. As shown in Fig. 4*A*, however, the phase corresponding to this branch is the first arrival over a range of a few degrees only, and even then is of such low amplitude that it could be obscured by noise at many recording stations. Moreover, slight changes in the velocity structure could make the branch unobservable. For example, a decrease in the separation of the two discontinuities would make the phase corresponding to the *pq* branch a second arrival, always masked by the larger amplitudes of the *ab* and *cd* branches. A velocity decrease just below 280 km would make the amplitude along *pq* extremely small and could even cause a shadow zone for part of the branch. Differences in thermal gradient, chemical inhomogeneity, and degree of partial melting are the most likely causes of regional differences in upper mantle structure[12]

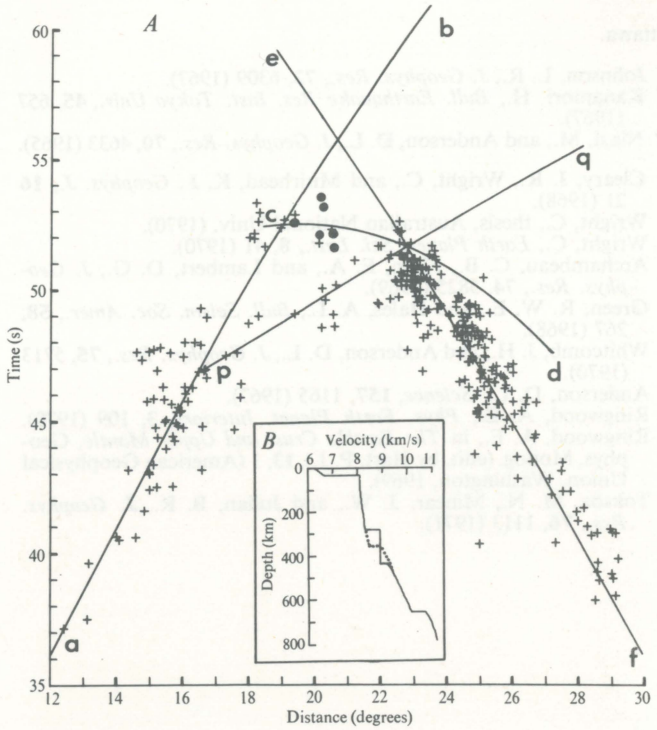

Fig. 4 *A*, The same travel times shown in Fig. 2 and the travel time curves derived from velocity model II. *B*, Velocity models I (. . .) and II (——).

and in these respects the complex trench region to the north of Australia may not be typical of the upper mantle as a whole[13].

If for any of these reasons only the branches *ab* and *cd* are observed, a single discontinuity at an intermediate depth will satisfy the travel time and $dT/d\Delta$ data as shown in Fig. 2*A*. The combination, therefore, of a low noise recording site and an upper mantle structure altered by the temperatures in a subduction zone may be the reason why the *pq* branch is observed for the first time.

We thank Professor D. I. Gough and Dr R. C. Liebermann for critically reading our manuscript.

D. W. SIMPSON
C. WRIGHT*
J. R. CLEARY

Department of Geophysics and Geochemistry,
Australian National University,
Canberra ACT

Received May 26, 1971.

* Present address: Department of Energy, Mines and Resources,

Ottawa.

[1] Johnson, L. R., *J. Geophys. Res.*, **72**, 6309 (1967).
[2] Kanamori, H., *Bull. Earthquake Res. Inst. Tokyo Univ.*, **45**, 657 (1967).
[3] Niazi, M., and Anderson, D. L., *J. Geophys. Res.*, **70**, 4633 (1965).
[4] Cleary, J. R., Wright, C., and Muirhead, K. J., *Geophys. J.*, **16** 21 (1968).
[5] Wright, C., thesis, Australian National Univ. (1970).
[6] Wright, C., *Earth Planet, Sci. Lett.*, **8**, 41 (1970).
[7] Archambeau, C. B., Flinn, E. A., and Lambert, D. G., *J. Geophys. Res.*, **74**, 5825 (1969).
[8] Green, R. W. E., and Hales, A. L., *Bull. Seism. Soc. Amer.*, **58**, 267 (1968).
[9] Whitcomb, J. H., and Anderson, D. L., *J. Geophys. Res.*, **75**, 5713 (1970).
[10] Anderson, D. L., *Science*, **157**, 1165 (1967).
[11] Ringwood, A. E., *Phys. Earth Planet. Interiors*, **3**, 109 (1970).
[12] Ringwood, A. E., in *The Earth's Crust and Upper Mantle*, Geophys. Monog. (edit. by Hart, P. J.), **13**, 1 (American Geophysical Union, Washington, 1969).
[13] Toksöz, M. N., Minear, J. W., and Julian, B. R., *J. Geophys. Res.*, **76**, 1113 (1971).

Travel Times and Amplitudes from Explosions in Northern Australia

D. Denham, D. W. Simpson, P. J. Gregson and D. J. Sutton

REPRINTED FROM

Geophys. J. R. astr. Soc. (1972) **28**, 225–235

PUBLISHED BY

BLACKWELL SCIENTIFIC PUBLICATIONS
OXFORD LONDON EDINBURGH MELBOURNE

PRINTED IN ENGLAND BY

C. F. HODGSON & SON LTD., LONDON

Geophys. J. R. astr. Soc. (1972) **28**, 225–235.

Travel Times and Amplitudes from Explosions in Northern Australia

D. Denham, D. W. Simpson, P. J. Gregson and D. J. Sutton

(Received 1972 February 21)

Summary

Two large ($\sim 500\,t$) chemical explosions, detonated in 1970 and 1971, in northern Australia each produced seismic amplitudes equivalent to about a magnitude $4\frac{1}{2}$ earthquake. Arrivals from these explosions were recorded to a distance of 25° by 36 seismograph stations and provided an opportunity to measure seismic velocities over a large part of the Australian continent.

A P_n velocity of $8{\cdot}27 \pm 0{\cdot}01$ km s^{-1} and a crustal thickness of approximately 40 km were obtained from stations in the central and western regions of the continent. Stations to the east of the shot point give a lower P_n velocity of $8{\cdot}17 \pm 0{\cdot}02$ km s^{-1} and indicate a significant difference in travel times in this direction. A change in slope of the P wave travel-time curve, to $8{\cdot}85 \pm 0{\cdot}08$ km s^{-1} at a distance of 1400 km has not been observed before in Australia but corresponds to similar observations made from large explosions in North America.

The S wave travel times also show a change in slope, near 1400 km, to 4·84 km s^{-1}, but between 400 and 1400 km they indicate some complexity, not seen on the P wave curves, which may indicate a low velocity S layer in the upper mantle.

1. Introduction

On 1970 June 21 and 1971 May 2, two large chemical explosions were detonated during quarrying operations near the Ord River dam site in northern Australia. Because of their size (both larger than 450 t*) and the method of blasting, the explosions were excellent seismic sources, and were the first in the Australian region to provide reliable data beyond 1000 km.

2. The explosions

The wall of the main storage dam for the Ord River Irrigation Project contains approximately $1{\cdot}5 \times 10^6$ m^3 of rock fill obtained from a hill of quartzite situated close to the dam site. Conventional methods of quarrying, using many small separate charges, were uneconomical in the hard massive quartzite, and instead a special type of tunnel-blasting, referred to as 'coyote' blasting, was used. Horizontal tunnels were cut in the base of the hill and filled with explosives as shown in Fig. 1. Each tunnel was stemmed with sandbags to prevent blowout and as an additional precaution the direction of the tunnel was changed abruptly near the open end. Unlike

*t ≡ tonne ≡ 10^3 Kg = 2204·6 lb

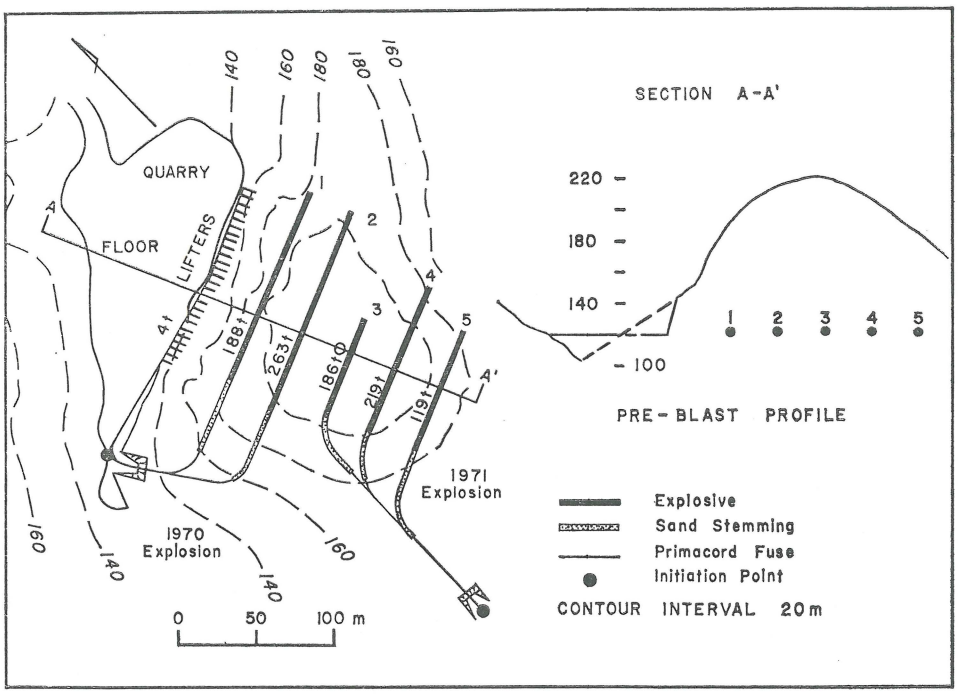

FIG. 1. Shot point details for 1970 and 1971 Ord River blasts.

other quarrying techniques there was no delay between charge groups and the effect was to produce a large, well contained, almost instantaneous explosion well suited for use as a seismic source.

In the June 1970 explosion a total of 455 t of an ammonium nitrate base explosive, Dupont Nilite, was detonated. Most of the explosive was placed in tunnels 1 and 2 which contained 188 t and 263 t respectively. An additional 4 t was located in a series of 50 lifter tunnels designed to blow out the lower part of the hill so that the main body of rock could slide down onto a prepared quarry floor.

The May 1971 explosion used 524 t of explosive, of which 82 per cent was Nilite and the remainder dynamite. The dynamite was included to increase the overall density of the explosive in an effort to break up the rock more effectively. Tunnels 3, 4 and 5 were used and contained 186, 219 and 119 t of explosives, respectively.

Since both explosions were detonated with primacord fuse it was necessary to determine the shot instants by placing a recording instrument as near as possible to the blast site. The origin times, accurate to better than 0·05 s, were 02 h 58 m 48·4 s UT on 1970 June 21, and 03 h 00 m 07·6 s UT on 1971 May 2. The shot point co-ordinates adopted for both explosions were 16° 07·6′ S, 128° 44·1′ E with an elevation of 120 m above sea level.

3. Recording stations

The two explosions were recorded at distances up to 25° by 36 seismic stations throughout the continent. The locations of the shot point and stations are shown in Fig. 2 and the station coordinates and operating authorities are given in Table 1. Only three temporary stations were installed in 1970 (DAM, KAT, and OOD) but the following year 16 temporary stations were set up along different azimuths from

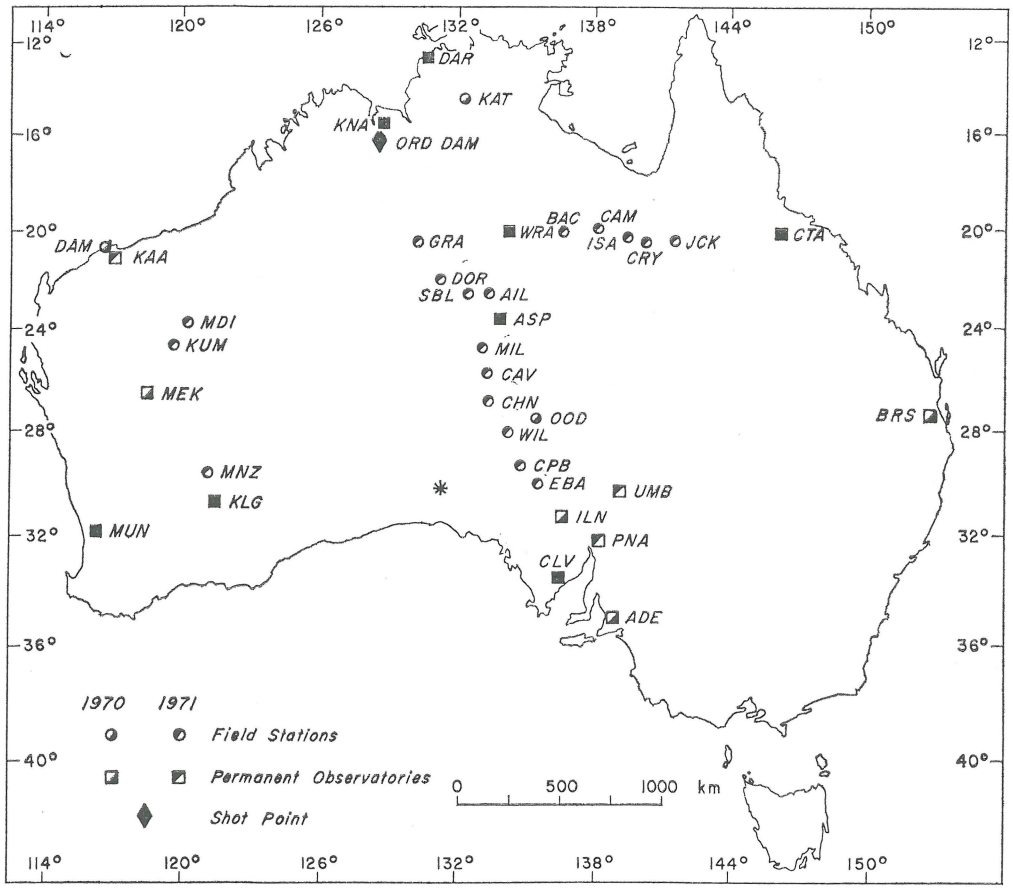

FIG. 2. Location of shot point and stations. The star indicates the location of the 1956 Maralinga explosion used by Bolt, Doyle and Sutton (1958)

the shot point in order to investigate regional variations in upper mantle velocities. The stations comprised three main groups. The most complete coverage was to the south along a line from GRA (520·8 km) to ADE (2312·0 km) where 17 stations recorded one or both of the explosions. To the west, eight stations in Western Australia provided data from 1227·4 km (MDI) to 2165·3 km (MUN), while to the east, records were obtained from seven stations from WRA to CTA in the distance range 728·6 km to 1904·3 km. In addition to these lines, the stations KNA, DAR, KAT and BRS also recorded the explosions.

Distances and travel times for each station are given in Table 2 and where the instrument magnification was known a ground displacement for the *P* phase is included. The distances in km were based on the Australian National Spheroid (Robbins 1962) and those in degrees were calculated using the standard expressions given by Bullen (1963). Where different times for the two explosions are listed for the same station, the time with the least estimated uncertainty was used in the velocity analyses.

Five records, which indicate the quality of the results at different distances and on different instruments, are shown in Fig. 3.

Table 1

Station information

Station	Code*	Lat, S deg min	Long, E deg min	Elevation (m)	Operator**
Kununurra	KNA ⊕	15 45·0	128 46·0	60	PWD
Katherine	KAT ○	14 29·6	132 21·1	50	BMR
Darwin	DAR ⊕	12 24·5	130 49·1	5	BMR
The Granites	GRA +	20 34·3	130 21·2	430	BMR
Mount Doreen	DOR +	22 02·6	131 19·7	520	BMR
Warramanga array	WRA ⊕	19 56·7	134 20·5	365	ANU
Stuart Bluff	SBL +	22 45·6	132 29·0	610	BMR
Aileron	AIL +	22 37·2	133 18·5	685	BMR
Barry Caves	BAC +	20 02·9	136 40·2	290	BMR
Alice Springs	ASP ⊕	23 41·0	133 53·8	600	BMR
Mill Ridge	MIL +	24 52·0	133 09·2	410	ANU
Camooweal	CAM +	19 53·4	138 09·4	260	BMR
Mount Cavenagh	CAV +	25 54·6	133 07·9	550	ANU
Mount Isa	ISA +	20 26·3	139 25·5	400	BMR
Mundiwindi	MDI +	23 47·1	120 14·8	570	BMR
Mount Chandler	CHN +	26 59·8	133 19·4	380	ANU
Kumarina	KUM +	24 42·7	119 36·9	610	BMR
Cloncurry	CRY +	20 41·7	140 32·6	300	BMR
Karratha	KAA +	20 46·6	116 51·5	15	BMR
Dampier	DAM ○	20 42·6	116 45·6	30	BMR
Mount Willoughby	WIL +	28 00·2	134 09·2	280	ANU
Oodnadatta	OOD ○	27 37·8	135 35·0	135	UA
Julia Creek	JCK +	20 38·6	141 43·3	115	BMR
Meekatharra	MEK ○	26 36·8	118 32·7	515	BMR
Coober Pedy	CPB +	29 15·7	134 58·4	205	UA
Menzies	MNZ +	29 40·9	121 01·5	435	BMR
Mount Eba	EBA +	30 03·6	135 37·7	200	UA
Kalgoorlie	KLG ⊕	30 47·0	121 27·5	360	BMR
Island Lagoon	ILN ○	31 23·6	136 52·2	135	UA
Umberatana	UMB +	30 14·4	139 07·7	610	UA
Charters Towers	CTA ⊕	20 05·3	146 15·3	355	QLD
Partacoona	PNA +	32 00·4	138 09·9	200	UA
Cleve	CLV ⊕	33 41·5	136 29·7	240	UA
Mundaring	MUN ⊕	31 58·7	116 12·5	255	BMR
Adelaide	ADE ○	34 58·0	138 42·5	655	UA
Brisbane	BRS ○	27 23·5	152 46·5	525	QLD

*Permanent seismograph station underlined, (○ Recorded 1970 explosion; + recorded 1971 explosion)

**BMR, Bureau of Mineral Resources; ANU, Australian National University; UA, University of Adelaide; QLD, Queensland University; PWD, Public Works Department, Western Australia.

Table 2

Travel times and amplitudes of main phases

Station code and year		Distance degrees	km	Travel times, seconds *P*	*S*	Period *P* wave sec	Ground Amplitude A/T, mμ/s
KNA	70	0·38	41·8	7·0B	11·7C	0·3	3900
KNA	71			6·8A	10·8C	0·2	3850
KAT	70	3·85	428·4	59·6A			
DAR	70	4·21	468·8	65·0B	111·5C	0·2	220
				76·5C(P_1)			
DAR	71			65·6B	111·6B	0·2	190
				77·5B(P_1)	127·1C(S_1)		
GRA	71	4·68	520·8	71·59A	121·2B		
DOR	71	6·38	709·4	94·65A	161·5B		
WRA	70	6·55	728·6	95·10A	167·6B		
WRA	71			95·10A	167·6B		
SBL	71	7·49	832·9	109·62A	188·3B		
AIL	71	7·77	864·5	113·5A	193·4B		
BAC	71	8·49	945·1	121·7B	215·2C		
ASP	70	8·95	995·7	129·2A	226·6B	0·5	40
ASP	71			129·3B	225·4B	0·5	28
MIL	71	9·63	1071·5	138·7A	240·7C		
CAM	71	9·71	1080·8	138·1B	243·5C		
CAV	71	10·56	1175·3	151·0A	263·2D		
ISA	71	11·02	1226·4	155·9D			
MDI	71	11·03	1227·4	157·4B	276·2B	0·25	60
CHN	71	11·63	1293·6	165·1A	289·6B		
KUM	71	12·08	1344·1	171·0B	299·9C	0·4	22
CRY	71	12·09	1345·6	170·8C	298·5C		
KAA	71	12·18	1355·4	171·6B	300·6C	0·5	30
DAM	70	12·24	1362·5	172·4B	302·2C	0·3	37
WIL	71	12·84	1428·5	181·4A	320·0C		
OOD	70	13·09	1456·3	185·1C	325·6D		
JCK	71	13·12	1459·9	182·8D			
MEK	70	14·10	1568·5	197·4B	348·6D	0·2	15·4
CPB	71	14·28	1588·7	198·5A	350·8C		
MNZ	71	15·24	1695·5	212·7B	374·1C		
EBA	71	15·24	1695·9	212·2C	373·5B		
KLG	70	16·04	1784·1	220·3C	390·5C		
KLG	71			220·3B	390·5B	0·4	8·0
ILN	70	16·91	1881·6	232·6B			
UMB	71	16·97	1888·4	234·2C	415·4D		
CTA	70	17·11	1904·3	237·9D			
CTA	71			237·6D			
PNA	71	17·98	2000·9	245·4C			
CLV	70	18·84	2095·8	256·1C		0·5	8·0
CLV	71			256·1C	456·1D	0·5	8·0
MUN	70	19·46	2165·3	264·8C		0·35	12·8
MUN	71			264·8C		0·35	8·5
ADE	70	20·78	2312·0	281·6C			
BRS	70	24·93	2774·3	325·0B			

Uncertainty in travel time is assessed as follows: A $\leqslant$ 0·1 sec; B, 0·1 $\leqslant$ 0·5 sec; C, 0·5 $\leqslant$ 1 sec and D $>$ 1 sec.

4. Apparent velocities

Crustal phases

As the experiment was designed to take advantage of the large energy sources to determine travel times at distances beyond the range of crustal studies, no attempt was made to install temporary stations to record crustal phases. The limited data obtained from the nearer stations are not inconsistent with the P_1 and S_1 times observed from earlier studies (cf. Cleary 1972; Dooley 1972).

P_n

In Fig. 4 the travel times of first arrivals in the distance range 400–2400 km are shown on a reduced time scale. Also included are results obtained from stations to

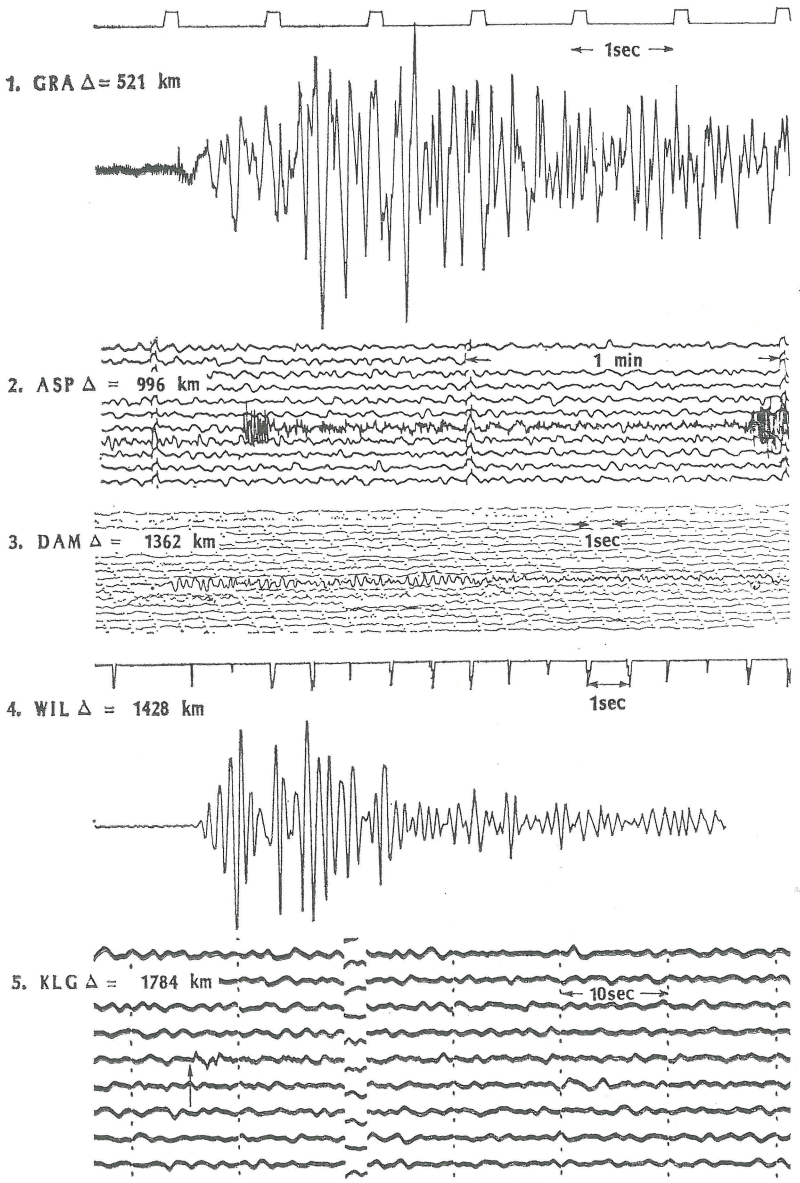

FIG. 3. Sample records.

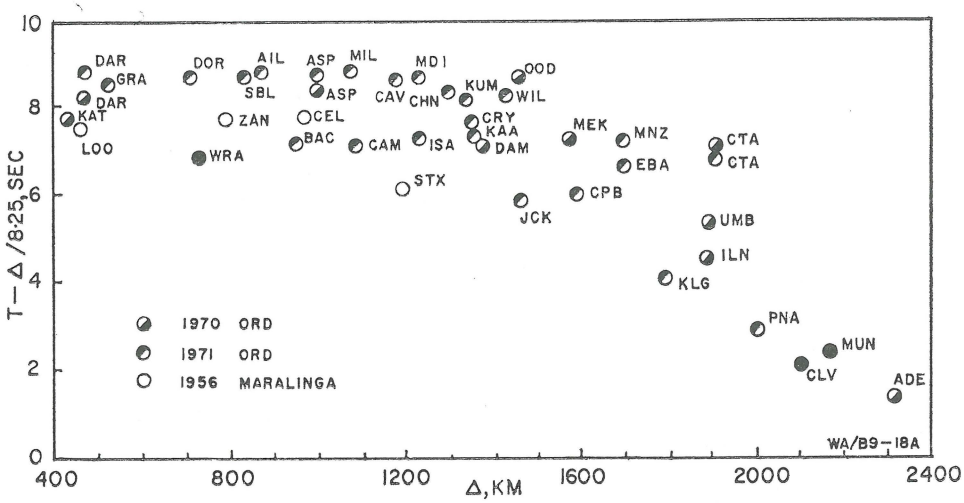

FIG. 4. Reduced P wave travel times.

the west of the 1956 nuclear explosion at Maralinga, South Australia (Bolt, Doyle & Sutton 1958). In the distance range 700–1400 km the arrivals at the eastern stations are in general earlier than those from the western and southern lines, and the two groups will be treated separately.

A least squares analysis of the ten points on the southern line from GRA (520·8 km) to OOD (1456·3 km) gives a P_n velocity of $8{\cdot}27 \pm 0{\cdot}01$ km s^{-1} and an intercept time of $8{\cdot}79 \pm 0{\cdot}20$ s. If the western stations of MDI, and KUM, are included the velocity obtained is $8{\cdot}27 \pm 0{\cdot}01$ km s^{-1} and the intercept time becomes $8{\cdot}85 \pm 0{\cdot}21$ s, which are not significantly different from the results using the southern data alone. Although a straight line fits the data adequately, there is some suggestion that curvature of the travel-time curve may occur over this distance range. The data to 864 km (GRA, DOR, SBL and AIL) treated separately give a velocity of $8{\cdot}20 \pm 0{\cdot}01$ km s^{-1} and an intercept time of $8{\cdot}14 \pm 0{\cdot}12$ s, both of which are less than the results from the complete range.

A formal least squares analysis of the arrivals at five stations on the eastern line from WRA (728·6 km) to CRY (1345·6 km) gives a P_n velocity of $8{\cdot}17 \pm 0{\cdot}02$ km s^{-1} and an intercept time of $5{\cdot}86 \pm 0{\cdot}34$ s. The record quality from some of these stations is not as good as for the other areas and both the values of the velocity and the intercept time may be in error by larger amounts than those indicated by the least squares analysis. Nevertheless, the arrivals to the east are consistently 1·5–2·0 s earlier than for the other lines and they appear to indicate a significant difference in travel times to these stations.

P arrivals beyond 1400 km

At a distance of about 1400 km the P travel-time curve undergoes an abrupt change of slope. From the first arrival data it is not clear precisely where the change of slope occurs, but beyond 1550 km the first arrivals all appear to be on the new branch. Using the seven stations from CPB (1588·7 km) to ADE (2312·0) km on the southern line, a P wave velocity of $8{\cdot}82 \pm 0{\cdot}10$ km s^{-1} is obtained with an intercept time of $19{\cdot}13 \pm 2{\cdot}53$ s. No significant difference results from the inclusion of the times to the western stations which gives a velocity of $8{\cdot}85 \pm 0{\cdot}08$ km s^{-1}, and an intercept time of $19{\cdot}90 \pm 2{\cdot}03$ s. The KAA and DAM arrivals may belong in this group but

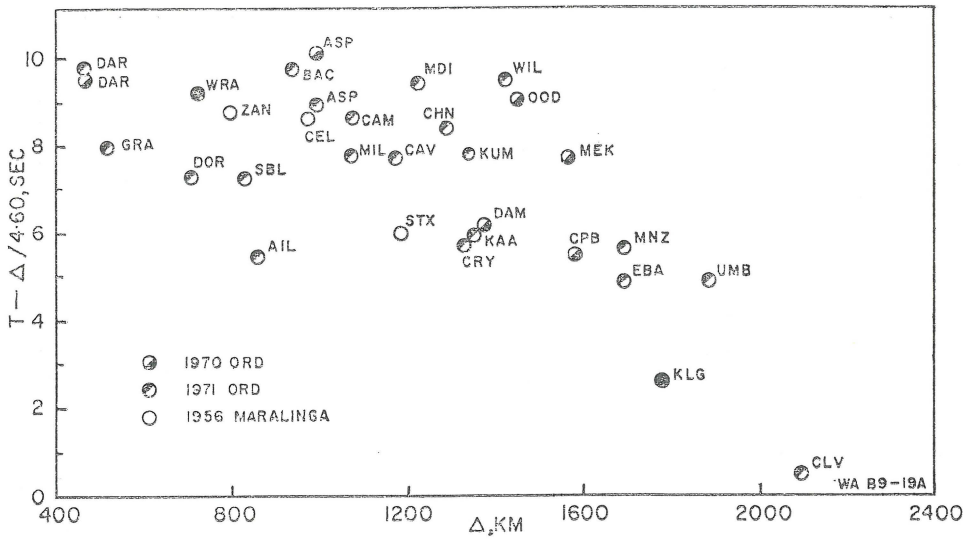

Fig. 5. Reduced *S* wave travel times.

they have not been included because of the uncertainty involved in identifying them with a particular branch.

A clear *P* wave arrival was recorded at BRS (2774·3 km) from the 1970 explosion. However, since this is an isolated point on a separate section of the travel-time curve, it is not possible to obtain an apparent velocity in the ADE, BRS distance range.

S wave arrivals

Fig. 5 shows reduced *S* wave travel times from the Ord River and Maralinga explosions. Because of the emergent nature of the *S* phase and the lack of horizontal component seismographs at many of the stations there is more uncertainty in these arrival times than those from the *P* wave data. There appears to be no obvious distinction between different azimuth ranges and all the *S* arrivals have been treated as one group.

As with the *P* arrivals, it is clear that the slope of the *S* wave curve changes near 1400 km, but the arrivals at shorter distances do not appear to fall on a continuous curve. If the six arrivals from DAR (468·8 km) to AIL (864·5 km) are grouped together the resulting velocity is $4{\cdot}75 \pm 0{\cdot}07$ km s^{-1} with an intercept time of $12{\cdot}52 \pm 2{\cdot}29$ s. If the group is extended to include the eight arrivals from BAC (945·1 km) to KUM (1344·1 km) and the arrivals at WIL (1428·5 km) and OOD (1456·3 km), the velocity is reduced to $4{\cdot}59 \pm 0{\cdot}02$ km s^{-1} and the intercept time to $7{\cdot}84 \pm 1{\cdot}04$ s.

At distances greater than 1500 km the seven arrivals from MEK (1568·5 km) to CLV (2095·8 km) give a velocity of $4{\cdot}84 \pm 0{\cdot}06$ km s^{-1} with an intercept time of $23{\cdot}33 \pm 4{\cdot}94$ s.

Comparisons with other investigations

Table 3 summarizes the results of the analysis of the *P* and *S* wave data from the Ord River explosions. Previous seismic studies of the crust and upper mantle in Australia have recently been reviewed by Cleary (1972) and Dooley (1972).

The P_n velocity of 8·27 km s^{-1} from the Ord River observations is consistent with earlier studies in the region, and the Maralinga results (Bolt *et al.* 1958) included in

Table 3

Apparent P and S wave velocities

Velocity (km s^{-1})	Intercept time (s)	Range (km)	Line
P wave data			
8·27± 0·01	8·79± 0·20	400–1500	south
8·27± 0·01	8·85± 0·21	400–1500	south & west
8·82± 0·10	19·13± 2·53	1400–2400	south
8·85± 0·08	19·90± 2·03	1400–2400	south & west
8·17± 0·02	5·92± 0·30	700–1400	east
S wave data			
4·75± 0·07	12·52± 2·29	400–900	all lines
4·59± 0·02	7·84± 1·04	400–1450	all lines
4·84± 0·06	23·33± 4·94	1500–2100	south & west

Fig. 4 indicate that an average P_n velocity of 8·25 km s^{-1} may be typical of most of the Precambrian shield of central and western Australia.

Assuming an average crustal velocity of 6·0 km s^{-1}, the western and southern Ord River data give a crustal thickness of about 40 km, which agrees with earlier studies. The P_n velocity and crustal thickness are also similar to the results obtained by Barr (1967), in the Canadian shield, who reports a 40 km thick crust and a P_n velocity of 8·23 km s^{-1}.

The increase of the apparent *P* velocity to 8·85 km s^{-1} near 1400 km has not been observed before in Australia, but it has been recognized from explosion studies in North America. Johnson (1967) and Hales (1969) summarize the observations of higher velocity branches between 600 and 2000 km. The crossover distance between the 8·27 km s^{-1} and 8·85 km s^{-1} phases from the Ord River data is greater than that reported from the North American results and indicates a velocity increase to 8·6 km s^{-1} at a depth of about 160 km.

The *S* wave velocity of 4·75 km s^{-1} for arrivals from 400 to 900 km agrees with the results reported by Bolt *et al.* (1958) from the Maralinga explosion and the 4·75 km s^{-1} reported by Barr (1967) in the Canadian shield. The decrease in the average apparent velocity to 4·59 km s^{-1} obtained by including the later arrivals from 900 to 1450 km may indicate an offset in the travel-time curve caused by a low velocity layer for *S* waves, similar to that described for *P* waves by Dowling & Nuttli (1964). The break in the data between AIL and BAC at approximately 900 km may be such an offset but scatter in the results precludes a detailed analysis at this stage.

The 4·82 km s^{-1} branch in the *S* travel times has not been reported before in the Australian region. It probably represents the bottom of a low velocity *S* layer and corresponds to the 8·85 km s^{-1} branch of the *P* wave curve.

5. Amplitude data

Table 2 contains the amplitude data for the *P* arrivals where the magnifications were known and where meaningful measurements of amplitude and period could be made. The maximum amplitude of the initial *P* phase was taken to obtain these values.

The magnitude (m) of a seismic event or explosion can be expressed in the form

$$m = \log (A/T) + A_2$$

where A is the ground amplitude, T the period and A_2 a function of distance and depth of the source.

Table 4

Amplitude data

Station	A_2	1970 log (A/T)	1970 m_B	1971 log (A/T)	1971 m_B
*KNA	0·03	3·59	3·62	3·59	3·62
DAR	2·38	2·34	4·72	2·28	4·66
ASP	3·00	1·60	4·60	1·45	4·45
MDI	3·16			1·78	4·94
KUM	3·21			1·34	4·55
KAA	3·22			1·48	4·70
DAM	3·22	1·57	4·79		
MEK	3·31	1·19	4·50		
KLG	3·43			0·90	4·33
CLV	3·51	0·90	4·41	0·90	4·41
MUN	3·52	1·11	4·63	0·93	4·45
Means and standard deviations			$4·61 \pm 0·14$		$4·56 \pm 0·20$

*KNA values not used to determine means

The magnitudes listed in Table 4 were calculated using the values of A_2 derived by Everingham (1968), for m_B, from Western Australian earthquakes. His curve for A_2 is continuous over the distance range 100–3000 km and agrees with Evernden's (1967) results for the eastern United States to better than 0·3 in the 500–3000 km range.

There is no statistical difference between the magnitudes of the two explosions. However, since the weight of explosive for the 1971 event was about 15 per cent greater than for the 1970 event, the first explosion was evidently a more efficient seismic source.

The magnitudes of both these explosions are higher than would normally be expected from 500 t explosions. An extrapolation of Basham's (1970) data based on high yield underground explosions predicts a magnitude of 3·7. Evernden's (1970) results using explosions detonated in a variety of media suggest a magnitude of 3·0 for an explosion of 500 t in hard rock, and in fact the 4·51 value for the 1970 explosion lies on his curve for detonation in water. The large amplitudes probably resulted from a combination of the excellent coupling between the explosives and the unweathered quartzite and the low attenuation associated with propagation paths in a shield area.

Acknowledgments

We are grateful for the assistance and co-operation at the shot point of Mr Guy Reid of Dravo Pty Ltd and Mr Barry Gale of the Public Works Department of Western Australia. We are indebted to: Dr J. Cleary of the A.N.U., and Mr P McGregor and Mr D. Finlayson of B.M.R. for valuable discussions throughout the project; Mr J. Cull of the B.M.R. for making available some computer programs; Dr J. Webb of the University of Queensland for making available the records from CTA and BRS; and all those who manned the field stations. Two of us (D.D. & P.J.G.) would like to thank the Director of the B.M.R. for permission to publish the B.M.R. results.

D. Denham:
Bureau of Mineral Resources, Canberra A.C.T. 2601, *Australia*

P. J. Gregson:
Bureau of Mineral Resources, Mundaring, W.A. 6073, *Australia*

D. W. Simpson:
Australian National University, Canberra A.C.T. 2601, *Australia*

D. J. Sutton:
University of Adelaide, Adelaide, 5001 S.A., *Australia*

References

Barr, K. G., 1967. Upper mantle structure in Canada from seismic observations using chemical explosions, *Can. J. earth Sci.*, **4**, 961–975.

Basham, P. W., 1970. Seismic magnitudes of high-yield underground explosions, *Can. J. earth Sci.*, **7**, 531–534.

Bolt, B. A., Doyle, H. A. & Sutton, D. J., 1958. Seismic observations from the 1956 atomic explosions in Australia, *Geophys. J. R. astr. Soc.*, **1**, 135–145.

Bullen, K. E., 1963. *An Introduction to the theory of Seismology*, 3*rd ed.*, Cambridge University Press, 381 pp.

Cleary, J. R., 1972. Australian crustal structure, *Tectonophysics*, in press.

Dooley, J. C., 1972. Seismological studies of the upper mantle in the Australian region, *Proc. Second Indian Symp. on the Upper Mantle Project, Hyderabad*, 1970, in press.

Dowling, J. & Nuttli, O., 1964. Travel-time curves for a low-velocity channel in the upper mantle, *Bull. seism. Soc. Am.*, **54**, 1981–1996.

Everingham, I. B., 1968. Mundaring Geophysical Observatory annual report 1966. *Bur. Miner. Resour. Aust. Rec.*, 1968/97, (inpubl.).

Evernden, J. F., 1967. Magnitude determination at regional and near-regional distances in the United States, *Bull. seism. Soc. Am.*, **57**, 591–639.

Evernden, J. F., 1970. Magnitude versus yield of explosions, *J. geophys. Res.*, **75**, 1028–1032.

Hales, A. L., 1969. A seismic discontinuity in the lithosphere, *Earth Planet Sci. Letters*, **7**, 44–46.

Johnson, L. R., 1967. Array measurements of *P* velocities in the upper mantle, *J. geophys. Res.*, **72**, 6309–6325.

Robbins, A. R., 1962. Long lines on the spheroid, *Emp. surv. Rev.*, **16**, 301–309.

Bulletin of the Seismological Society of America

A THREE-QUARTER WATT SEISMIC STATION

By K. J. Muirhead and D. W. Simpson

ABSTRACT

A low-power, low-cost instrument using slow speed, direct recording on magnetic tape provides continuous unattended seismic recording in excess of 1 month. The

Bulletin of the Seismological Society of America. Vol. 62, No. 4, pp. 985–990. August, 1972

A THREE-QUARTER WATT SEISMIC STATION

By K. J. Muirhead and D. W. Simpson

ABSTRACT

A low-power, low-cost instrument using slow speed, direct recording on magnetic tape provides continuous unattended seismic recording in excess of 1 month. The seismic signal is recorded at two gain levels separated by 26 db with a total dynamic range of greater than 70 db. A high-accuracy crystal clock with fully coded digital output and a crystal stabilized radio for reference time-signal reception provide timing to better than 0.1 sec throughout the recording period. Total power consumption is less than $\frac{3}{4}$ watts which enables operation for 1 month on dry cell batteries. The weight of the complete system including seismometer and batteries is less than 100 lb. Ten instruments have been used to record seismic signals ranging from localized microearthquake activity to explosions and teleseismic events.

Introduction

Many of the portable seismic instruments developed in recent years make use of FM (frequency modulation) recording on magnetic tape (Mereu and Kovach, 1970; Lewis and Meyer, 1968; Green and Hales, 1966; Lehner and Press, 1966). The FM method produces records of high quality, but suffers from the inherent disadvantage that recording time with standard tapes is limited to a few days. This is sufficient for many explosion studies where the recorder can be turned on at predetermined times. However, it is not suited for the recording of naturally occurring events, or for recording explosions where the shot time is beyond the control of the experimenter. Direct recording on the other hand permits much slower recording speeds and, hence, extended recording time, but it has not found wide usage in seismic applications, apparently because of power supply problems, timing difficulties and the fear of a loss of record quality.

The direct recording method is described by Pear (1967) and its application in a seismic instrument is discussed by Dibble (1964). In magnetic tape recording, there is an upper limit of about 4,000 cycles per inch of tape. As the maximum frequency of interest in most seismic applications is less than 100 Hz, tape speeds of only a few hundredths of an inch per second can be used, thus providing great economy in tape consumption. There is no lower limit to the frequency which can be recorded, but there are difficulties, with standard tape heads, in reproducing frequencies below 20 Hz. If, however, the playback speed is increased to a factor of 100 or more times the recording speed, the recorded frequencies are increased by the same amount and the seismic signals are reproduced in the audio range. This allows the signals to be processed with standard audio frequency equipment and also makes it possible to edit the tapes quickly by listening for events of interest.

The direct recording method does not provide the same degree of amplitude stability available from the FM process, but this is not serious in most seismic applications where small variations in amplitude are normally not significant. Because tape speed stability is less critical than in the FM method, less sophisticated tape transports can be used. Dibble (1964) showed that a slow speed, direct recording instrument can be developed at low cost and that the records obtained from such an instrument are of good quality. A similar

instrument has been used in Tasmania as part of a permanent seismic network (Muirhead and Read, 1966). Neither system includes an accurate clock or time encoder and this, together with the power required to drive the instruments for long periods, has made it difficult to utilize the full potential of the method. A crystal controlled clock has, however, been incorporated in a direct recording system used by Green and Hales (1968).

Advances in low-power semiconductor technology have enabled us to construct a complete seismograph system, including comprehensive timing facilities, with a total power consumption of less than $\frac{3}{4}$ W. This system is portable and battery operated, and is capable of recording unattended for periods in excess of 1 month.

Instrumentation

Tape transport. The tape transport has been adapted from the mechanical drive of a standard domestic Sony TC 105, tape recorder. As purchased, it is an a.c., three-speed ($1\frac{7}{8}$, $3\frac{3}{4}$ and $7\frac{1}{2}$ in/sec), four-track monophonic instrument accepting 7-in reels of $\frac{1}{4}$-in tape. All the electrical components are removed and the motor is replaced with a modified 250 rpm clock motor and 125:2 reduction gearbox to give tape speeds of 0.005, 0.010 and 0.020 in/sec. For a playback speed of $3\frac{3}{4}$ in/sec these give recorded frequency bands of approximately 0.05 to 20 Hz, 0.1 to 40 Hz and 0.2 to 80 Hz. Although four channels of information can be recorded by installing a four-channel head, the extra cost has been avoided by mounting an inverted two-channel head beside the existing one. To eliminate timing errors, one seismic channel and one time channel are recorded on each head. The offset between the heads is routinely measured by recording a pulse simultaneously on all four channels.

Recording system. A block diagram of the four-channel recording system is shown in Figure 1. Bias from a 2-kHz oscillator is added to all signals prior to recording. The

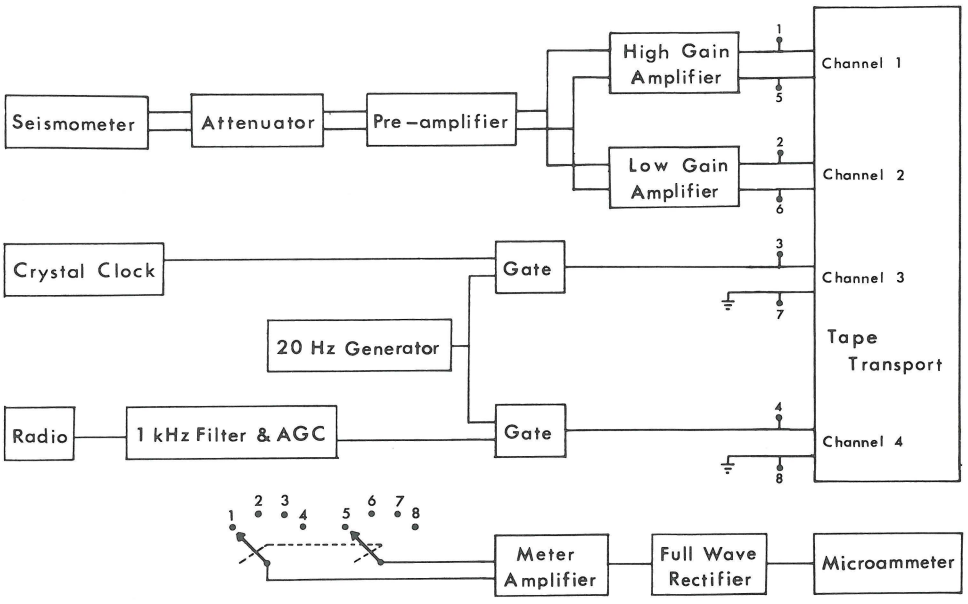

Fig. 1. Block diagram of the recording system.

seismometer output is first passed through a variable attenuator and preamplifier before being recorded on two tracks of the magnetic tape with a gain separation of 26 db. Each magnetic tape channel has a dynamic range of about 45 db before distortion becomes

significant, giving a total dynamic range of the system in excess of 70 db. The maximum gain is set such that background noise from a low-noise site can be recorded without attenuation, and corresponds to a total useful magnification of about 10^6 at 1.0 Hz. For noisier sites or for higher expected signal levels it is possible to introduce up to 30 db of attenuation in 6-db steps.

Timing. Absolute timing is obtained from a domestic radio receiver tuned to the Australian Post Office time service (VNG) on 7.5 MHz. To prevent drift, a crystal is added to the superheterodyne oscillator, and the signal-to-noise ratio is improved by adding a narrow band, 1-kHz filter and automatic gain control to the radio output. After full wave rectification the 1-kHz second tone (of length 0.05 sec) is used to gate the output of a 20-Hz oscillator which is recorded on the third tape channel.

Because radio signal fading occurs at night, continuity of time signals is provided by a crystal clock, the output of which is recorded on the fourth tape channel. A complete time code provides a method of determining the time on any part of the tape. The clock consists of a 4.194304 MHz crystal-controlled oscillator and a series of dividing and decoding circuits. The oscillator frequency is reduced to 1 pulse per second using straight binary division, after which binary dividers incorporating feedback loops are used to provide minute, hour, and day counts. Each minute, the outputs of these counters are gated into a parallel-to-serial shift register, and, from this, they are gated onto the tape giving a binary registration of the hour, minute and day during the first 30 sec of each minute. A sample time code recovered from the tape is shown in Figure 2. A 0.5-sec pulse

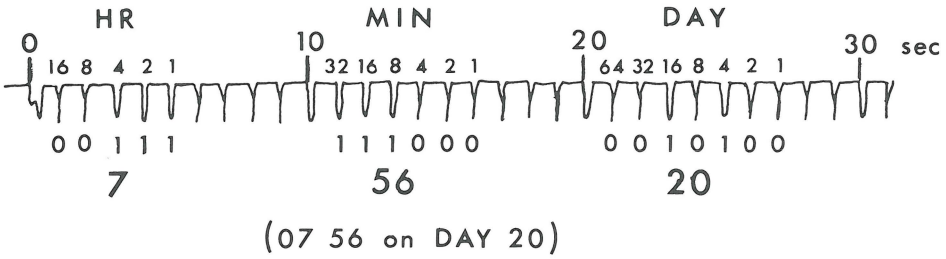

FIG. 2. Sample time code as recovered from the tape.

identifies the start of the minute, a 0.25-sec pulse identifies 10-sec intervals as well as logical "ones" in the time code, while a 0.125-sec pulse is used for all other seconds. To keep power consumption to a minimum, COS-MOS integrated circuits have been used throughout the clock logic, and the use of a crystal oven has been avoided by selecting a crystal with a stability of better than ± 0.5 ppm over the temperature range 0 to 60°C, which corresponds to a variation of less than ± 0.05 sec per day. A separate circuit incorporating a digital display is used to set the clock at commencement of recording.

Test circuits. For a portable instrument of this nature, it is essential that means should be available for fully checking its operation in the field with the minimum amount of test equipment. This is accomplished using an inbuilt test amplifier followed by a full-wave rectifier and microammeter. The operation of the seismic amplifiers, the radio, the clock (together with its time encoding circuitry) and the bias oscillator can be checked by switching the test amplifier to the input of the four tape channels. This feature together with a spare set of printed circuit boards ensures that any damage incurred in transporting the system can be repaired in the field.

Assembly. Except for the seismometer, the complete system together with sufficient dry cells for over 1 month's operation is contained in a single fibre-glassed wooden box, as shown in Figure 3. To prevent vandalism and to maintain a constant temperature for

the clock, the instruments are normally completely buried except for the radio aerial. Complete water-proofing is, therefore, essential. This has been achieved with a snug-fitting brass lid, the join being sealed with 2-in wide moisture-resistant tape. This is much simpler and more satisfactory under field conditions than an "O" ring seal.

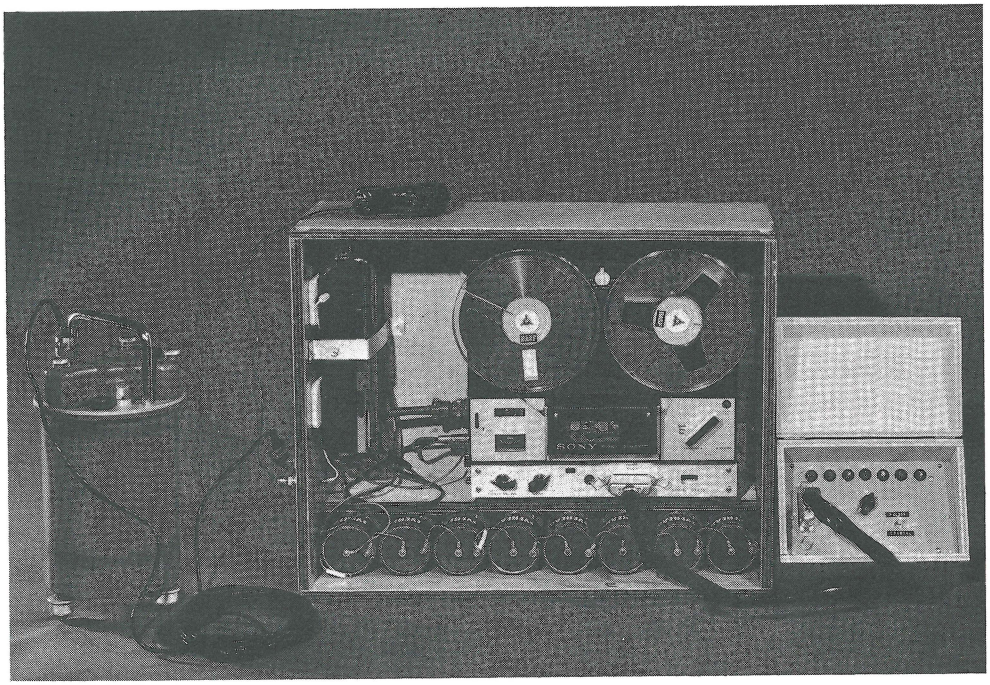

FIG. 3. Complete field system with clock set-up box shown connected at right.

Playback. As mentioned previously, a high-speed playback is necessary to recover the signals. For this purpose, we use a multichannel a.c. Oscillomink "jet pen" recorder with a frequency response up to 800 Hz, and a modified playback tape recorder having a frequency response down to 20 Hz and seven tape speeds between $\frac{15}{64}$ and 15 in/sec. The normal procedure is to locate an event aurally using a high playback speed and then to transcribe the event to paper using a playback speed which brings the signal within the frequency band of the pen recorder.

COST, WEIGHT AND POWER CONSUMPTION

As with any equipment developed within a research organization, the total cost of this nstrument is difficult to determine but the component cost excluding the seismometer is less than $800 and about 3 weeks technical time is required for the complete assembly. The Mark II Willmore has been used in our experiments although a much smaller and less expensive seismometer could easily be substituted.

The weight of the complete field recording system is 88 lb, including 17 lb of dry cells (sufficient for 1 month's operation) and the 32 lb Willmore seismometer.

Total power consumption is 0.65 W including 0.40 W for the motor and 0.10 W for the radio. This could be reduced still further by modifications to the radio and motor circuits, but at present eight Eveready no. 6 dry cells provide sufficient power to exhaust a 2,400 ft spool of tape over 1 month's operation.

Applications

The range of applications for which the instrument is suitable is indicated by the sample records shown in Figure 4. In experiments involving man-made explosions, a continuous recorder has the advantage over a programmed or manned system of being independent of the time of the explosion, thus eliminating the necessity of complicated shooting schedules or shot point to receiver communication links. This, along with the ease of installation, makes it possible to set up a number of stations with a minimum of

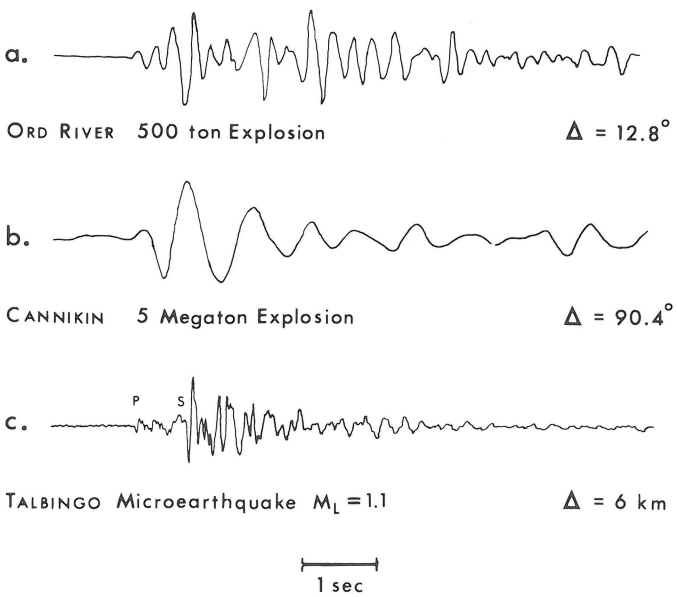

Fig. 4. Sample records.

personnel. Four of our instruments recorded the Ord River explosion in central Australia (Denham *et al.*, 1972) (Figure 4a) and ten were used to record the U.S. nuclear explosion CANNIKIN (Cleary *et al.*, 1972) (Figure 4b).

The instruments are also well suited for temporary installation to monitor localized earthquake activity and aftershock sequences or for detailed microearthquake studies. Microearthquake activity associated with the filling of the Talbingo reservoir in the Snowy Mountains of southeastern Australia has been monitored on three of the instruments, and one of the small events detected is shown in Figure 4c.

Acknowledgments

We wish to thank Dr. John Cleary for advice and encouragement, and Mr. E. Penikis for design assistance.

References

Cleary, J. R., D. W. Simpson, and K. J. Muirhead (1972). Variations in Australian upper mantle structure, from observations of the CANNIKIN explosion, *Phys. Sci.* **236**, 111–112.

Denham, D., D. W. Simpson, P. J. Gregson, and D. J. Sutton (1972). Travel times and amplitudes from explosions in northern Australia, *Geophys. J.* (in press).

Dibble, R. R. (1964). A portable slow motion magnetic tape recorder for geophysical purposes, *New Zealand J. Geol. Geophys.* **7**, 445–465.

Green, R. W. E. and A. L. Hales (1966). Seismic refraction measurements in the Indian Ocean, *J. Geophys. Res.* **71,** 1637–1647.

Green, R. W. E. and A. L. Hales (1968). The travel times of *P* waves to 30° in the central United States and upper mantle structure, *Bull. Seism. Soc. Am.* **58,** 276–289.

Lehner, F. E. and F. Press (1966). A mobile seismograph array, *Bull. Seism. Soc. Am.* **56,** 889–897.

Lewis, B. T. R. and R. P. Meyer (1968). A seismic investigation of the upper mantle to the west of Lake Superior, *Bull. Seism. Soc. Am.* **58,** 565–596.

Mereu, R. F. and R. J. Kovach (1970). A portable inexpensive seismic system for crustal studies, *Bull. Seism. Soc. Am.* **60,** 1607–1613.

Muirhead, K. J. and L. Read (1966). Slow-speed tape recording of seismic signals, *Nature* **210,** 929–930.

Pear, C. B. (1967). *Magnetic Recording in Science and Industry*, Reinhold, New York.

Department of Engineering Physics (K.J.M.)
Department of Geophysics and Geochemistry (D.W.S.)
Research School of Physical Sciences
The Australian National University
Canberra, A.C.T., Australia

Manuscript received January 14, 1972